Manufacture and Testing Carbon Fibre Lattice Core Sandwich Structures

Thesis submitted in accordance with the requirements of the
University of Liverpool for the degree of
Doctor of Philosophy

By
S Kanna Subramaniyan

February 2019

Acknowledgements

Firstly, I would like to thank and express my sincere gratitude to my supervisors, Dr Z. Guan and Professor W. J. Cantwell for their help, guidance and outstanding supervision throughout this research project. They have been actively interested in my work and their readiness to share knowledge, experience and expertise have been invaluable and highly appreciated. I am also grateful for the scholarship, financial support and encouragement from the Universiti Tun Hussein Onn Malaysia (UTHM) and the Government of Malaysia.

I would also like to extend my thanks to the technical team of the School of Engineering at the University of Liverpool, Mr S. Pennington, Mr J. Curran, Mr J. Mathew, Mr G. J Friel, Mr D. Atkinson, Mr J. Carter-Hallam for their help and technical support during this study. My appreciation to my colleagues, including Dr M. Zuhri, Dr R. A. Alia, Dr A. K. Haldar, Dr T. Boonkong, Dr S. S. Zaini, Mr Azimin and Miss Ziwen Xu for their valuable ideas.

Finally I would like to thank my family, especially my parents, for all of the support, love and encouragement that they have given me over the years. Special thanks to my friends, Dr P. Kongphan and Dr G. Fleming for their thoughts and motivation. I am delighted to thank my parent-in-laws for their prayers and encouragement. I wish to thank my lovely wife, Yogabhairavi Armugam for her unconditional love, support, understanding and patience throughout the ups and downs in finishing this study. I was also fortunate enough to be blessed with one daughter, Lakhsmiivardhini during this study.

Publications

Conference Paper

- S.K. Subramaniyan, Z.W. Guan and W.J. Cantwell, Crushing behaviour of carbon fibre lattice structures, In: Presented at the ICCM21 International Conferences on Composite Materials, Xi'an, 2017.

Journal Papers to be Submitted

- Structural response of carbon fibre lattice cores subjected to quasi-static and dynamic loadings, Polymer Testing.
- Prediction of load carrying capacities of carbon fibre lattice core sandwich structures, Composites Part B Engineering.

Abstract

The aim of the research is to manufacture composite lattice core sandwich structures based on a number of core truss configurations. Here, a novel manufacturing method is presented to manufacture carbon fibre reinforced composites (CFRC) lattice truss sandwich structures using a combination of sacrificial mould method and vacuum assisted resin infusion process (VARTM) technology in a single manufacturing operation to fully integrate the core with facesheets. Following this, the composite lattice core sandwich panel structures with different relative densities were produced and their mechanical properties and energy absorbing characteristics were examined under quasi-static and dynamic loading conditions.

Lattice sandwich structures based on columnar, pyramidal and modified pyramidal truss-based topologies were manufactured using sacrificial mould method. The influence of fibre volume fraction on vertical columnar lattice truss based on strut diameters of 2, 3 and 4mm were investigated under quasi-static compression loading. Specific compression strength and modulus values showed an increase when fibre volume fraction within individual struts increased. The maximum value of specific energy absorption value (SEA) is approximately 39 kJ/kg for columnar lattices based on 4 mm diameter struts with a higher fibre volume fraction. Pyramidal lattice cores and modified-pyramidal lattice cores based on varying complexity design were manufactured and tested under quasi-static compression and low velocity impact tests. Key mechanical properties, such as the elastic modulus, peak strength and energy absorption, were recorded for each of lattice core sandwich structures. It has been shown that by adding a vertical strut to the plain pyramidal unit cell, the mechanical properties of the lattice are improved significantly. It is likely that optimisation of the unit cell geometry could further enhance these properties and increase the potential for uses in load-bearing and energy absorption applications. The possibility of manufacturing such the lattices with complex configurations using sacrificial mould method proved to be an advantage over other techniques, which is extremely challenging for the manufacture using composite material. Dynamic testing has shown an increase in the peak load of the range of lattices structures studied. However, the overall energy absorption capacity of lattice structures subjected to dynamic loading demonstrated a decrease of approximate 30% compared to structures tested in most of quasi-static cases due to more significant drop of the load carrying capacity after the damage initiation. Finally, the static crushing response of the lattice structures were predicted using the analytical models presented in this research. The peak failure strengths of the lattice cores were predicted with reasonable agreement with the experimental data. However, there some discrepancies between the predicted and measured stiffnesses due to ignoring material imperfections during manufacturing. Overall, it has been shown that composite based lattice structures manufactured using the sacrificial mould method offer the potential to produce higher elastic modulus, peak strength and energy absorption by employing higher volume fibre fraction within individual struts. These novel lattice structures are expected to fill gaps of the low-density region in material property space.

Contents

Contents

List of Figures

List of Tables

1 Introduction

This chapter contains a brief introduction to the research project and an overview of the relevant composite materials and sandwich structures along with their applications. Following this, the motivation, objectives of the research and significance of the study are discussed. The chapter concludes with an outline of the thesis.

1.1 Overview

Over the years, industrial sectors such as automobiles, naval ships and aircrafts have been evolving with efforts focused on increasing performance and improve passenger comfort and most importantly safety. However, the rising of global oil price and environmental issues have led to an immense attention on the reduction of fuel consumption as well as carbon dioxide emissions.

One important aspect that helps to improve fuel efficiency and reduce polluting gas emissions is to minimise the structural weight of any transportation system. This must be done without sacrificing the performance of the system while reducing fuel consumption and consequently lowering emissions. Therefore, this engineering challenge has encouraged researchers to design and manufacture lightweight structures that can offer a higher strength and absorb more energy under various loading conditions.

In the past decades, introducing composite materials in the structural development substituting metals has provided major weight savings in the structure. A composite material is a combination of two or more materials, and it creates a new material with a unique combination of properties. Generally, a composite material is formed by reinforcing the fibres in a matrix resin. Composites made with a polymer matrix, e.g. a carbon fibre reinforced plastics (CFRP), have become more common and are extensively utilised in various engineering fields. Recently, composites have been widely used either in monolithic form or in a sandwich structures. Usage of composite materials and sandwich structures have become a common approach to reduce weight of structures and potentially improves the structural efficiency, including reduction of fuel consumption.

A sandwich structure consists of two thin and stiff facesheets separated by a thick, low-density core as shown in Figure 1.1. Sandwich structure has been regarded as an ideal structure since it offers high stiffness and strength to weight ratio and substantial energy absorption capacity. The use of sandwich structures continues to increase rapidly in applications ranging from satellites, aircraft, ships, automobiles, train carriages, wind energy systems, and bridge constructions, to mention only a few. The various advantages of sandwich constructions, the development of new materials, and the need for high performance but low weight structures insure that sandwich structures will continue to be in demand. Consequently, the core construction plays a critical role in the overall performance of the sandwich structure, especially energy absorption. Foams and honeycombs are usually used for core designs for sandwich structures.

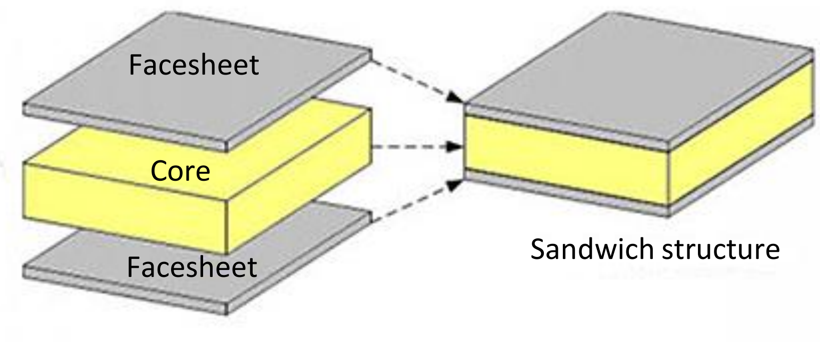

Figure 1.1. Schematic of a sandwich structure.

Foams offer easy handling, cheap, large surface area and high damping ratio making them preferable materials for thermal and sound insulation as well as for energy absorption applications. However, they lack strength and stiffness, limiting their application for heavy duty loading [1]. A honeycomb is regarded as the optimal core material in terms of strength, stiffness and lightness. However, this type of structures provides a limited access to core region for additional functions [2]. Nevertheless, some researchers have also attempted to use open cell foam structures, but their mechanical properties are far from optimal. This can be attributed to the fact that open cell foams have a low nodal connectivity and the cell walls usually deform by local buckling [3, 4]. As a result, they have low compressive stiffness and strengths, especially at low density.

The search for structurally-efficient cellular cores has led to the development of open cell microstructures called lattice truss core structures (periodic cellular structures). Lattice structures have high a nodal connectivity, which deform by the stretching of the constituent cell member. They have been shown to exhibit superior mechanical properties to closed cell foams with an identical density made from the same material. Since early year 2000s, lattice truss structures have been studied as a potential replacement for conventional sandwich cores (such as polymer foams and aluminium honeycomb. This kind of lattice structure is found to be competitive to honeycombs and superior to stochastic foams. Notably, lattice cores provide multifunctional opportunities such as actuation and cooling owing to the easy access to the core region.

The emergence of manufacturing technologies for constructing metallic three-dimensional periodic cores and the more recent development of techniques to manufacture composite truss cores have opened new opportunities for optimizing multifunctional core structures.

The mechanical properties of cellular structures depend on the intrinsic properties of the solids from which they are made of as well as the geometric arrangement of the components. Hence, stiffer and stronger materials are desirable for fabricating cellular structures with improved characteristics. Consequently, fibre reinforced composite cellular structures with lattice truss topologies have been shown as a promising alternative to metallic materials over the last decade. Carbon fibre reinforced composites that offer low density and high mechanical properties have been used to make lattice cores for sandwich structures [5]. Composite lattice structure offers the potential to fill the gap between existing engineering materials and the attainable material space, as illustrated in Figure 1.2.

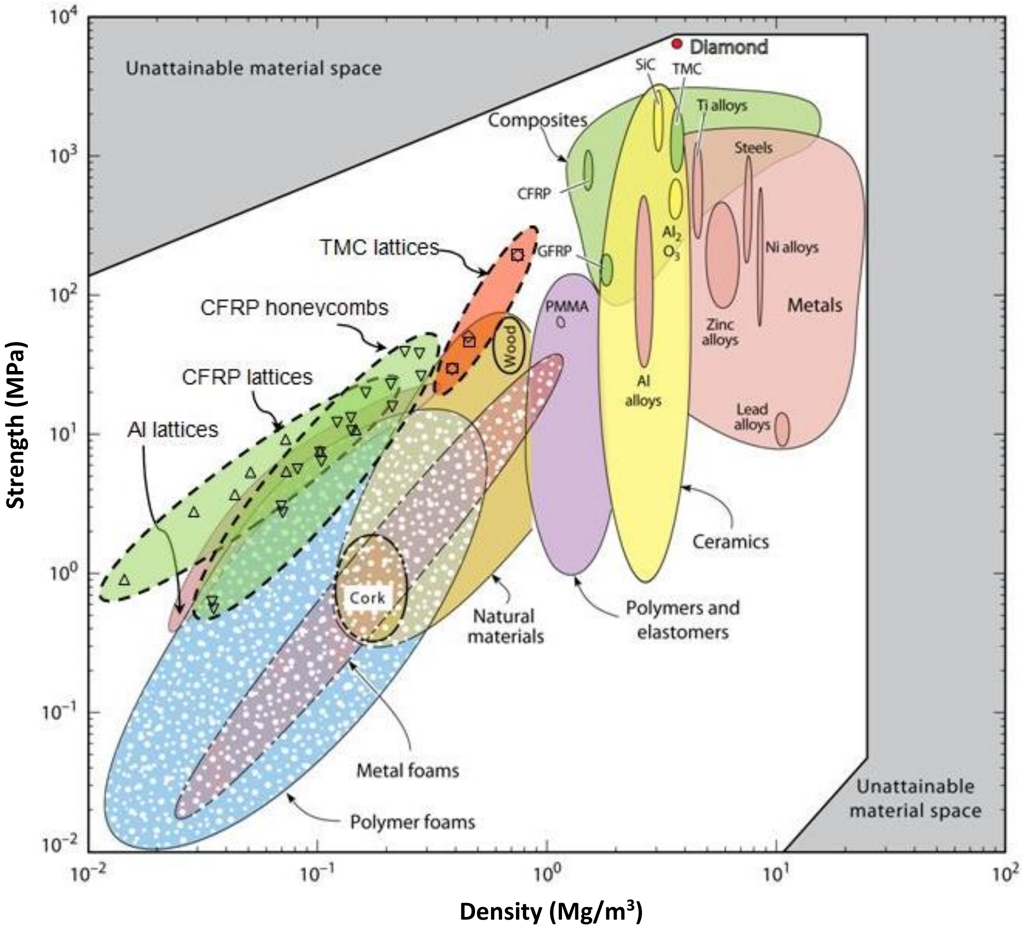

Figure 1.2. A material property chart comparing the strength and density of engineering materials including foams, honeycombs and lattices [6].

This research presents a contribution towards the development of all-composite sandwich structures with lattice truss core constructions. The lattice truss cores and the facesheets (or skins) are manufactured in a single manufacturing process without secondary bonding. Inevitably, this will prevent the weak interface between the core and skins that is considered the most vulnerable part of the sandwich structure.

1.2 Applications

This section describes some of the potential applications offered by sandwich structures based on cellular cores. Interest today in cellular materials is being driven by new vehicles which need to be lighter than ever but are also stiff, strong and capable of absorbing mechanical energy.

1.2.1 Automotive applications

The use of energy absorbing materials is essential for protecting passengers from impact when designing a vehicle. Cellular materials are able to absorb considerable energy in an impact event from a core. The peak force transmitted through the structure must be kept below the limits that an occupant can withstand. The energy absorbing behaviour of cellular core can be tailored to meet a certain range depending on the core topology and parent material from which the core is made. This makes cellular lattice core ideal candidate materials for crash-resistant components in automotive industry [7].

1.2.2 Aerospace applications

In the aerospace industry, sandwich structures based on cellular core offer high performance and low-cost designs of aircraft fuselages and wing structures for both military and civil aircraft. With far superior synthetic materials now available from which to make cellular material, materials scientists and mechanical engineers are beginning to fabricate cellular solids that rival those of nature. Figure 1.3 shows an example of curved aerospace sandwich structures in wing application [8].

1.2.3 Heat exchanger applications

For cellular core structures, the open topologies with high surface area density have thermal exchange efficiencies that may render them suitable for applications which require a structure for heat dissipation as well as structural efficiency. These combinations make the cellular materials being capable of heat dissipation media that can be used effectively for coupled thermal and structural applications. Periodic cellular structures have anisotropic pore structures. For instance, prismatic structures have one low friction flow direction, pyramidal lattices have two and the 3D Kagome and tetrahedral topologies have three easy flow directions. Textile and co-linear structures have one very easy flow direction while flow in others lies between that of the lattices and prismatic structures. The thermal characteristics of periodic cellular structures are therefore orientation dependent [9].

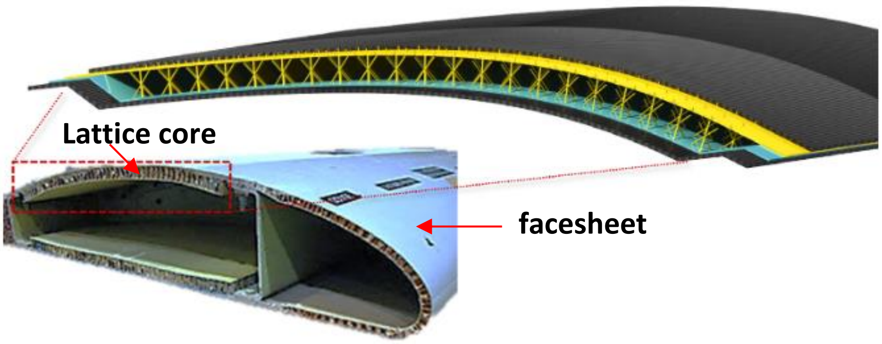

Figure 1.3. Curved sandwich structures in aerospace wing application [8].

1.3 Motivation and significance of the study

Many fabrication approaches have been developed to produce composite lattice core sandwich structures [3-10]. For example, Finnegan et al. [5] produced composite pyramidal lattice core by a waterjet cutting process and a snap fitting method. Thereafter, various technologies have emerged to manufacture composites lattice cores with different topologies for sandwich structures, such as hot press moulding method [10,11], thermal expansion moulding method [12,13], intertwining [14], interlocked method [15], electrical discharge machining [16] and stitching technology [17-19]. Although all these manufacturing methods for composites lattice cores are innovative, they generally involve complicated tooling approaches and high production costs. It is also worth mentioning that there is a problem of a relatively low bonding strength and stiffness on the core-facesheets interface for truss core sandwich structures [17]. Potluri et al. [20,21] has been suggested such problems could be improved by employing stitching technology using through-the-thickness reinforcement in the sandwich structures. This motivates an approach to fabricate lattice truss core sandwich structure as a single structure without secondary bonding process by integrally stitching the fibre through facesheets.

Therefore, the aim of this project is to develop a new method to fabricate composite lattice core sandwich structures. The lattice truss cores and the face sheets (or skins) are manufactured in a single fabrication process. This approach uses a sacrificial mould method to fabricate the lattice core sandwich structures. The sacrificial mould replicates the shape of the lattice truss in which the continuous carbon fibre tow incorporated in the core construction and extended to link the skins. This method efficiently uses the material whereby fibres are aligned along the truss direction and thus the design fully exploits the intrinsic strength of fibre reinforced composites. This process results in a stitched structure that is impregnated with a thermosetting resin using the vacuum assisted resin infusion process.

The outcomes of this research project have wider significance and implications, which are highlighted below.

(i) The manufacturing method for producing the lattice truss core sandwich structures as a fully integrated single structure is innovative and this thesis contributes the new knowledge for their designs and uses in sandwich applications.

(ii) This study will be highly beneficial to applications in various engineering problems, particularly to lightweight structural designs because of their high efficiency and multifunctional potential.

(iii) The resulting data generated from this research fills the gap in the material property chart on cellular core materials.

1.3.1 Project objectives

The primary aim of this project is to manufacture all-composite lattice core sandwich structures with a robust integration of the core and the skins. The resulting structures are then tested mechanically to characterise the behaviour under different loading conditions. The details of the objectives of this project can be summarised as follows:

(i) Designing and developing a manufacturing method to fabricate a range carbon fibre composite lattice core sandwich structures.

(ii) Investigating the mechanical response of lattice structures and their failure mechanisms subjected to quasi-static and dynamic loading.

(iii) To propose analytical models to predict the mechanical response of the lattice core sandwich structures.

(iv) To compare the measured mechanical response of the manufactured lattice core structures with analytical modelling results.

1.4 Thesis outline

This thesis consists of a further five chapters as follows:

Chapter II: Literature Review; this chapter gives an overview of the lattice materials and their manufacturing route to fabricate lattice core sandwich structures. Attention is focused on mechanical behaviour of sandwich cores under quasi-static and dynamic loading.

Chapter III: Experimental Procedure; this chapter describes the design and experimental procedure in this study, consists of specimen preparation, experimental testing (burn-off, quasi-static and low velocity impact tests). It also gives the details of the equipment necessary for these tests carried out, together with the related methods.

Chapter IV: Experimental Results; this chapter presents and discusses the experimental results of material and sandwich structure tests and the failure mechanisms of the structures. The load-displacement traces and energy absorption of various lattice structures are included.

Chapter V: Analytical Model; this chapter presents the analytical approach to estimate the stiffness and strength of lattice-core sandwich structures and compares the predicted values with experimental results.

Chapter VI: Conclusions and Recommendations; this chapter summarises the overall findings and observations based on the mechanical responses of the range of carbon fibre lattice structures. In addition, recommendations of possible future work are also given.

References

[1] M.F. Ashby, A.G. Evans, N.A. Fleck, L.J. Gibson, J.W. Hutchinson and H.N.G. Wadley, Metal foams: A Design Guide, Butterworth-Heinemann, 2000.

[2] T. Bitzer, Honeycomb Technology: Materials, Design, Manufacturing, Applications and Testing, Springer, 1997.

[3] G.W. Kooistra and H.N.G. Wadley, Lattice truss structures from expanded metal sheet, Materials & Design, 28, 2007, pp507–514.

[4] T. George, V.S. Deshpande, K. Sharp and H.N.G Wadley, Hybrid core carbon fibre composite sandwich panels: Fabrication and mechanical response, Composite Structures, 108, 2014, pp696–710.

[5] K. Finnegan, G. Kooistra, H.N.G. Wadley, and V.S. Deshpande, The compressive response of carbon fibre composite pyramidal truss sandwich cores, International Journal of Materials Research, 98, 2007, pp1–9.

[6] http://www.virginia.edu/ms/research/wadley/celluar-materials.

[7] H.P. Degischer and B. Kriszt, Handbook of Celllular Metals, Wiley-VCH, 2002.

[8] I. Ullah, J. Elambasseril, M. Brandt and S. Feih, Performance of bio-inspired Kagome truss core structures under compression and shear loading, Composite Structures, 118, 2014, pp294–302.

[9] H.N.G. Wadley and D.T. Queheillalt, Thermal applications of cellular lattice structures, Material Science Forum, 539-543, 2007, pp242–247.

[10] Y. Sun and L. Gao, Mechanical behaviour of all-composite pyramidal truss cores sandwich panels, Mechanics of Materials, 65, 2013, pp. 56–65.

[11] M. Li, L. Wu, L. Ma, B. Wang and Z. Guan (2011). Mechanical response of all-composite pyramidal lattice truss core sandwich structures, Journal of Materials Science and Technology, 27(6), pp570–576.

[12] B. Wang, L. Wu, L. Ma, Y. Sun and S. Du, Mechanical behavior of the sandwich structures with carbon fiber-reinforced pyramidal lattice truss core. Materials and Design, 31(5), 2010, pp2659–2663.

[13] S. Yin, L. Wu and S.R. Nutt, Compressive efficiency of stretch–stretch-hybrid hierarchical composite lattice cores, Materials & Design, 56, 2014, pp731–739.

[14] H. Fan, W. Yang, B. Wang, Y. Yan, Q. Fu, D. Fang and Z. Zhuang, Design and manufacturing of a composite lattice structure reinforced by continuous carbon fibers, Tsinghua Science and Technology, 11(5), 2006, pp515–522.

[15] H. Fan, F. Sun, L. Yang, F. Jin and D. Zhao, Interlocked hierarchical lattice materials reinforced by woven textile sandwich composites, Composites Science and Technology, 87, 2013, pp142–148.

[16] J. Xiong, B. Wang, L. Ma, J. Papadopoulos, A. Vaziri and L. Wu, Three-dimensional composite lattice structures fabricated by electrical discharge machining, Experimental Mechanics, 54(3), 2013, pp405–412.

[17] L. Che, G. Xu, T. Zeng, S. Cheng, X. Zhou and S. Yang, Compressive and shear characteristics of an octahedral stitched sandwich composite, Composite Structures, 112, 2014, pp179–187.

[18] H. Kim, B.H. Cho, H.-K. Hur and K.-J. Kang. A Composite Sandwich Panel Integrally Woven with Truss Core, Materials and Design, 2014.

[19] Z. Song, S. Cheng, T. Zeng, F. Yang, S. Jing and D. Fang, Compressive behavior of C/SiC composite sandwich structure with stitched lattice core, Composites Part B: Engineering, 69, 2015, pp. 243–248.

[20] P. Potluri, E. Kusak and T.Y. Reddy, Novel stitch-bonded sandwich composite structures, Composite Structures, 59, 2003, pp. 251–259.

[21] A. Aktas, P. Potluri and I. Porat, Development of Through-Thickness Reinforcement in Advanced Composites Incorporating Rigid Cellular Foams, 20, 2013, pp. 553–568.

2 Literature Review

This chapter provides a literature review of the relevant work and commences with an overview of the cellular solids, followed by a discussion of lattice materials. As the engineering applications of the lattice core sandwich structures grow, many methods were developed to manufacture the lattice truss cores. Although there are many manufacturing methods for producing lattice core sandwich structures with different topologies, those manufacturing approaches are based on a similar principle, i.e. to create an open architecture with multifunctional capabilities. A review of the manufacturing lattice core sandwich structures is presented mainly with brief discussion on metallic lattices, followed by composite lattice truss cores. An emphasis is given to composite lattice core sandwich structures, with detailed discussion on their mechanical performance. This chapter primarily gives the review of the mechanical responses of the composite lattice core sandwich structures subjected to quasi-static compression and low velocity impact test. It also discusses numerical investigations on lattice core sandwich structures.

2.1 Cellular solids

Nature has always given many inspirations in developing engineered materials. As such, cellular solids (or structures) which appear broadly in nature can be constructed efficiently to meet desired structural as well as functional demands. A cellular solid is an assembly of cells with edges and faces from an interconnected system of solid struts or plates [1]. Some examples of these cellular solids exist in nature are wood, cork, sponge and coral. These materials are generally lightweight yet mechanically robust with random cell sizes and shapes. In structural perspective, voids and pores are generally considered as defects since they decrease overall structural performance [2,3]. However, natural materials, such as those shown in Figure 2.1, have dictated that cellular materials with aptly structured voids and pores can be efficiently used to support load. From these natural inspirations, synthetic cellular solids have been evolved, such as stochastic foams and honeycombs for use in numerous engineering applications.

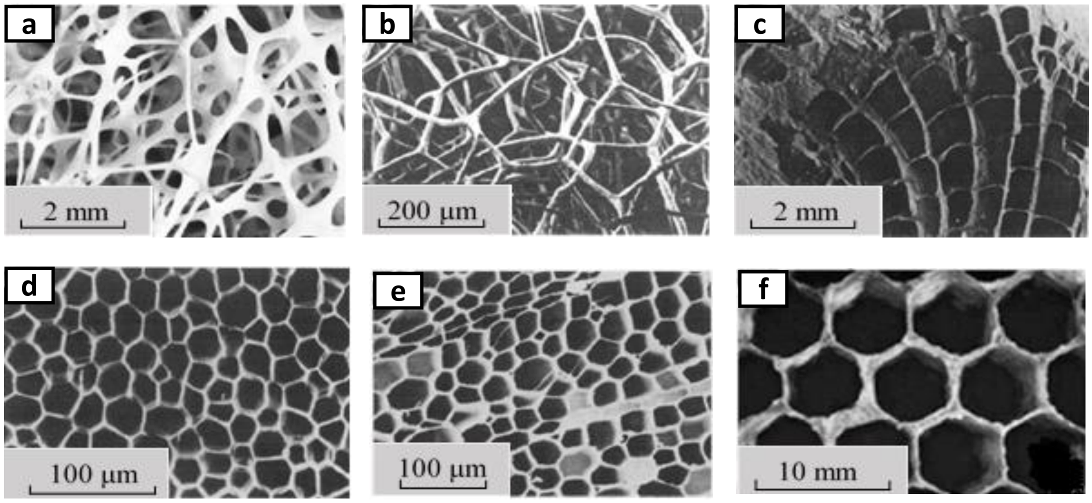

Figure 2.1. Natural cellular materials. a) cancellous bone b) sponge c) coral d) cork e) wood f) bee honeycomb [1].

The most widespread cellular solids are foams. The first synthetic cellular solids of foams were made from polymers to which foaming agents were added in a liquid state [4]. Since then, significant growth in the manufacturing of engineered foams and foaming technologies were taken place over the time, which has resulted in a wide range of foam materials from polymers [4], metals [2] and ceramics [5]. Polymers, in particular, can be made into flexible or stiff foams depending on the properties of the parent material from which they are made. Solid foams are often preferred for a given application due to their excellent energy absorption or cushioning properties. Despite this, it has been shown that such foams are suitable for use in a wide range of applications, from sandwich cores, damping and vibration control applications, thermal and acoustics management, packaging and energy absorption. Figure 2.2 illustrates some commercial foams available in the market.

Most foams are stochastic in nature, made by variants of foaming in the liquid, solid or semi-solid state. Foams that made from this process produces cellular architectures that are either closed cells or open cell structures. Closed cell stochastic structures are useful, for example, sound attenuation, fire retardation and impact energy absorption. However, they do not provide for fluid throughput. Fluids do however, flow through open cell stochastic foams because of the interconnected nature of the porosity. Open cell stochastic foams are useful, for example, for lightweight heat exchangers or as electrodes in nickel metal hydride batteries. Open cell foams have a low nodal connectivity and are usually deform predominately through bending of their cell edges, meanwhile closed cell foams have cell edges which both bend and stretch during compression and have cell faces which also stretch.

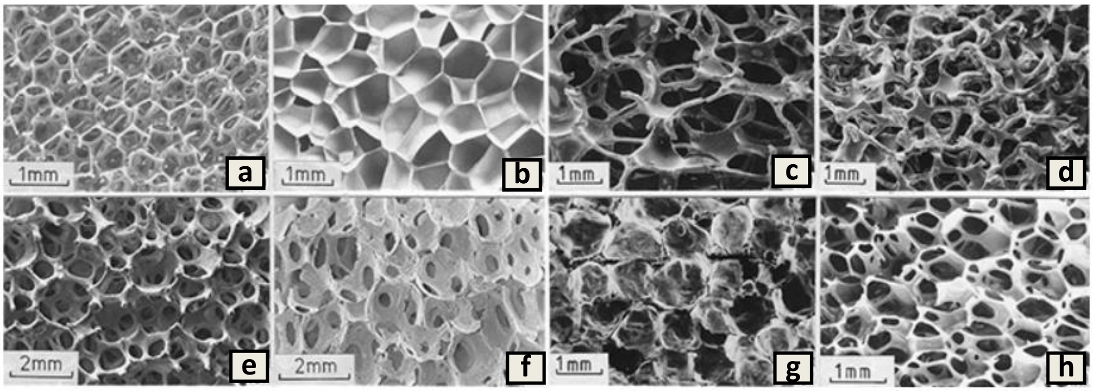

Figure 2.2. (a) Open-cell polyurethane (b) closed-cell polyethylene (c) nickel (d) copper (e) zirconia (f) mullite (g) glass foams and (h) a polyether foam with both open and closed cell [1].

One prominent feature of a cellular solid is its relative density, $\bar{\rho}$ defined as the ratio of density of cellular material to that of the solid from which the cell walls are made. As such, Gibson and Ashby [1] have described that the Young's modulus and strengths of foams depends on the foams cell topology (open or closed cell) and its relative density. The modulus, E and plateau strengths, σ_{pl} of the open cell foams vary with relative density according to the following power law relations.

$$\frac{E}{E_s} = C\bar{\rho}^{\,2} \tag{2.1}$$

$$\frac{\sigma_{pl}}{\sigma_{ys}} = C_1\bar{\rho}^{\,3/2} \tag{2.2}$$

where E_s and σ_{ys} are elastic modulus and yield strength of the solid material from which it is made. C is a cell topology dependent constant (approximately equal to unity for many open cell foams) and C_1 is a constant of proportionality. For closed cell foams that includes contributions from the cell edges and faces, resulting in mechanical property – relative density relationships are in the following forms.

$$\frac{E}{E_s} = C_2\phi^2\bar{\rho}^{\,2} + C'_2(1-\phi)\bar{\rho} \tag{2.3}$$

$$\frac{\sigma_{pl}}{\sigma_{ys}} = C_3(\phi\bar{\rho})^{3/2} + C'_3(1-\phi)\bar{\rho} \tag{2.4}$$

where C_2/C_3 and C'_2/C'_3 are the constants of proportionality for the cell edges (bending structures) and cell faces (which deforms by membrane stretching), and ϕ is the fraction of the solid in the cell edges. Due to effects of stretching in closed cell foams, the modulus and plateau strengths are higher than their open cell counterparts.

The power law dependence on relative density indicates a rapid property loss with decreased density of the foams. Consequently, their mechanical properties are often altered by changing the material and/or the degree of porosity by means of the relative density. Since it is difficult to control placement of the solid material at the cell level, they normally possess a random pore architecture with non-uniform, curved cell walls/edges and numerous imperfections [6]. One disadvantage to this is that it complicates prediction of the physical properties based on the material and structural design. Moreover, it is challenging to produce foams with well-controlled directional properties. The drawbacks of foams cause the mechanical properties of stochastic foams which are inferior to those of periodic, less defective cellular structures like hexagonal honeycomb in Figure 2.3 [6].

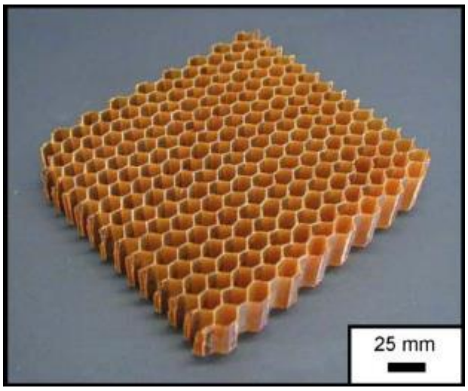

Figure 2.3. Aramid-fibre (Nomex®) reinforced honeycomb [6].

Synthetic honeycombs are inspired from an efficient design of a honeybee's nest (contains their brood and stores of honey). It has been reported that honeycomb have superior features to stochastic foams. This is because their manufacturing and optimization design process are more controllable. Therefore, the actual mass distribution in periodic cellular structures is significantly consistent with the ideal one. Honeycombs are the current state-of-the art for lightweight applications such as aircraft and satellite structures [7-9]. However, they do provide some disadvantages when used as cores for sandwich panels. There are difficulties to manufacture them into complex curved configurations due to induced anticlastic curvature. Moreover, due to nature of closed cell architectures, honeycomb sandwich structures are susceptible to moisture rise and gas retention which eventually lead to internal corrosion and skin debonding [8,10]. Despite of these drawbacks, honeycombs have a low relative density, high strength-to-weight ratio and good energy absorption characteristics. Interestingly, elastic modulus and strength of regular hexagonal honeycombs scale with $\bar{\rho}^{\,3}$

and $\bar{\rho}^2$, respectively, at low relative densities under out-of-plane compression loading [11]. The property-relative density scaling relations indicated that the mechanical properties of the regular honeycomb are superior compared to that of foams at low relative densities [6,8]. These differences are a consequence of cell walls/edges deformation along with minor defects. Cells in foams deform by local bending, whilst honeycomb structures deform in more desirable stretching or compression mode of deformation that improve cellular performance.

Cellular solids such as foams and honeycomb profoundly created an opportunity to produce highly ordered architectures with open cell microstructures and in a periodic manner. Although the bee stimulated honeycomb regarded as the optimal core material in terms of stiffness and strength, however, access to its interior space for additional functions is limited [12]. This has led to a search for open cell microstructures with high nodal connectivity that deform by the stretching of constituent cell members, giving a much higher stiffness and strength per unit mass. As such, cellular solids known as lattice truss has emerged as candidate for stretch-dominated structures. The following section illustrates the concept of lattice truss materials.

2.2 Lattice materials

Lattice materials are a structure made up of struts in a periodic manner [13-17]. In a structural engineering viewpoint, a lattice truss or space frame means an array of struts that can be treated a pin-jointed or rigidly bonded at their nodal connections [14]. Their motivation is to create stiff and strong load-carrying structures using as little material as possible, hence being lightweight. However, lattice materials are different from structural lattices (truss or frame) in one critical aspect that of scale [14]. Scale of the unit cell of lattice materials is one of millimetres or micrometres, and it is this that enable them to be seen both as structures and as materials [14,15]. At one level, classical methods of mechanics can be used to analyse them in a similar manner of any space frame analysed. But at another level, lattices are not only treated as a set of connected struts, but as a 'material' in its own right, with its own set of effective properties, allowing direct comparison with those of fully dense, monolithic materials [14,17].

Lattice materials as a periodic structure can be classified as planar lattices and spatial lattices [15]. Planar lattices are two dimensional (2-D), in which the unit cells are translated in two dimensions to create a prismatic material. An example of a prismatic cellular material is the honeycomb structure, contains regular polygons such as triangle, square and hexagon [18-20]. All honeycombs are closed cell structures and exhibits an anisotropic mechanical behaviour. Other examples of planar lattices are corrugated structures with different topologies such as triangular, diamond and web truss [20]. These prismatic structures are open (easy flow) cells in one direction and a closed cell structure in the other two orthogonal directions. Figure 2.4 shows the range of planar lattices as aforementioned here. Three dimensional (3-D) or spatial lattices is another type of periodic materials, in which the unit cell is tessellated along three axes to create lattice truss materials. The trusses can be arranged in many different configurations depending upon the intended application [13]. Figure 2.5 shows six examples of lattice truss structures that commonly available in literature search [17, 20, 21].

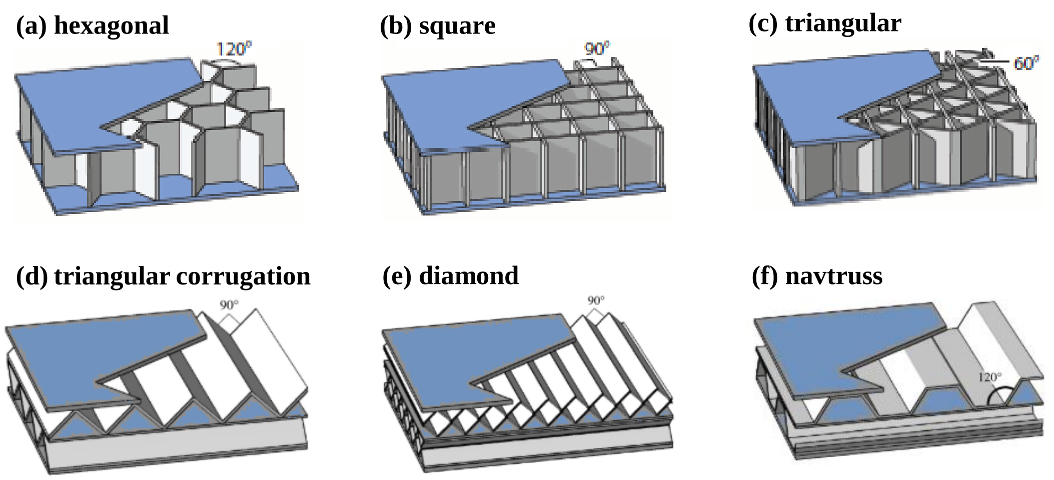

Figure 2.4. Examples of 2-D lattices. (a)-(c) prismatic honeycomb structures (d)-(f) prismatic corrugation structures [18,20].

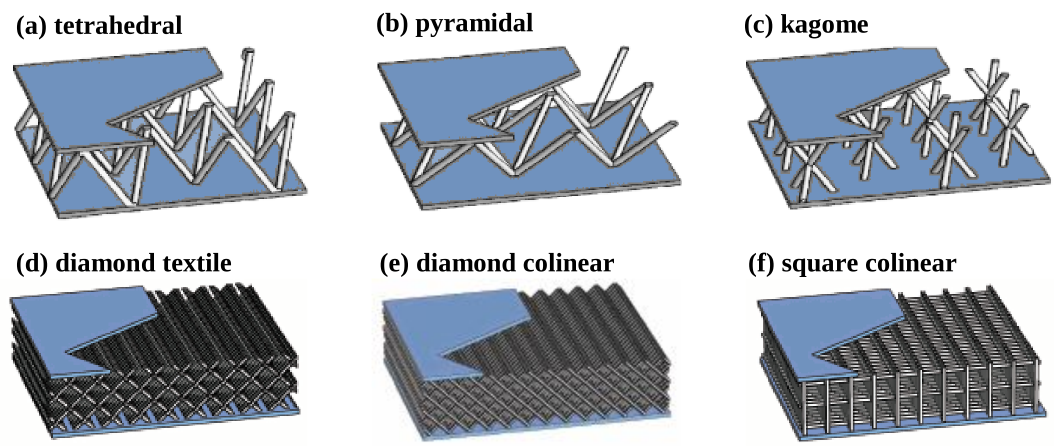

Figure 2.5. (a)-(f) Examples of 3-D lattices (lattice truss) topologies configured as the cores of sandwich panel structures. Many can be made with solid or hollow trusses. The truss cross sections can also be shaped (for example, square or circular) [20,21].

The structural performance of a lattice material is strongly reliant upon its topology [16]. Moreover, topology of nodes and inter-node struts of a unit cell of lattice materials dictates its physical behaviours. Deshpande et al. [22,23] indicates that the macroscopic properties are largely dictated by the connectivity of joints rather than by the regularity of the microstructure. As such, the mechanical properties of cellular materials lie on the nature of deformation mechanisms [23]. Foams, stochastic in nature have low nodal connectivity of three (3)-four (4) adjoining bars per joint [24]. They are referred as a bending dominated structure since the deformation is primarily governed by bending of the constituent struts and cell walls and thus, stiffness and strength follow non-linear scaling law as pointed in the section 2.1. However, lattice materials, for example, octet truss has a nodal connectivity of twelve (12) and is a stretching dominated structure because constituent struts deform by stretching [16,22,24]. Interestingly, lattice material exhibits ideal linear scaling of mechanical properties. As a result, lattices with $\bar{\rho} = 0.1$ are predicted to be about ten times stiffer and about three times stronger than the equivalent relative density foams [25-27]. Figure 2.6 illustrates the influence of cellular architecture on the scaling of mechanical properties [19]. Considerably, even small differences in scaling can have a large effect on strength and modulus at very low densities.

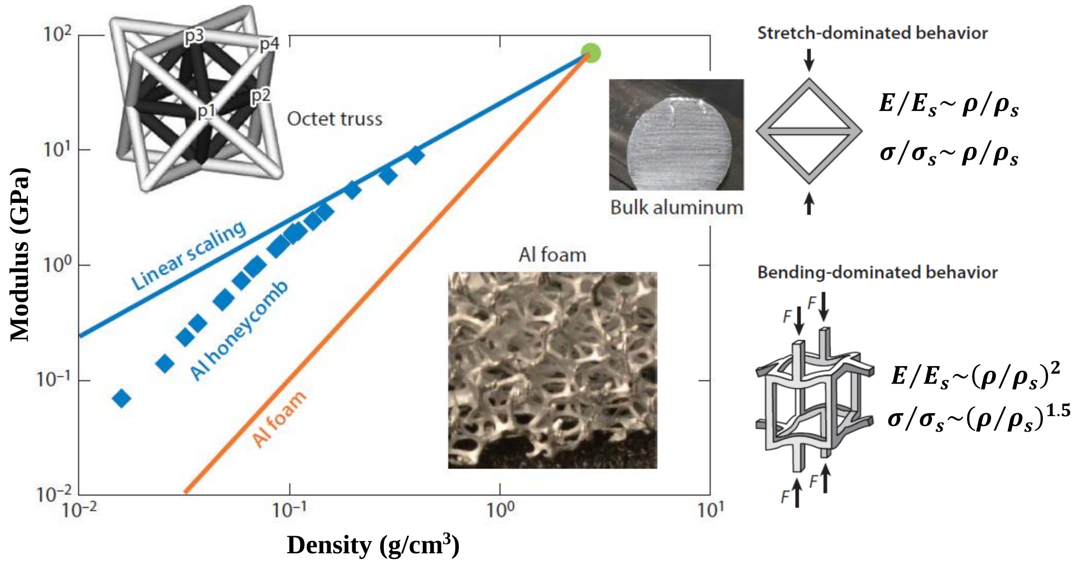

Figure 2.6. Trends of cellular architecture on the scaling of mechanical properties with density exemplified by aluminium foam, honeycomb, and octet truss [19].

The criteria for the deformation of lattice materials to be stretching dominated is that the unit cell of the structure satisfies Maxwell's criterion, $M = b - 3j + 6 > 0$ [22,23]. Here the b and j are number of struts and nodes, respectively. Furthermore, the principle dictates the minimum node connectivity for a special class of lattice structured materials to be stretching-dominated is 6 and 12 for 2-D and 3-D lattice materials [14, 16, 23], respectively. Such stretching dominated lattices can be treated as a collection of pin jointed struts [23], with struts that only sustain uniaxial forces and elongations as shown in Figure 2.7. The point has been made that stretch-dominated structures offer greater stiffness and strength per unit weight than those with the bending dominant mode of deformation. It should be realised that minimal stretch-domination offers only marginal gain. However, for the full gain to be realised, the structure must be predominantly stretch-dominated. Therefore, stretching dominated lattices are preferred as they are structurally efficient.

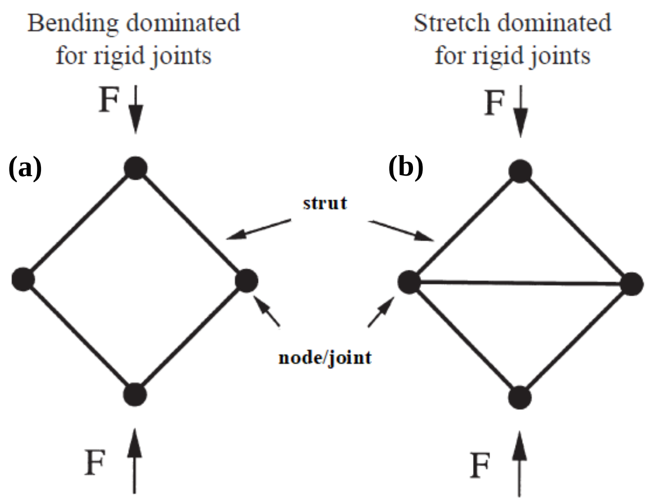

Figure 2.7. Picture showing (a) a mechanism and (b) a structure. The joints are pin-jointed. Note that (a) is kinematically indeterminate structure with one mechanism and (b) is a statically and kinematically determinate or simply stiff structure [23].

Furthermore, lattice materials are also offering unprecedented opportunities for multifunctionality [28]. The open topologies with high surface area density have thermal attributes that may enable applications which require a structure for heat dissipation as well as mechanical stiffness/strength. The structures have a high surface area density and may be constructed out of high conductivity materials. These combinations make the cellular materials as a heat dissipation media that can be used effectively for coupled thermal and structural applications, for example as a jet blast deflector on an aircraft carrier. By tailoring the architecture, the properties also can be varied to match location-specific requirements. Figure 2.8 shows a notional example in which the relative density of the core of a wing can be varied by adjusting pore and struts dimensions to increase strength where necessary corresponding to critical loading requirements whereas the density is minimized in other locations to save mass [19]. Additionally, the core architecture can be tailored to ensure that the centre of gravity is aligned with design targets, or the open cellular architecture can be optimized for thermal management.

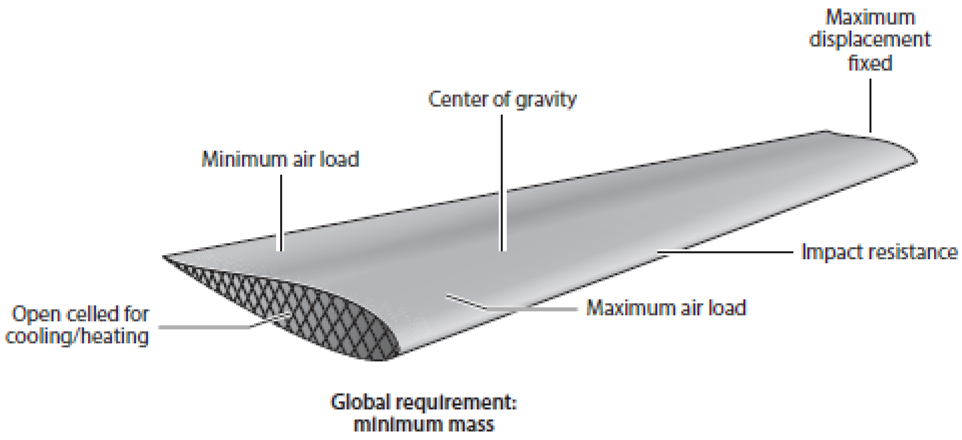

Figure 2.8. Multifunctional exploration by tailoring the cellular architecture to local requirements [19].

2.3 Manufacturing lattice core sandwich structures

The interest in lattice truss structures has been driven by both structural and multi-functional applications of these materials. Now, many methods used to manufacture lattice truss structures have been emerged and being developed over the time. In this section we describe the processes that can used to manufacture lattice core sandwich structures.

2.3.1 Manufacturing metallic lattice core sandwich structures

Several approaches can be used to manufacture metal lattices as a core in sandwich construction. They result in materials that can be classified by the size of their cells and the relative density of the structures. From the literature searches, it was well described that metal lattices can be produced from conventional manufacturing processes to modern technologies includes additive manufacturing processes. From this, manufacturing metallic lattices can be classified into a few processes such as investment casting, deformation forming, metal wires approaches, snap-fitting method and additive manufacturing.

The first 3-D lattice truss materials/structures were developed by JAMCORP, which are known as lattice block materials from investment casting [28]. Investment casting is a precision casting process using lost wax method to make components in any cast alloys. Earlier, injection moulding was used to create a wax or polymer template of the truss core that could be used as a sacrificial pattern for investment casting [29]. However, the cost of die fabrication is often high due to the nature of design complexity. Moreover, if the lattice core design has to change for sandwich panels, a new die required with additional costs. The emergence of rapid prototyping approaches [30,31] has automated the creation of sacrificial pattern for investment casting with less expensive and offers design flexibility. This pattern, together with a system of gating and risers, is coated with a ceramic casting slurry and dried. The wax or polymer is removed by melting or vaporization and the empty mould filled with liquid metal. Figure 2. 9 illustrated an example of investment casting approach.

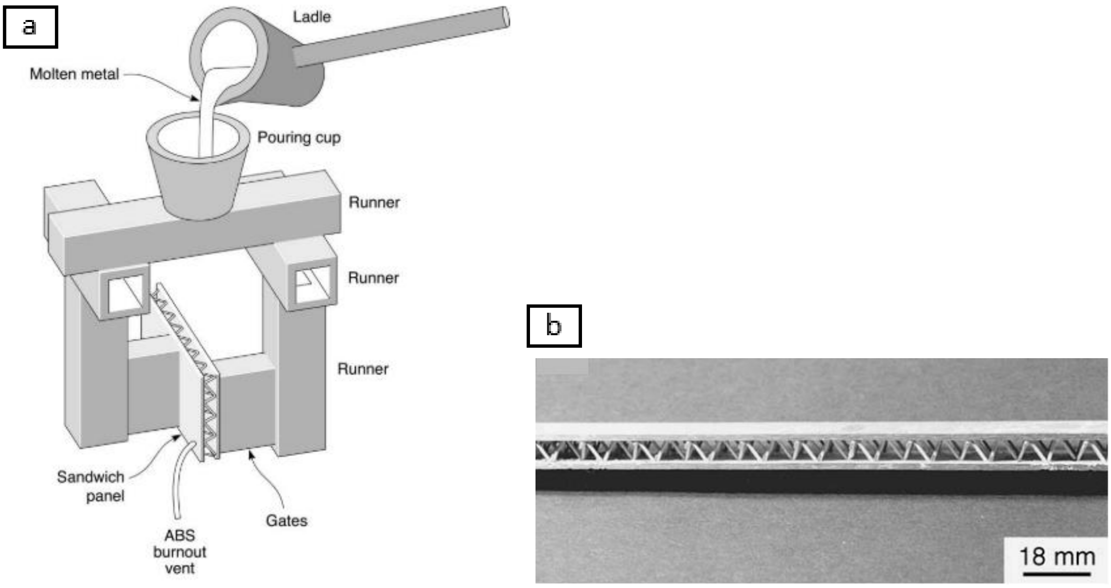

Figure 2.9. An example of an investment casting approach. (a) Molten metal is poured into cavity after the sacrificial pattern burnout process. (b) As manufactured aluminium alloy tetrahedral truss core sandwich specimen [30, 32].

Many metallic lattice materials were produced by this approach such as aluminium/silicon [22, 29,32-33], beryllium/copper alloy [30-31], Copper Alloy [34,35] and IN 718 & Mar-M247 superalloys [36] with a range of lattice truss topologies. However, structures with near optimal, low relative density cores are difficult to fabricate from investment casting approach due to tortuous metal paths. Furthermore, the resulting components susceptible to defects caused by the inability of the fluid to access all parts of the truss structure. Thus, to overcome these issues, forming operation can be used to fabricate lattices with low relative density from high formability alloys with minimal defects.

Deformation forming is another method of fabricating metal lattice structure by press forming operation [21,28]. This operation can be classified as two approaches, i.e. (1) sheet perforation and shaping techniques, (2) Expanded metal sheet folding. Figure 2.10 shows the perforating metal sheet forming to produce metal lattice truss core. Liu et al. [37] has used this approach to produce aluminium alloy tetrahedral lattice truss and then bonded them to facesheets using brazing method. Stainless steel pyramidal lattice trusses were also produced by this approach by Dharmashena et al. [38], Biagi et al. [39] and Wadley et al. [40] in which brazing method and laser welding were adopted for bonding purpose. Lim et al. [41] has demonstrated expanded metal sheet folding approach using low carbon steel sheet in which cut was performed using YAG laser, and expanded width wise to form a metal mesh. The metal mesh was later bent along the lines connecting the longer ends of the diamond shapes, forming a corrugated sheet to produce Kagome lattice truss as shown in Figure 2.11. Kooistra and Wadley [42], Jiang et al. [43] were also used expanded metal sheet approach to produce pyramidal lattice truss from aluminium and stainless steel respectively and however, the cut on metal sheets were performed using punching on die.

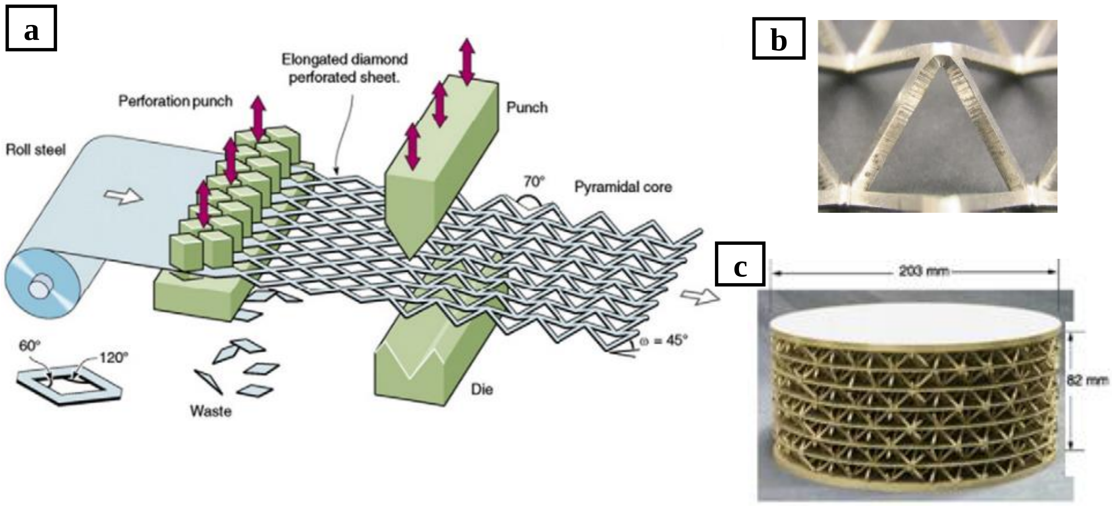

Figure 2.10. Sheet perforation and shaping process. (a) lattice fabrication, (b) as manufactured single layer pyramidal lattice truss [39], (c) multilayer assembly [40].

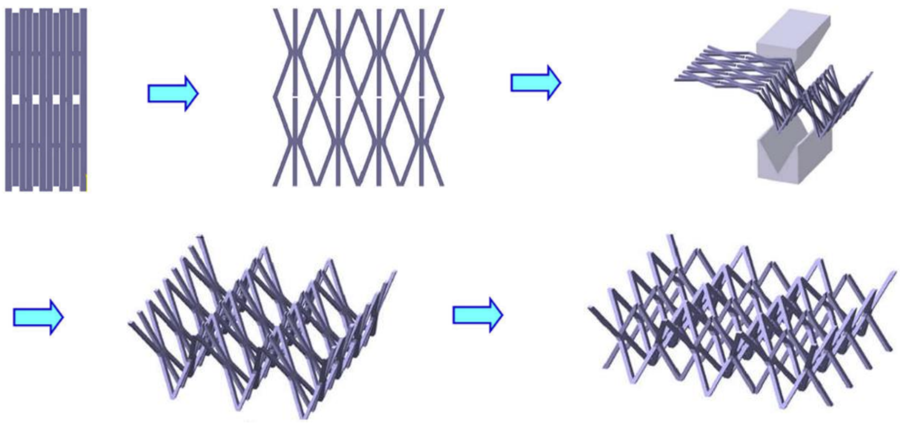

Figure 2.11. Expanded-metal forming process which involves laser cutting, expanding sheet, bending and corrugated forming to produce Kagome lattice truss core [41].

Another manufacturing route to fabricate metal lattice truss assembly is metal wire approaches which comprise of woven and non-woven metal textiles. Woven metal textile approach is a simple, inexpensive method of weaving, braiding and sewing of wire drawn from metal alloy to produce 3-D lattice materials. Sypeck et al. [44] and Tian et al. [45] described the woven metal textile approach using nichrome wire and copper/stainless wires to produce square or diamond textiles lattices, as shown in Figure 2.12. Meanwhile, non-woven metal textile approach produces textiles by layering wires and tubes from metal such as stainless steel and subsequently joined together by brazing. Figure 2.13 shows the approach for creating the lattice truss architecture, square or diamond colinear [46].

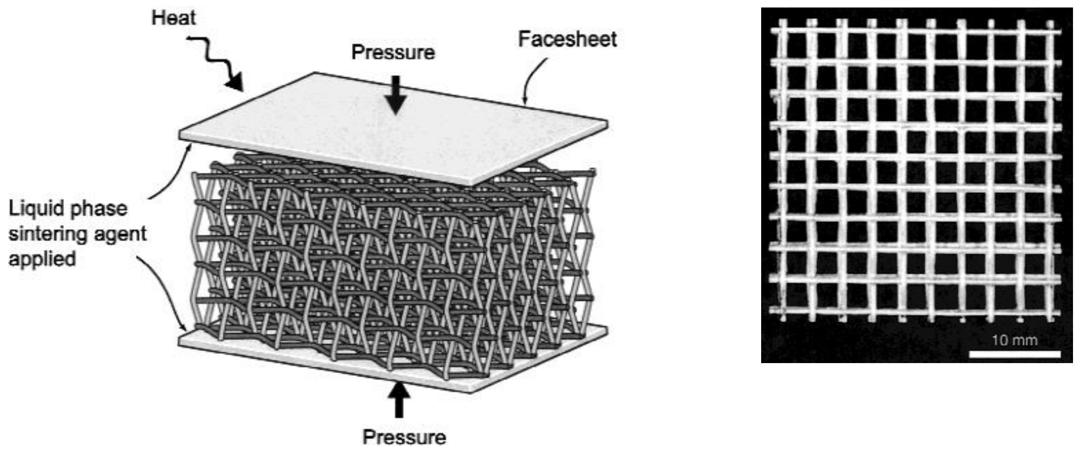

Figure 2.12. Woven metal textile and the resulting square metal textile lattices [44].

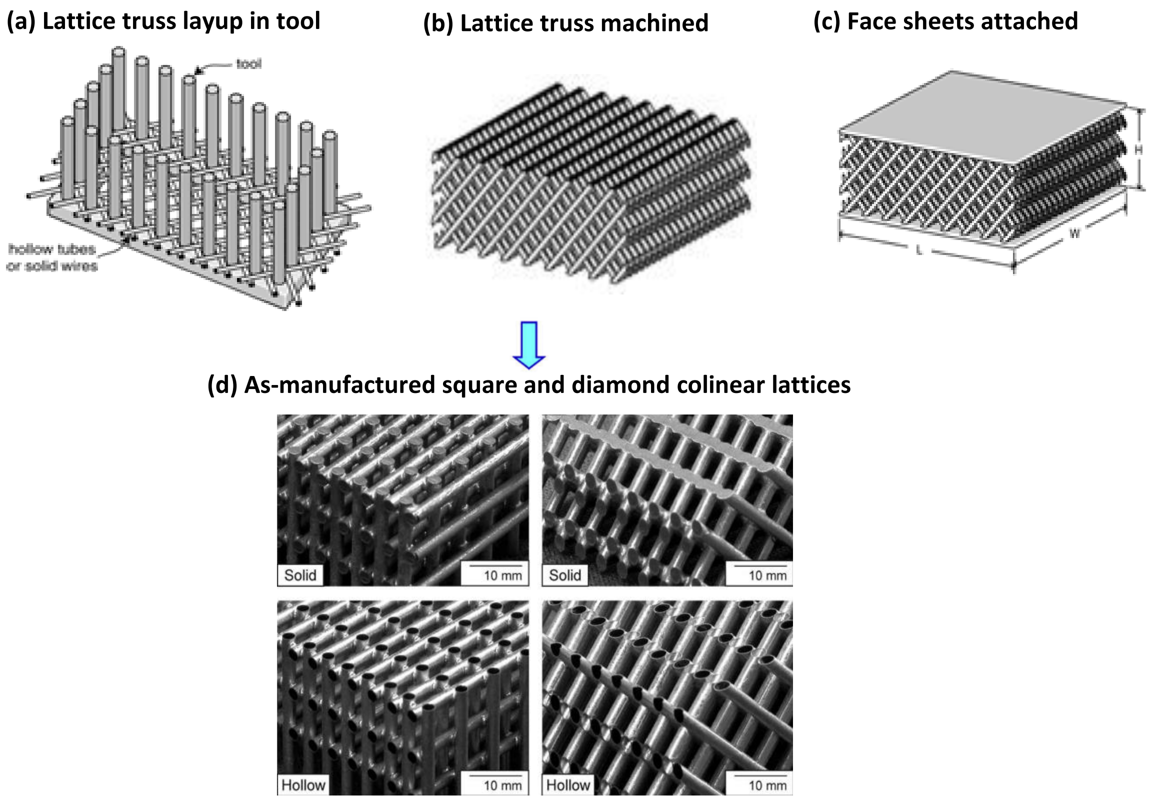

Figure 2.13. Non-woven metal textiles, solid and hollow micro truss [46].

Slot/snap-fitting method is another alternative method to manufacture metallic pyramidal and octet truss lattice truss [47-49]. First, continuous 2-D slot-fitting truss patterns were cut from the stacked metal alloy sheets using wire electro discharge machining or water jet. Then, these were cropped into the required dimension and slot-fitted into each other to build the successive truss core topology. Figure 2.14 illustrates the procedure to manufacture titanium/aluminium alloy octet-truss lattice structures [49]. In the above-mentioned conventional manufacturing techniques, strut size in the lattice structure tends to be large and so only a small number of cells are possible in the depth of the core. The emergence of additive manufacturing techniques made possible the fabrication of metallic lattice structures at the geometry of micrometre level with high complexity [50]. One of these techniques is selective laser melting (SLM). SLM is a layered manufacturing technology developed from selective laser sintering that uses a high-quality fibre laser to selectively melt a metal powder to produce a solid material [51,52]. An example of SLM process is shown in Figure 2.15. SLM can be used to manufacture lattice structures that were hitherto virtually impossible to manufacture. Gumruk and Mines [53] has investigated the mechanical static compression behaviour of 316L stainless steel micro-lattice materials manufactured using SLM method. Ullah et al. [54] analysed the performance of Ti-6Al- 4V Kagome truss core structures produced by SLM for composite sandwich structures.

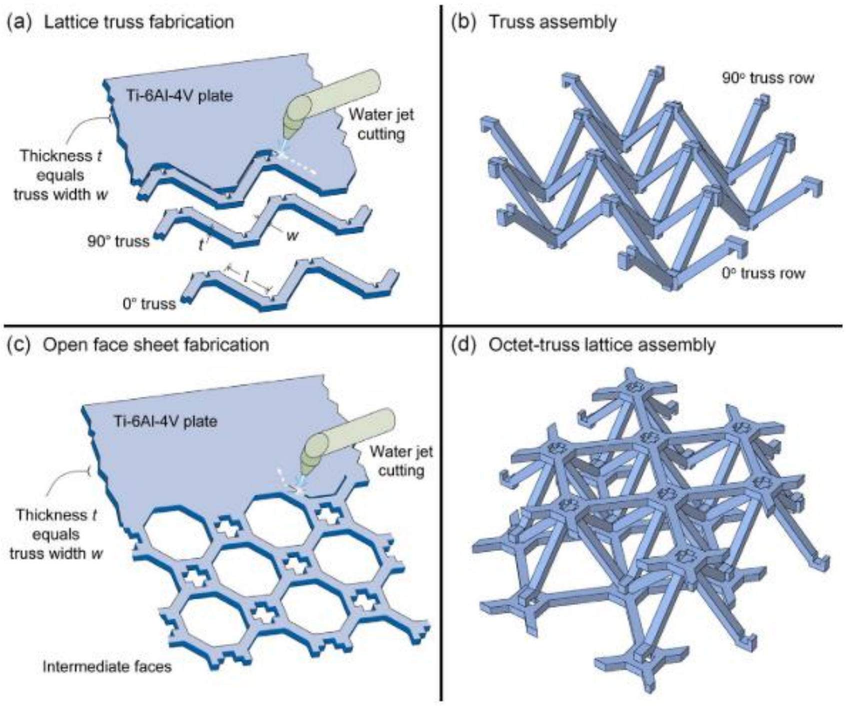

Figure 2.14. The schematic diagram of the slot fitting truss fabrication and assembly method for Ti–6Al–4V octet-truss lattice construction [49].

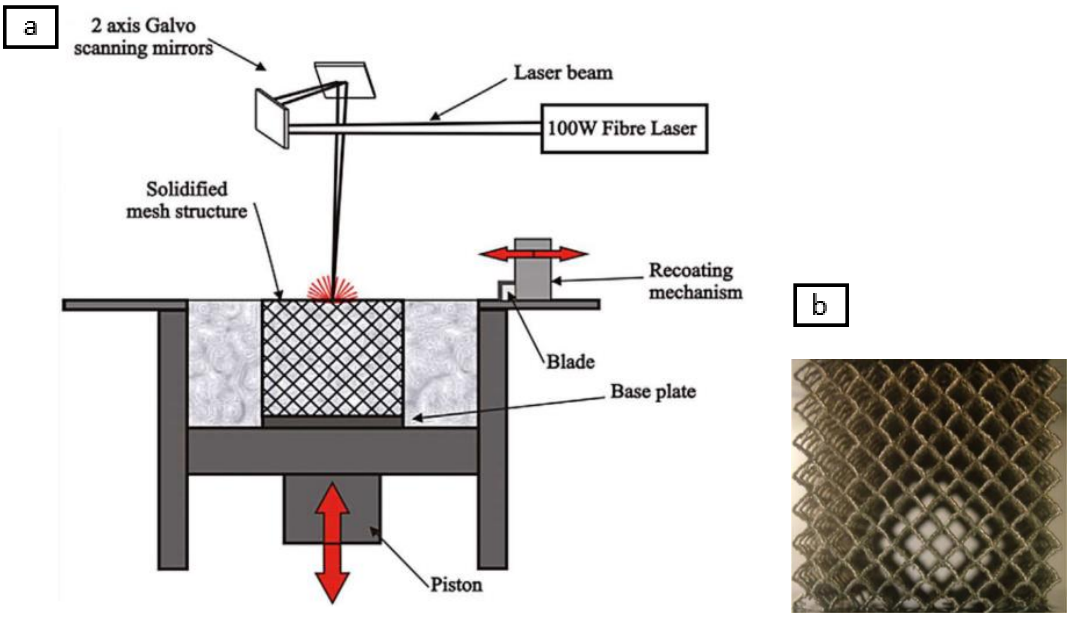

Figure 2.15. Schematic of the SLM process (b) as manufactured a stainless steel 316L micro-lattice (octahedral lattice known as BCC structures) [55-57].

It was elucidated that these metallic lattice structures had potential to occupy the low-density region of material property chart. It was also revealed that there is a gap to fill the space in the material property chart between existing lattice materials and the unattainable materials limit. As a result, optimized lattice topology and parent material properties can be combined to expand the space in the chart by creating new engineering materials. As such, composite lattice material has occupied the partial gap of material property chart at very low-density region and therefore, continuous development and improvements are needed to fill the space within material chart, as shown in Figure 2.16 [58]. Therefore, significant efforts were carried out on carbon fibre reinforced composite (CFRP) lattices as a candidate for cores of ultra-light sandwich structures. However, there remains a challenge to manufacture composite lattice truss sandwich structures. The fabrication technology of composite lattice core sandwich structure is known to influence the mechanical performance of the structures. In the next section, some of the proven manufacturing processes along with some latest fabrication route to manufacture composite lattice core sandwich structures will be discussed.

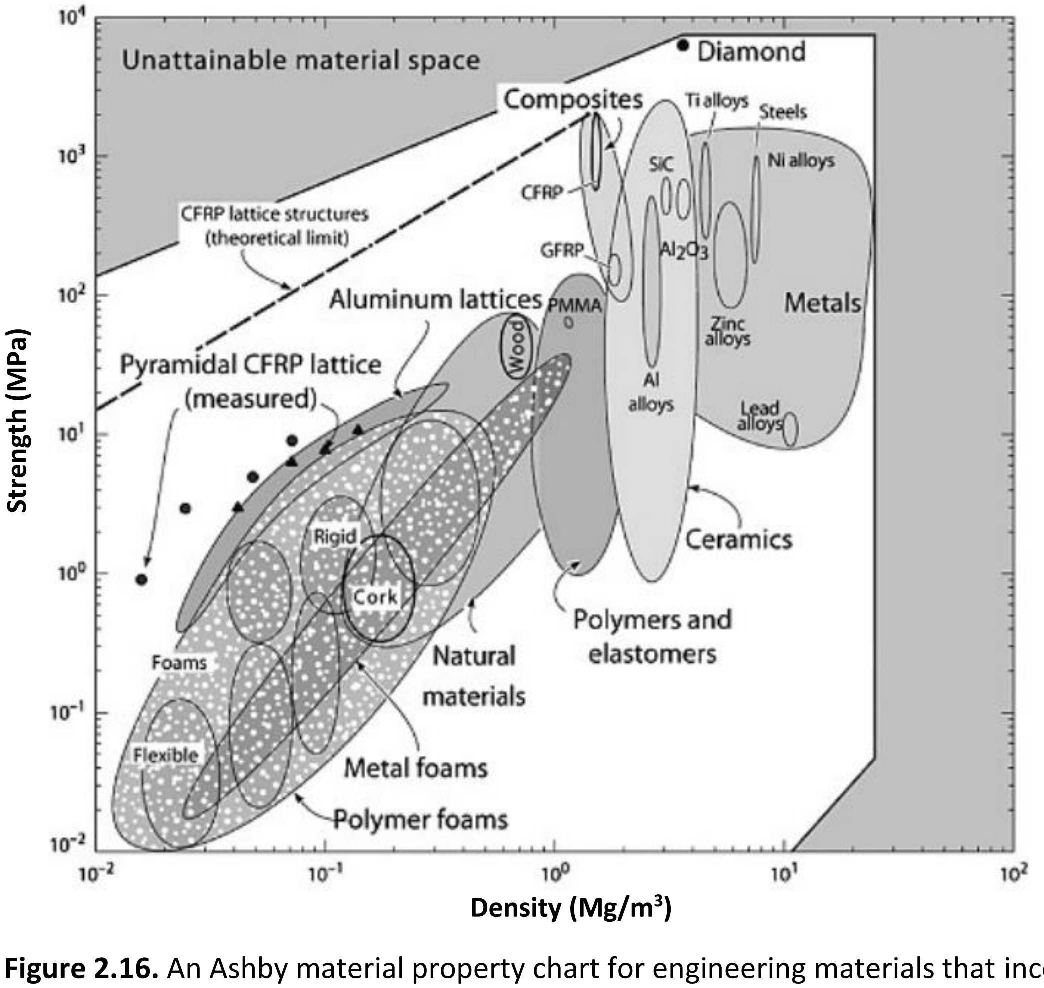

Figure 2.16. An Ashby material property chart for engineering materials that incorporated lattice materials [58].

2.3.2 Manufacturing composite lattice core sandwich structures

Composite lattices are hybrids of fibrous composites and optimized lattice topologies and thus, more efficient than their metallic counterparts due to high specific properties of the parent materials. These structures simultaneously enlarge the design space and fills the gap in material property chart. The applications of the composite lattice core sandwich structures can be realized if affordable manufacturing methods exits for deployment in many engineering applications. Fan et al. [59] has studied the feasibility of manufacturing of a composite lattice structure reinforced by continuos carbon fibres via two manufacturing routes, namely laminae assembly approach and intertwined/interlacing method. He found that an intertwining method was the best route to manufacture CFRP lattice core sandwich structure as it offered optimal specific properties and larger shear strength than that of stacking-assembled lattice structure. Intertwined lattice structure was manufactured from repeated process to weave fibres diagonally from the bottom hole to a hole on the upper plate until the desired configuration was achieved, followed with curing step in autoclave. Figure 2.17 shows the intertwining process to manufacture carbon fibre reinforced epoxy composite lattice core sandwich structures. In spite of this, it was reported that defects such as strut waviness and non-circular cross sections due to the manufacturing imperfections were noticeable [60]. However, the tested stiffness and strength were considerably higher than those of carbon foams and aluminum honeycombs with the same relative density.

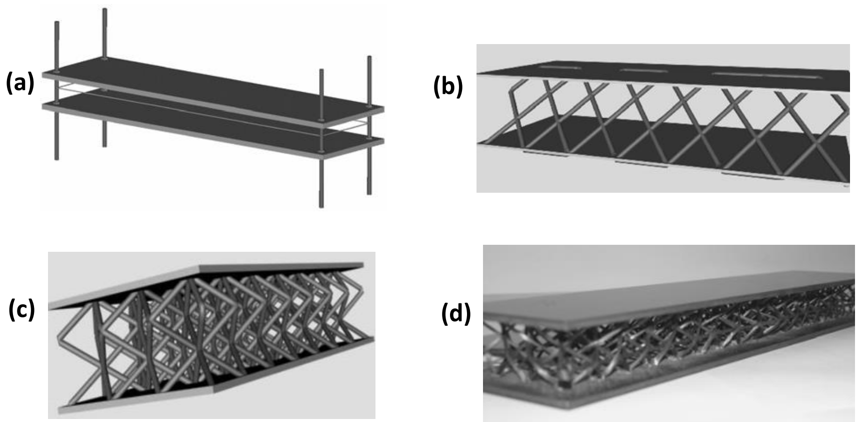

Figure 2.17. Intertwining/interlacing manufacturing approach (a) top and bottom plates positioned by nuts on four threaded columns; (b) construction of an inclined lattice lamina; (c) completed lattice structures; (d) as manufactured lattice sandwich structure [59,60].

A significant effort on manufacturing CFRP lattice core sandwich structures was made by Finnegan et al. [58], where composite pyramidal truss cores were manufactured by using water-jet cutting process in combination with the snap-fitted also known as slot-fitted method. Pyramidal truss sandwich cores with relative densities in the range 1 - 10% have been manufactured from carbon fibre reinforced polymer laminates using snap-fitting method, with their compression properties being studied. Initially, the truss patterns were cut from CFRP laminate sheets using water jet cutting process. Thereafter, these patterns were then snap-fitted into each other to produce a pyramidal truss. Finally, the pyramidal truss was bonded to composite face sheets using an adhesive bonding to form sandwich panel as depicted in Figure 2.18. George et al. [61] explored the same manufacturing route to manufacture CFRP pyramidal lattice truss structures and investigated the panels in-plane shear stiffness and strength. However, only half of the fibres are aligned in the direction of the truss struts and thus, the intrinsic strength of the fibre reinforced composite not fully exploited by the truss lattice structure. Yin et al. [62] also tried the similar fabrication concept in developing hierarchical composite pyramidal lattice cores with foam-core sandwich struts using two approaches, one is patterns cut from flat foam sandwich plate and another one is fabricating a corrugated foam sandwich plate with a specially designed steel mould followed by snap fitting method. It was reported that the former approach was more efficient than the latter approach from structural efficiencies viewpoint. Norouzi and Rostamiyan [63] also used this manufacturing route to manufacture CFRP lattice sandwich panels from laminate sheets that were manufactured with VARTM (Vacuum Assisted Resin Transfer Moulding) method to achieve a laminate without any fault. Furthermore, Dong and Wadley [64,65] explored the application of snap fitting method for fabricating octet-truss cellular materials from CFRP laminate materials with relative densities in the range 1.7 - 16%.

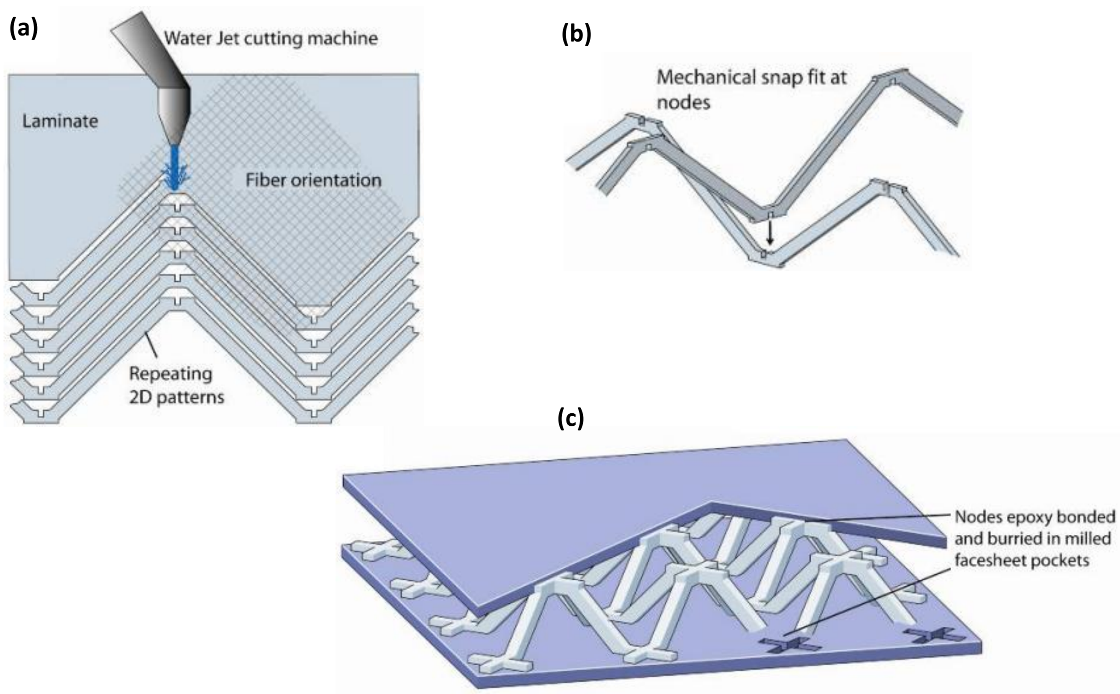

Figure 2.18. Illustration of the manufacturing route for making the composite pyramidal lattice core sandwich panels [58,61].

The remarkable work from Finnegan has initiated a rapid grow in the manufacturing of composite lattice core sandwich structures, particularly those made from CFRP. Another method which was used extensively to manufacture composite lattice core sandwich structures is hot-press moulding technique [66-69]. This technique can be carried out in two ways either with or without secondary bonding. Xiong et al. [66,67] exploited the fabrication of carbon fibre composite pyramidal lattice structures in two steps using hot press method to produce single and double-layer composite pyramidal core sandwich panels, respectively. The fabrication process involved many tooling approaches for moulding. Here, the fibre reinforced laps which were cut from prepreg sheets were inserted into the strut compaction areas to build the composite lattice truss structures. The composite was then cured in a hot press machine with predetermined conditions. Finally, the composite pyramidal cores were removed from the mould after solidification of the resin and then attached to the face sheets with adhesive bonding. Figure 2.19 illustrates the stages taken to produce lattice cores sandwich panels by hot press method. Sun and Gao [69] enhanced this process by introducing post-forming process with hot press method to increase the secondary adhesive area between face sheets and lattice cores.

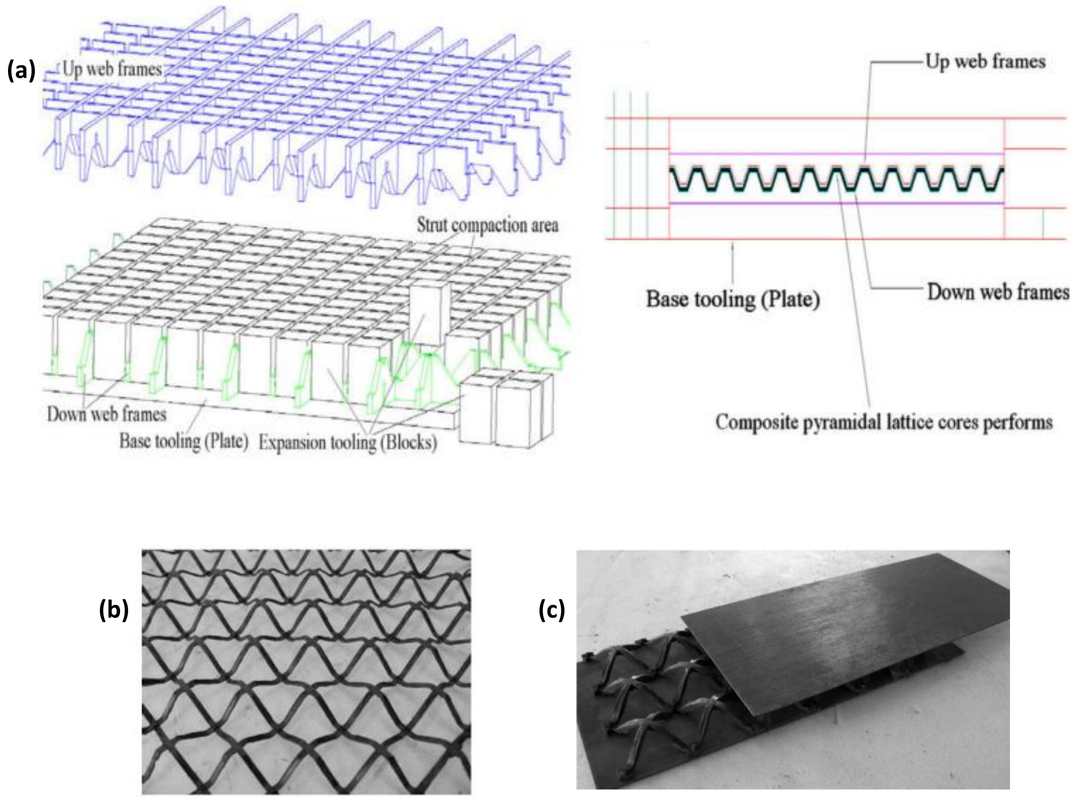

Figure 2.19. Hot press moulding (a) manufacturing mould with tooling blocks and frames (b) as manufactured CFRP pyramidal lattice core (c) sandwich panel [66].

Interestingly, there were also some efforts to manufacture all composite lattice core sandwich panels in one manufacturing process without secondary bonding [68, 70-73]. This was carried out by embedding the carbon prepregs into top and bottom face sheets to integrally connect them with cores. Wang et al. [70] and Li et al. [72] explored hot compression moulding method to fabricate composite pyramidal truss core sandwich structures using carbon/epoxy prepregs in one manufacturing route. A set of trapezoidal moulds with semicircular grooves were machined first. Then, the carbon/epoxy prepregs were cut into the required dimension. These prepregs were rolled into circular rods as truss member. In this manufacturing process, all the continuous fibres of composites are aligned in the direction of truss members. Therefore, the truss structure can fully exploit the intrinsic strength of the fibre-reinforced composite. Then, the composite struts were inserted into the holes of the moulds through the plies of predrilled prepreg. The ends of the struts were split into many parts and embedded gradually into the top and bottom face sheets. Additional plies of prepreg were laid on the prepreg laid earlier with desired stacking sequence. The face sheets were interconnected with pyramidal truss cores, and the face sheets and truss cores were fabricated in one manufacturing process without subsequent bonding. Finally, the preformed sandwich panels were cured in hot press conditions and followed by removal of moulds as shown in Figure 2.20. Similar approach was carried out by Wang et al. [74] and Liu et al. [75] to produce 2-D and 3-D composite pyramidal lattice truss sandwich panels.

Yin et al. [77,78] studied manufacturing concept to produce hollow composite pyramidal lattice core sandwich panels using thermal expansion molding, an approach like hot press method but the curing process conducted in an oven (autoclave). In their work it also reported the hybrid concept whereas to embed the hollow space with wood and rubber as cores to create hybrid lattice truss. Thereafter, Yin et al. [79] explored hierarchical composite lattice cores which were fabricated with a two-step approach using thermal expansion moulding technique. Xiong et al. [80] presented a novel method for fabricating carbon fibre composite near-pyramidal truss core sandwich panels by means of hot press method and electrical discharge machining (EDM). EDM process of precision cutting method was selected to convert corrugated core sandwich panel into truss core sandwich panel by enabling greater bonding area between core and face sheets. George et al. [81,82] provided an approach for fabricating carbon fibre reinforced composite (CFRC) pyramidal lattice structures from a braided carbon fibre net together with closed cell polymer foams to produce hybrid truss/foam core sandwich panels. This dry panel was stitched to CFRC faces using Kevlar fibre and then infused with resin by vacuum assisted resin transfer moulding (VARTM), as shown in Figure 2.21 [82].

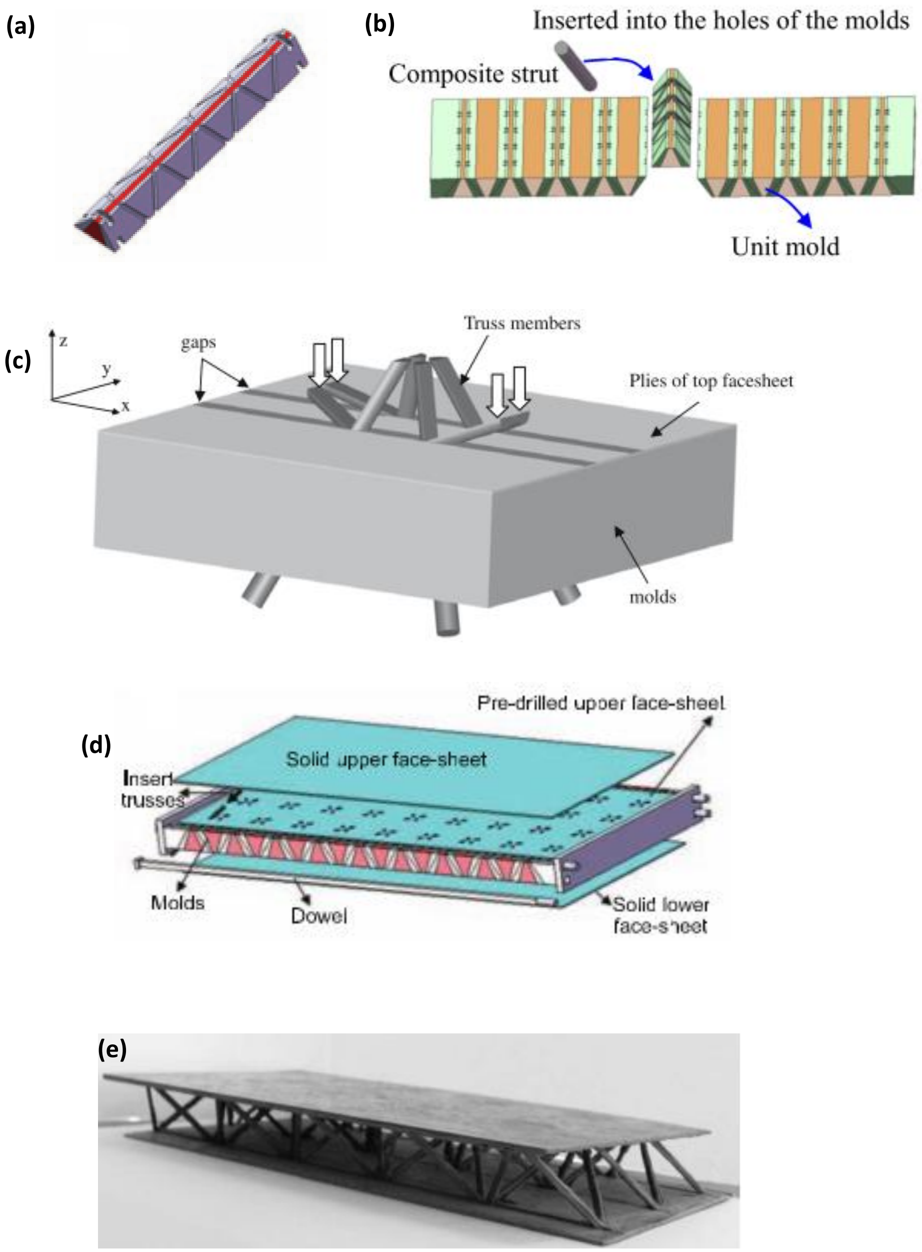

Figure 2.20. Hot press moulding in one manufacturing process (a) a piece of mould with unit cell; (b) composite prepreg rolled into circular rod inserted into mould assembly of mould with embedded carbon rods onto upper and bottom face sheets; (c) method for embedding truss members into face sheet; (d) assembly of mould with embedded carbon rods onto upper and bottom face sheets; (e) as-manufactured sandwich panel with pyramidal lattice truss [70,72,76].

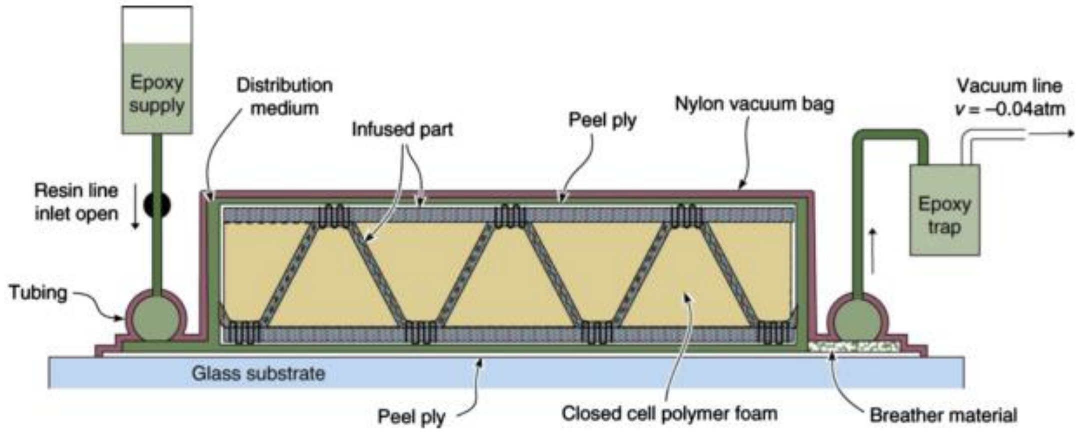

Figure 2.21. Schematic illustration of setup used for the vacuum assisted resin infusion process [82].

Furthermore, Kim et al. [83] and Song et al. [84] demonstrated techniques dealing with continuous fibre tow by means of fibre stitching to develop composite sandwich panel integrally woven with lattice truss cores. Figure 2.22 shows the process of this method by stitching of dry or prepreg yarn between two face sheets that separated from each other at a constant distance. By repeating the stitching pattern at regular intervals, a desired lattice topology could be constructed. Che et al. [85] manufactured an octahedral composite lattice core sandwich structure using stitching of carbon fibre towpreg and followed by vacuum bagging and autoclave curing. Meanwhile, Xu et al. [86] developed a new graded lattice core sandwich structure based on stitching and hot press method. It was stipulated that the stitching method has provided a good resistance against facesheet - core debonding of the composite lattice core sandwich structures given that only small area of cores contacted with the face sheets.

The composite lattice core sandwich structure construction discussed here provides a pathway to design lattice structures with increased density-specific performance and multifunctional characteristics by judicious selection of material and geometries. The construction concept is equally applicable to variety of lattice topologies. However, each of the conventional manufacturing methods explained in this section has its own limitations. Table 2.1 summarises limitations in the some of the existing techniques discussed here.

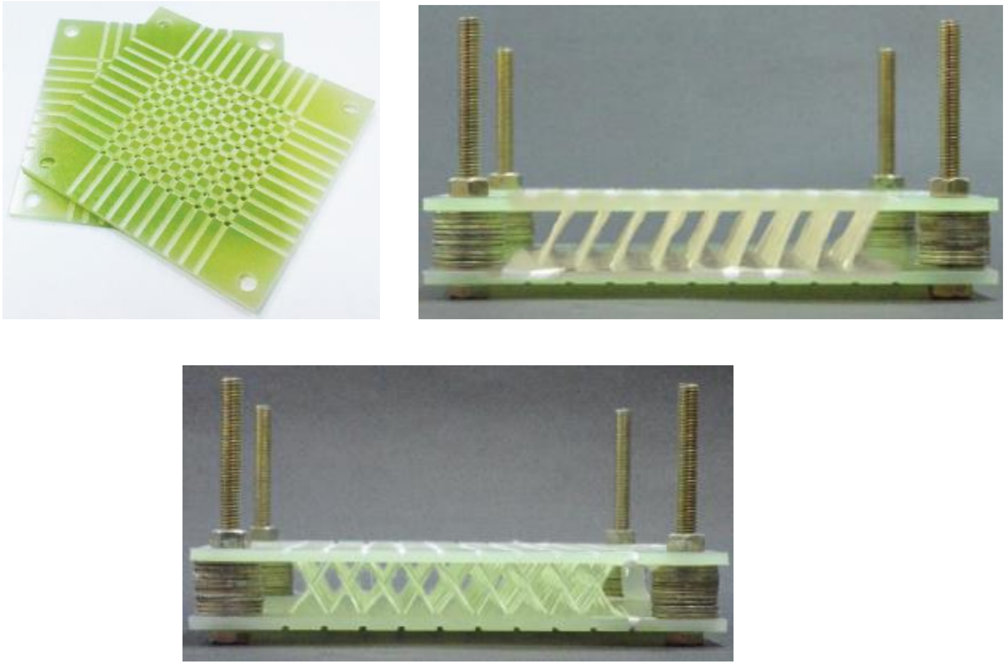

Figure 2.22. An example of stitching-based manufacturing approach [83].

Table 2.1. General limitations of some conventional fabrication techniques.

Fabrication Technique	Limitations
Intertwining method/ Sewing process [59-60, 83-84].	• The operation to form the lattice pattern is complicated and is not capable of manufacturing complex lattice structures patterns. • Defects such as strut waviness and non-circular cross sections due to the manufacturing imperfections.
Snap fitting method [59, 61-65].	• High-cost machining operation. • Heat generated during the machining operation that could lead to reduction of mechanical properties of the structure. • Not all fibers could be aligned with truss/struts direction, thus the intrinsic properties of the composite were not fully exploited by the structure. • Involves joining method that could weaken the lattice structure.
Hot compression molding [77-80].	• Complex mold design that leads to high precision machining operation, which makes the manufacturing expensive. • Complicated mold assembly consists of various blocks and dies. • Difficult to manufacture lattices with a complex topologies.

Up to now, it has proved that difficult to manufacture many optimized lattice structures due to their complexity and due to limitations in manufacturing method. Despite, all these manufacturing routes indicate that there still remains much room for improvements and developments of construction of composite lattice core sandwich structures. Therefore, a simple fabrication technique could afford an opportunity to design composite lattices with enhanced properties. Thus, new technique to manufacture pyramidal lattices that considered as near-ideal stretch-dominated structures is primary focus in this study.

2.4 Mechanical behaviour of the composite lattice core sandwich structures

The primary aim of most researches on the composite lattice core sandwich structures was to focus on the manufacturing methods and the subsequent objectives were to obtain mechanical responses of these structures for various mechanical loadings, i.e. compression, shear, bending and impacts. The following section describes the mechanical behaviour of composite lattice core sandwich structures under quasi-static compression and low velocity impact to help a better understanding of the mechanical performance of these structures.

2.4.1 Quasi-static compression properties

Fan et al. [59] manufactured 3-D intertwined pyramidal lattice structure with a relative density just 0.017 and tested in compression to determine the stiffness of the structure. It was reported that the stiffness and strength of the lattice structure were about 46 MPa and 0.77 MPa, respectively, exceeded that of carbon foams and honeycombs. It was also concluded that imperfections caused bending effects of the wavy struts and non-circular cross sections reduced the experimental values are about one magnitude lower than these predicted data. Fan et al. [87] also fabricated sandwich panels with Kagome lattice cores reinforced by carbon fibres using interlocked method. The author reported that the in-plane and out-of-plane compression tests reveal that the lattice grids are much stiffer and stronger than other cellular materials such as metallic lattices and carbon foams. The failure modes under out-of plane compression were attributed by delaminating, buckling and shearing. In contrast, two different failure modes were detected under in-plane compression tests such as buckling and debonding [87]. Subsequently, Fan et al. [88] manufactured a more softer CFRC Kagome lattices with thinner skins which resulted in relative density of the grid core was just 0.043, a half of the Kagome lattice made by Fan et al. [87]. In his work, more compliant skins were designed to restrict the debonding failure as revealed by Fan et al. [87] in his previous research.

Due to superior mechanical performance of the composite lattice structures compared to that of other cellular structures, it has exhibited potential applications as cores in sandwich structures. Table 2.1 lists the compressive properties, particularly their out-of-plane (flatwise) compression tests results for some of as manufactured composite lattice core sandwich structures. The composite lattice core sandwich structures responses to compressive loading with initial linear stage, usually less than 2-3% of strain values followed by nonlinear region due to progressive failure of struts made up the lattice cores. Finnegan et al. [58] conducted compression tests on pyramidal sandwich core specimens that were bonded to the platens of the test machine to prevent the relative sliding of the two face-sheets. Two designs of pyramidal core were investigated that varied in node design with the design 1 comprising of significantly smaller nodes compared to the design 2. The measured compressive nominal stress versus strain curves of these specimens and the resulting failure modes were shown in Figure 2.23. The significant nonlinear behaviour prior to attainment of the peak stress suggested that strut delamination is the failure mode rather than microbuckling in most of the tests.

Wu et al. [90] manufactured composite pyramidal lattice truss core sandwich structure with improvement between core and face sheets connection. In his work, the lattice core is integrally strengthened by using aluminium frames between the core and face sheets in which by strengthened the design using top and bottom aluminium connectors. By this method, the bonding strength between the core and face sheets were effectively enhanced by increasing the bonding area between the aluminium connectors and the face-sheets. Interestingly, the authors manufactured the lattice core in way which all of the continuous fibres were aligned in the truss direction, so that it could fully exploit the intrinsic strength of the fibre reinforced composites in contrast to the work done by Finnegan in which only half the fibres were aligned with the load. As a result of this, compression strength of the composite lattice truss core in his work was superior to all of the other composite lattice truss cores with low relative densities [90], particularly it was enhanced by 27% higher than that as compared to Finnegan et al. [58].

Table 2.2. Compression properties of the composite lattices

Fabrication Method	Lattice Type	Relative Density (%)	Strength (MPa)	Modulus (MPa)
Interlocked method [88]	Kagome	4.30	5.63	115.47
Snap fitting method [58]	Pyramidal	1	0.70	90
		2	3.10	185
		3	4.00	225
		5	5.90	295
		7	8.10	300
		10	11.60	420
Hot press method (O*) [70]	Pyramidal	1.20	0.84	25.10
Hot press method (T**) [66]	Pyramidal	1.25	0.31	45.80
		1.81	3.17	70.30
		4.70	6.18	241.50
Thermal expansion molding [77]	Pyramidal (H***)	1.07	0.60	35.70
		2.21	1.91	72
		4.53	4.68	160
Hot press method (O) [72]	Pyramidal	2.24	2.62	280.80
Thermal expansion molding [89]	Tetrahedral	3.45	4.60	320.30
Hot press method (T) [69]	Pyramidal	2.72	4.83	125.75
Hot press method (O) and stitching [85]	Octahedral	0.75	0.33	45.83
		1.41	1.14	69.46
		2.26	2.57	129.85
Snap fitting method [64]	Octet	1.70	0.73	75
		5.40	4.39	295
		9.40	7.98	556
		13	9.90	753
		15.90	11.39	983

Notes: *O refers to one step manufacturing process; **T refers to two step manufacturing process; ***H refers to hollow truss

On the other hand, Gao et al. [69, 91] used cross bars to manufacture a strengthened pyramidal truss core. It was shown that the introduction of cross bars to the node design has significantly improved mechanical performance of the structure [69]. They further improved the cross bars applications by using interlacing laminate form to substitute the original non-weave laminate one as demonstrated in Figure 2.24. It was found that the new interlacing laminate form of the adjacent nodes greatly improves the integrity between cores and cross bars, taking full advantage of the cross-bars to suppress the growth of the local failure. It was noticed an improved performance in compression modulus with 7 % increase and only slim increases in compression st rength [91].

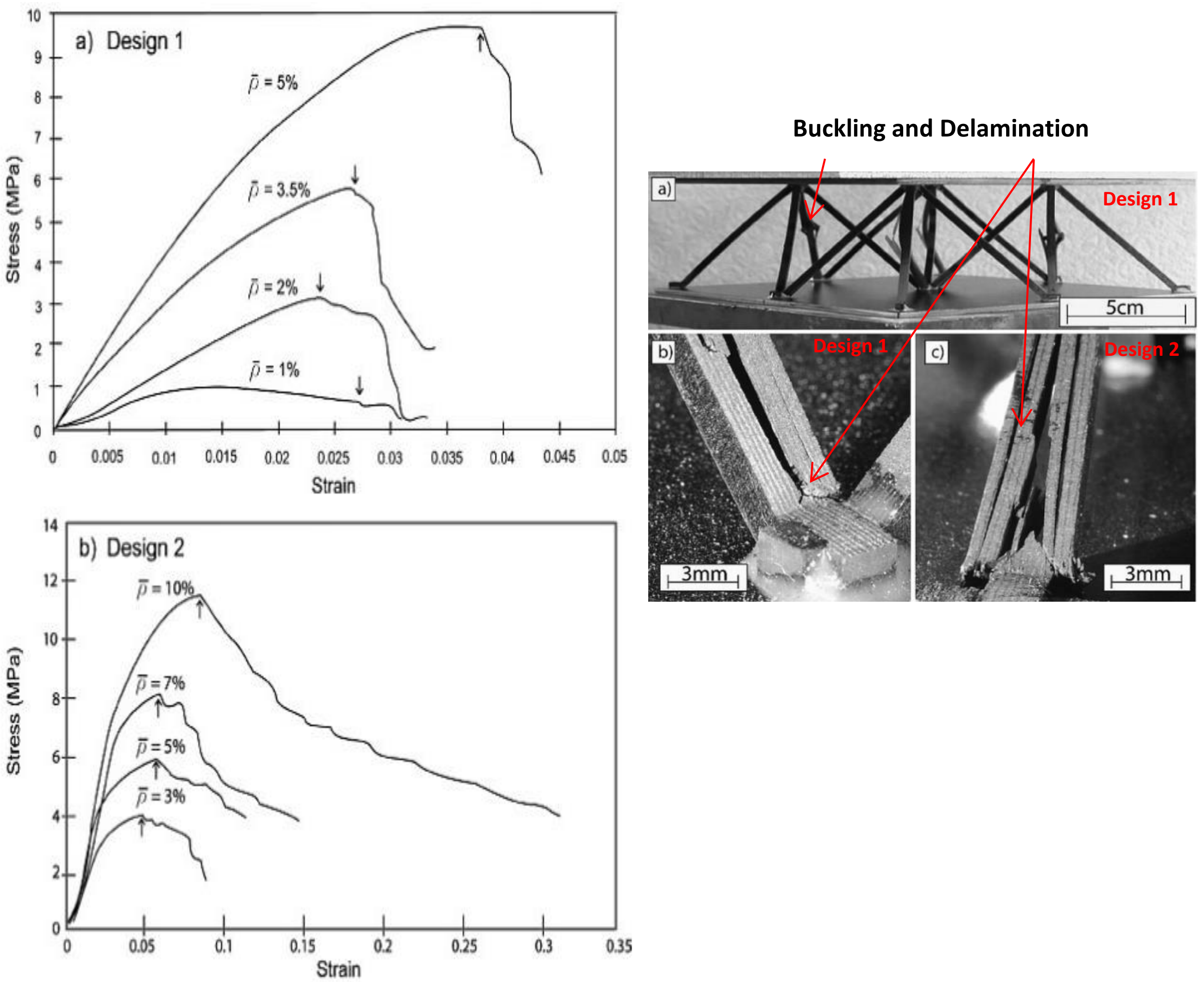

Figure 2.23. Compressive stress-strain response of pyramidal truss cores and their failure mechanisms [58].

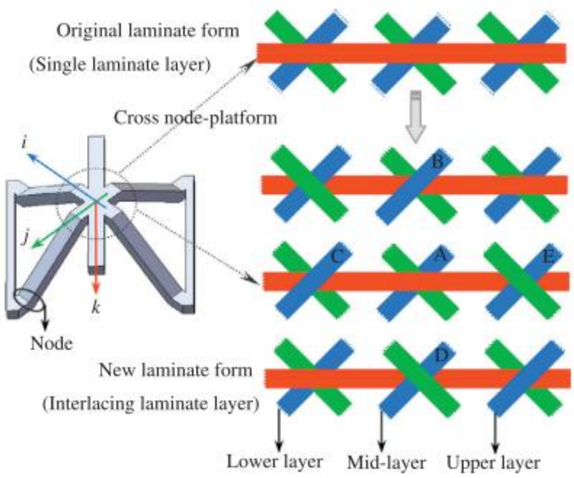

Figure 2.24. Improved laminate form of pyramidal truss cores [91].

Liu et al. [71, 75, 92] conducted investigations mainly on thermal effects on mechanical behaviour of carbon fibre composite truss core sandwich structures and found that thermal exposure temperature and time were the important factors affecting the failure of sandwich panels. They were also found that the decrease in compressive modulus and strength was mainly attributed to the degradation of the matrix and fibre–matrix interface properties, as well as the formation of delamination when specimens were exposed to higher temperatures around 300 °C. Mei et al. [93] in his research presented a novel hot-press mould technology to fabricate composite sandwich panel with tetrahedral truss cores. The out-of-plane compression showed that the tetrahedral truss core sandwich panels had a distinct superiority in compressive specific strength and observed node failure as a main failure mode. Interestingly, Hu et al. [94] found out that a corrugated carbon fibre composite lattice truss sandwich panel which was manufactured through mould pressing method had advantages compared with previous lattice truss composites. By their fabrication method, co-curing process ensured a strong adhesive strength, while mould pressing improved the volume fraction of the carbon fibre in the lattice structure, hence assured the strut strength. Importantly, the corrugation design enlarged the node area and improved the shear strength notably [94]. They also highlighted that strut fracture and strut buckling are the potential failure modes in compression.

There are also some investigations carried out on the role of defects in mechanical behaviour of the composite lattice core sandwich panels. Chen et al. [95] investigated the effect of defects on the mechanical performance of carbon fibre composite lattice structures and found that the struts were the main components carrying external loads. Owing to the effect of defect in which introduced by missing strut, the compressive stiffness and strength of sandwich panel decreased linearly with the fraction of missing members. Wallach and Gibson [96] and Wang and McDowell [97] obtained the similar trends of stiffness and strength with the increasing of moving cell walls in the investigation on truss and honeycomb structure by experiments, respectively. Fan et al. [60] mentioned that imperfections, such as waviness of struts and non-circular cross-sections of the 3-D lattice material and cantilever ribs of the 2-D lattice grid had degraded their mechanical performance. Biagi and Smith [39] investigated the presence of the unbound nodes between the core and face sheets and highlighted the impact of the spatial configurations of these imperfect nodes. Using the effects of the spatial configuration, the upper and lower limits on stiffness and strength were determined based on unbound node connectivity and edge node constraints for compression and shear loadings. Fan et al. [98] investigated the edge effects of composite lattice structures using the finite element method. It was concluded that the equivalent specific stiffness is greatly influenced by the strengthened edges because strengthened edges keep the deformation mechanism of the stretching dominated strut of lattices unchanged.

The literature review above highlighted many ways to improve mechanical performances of the lattice core sandwich structures mainly by some novel fabrication technologies, use of strengthening methods, optimization of lattice truss topologies and use of composite materials. The reviews here mainly showcased the mechanical responses of the carbon fibre reinforced composite lattice truss sandwich panels. However, the research has also advanced for utilizing natural fibre reinforced composite lattice. Xu et al. [99] studied the performance of flax fibre-reinforced lattice cores which were manufactured by vacuum-assisted resin infusion and slot assembly method. The flax fibre-reinforced composite lattice structures were found to be superior to several metallic lattice structures, foam filled corrugated materials, and competitive with Nomex honeycombs. Moreover, the flax fibre-reinforced lattice structures can fill low-cost gaps in the property-cost chart, although their mechanical properties are not comparable with carbon fibre-reinforced counterparts as illustrated in Figure 2.25. In between these, Hou et al. [100] recently presented novel integrated manufacturing process based on continuous fibre reinforced thermoplastic composites 3D printing of continuous fibre reinforced composite lightweight structures. It was showed that a compression strength of 17.17 MPa was obtained for corrugated structure with only 11.5% fibre content. Moreover, this new and improved process has a great potential for fabricating carbon fibre composite lattice cores with complex shapes, high mechanical properties, and multifunctional benefits. Although use of materials for lattice structures was varied from metals to fibre-reinforced composites of synthetic and natural fibre, the research on carbon fibre composite lattice cores still perceive much attention till to date owing to its superior specific properties and engineering applications.

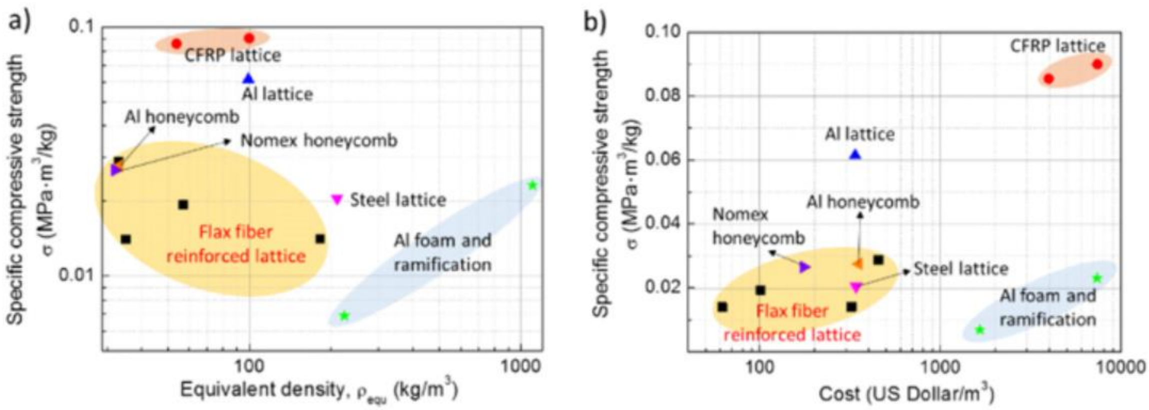

Figure 2.25. Flax lattice, CFRP lattice and other structure and their cost per volume [99].

2.4.2 Energy absorption

There are few studies which focused on lattice cores sandwich panels in evaluating the energy absorption capacity of the resultant panels. These were motivated due to the fact that struts member of lattice core sandwich panels deforms by stretching as oppose to stochastic foams that tends to deform by cell walls bending. Generally, it is well known that stochastic foams such as metallic and polymeric foams possess excellent energy absorption capabilities. Lattice truss core structures offer several other practical advantages. Since lattice core sandwich panes have shown potential as lightweight structures in structural applications to mitigate impact loadings, it is important to understand energy absorbed by these structures.

Yin et al. [77,78] presented investigation on pyramidal composite lattice structures with hollow truss and studied the influence incorporated core materials such as wood and silicone rubber into the hollow trusses in his latter study. He postulated that the specific energy absorption capacity of hollow truss composite lattice structures surpassed that of both hybrid truss and hollow truss metallic lattice structures. Figure 2.26 shows energy absorption values of studied structures in his works. Xiong et al. [67] estimated the energy absorption of two-layer pyramidal lattice core sandwich panels. The compression curves reveal long deformation plateaus suggesting that multi-layered sandwich panels as good energy absorbing materials. The authors reported that specific energy absorption of two-layer composite pyramidal lattice core sandwich panel is about 6.06 kJ/kg for the panel with 2.27 % relative density.

Zhang et al. [48] conducted a study on energy absorption response of polyurethane (PU) foam filled pyramidal lattice core sandwich panels. They suggested that the energy absorption of foam filled sandwich panels owning lower relative density (1.83%)

lattice cores is insignificant to that of the unfilled specimens compared to that of lattice cores with higher relative densities (2.58% and 3.17%) [48]. Alternatively, George et al. [82] carried out the work on carbon fibre composite sandwich panels with hybrid foam filled composite pyramidal lattice cores. The panels were assembled from a carbon fibre braided net, 3D woven face sheets and various polymeric foams (PU, polyvinylchloride (PVC) Divinycell and synfoam) and infused with resin through VARTM process. The authors suggested that energy absorption capacity significantly exceeded those of the materials from which they were fabricated. They compare favourably with other lightweight energy absorbing materials and structures, as shown in Figure 2.27.

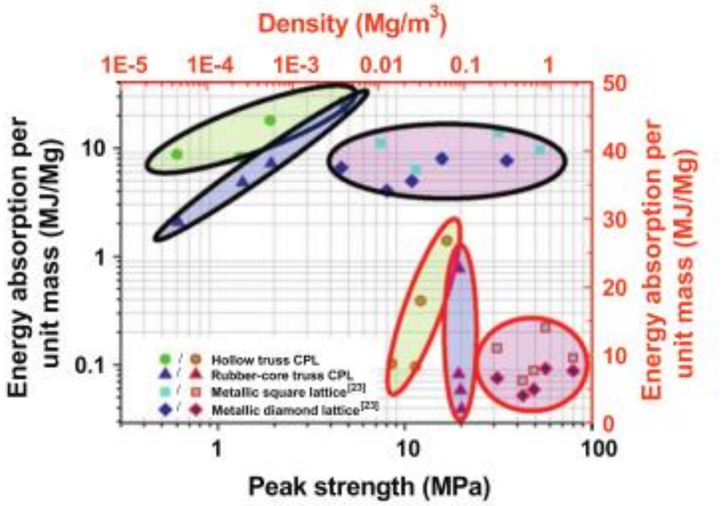

Figure 2.26. Specific energy absorption with respect to peak strength [77,78].

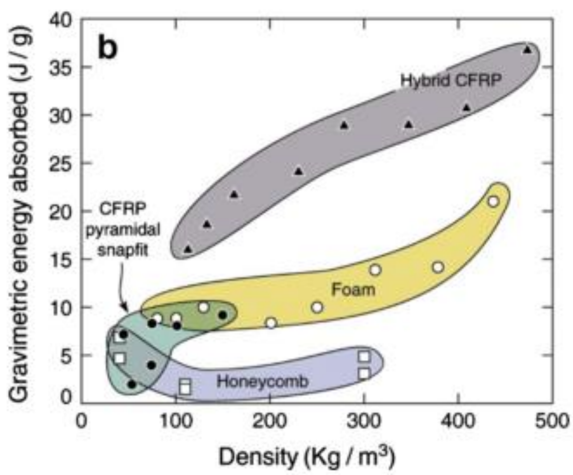

Figure 2.27. Comparable specific energy absorption for low density cellular materials [82].

2.4.3 Low velocity impact responses

On another aspect, composite sandwich structures are susceptible to impact damage due to the nature of brittleness which may severely decrease the structural stiffness, stability and load-carrying capacity [101,102]. Therefore, the behaviour and responses of these sandwich panels must be investigated under the expected in-service loading conditions. As such, one common loading scenario for sandwich structures used in the automotive, aerospace, marine and recreational equipment industries is an impact on one of the sandwich facesheets. Relatively, one major performance issues with sandwich structures is their foreign object impact performances such as tools drop, hail, runaway debris and bird strike. Although the induced damage may be barely visible, especially for low velocity impacts, the strength and reliability of the structure could be severely affected. Cantwell and Morton [103] categorised impact conditions either low or high velocity incidents by considered test techniques. The low velocity impact is generally simulated using a falling weight or a swinging pendulum, while high velocity impact using a gas gun or some other ballistic launcher. Impact can give rise to sub critical damage, or partial and full penetration [10]. It was also postulated that sandwich structures can offer excellent damage tolerance if the core is properly designed. In this section we will review some of the investigations undertaken on low velocity impact responses of the lattice core sandwich structures mainly on composite lattice core sandwich panels, also some other lattice materials for comparisons and offering ideas.

Vaidya et al. [104] reported low velocity impact response of three-dimensional multifunctional sandwich composites with hollow core (E-glass woven lattices) and a polyurethane (PUR) foam filled core. The impact tests were conducted using drop-weight impact machine with an instrumented striker with impact energies ranging from 5 to 73 J. It was concluded that the mode of failure of the unfoamed specimens was primarily the buckling of the core piles and the rupture of the facesheets, whilst for the foamed specimens, the foam core crushing along with the core piles failure were the primary modes of failure. The foam filled specimens could withstand the energies up to 70 J with a complete punch through for 73 J of impact energy. Low velocity impact test was performed and explained by Wang et al. [105] on carbon fibre composite lattice core sandwich structures to study the panel impact characteristics using experimental and numerical methods. An instrumented drop-weight machine was used for impact tests on sandwich panels with lattice columns, which were conducted on two locations, i.e. 1) at the centre of four columns and 2) at a fibre column. It was reported that no visible damage was found in former situation, while new damage mode was observed for latter location namely “band mode” damage mode under the same impact energy. The finite element simulation using Abaqus/Explicit with user subroutine

(VUMAT) was used to analyse the low velocity impact and it was found that the numerical predictions coincide well with experimental results.

Furthermore, the residual tensile strength of carbon fibre composite lattice core sandwich structures after low velocity impact test was investigated by numerical and experimental methods [106]. Initially, lattice core sandwich structure samples were impacted with 6.17 kg impactor using drop tower machine with different energies by adjusting the drop height. After the impact test the specimens were cut for tensile tests for acquiring tensile properties after the impact events. Impact force and residual tensile strength of carbon fibre composite lattice core sandwich structures were predicted well by the finite element explicit model. A user subroutine was produced to enhance the damage simulation which includes Hashin and Yeh failure criteria. According to the FE analysis results, degradation of residual tensile strength in sandwich structures can be divided to three stages, such as lower impact energy degradation stage, plateau stage and higher impact energy degradation stage. Xiong et al. [67] reported penetration impact testing of two-layer composite pyramidal core sandwich panels using a guided drop-weight impact rig. Three nominal impact energies were selected to cause partial damage to the samples such as 20, 40 and 60 J to impact at the centre of the specimen. The damage caused by the low velocity impact was mainly crushing of pyramidal truss cores with low relative density. On the other hand, for medium and high relative densities two-layer panels the impact damage included tearing of facesheets, debonding, fracturing and delamination of pyramidal truss cores. The results provided insight into the mechanical behaviour of multi-layer composite cores under low velocity concentrated impact.

The response of sandwich structures with pyramidal truss core consisting of carbon fibre reinforced polymer facesheets and aluminium alloy cores were also studied and tested in low velocity impact tests [107]. The tests were carried out to investigate the damage resistance of such structures. It was reported that the failure of matrix cracking, fibre breakage, delamination of CFRP facesheets and buckling of truss members occurred in impact test and the extent of damage was significantly affected by the impact location either at nodes or middle point of the four adjacent nodes. The samples suffered more serious damage when the impact locations were among the nodes. Subsequently, Zhang et al. [47] presented a combined experimental and numerical study to assess the effects of impact energy, impact location and core density on the compression-after-impact (CAI) strength of pyramidal truss core sandwich structures. The degree of CAI strength reduction is found to be closely related to the impact location. Under the same impact energy (5 J), the CAI strength of specimens impacted on the middle point of four adjacent nodes drops by as much as 25%, while the CAI strength only drops by 7% for the specimens impacted on the node. Moreover, it was found that the CAI strength of specimens impacted on the node decreases with the impact energy increase. In parallel, the failure modes in the simulation based on the ABAQUS are in a good agreement with the experiments.

There was also an attempt to study the low velocity impact responses of all-composite pyramidal truss core sandwich panel after high temperature exposure [76]. The results indicate that the high temperature exposure has a significant effect on impact properties and damage mechanisms of specimens. The fibre fracture, node failure, delamination and buckling were observed during low velocity impact tests and the extent of damage area was significantly affected by exposure to high temperature. In addition, the absorbed energy increased with increasing exposure to temperature, while the maximum impact force and compressive failure load after impact decreased with increasing exposure to temperature due to the degradation of the matrix properties and fibre–matrix interface properties at higher temperatures. This has provided insight into for the designers to understand the mechanisms involved in the low velocity impact event on lattice core sandwich panels and therefore help design impact-resistant lightweight structures.

2.5 Numerical simulation of lattice core-based sandwich structures

Computational modelling and simulation are among the most significant developments in the practice of scientific research [108]. In the past, the finite element (FE) method has become the prevalent technique used for analysing physical phenomena in the field of structural, solid and fluid mechanics as well as for the solution of field problems [109]. The accuracy and practicality of FE method are dependent on the governing theories, model complexity, mesh refinement, user's skills (in the representation of the geometric structures, material properties, boundary conditions and loads), and a given computer's memory capacity, speed and precision [110]. On the other hand, dealing with extensive experimental tests on cellular structures can be an extremely time-consuming process and sometimes could be very expensive. FE simulations, if correctly formulated and properly validated, help to greatly reduce the amount of laboratory tests required to characterise the response of a cellular structure subjected to various loading conditions [52]. FE analysis can also offer the detailed stress-strain distributions in the structures, which are difficult to measure experimentally and are useful in the optimisation of the structures. Recently, several modelling approaches has been developed using the FE method that attempts to capture the response of the lattice core sandwich structures.

The dynamic out-of-plane compressive responses of stainless steel corrugated and Y-frame sandwich cores were investigated for impact velocities ranging from quasi-static values to 200 ms^{-1} by Tilbrook et al. [111]. Two-dimensional FE simulations were performed using the explicit time integration version of the commercially available FE code ABAQUS/Explicit, in which the geometries were modelled using four-noded plane strain quadrilateral elements (CPE4R) with reduced integration. A mesh with approximately square elements of size $t/8$, where t is the web-thickness, was employed in all calculations that obtained from mesh sensitivity studies. The geometric imperfections in the form of the first static eigenmode of elastic buckling were introduced in the FE geometries of the corrugated and Y-frame cores and no material imperfections were considered in the analysis. Two types of simulations were performed namely impact simulations and constant velocity compression of the core. It was found that The FE predictions of both the deformation modes and stress versus strain histories are in a good agreement throughout the collapse response over the range of impact velocities investigated.

An effective single layer computational model was implemented in FE simulations by Liu et al. [112] to predict the structural behaviour of cellular sandwich structures having 2D prismatic or 3D truss cores. Three different types of cellular core topology were considered, i.e. pyramidal truss core (3D), Kagome truss core (3D) and corrugated core (2D) that made from steel. An effective single-layer model used one single displacement expansion through the entire thickness of the multilayer structure, unlike multilayer theories which deal with the principal layers of the sandwich structures separately. Even though multilayer theories can provide more accurate predictions on the behaviours of sandwich structures, they are more difficult to be implemented, since many independent field variables are involved. The ANSYS finite element code was used for the simulations and an 8-node layered plate/shell element, denoted as Shell91 in the commercially available ANSYS code, was employed to examine the applicability of the effectiveness of the single layer model. The FE analysis found that the single layered computational model has given acceptable predictions for both the static and dynamic behaviours of orthotropic truss core sandwich panels. Velea et al. [113] also presented numerical simulations of the mechanical behaviour of various periodic cellular cores (honeycomb, corrugated, pyramidal lattice truss and ExpaAsym) for sandwich panels using ABAQUS/Standard software.

On the other hand, there were also attempts to use FE simulations to present the response of metallic lattice core sandwich panels for different loading conditions. Wadley et al. [40] has modelled the compressive response of multi-layered pyramidal lattices during underwater shock loading using the FE code ABAQUS. The compression and shear responses of the stainless steel pyramidal and X-type lattice core sandwich structures were performed in the FE simulation using ABAQUS code by Zhang et al.

[114,115]. St-Pierre et al. [116] used the finite element method to simulate the compressive response of a pyramidal lattice made from tubes (*t/d = 0.1*) or solid struts (*t/d = 0.5*), both with an inclination angle, *x* =55°. Both annealed and carburised stainless steels were modelled as rate-independent, elastic-plastic solids in accordance with J2-flow theory and analysed using implicit solver within the FE code Abaqus. The simulations suggested that surface carburisation can significantly enhance the strength of lattice materials, and this combination has the potential to expand the current material space. Some researchers also highlighted numerical modelling of microlattice structures [52, 117, 118].

FE simulations have also been successfully used for the analysis and design of composite lattice core sandwich structures. Wang et al. [106] used ABAQUS/Explicit to simulate low velocity impact characteristics and predicted residual tensile strength of carbon fibre composite lattice core sandwich structures. A user-defined material subroutine (VUMAT) was created in the modelling to simulate the damage of carbon fibre composite lattice sandwich structures (facesheets and fibre columns lattice core) under impact load. The sandwich plate was modelled as a rectangular plate and clamped at its top and bottom circumferential edges to simulate the clamped condition that used in experimental method as illustrated in Figure 2.28. In his modelling, fibre columns core was assumed to be perfectly bonding with facesheets in FE model. It was found that the FE result coincides well with experimental data for the contact forces and the onset of the damage. Despite some differences existed between FE results and experimental data, the authors conclude that the FE programme developed can effectively be used in simulation of low-velocity impact events for carbon fibre composite lattice core sandwich structures.

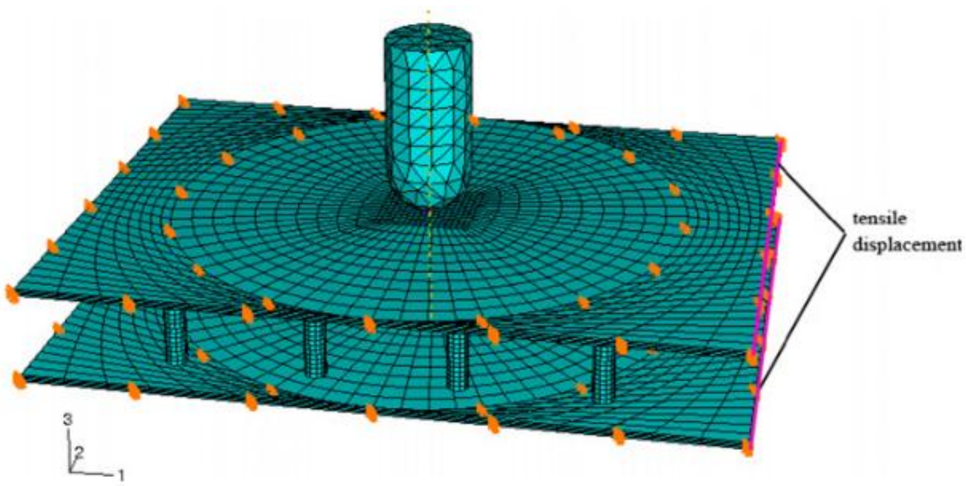

Figure 2.28. Representative of FE model of carbon fibre columns truss core sandwich panel with rigid impactor [106].

Li et al. [119] showed that node strength is the key of improving the failure load by studying the relationship between the failure mechanism maps and material mechanical properties of all-composite sandwich column with pyramidal truss core. He conducted numerical simulations to obtain failure loads and failure modes that were compared with those derived from analytical predictions and validated against the experimental measurements. Numerical simulations of the sandwich column loaded in end compression were conducted using an implicit element code ABAQUS/Standard. Two types of models were developed in this simulation, namely equivalent model and actual model. The facesheets of the sandwich column were modelled as single layer homogeneous shells for equivalent model and as composite laminate shells for actual model, respectively. Meanwhile the composite truss was treated as isotropic elastic material. It was concluded that the simulated results were in a good agreement with predicted ones. Torsional effects of carbon fibre composite pyramidal core sandwich plates were also simulated by Li et al. [120] using two types of FE models which were an equivalent material properties model and an actual geometry model. The authors pointed out that these two types of finite element models connect the analytical predictions with the experimental results like a bridge.

Sadighi and Hosseini [121] showed that the FE simulation could be used instead of time-consuming experimental procedures to study the effect of different parameters on mechanical properties of the 3D woven lattice sandwich composites. A 3D finite element model was constructed to predict the mechanical behaviour of 3D woven glass fibre sandwich composites under different mechanical loads using CATIA programme. It was concluded that the finite element predictions and experimental data were correlated well. Xiong et al. [122] modelled carbon fibre composite sandwich columns with prismatic lattice cores (3D honeycomb) under in-plane compression to investigate the Euler buckling of sandwich beams because this failure regime was not tested in the experimental study. The results from simulation had a good agreement with the analytical predictions. Parametric studies were conducted by Schneider et al. [123] using commercial finite element software Hypermesh to investigate how different geometrical parameters affect the mechanical properties of novel thermoplastic carbon fibre and poly-ethylene terephthalate fibre composite lattice structures. It was explained that the effect of core strut cross-section geometry and the effect of expansion and corrugation angle on out-of-plane compressive response lattice truss core is important.

A numerical simulation was performed by Sebaey and Mahdi [124] to check the damage mechanism and the hole sensitivity of CFRP pyramidal truss core sandwich composites under biaxial loading. The ABAQUS software was used with the physically-based failure criteria, denoted LaRC, to simulate the damage initiation and property degradation related to the damage propagation. The damage criteria were implemented in a user subroutine. The model was validated against experimental results from the literature with a good agreement. Norouzi and Rostamiyan [63] conducted numerical study of flatwise compression behaviour of carbon fibre composite sandwich panels with new lattice cores and the results were compared with experimental results. The geometric model was created in Solid Works program and FE simulation performed using ABAQUS/Explicit. Notably, FE simulation was considered till the point of compression strength peak only. The geometric imperfection, in terms of the buckling modes was imported into the ABAQUS/explicit analysis. It was noted that there was a good agreement between the predicted and experimental force - extension curves. However, the predicted yield loads are slightly lower than the experimental data in his work. The full-scale model simulating the out-of-plane compressive and shear response of composite sandwich panel with tetrahedral truss cores was developed in ABAQUS/Standard by Mei et al. [93]. A continuum damage model (CDM) based on Hashin failure criteria was implemented in ABAQUS by a user subroutine UMAT for this simulation. The authors showed that the stress-strain curves of numerical and experimental results were coincident approximately. However, it was found that the compressive and shear stiffness of numerical analysis were slightly higher than test results due to the simplification of the FE model.

The FE analysis using ABAQUS/Explicit was applied to evaluating the mechanical behaviour of a novel glass fibre reinforced composite lattice sandwich panel under flatwise compression by Liu et al. [125]. The progressive failure of composites was implemented in the model by ABAQUS user-subroutine VUMAT. Cohesive model was also considered in this simulation to model interface behaviour. It was found that the modulus and strength calculated in the finite element model were in accordance with the experimental result with a relative error of 10.3 % and 19.4 %, respectively. Yin et al. [126] used LS-DYNA to build a model for impact simulations of a double-curvature composite sandwich hood with a pyramidal lattice core. The effects of geometrical variables, material selection and core types on the structural response were discussed. Among various material selections, hoods designed with carbon fibre reinforced composite (CFRC) panels and a flax fibre reinforced composite (FFRC) lattice core led to the minimum head injury. The literature review on the FE simulations shows that the accuracy of the simulated results can be validated by means of experimental results, which may be extended parametric studies.

2.6 Summary

The literature review in this chapter has revealed the past and present research work associated on lattice core sandwich structures. The review commenced with the overview of cellular solids, followed by lattice materials. The manufacturing of lattice core sandwich structures was discussed with brief review on manufacturing processes of metallic lattice core sandwich panels and evolution of these techniques in producing composite lattice core sandwich structures, in particularly. Following this, the response of composite lattice core sandwich structures under compression and low-velocity impact conditions were reviewed. Finally, the development of the finite element techniques to model the response of the lattice core sandwich structures using commercially available FE codes have been reviewed.

The literature review has signified that the manufacturing process of the composite lattice core sandwich structures influences the mechanical properties and failure mechanism of these structures. As the manufacturing technique and procedure play a key role on the outcome, an emphasis should be placed on the fabrication technology and mechanical property. Relatively, this has provided a gap to explore hybrid manufacturing process in which combining two or more manufacturing techniques in producing composite lattice core sandwich structures. Furthermore, another critical factor is the connection between the cores and the face sheets during the preparation of sandwich structures. Particularly, composite truss cores contact with the facesheets at points with small area, rather than on lines as done by conventional cores. Consequently, the adhesive joints between a lattice core and the face sheets are likely to be more vulnerable to pull-out failure than the other sandwich combinations due to the tensile force acting in the struts, even if the ends of the struts are partly or completely inserted into the face sheets along grooves or through holes, respectively, as carried out in the past researches. Alternatively, the literature review has suggested that the lattice truss cores and the facesheets must be manufactured in one process without bonding, which effectively improves the connection strength of the facesheets and core. This has led to the idea of manufacturing composite lattice core sandwich structures using integrative forming method in one manufacturing to improve the connectivity between core and facesheet by stitching technology.

It is well known that the response of the sandwich structures primarily depends on the topology and the parent materials. Yet, carbon fibre composites (CFRP) have a high specific strength and stiffness and are therefore a promising material for making stiff and potentially strong cellular structures with optimized lattice topology. The pyramidal lattice structure is one of the most representative lattice sandwich structures with high specific strength and stiffness, having attracted more research attention.

Therefore, this research proposes a new manufacturing approach to manufacture carbon fibre reinforced lattice core sandwich structures in one manufacturing process by highlighting the gap identified in the literature review. A simpler lattice core consisting composite column will be explored first and subsequently a more known pyramidal lattice truss core will be investigated in this research. Finally, the proposed structures have potential to fill the gap in the material-property space.

References

[1] L.J. Gibson and M.F. Ashby, Cellular Solids: Structure and Properties, 1st Edition, Pergamon Press, 1988.

[2] M.F. Ashby, A.G. Evans, N.A. Fleck, L.J. Gibson, J.W. Hutchinson and H.N.G. Wadley, Metal Foams: A Design Guide, Butterworth-Heinemann, 2000.

[3] M. Ashby, D.R.H. Jones, Engineering Materials 2: An Introduction to Microstructures, Processing and Design, 3rd Edition, Butterworth-Heinemann, 2005.

[4] N. Mills, Polymer Foams Handbook: Engineering and Biomechanics Applications and Design Guide, 1st Edition, Butterworth-Heinemann, 2007, pp10–36.

[5] M. Schiffler and P. Columbo, Cellular Ceramics: Structure, Manufacturing, Properties and Applications, Wiley, 2005.

[6] D.J. Sypeck, Cellular truss core sandwich structures, Applied Composite Materials, 12, 2005, pp229–246.

[7] HexWeb, Honeycomb attributes and properties, Hexcel Composites Publication No. TSB 120, http://www.hexcel.com/Resources/DataSheets/Brochure-Data Sheets/Honeycomb_Attributes_and_Properties.pdf.

[8] D.J. Sypeck and H.N.G. Wadley, Cellular metal truss core sandwich structures, Advanced Engineering Materials, 4, 2002, pp759-64.

[9] T. Bitzer, Honeycomb Technology: Materials, Design, Manufacturing, Applications and Testing, Springer, 1997.

[10] R.A.W. Mines, S. Tsopanos, Y. Shen, R. Hasan, S.T. McKown, Drop weight impact behaviour of sandwich panels with metallic micro lattice cores, International Journal of Impact Engineering, 60, 2013, pp120-132.

[11] O.E. Sotomayor and H.V. Tippur, Role of cell regularity and relative density on elasto-plastic compression response of random honeycombs generated using Voronoi diagrams, International Journal of Solids and Structures, 51, 2014, pp3776-3786.

[12] D.J. Sypeck, Wrought aluminum truss core sandwich structures, Metallurgical and Materials Transactions B, 36, 2005, pp125–131.

[13] A.G. Evans, J.W. Hutchinson, N.A. Fleck, M.F. Ashby and H.N.G. Wadley, The topological design of multifunctional cellular metals, Progress in Materials Science, 46, 2001, pp309-327.

[14] M.F. Ashby, The properties of foams and lattices, Philosophical Transactions of the Royal Society A, 364, 2006, pp15–30.

[15] N.A. Fleck, V.S. Deshpande and M.F. Ashby, Micro-architectured materials: past, present and future", Proceedings Royal Society A, 466, 2010, pp2495–2516.

[16] H.L. Fan, T. Zeng, D.N. Fang and W. Yang, Mechanics of advanced fiber reinforced lattice composites, Acta Mechanica Sinica, 26, 2010, pp825–835.

[17] T.J. Lu, F. Xu and T. Wen, Thermo-fluid Behaviour of Periodic Cellular Metals, Springer-Verlag, 2013.

[18] A.H. Azman, Method for integration of lattice structures in design for additive manufacturing" Ph.D. Thesis, University Grenoble Alpes, 2017.

[19] T.A. Schaedler and W.B Carter, Architected cellular materials, Annual Review of Materials Research, 46, 2016, pp187–210.

[20] H.N.G. Wadley, Multifunctional periodic cellular metals, Philosophical Transactions of the Royal Society A, 364, 2006, pp31–68.

[21] H.N.G. Wadley, N.A. Fleck and A.G. Evans, Fabrication and structural performance of periodic cellular metal sandwich structures, Composites Science and Technology 63, 2003, pp2331–2343.

[22] V.S. Deshpande, N.A. Fleck and M.F. Ashby, Effective properties of the octet-truss lattice material, Journal of the Mechanics and Physics of Solids, 49, 2001, pp1747–1769.

[23] V.S. Deshpande, M.F. Ashby and N.A. Fleck, Foam topology bending versus stretching dominated architectures, Acta Materialia, 49, 2001, pp1035–1040.

[24] R.G. Hutchinson and N.A. Fleck, Microarchitectured cellular solids – the hunt for statically determinate periodic trusses, Journal of Applied Mathematics and Mechanics, 85, 2005, pp607–617.

[25] S. Engelbrecht, L. Folgar, D.W. Rosen, G. Schulberger and J. Williams, Cellular Structures for Optimal Performance, In: Proceedings of SFF Symposium, Austin, 2009, pp831–842.

[26] D.T. Queheillalt, V.S. Deshpande, H.N.G Wadley, Truss waviness effects in cellular lattice structures, Journal of Mechanics of Materials and Structures, 2, 2007, pp1657–75.

[27] D. Rosen, S. Johnston and M. Reed, Design of general lattice structures for lightweight and compliance applications, Rapid Manufacturing Conference, Loughborough, UK, 2006, pp1–14.

[28] H.N.G. Wadley, Cellular metals manufacturing, Advanced Engineering Materials, 4, 2002, pp726–733.

[29] V.S. Deshpande and N.A. Fleck, Collapse of truss core sandwich beams in 3-point bending, International Journal of Solids and Structures, 38, 2001, pp6275–6305.

[30] S. Chiras, D.R. Mumm, A.G. Evans, N. Wicks, J.W. Hutchinson, K. Dharmasena, H.N.G. Wadley and S. Fichter, The structural performance of near-optimized truss core panels, International Journal of Solids and Structures, 39, 2002, pp4093–4115.

[31] J. Wang, A.G. Evans, K. Dharmasena, and H.N.G. Wadley, On the performance of truss panels with Kagomé cores, International Journal of Solids and Structures, 40, 2003, pp6981–6988.

[32] Y. Sugimura, Mechanical response of single-layer tetrahedral trusses under shear loading, Mechanics of Materials 36, 2004, pp715–721.

[33] J. Zhou, P. Shrotriya, and W.O. Soboyejo, On the deformation of aluminum lattice block structures: From struts to structures, Mechanics of Materials, 36, 2004, pp723–737.

[34] J. Mun, J. Ju, and J. Thurman, Indirect Fabrication of Lattice Metals with Thin Sections Using Centrifugal Casting, Journal of Visualized Experiments, 111, 2016, pp1–9.

[35] J. Mun, J. Ju, and J. Thurman, Indirect additive manufacturing of a cubic lattice structure with a copper alloy, International Solid Freeform Fabrication Symposium – An Additive Manufacturing Conference, 2014, pp665–687.

[36] M.V. Nathal, J.D. Whittenberger, M.G. Hebsur, P.T. Kantzos and D.L. Krause, Superalloy lattice block structures, The Minerals, Metals and Materials Society, 2004, pp431–439.

[37] J. Liu, S. Pattofatto, D. Fang, F. Lu, and H. Zhao, Impact strength enhancement of aluminum tetrahedral lattice truss core structures, International Journal of Impact Engineering, 79, 2015, pp3–13.

[38] K.P. Dharmasena, H.N.G. Wadley, K. Williams, Z. Xue, and J.W. Hutchinson, Response of metallic pyramidal lattice core sandwich panels to high intensity impulsive loading in air, International Journal of Impact Engineering ,38, 2011, pp275–289.

[39] R. Biagi and H. Bart-Smith, Imperfection sensitivity of pyramidal core sandwich structures, International Journal of Solids and Structures, 44, 2007, pp4690–4706.

[40] H. Wadley, K. Dharmasena, Y. Chen, P. Dudt, D. Knight, R. Charette and K. Kiddy, Compressive response of multilayered pyramidal lattices during underwater shock loading, International Journal of Impact Engineering, 35, 2008, pp1102–1114.

[41] C.H. Lim, I. Jeon, and K.J. Kang, A new type of sandwich panel with periodic cellular metal cores and its mechanical performances, Materials and Design, 30, 2009, pp3082–3093.

[42] G.W. Kooistra and H.N.G. Wadley, Lattice truss structures from expanded metal sheet, Materials and Design, 28, 2007, pp507–514.

[43] W. Jiang, B. Yang, B.Y. Wang, H. Chen, and J.M. Gong, Experimental and numerical study on the residual stress in a lattice truss sandwich structure: Effect of geometrical dimensions of punching die, Materials and Design, 49, 2013, pp1048–1055.

[44] D.J. Sypeck, H.N.G. Wadley, Multifunctional microtruss laminates: textile synthesis and properties, Journal of Materials Research, 16, 2001, pp890–897.

[45] J. Tian, T.J. Lu, H.P. Hodson, D.T. Queheillalt, and H.N.G. Wadley, Cross flow heat exchange of textile cellular metal core sandwich panels, International Journal of Heat and Mass Transfer, 50, 2007, pp2521–2536.

[46] D.T. Queheillalt and H.N.G. Wadley, Cellular metal lattices with hollow trusses, Acta Materialia, 53, 2005, pp303–313.

[47] G. Zhang, B. Wang, L. Ma, J. Xiong, J. Yang, and L. Wu, The residual compressive strength of impact-damaged sandwich structures with pyramidal truss cores, Composite Structures, 105, 2013, pp188–198.

[48] G. Zhang, B. Wang, L. Ma, L. Wu, S. Pan, and J. Yang, Energy absorption and low velocity impact response of polyurethane foam filled pyramidal lattice core sandwich panels, Composite Structures, 108, 2014, pp304–310.

[49] L. Dong, V. Deshpande, and H. Wadley, Mechanical response of Ti-6Al-4V octet-truss lattice structures, International Journal of Solids and Structures, 60–61, 2015, pp107–124.

[50] R.A.W. Mines, On the characterisation of foam and micro-lattice materials used in sandwich construction, Strain, 44, 2008, pp71–83.

[51] J. Sun, Y. Yang, and D. Wang, Mechanical properties of a Ti6Al4V porous structure produced by selective laser melting, Materials and Design, 49, 2013 pp545–552.

[52] M. Smith, Z. Guan, and W.J. Cantwell, Finite element modelling of the compressive response of lattice structures manufactured using the selective laser melting technique, International Journal of Mechanical Sciences, 67, 2013, pp28–41.

[53] R. Gümrük and R.A.W. Mines, Compressive behaviour of stainless steel micro-lattice structures, International Journal of Mechanical Sciences, 68, 2013, pp125–139.

[54] I. Ullah, J. Elambasseril, M. Brandt, and S. Feih, Performance of bio-inspired Kagome truss core structures under compression and shear loading, Composite Structures, 118, 2014, pp294–302.

[55] J. Xiong, R.A.W Mines, R. Ghosh, A. Vaziri, L. Ma, A. Ohrndorf, H.J. Christ, and L. Wu, Advanced micro-lattice materials, Advanced Engineering Materials, 17, 2015, pp1253–1264.

[56] S. McKown, Y. Shena, W.K. Brookes, C.J. Sutcliffe, W.J. Cantwell, G.S. Langdon, G.N. Nurick, and M.D. Theobald, The quasi-static and blast loading response of lattice structures, International Journal of Impact Engineering, 35, 2008, pp795–810.

[57] G.N. Labeas and M.M. Sunaric, Investigation on the static response and failure process of metallic open lattice cellular structures, Strain, 46, 2010, pp195–204.

[58] K. Finnegan, G. Kooistra, H.N.G. Wadley, and V.S. Deshpande, The compressive response of the carbon fiber composite pyramidal truss sandwich cores, International Journal of Materials Research, 98, 2007, pp1–9.

[59] H. Fan, W. Yang, B. Wang, Y.Yan, Q. Fu, D. Fang, and Z. Zhuang, Design and manufacturing of a composite lattice structure reinforced by continuous carbon fibers, Tsinghua Science and Technology, 11, 2006, pp515-522.

[60] H.L. Fan, F.H. Meng, and W. Yang, "Mechanical behaviors and bending effects of carbon fiber reinforced lattice materials," Archive of Applied Mechanics, 75, 2006, pp635–647.

[61] T. George, V.S. Deshpande, and H.N.G. Wadley, Mechanical response of carbon fiber composite sandwich panels with pyramidal truss cores, Composites: Part A, 47, 2013, pp31–40.

[62] S. Yin, L. Wu, and S. Nutt, Stretch–bend-hybrid hierarchical composite pyramidal lattice cores, Composite Structures, 98, 2013, pp153–159.

[63] H. Norouzi and Y. Rostamiyan, Experimental and numerical study of flatwise compression behavior of carbon fiber composite sandwich panels with new lattice cores, Construction and Building Materials, 100, 2015, pp22–30.

[64] L. Dong and H. Wadley, Mechanical properties of carbon fiber composite octet-truss lattice structures, Composites Science and Technology, 119, 2015 pp26–33.

[65] L. Dong and H. Wadley, Shear response of carbon fiber composite octet-truss lattice structures, Composites: Part A, 81, 2016, pp182–192.

[66] J. Xiong, L. Ma, L. Wu, B. Wang, and A. Vaziri, Fabrication and crushing behavior of low density carbon fiber composite pyramidal truss structures, Composite Structures, 92, 2010, pp2695–2702.

[67] J. Xiong, A. Vaziri, L. Ma, J. Papadopoulos, and L. Wu, Compression and impact testing of two-layer composite pyramidal-core sandwich panels, Composite Structures, 94, 2012, pp793–801.

[68] B. Wang, L. Wu, L. Ma, Q. Wang, and S. Du, Fabrication and testing of carbon fiber reinforced truss core sandwich panels, Journal of Materials Science and Technology, 25, 2009, pp547–550.

[69] Y. Sun and L. Gao, Mechanical behavior of all-composite pyramidal truss cores sandwich panels, Mechanics of Materials, 65, 2013, pp56–65.

[70] B. Wang, L. Wu, L. Ma, Y. Sun, and S. Du, Mechanical behavior of the sandwich structures with carbon fiber-reinforced pyramidal lattice truss core, Materials and Design, 31, 2010, pp2659–2663.

[71] J. Liu, Z. Zhou, L. Wu, and L. Ma, Mechanical Behavior and Failure Mechanisms of Carbon Fiber Composite Pyramidal Core Sandwich Panel after Thermal Exposure, Journal of Materials Science and Technology, 29, 2013, pp846–854.

[72] M. Li, L. Wu, L. Ma, B. Wang, and Z. Guan, Mechanical Response of All-composite Pyramidal Lattice Truss Core Sandwich Structures, Journal of Materials Science and Technology, 27, 2011, pp570–576.

[73] B. Wang, G. Zhang, S. Wang, L. Ma, and L. Wu, High velocity impact response of composite lattice core sandwich structures, Applied Composite Materials, 21, 2013, pp377–389.

[74] B. Wang, G. Zhang, Q. He, L. Ma, L. Wu, and J. Feng, Mechanical behavior of carbon fiber reinforced polymer composite sandwich panels with 2-D lattice truss cores, Materials and Design, 55, 2014, pp591–596.

[75] J. Liu, X. Zhu, Z. Zhou, L. Wu, and L. Ma, Effects of thermal exposure on mechanical behavior of carbon fiber composite pyramidal truss core sandwich panel, Composites: Part B, 60, 2014, pp82–90.

[76] J. Liu, X. Zhu, T. Li, Z. Zhou, L. Wu, and L. Ma, Experimental study on the low velocity impact responses of all-composite pyramidal truss core sandwich panel after high temperature exposure, Composite Structures, 116, 2014, pp670–681.

[77] S. Yin, L. Wu, L. Ma, and S. Nutt, Pyramidal lattice sandwich structures with hollow composite trusses, Composite Structures, 93, 2011, pp3104–3111.

[78] S. Yin, L. Wu, L. Ma, and S. Nutt, Hybrid truss concepts for carbon fiber composite pyramidal lattice structures, Composites: Part B, 43, 2012, pp1749–1755.

[79] S. Yin, L. Wu, and S. R. Nutt, Compressive efficiency of stretch–stretch-hybrid hierarchical composite lattice cores, Materials and Design, 56, 2014, pp731–739.

[80] J. Xiong, B. Wang, L. Ma, J. Papadopoulos, A. Vaziri, and L. Wu, Three-dimensional Composite Lattice Structures Fabricated by Electrical Discharge Machining, Experimental Mechanics, 54, 2014, pp405–412.

[81] T. George, V.S. Deshpande, and H.N.G. Wadley, Hybrid carbon fiber composite lattice truss structures, Composites: Part A, 65, 2014, pp135–147.

[82] T. George, V.S. Deshpande, K. Sharp, and H.N.G. Wadley, Hybrid core carbon fiber composite sandwich panels: Fabrication and mechanical response, Composite Structures, 108, 2014, pp696–710.

[83] H. Kim, B. H. Cho, H.-K. Hur, and K.-J. Kang, A composite sandwich panel i ntegrally woven with truss core, Materials and Design, 65, 2014, pp231–242.

[84] Z. Song, S. Cheng, T. Zeng, F. Yang, S. Jing, and D. Fang, Compressive behavior of C/SiC composite sandwich structure with stitched lattice core, Composites: Part B, 69, 2015, pp243–248.

[85] L. Che, G. Xu, T. Zeng, S. Cheng, X. Zhou, and S. Yang, Compressive and shear characteristics of an octahedral stitched sandwich composite, Composite Structures, 112, 2014, pp179–187.

[86] G. Xu, J. Zhai, T. Zeng, Z. Wang, S. Cheng, and D. Fang, Response of composite sandwich beams with graded lattice core, Composite Structures, 119, 2015, pp666–676.

[87] H. L. Fan, F. H. Meng, and W. Yang, Sandwich panels with Kagome lattice cores reinforced by carbon fibers, Composite Structures, 81, 2007, pp533–539.

[88] H. Fan, L. Yang, F. Sun, and D. Fang, Compression and bending performances of carbon fiber reinforced lattice-core sandwich composites, Composites: Part A, 52, 2013, pp118–125.

[89] G. Zhang, L. Ma, B. Wang, and L. Wu, Mechanical behaviour of CFRP sandwich structures with tetrahedral lattice truss cores, Composites: Part B, 43, 2012, pp471–476.

[90] Q. Wu, L. Ma, L. Wu, and J. Xiong, A novel strengthening method for carbon fiber composite lattice truss structures, Composite Structures, 153, 2016, pp585–592.

[91] L. Gao, Y. Sun, L. Cong, and P. Chen, Mechanical behaviours of composite sandwich panel with strengthened pyramidal truss cores, Composite Structures, 105, 2013, pp149–152.

[92] J. Liu, Z. Zhou, L. Ma, J. Xiong, and L. Wu, Temperature effects on the strength and crushing behavior of carbon fiber composite truss sandwich cores, Composites: Part B, 42, 2011, pp1860–1866.

[93] J. Mei, J. Liu, and J. Liu, A novel fabrication method and mechanical behavior of all-composite tetrahedral truss core sandwich panel, Composites: Part A, 102, 2017, pp28–39.

[94] Y. Hu, W. Li, X. An, and H. Fan, Fabrication and mechanical behaviors of corrugated lattice truss composite sandwich panels, Composites Science and Technology, 125, 2016, pp114–122.

[95] M. Chen, X. Zhu, H. Lei, H. Chen, and D. Fang, Effect of defect on the compressive response of sandwich structures with carbon fiber pyramidal truss cores, International Journal of Applied Mechanics, 7, 2015, pp1550004-1550024.

[96] J. Wallach and L. Gibson, Defect sensitivity of a 3D truss material, Scripta Materialia, 45, 2001, pp639–644.

[97] A. Wang and D. McDowell, Effects of defects on in-plane properties of periodic metal honeycombs, International Journal of Mechanical Sciences, 45, 2003, pp1799–1813.

[98] H. Fan, F. Jin and D. Fang, Characterization of edge effects of composite lattice structures, Composites Science and Technology, 69, 2009, pp1896–1903.

[99] J. Xu, X. Gao, C. Zhang, and S. Yin, Flax fiber-reinforced composite lattice cores: A low-cost and recyclable approach, Materials and Design, 133, 2017 pp444–454.

[100] Z. Hou, X. Tian, J. Zhang, and D. Li, 3D printed continuous fibre reinforced composite corrugated structure, Composite Structures, 184, 2018, pp1005–1010.

[101] G.B. Chai and S. Zhu, A review of low-velocity impact on sandwich structures, Proceedings of the Institution of Mechanical Engineers, Part L: Journal of Materials: Design and Applications, 225, 2011, pp207–230.

[102] A. Ahmed and L. Wei, The low-velocity impact damage resistance of the composite structures - a review, Reviews on Advanced Materials Science, 40, 2015, pp127–145.

[103] W.J. Cantwell and J. Morton, The impact resistance of composite materials - a review, Composites, 22, 1991, pp347–362.

[104] A.S. Vaidya, U.K. Vaidya, and N. Uddin, Impact response of three-dimensional multifunctional sandwich composite, Materials Science and Engineering A, 472, 2008, pp52–58.

[105] S.X. Wang, L.Z. Wu, and L. Ma, Low-velocity impact characteristics of carbon fiber composites lattice core sandwich structures, Advanced Materials Research, 79-82, 2009, pp127-130.

[106] B. Wang, L.-Z. Wu, L. Ma, and J.-C. Feng, Low-velocity impact characteristics and residual tensile strength of carbon fiber composite lattice core sandwich structures, Composites: Part B, 42, 2011, pp891–897.

[107] G. Zhang, B. Wang, L. Ma, J. Xiong, and L. Wu, Response of sandwich structures with pyramidal truss cores under the compression and impact loading, Composite Structures, 100, 2013, pp451–463.

[108] T. Strek, H. Jopek, B.T. Maruszewski, and M. Nienartowicz, Computational analysis of sandwich-structured composites with an auxetic phase, Physica Status Solidi (B) Basic Research, 251, 2014, pp354–366.

[109] J. Mackerle, Finite element analyses and simulations of manufacturing processes of composites and their mechanical properties: a bibliography (1985–2003), Computational Materials Science, 31, 2004, pp187–219.

[110] A.N. Palazotto, E.J. Herup, and L.N.B. Gummadi, Finite element analysis of low velocity impact on composite sandwich plates, Composite Structures, 49, 2000, pp209–227.

[111] M.T. Tilbrook, D.D. Radford, V.S. Deshpande, and N.A. Fleck, Dynamic crushing of sandwich panels with prismatic lattice cores, International Journal of Solids and Structures, 44, 2007, pp6101–6123.

[112] T. Liu, Z.C. Deng, and T.J. Lu, Structural modeling of sandwich structures with lightweight cellular cores, Acta Mechanica Sinica, 23, 2007, pp545–559.

[113] M.N. Velea and S. Lache, Numerical simulations of the mechanical behavior of various periodic cellular cores for sandwich panels, Procedia Engineering, 10, 2011, pp287–292.

[114] Q. Zhang, A. Chen, C. Chen, and T. Lu, Ultralight X-type lattice sandwich structure (II): Micromechanics modeling and finite element analysis, Science in China Series E: Technological Sciences, 52, 2009, pp2670–2680.

[115] Q. Zhang and T. Lu, Experimental and simulated compressive properties of work-hardened X-type lattice truss structures," Acta Mechanica Solida Sinica, 25, 2012, pp111–116.

[116] L. St-Pierre, N.A. Fleck, and V.S. Deshpande, The predicted compressive strength of a pyramidal lattice made from case hardened steel tubes, International Journal of Solids and Structures, 51, 2014, pp41–52.

[117] M. R. Karamooz Ravari, M. Kadkhodaei, M. Badrossamay, and R. Rezaei, "Numerical investigation on mechanical properties of cellular lattice structures fabricated by fused deposition modeling, International Journal of Mechanical Sciences, 88, 2014, pp154–161.

[118] Y. Liu, T.A. Schaedler, A.J. Jacobsen, and X. Chen, Quasi-static energy absorption of hollow microlattice structures, Composites: Part B, 67, 2014, pp39–49.

[119] M. Li, L. Wu, L. Ma, B. Wang, and Z. Guan, Structural response of all-composite pyramidal truss core sandwich columns in end compression, Composite Structures, 93, 2011, pp1964–1972.

[120] M. Li, L. Wu, L. Ma, J. Xiong, and Z. Guan, Torsion of carbon fiber composite pyramidal core sandwich plates, Composite Structures, 93, 2011, pp2358–2367.

[121] M. Sadighi and S.A. Hosseini, Finite element simulation and experimental study on mechanical behavior of 3D woven glass fiber composite sandwich panels, Composites: Part B, 55, 2013, pp158–166.

[122] J. Xiong, M. Zhang, A. Stocchi, H. Hu, L. Ma, L. Wua, and Z. Zhang, Mechanical behaviors of carbon fiber composite sandwich columns with three dimensional honeycomb cores under in-plane compression, Composites: Part B, 60, 2014 pp350–358.

[123] C. Schneider, M.N. Velea, S. Kazemahvazi, and D. Zenkert, Compression properties of novel thermoplastic carbon fibre and poly-ethylene terephthalate fibre composite lattice structures, Materials and Design, 65, 2015, pp1110–1120.

[124] T.A. Sebaey and E. Mahdi, Behavior of pyramidal lattice core sandwich CFRP composites under biaxial compression loading, Composite Structures, 116, 2014, pp67–74.

[125] Y. Liu, C. Zhou, B. Cen, Z. Zeng, X. Lu, and X. Zhu, Compression property of a novel lattice sandwich structure, Composites Part B, 117, 2017, pp130–137.

[126] S. Yin, H. Chen, Y. Wu, Y. Li, and J. Xu, Introducing composite lattice core sandwich structure as an alternative proposal for engine hood, Composite Structures, 201, 2018, pp131–140.

3 Manufacture and Testing Procedure

This chapter focuses on the novel fabrication technique to manufacture all-composite lattice truss core sandwich structures and recording their resulting mechanical responses of the structures under static and dynamic loadings. Initial attention was deemed to explore the viability of the fabrication technique which uses sacrificial mould method with combination of vacuum assisted resin infusion process (VARTM) by manufacturing sandwich structures with simple carbon fibre composite column lattice trusses. Then, the structures were tested under quasi-static flatwise compression to investigate their mechanical properties and failure mechanisms of the composite columnar lattice core sandwich panels. The influence of fibre volume fraction and strut diameter of columnar lattice truss structures were also examined. Following this, the work was extended to manufacture sandwich structures made with carbon fibre composite pyramidal and modified pyramidal lattice cores using the sacrificial mould method. Furthermore, more complex lattice structures based on pyramidal topology were manufactured to explore the potential of this fabrication method. The experimental investigations were carried out to evaluate the compressive and impact responses of these structures and their subsequent failure mechanisms. As the investigation focuses on the energy absorption performance of the novel lattice core sandwich structures, only the structural response of the structures subjected to compressive loading was studied to obtain the load-displacement relationships and further to quantify the corresponding energy absorbing capabilities of those lattice sandwich panels produced. Therefore, the bending behaviour of the structures was not studied in the current research project.

3.1 Constituent materials

In this section, the constituent materials used to manufacture all-composite lattice truss core sandwich structure are initially described. Here, the all-composite lattice truss core sandwich structure was fabricated from carbon fibre reinforced epoxy resin composite. As it is known, carbon fibre reinforced composite has a high uniaxial specific stiffness and strength. If such a composite is used as trusses or struts of a lattice structure, the resulted lattice structures will be lighter and stronger than the existing structures made of metals [1] for a given mass. The facesheets and lattice truss cores were manufactured in one process without bonding, thus preventing the weak interface between the core and the facesheets.

3.1.1 Facesheets

The material used for facesheet is a commercially available woven carbon fabric preform purchased from Easy Composite Ltd, United Kingdom. This 2/2 twill weave fabric at the 200 g/m^2 weight is the most commonly used carbon fabric of all. It is suitable for use in wet-lay, vacuum bagging and resin infusion manufacture as well as for using as a single surface layer where parts are being made to look like carbon fibre (skinning).

The woven carbon fabric preform has a thickness of 0.28 mm with 3K fibre tow in weft and warp directions. '3K' is the filament count or tow size. This means that each 'bunch' of carbon fibres with this cloth is made up of 3000 individual carbon filaments. Fibres are bundled in various sizes, designated in thousands (K) of fibres. 1K, 3K, 6K, 12K, 24K, 50K are common bundle sizes. These fibres are woven into fabric with various weave patterns. 3K fabric is the most common one. The fibre will have the same “K” designation to indicate the number of fibres in the bundle. These numbers describe the size of the bundle used and have little to do with the quality of the fibre itself.

The carbon fibre used for the facesheets is from Mitsubishi-Rayon Pyrofil TR30S. Table 3.1 summarises the typical fibre properties used in this research. Both, the top and bottom facesheets of the lattice truss core sandwich structure are made up of sixteenth (16) layers of woven carbon fabric cloth with a 0/90 architecture. This ensured consistent for all types of the lattice truss sandwich structure.

Table 3.1. Typical properties of carbon fibre [2].

Property	Value
Tow Tensile Strength (MPa)	4410
Tow Tensile Modulus (GPa)	235
Typical Density (kg/m^3)	1790

3.1.2 Core

The material for making composite lattice truss core is a continuous carbon fibre tow preform in 12K bundle sizes. This carbon fibre tow preform was then threaded through the predrilled holes in the sacrificial mould that contains the lattice topology configurations and stitched together with the preform facesheets. Carbon fibre of 12K tow (Grafil 34-700 WD 12K) was purchased from Easy Composite Ltd, United Kingdom. Grafil 34-700 carbon fibre is a continuous, high strength, PAN based fibre. The specification and properties of this fibre are listed in Table 3.2.

Table 3.2. Typical specification and properties of Grafil 34-700 fibre [3].

Property	Value
Filament Diameter (μm)	7.0
Tensile Strength (MPa)	4,900
Tensile Modulus (GPa)	234
Tensile Strain (%)	2.0
Fiber Density (kg/m^3)	1800
Yield (g/km)	800
Size Content by Mass (%, w/w)	1.0

3.2 Sacrificial (lost) mould

One of the goals in this research is to manufacture a composite lattice core sandwich structure in a one manufacturing process. In order to achieve this, the sacrificial mould method has been adopted to fabricate the lattice sandwich structure. The sacrificial mould material contains the features of the truss core construction by means of drilling holes into it. Initially, vertical columns were simply created in the sacrificial mould to represent a simple column lattice. A vertical column truss was chosen as a core structure, due to the simplicity in order to study the feasibility of manufacturing a sandwich panel using the sacrificial mould method in a single manufacturing process. Following this, more complex lattices based on pyramidal topology by including more struts into the open pyramidal core structure were constructed. By a careful machining process, the lattice core construction of any topologies could be produced in the sacrificial mould for utilizing this concept.

Two materials were considered to act as the sacrificial mould, namely a Himalayan salt slab and a wax block. Himalayan salt is rock salt or halite from the Punjab region of Pakistan and it is being mined for commercialisation. Himalayan salt is used for skin therapy [4] and to flavour food. Himalayan salt is also manufactured into trendy glowing salt lamps, which are hollowed then lit with electric lighting. The wax block was made from Ferris File-A-Wax in USA. These blocks can be used for carving and machining to make model with ease and accuracy. These wax block comes with different colour coded that serves with different formulae and varying mechanical properties. Blue, purple and green wax blocks are available. The purple wax block was selected in this research due to easy machinability and it offers medium hardness with some flexibility for general purpose carving. The salt slabs and wax blocks were purchased from Westlab and Cousins respectively, located in the United Kingdom. Figure 3.3 shows images of the salt and wax blocks considered in this research.

(a) Himalayan salt (b) Wax

Figure 3.1. Typical sacrificial mould blocks.

Wax is generally easier to drill for any desired geometry with good accuracy. However, they require a higher temperature, approximately at 116°C (240°F) to melt and remove it completely [5]. This may have an influence on the mechanical properties of the finished structure. On the other hand, salt blocks can be easily removed by simply washing them under a continuous stream of water after the panel is fully cured. However, careful handling must be placed when dealing with salt blocks as it is more brittle in comparison to wax. The drilling of holes in the rock salt can sometimes be difficult, making it prone to breaking and chipping. Therefore, the drilling process must be carried out in a careful manner to produce the finished structure with a good quality. Furthermore, the removal of salt material during drilling must be cleaned off from the machine immediately after the machining process to avoid rusting of the lab equipment. In this work, the Himalayan salt block was extensively used as a sacrificial mould for specimen fabrication.

3.3 Design and specimen fabrication

In this section, the lattice core design and fabrication of sandwich structure are primarily described.

3.3.1 Lattice core design

In this work, a simple core topology that consists of a vertical truss (columnar) core lattice structure is initially presented. The unit cell of the columnar truss core is based on four by four vertical members and a representative unit cell is sketched in Figure 3.2 (a) with a height of $h = 39\ mm$, width of $w = 60\ mm$, a length of $b = 60\ mm$, and strut diameter of $d = 2, 3\ and\ 4\ mm$ respectively. The centreline distance between the struts is 15 mm. The relative density of the lattice core depends on the geometrical properties of the struts and the unit cell of the structures. Thus, the relative density, $\tilde{\rho}$, of the core structures is determined by 1) the volume occupied by the strut members in a unit cell of the core divided by the unit cell volume and/or 2) the ratio of core density (ρ_c) to that of the solid parent material (ρ_s) from which it is manufactured. The relative density, $\tilde{\rho}$, of the columnar truss core is given by:

$$\tilde{\rho} = \frac{\rho_c}{\rho_s} = \frac{4\pi d^2}{bw} \tag{3.1}$$

Following this, a pyramidal lattice truss core was designed and manufactured using the fabrication method described above. The unit cell of a pyramidal truss core is shown in Figure 3.2 (b) and it can be seen that the relative density of the core is given by:

$$\bar{\rho} = \frac{\pi d^2}{2 \sin\omega \, (\, l \cos\omega + \, t)^2} \tag{3.2}$$

where, the symbols l = 52.3 mm and $\omega = 45°$ denote the strut length and the inclined angle of the truss, respectively. The pyramidal core height is 37 mm and inclined strut centre distance, $t \; is$ 10 mm.

(a)

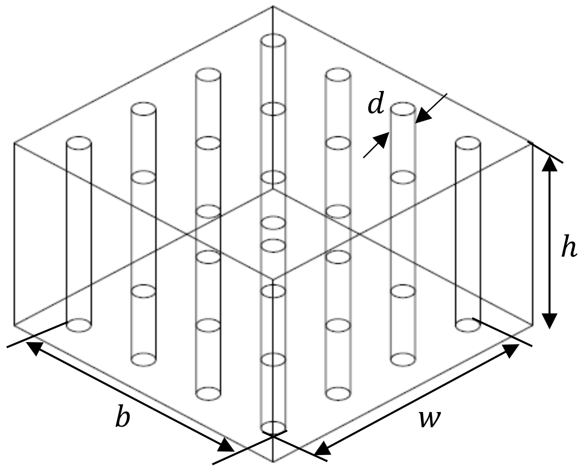

(b)

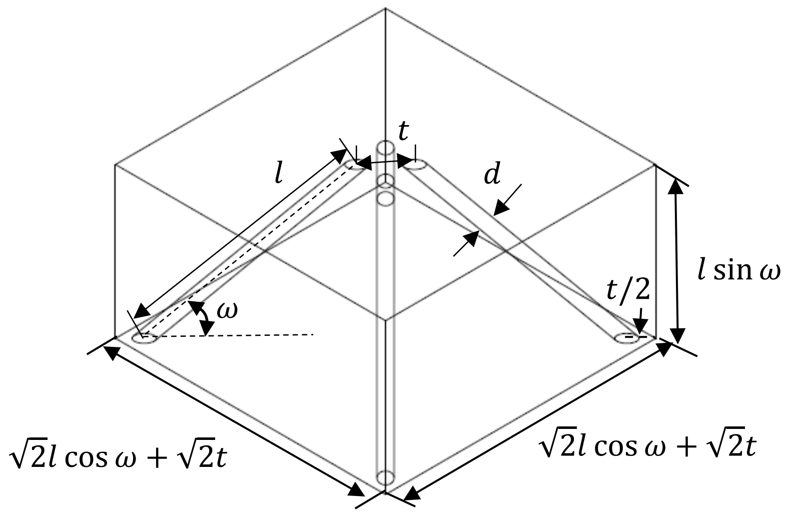

Figure 3.2. Schematic of the unit cell lattice truss core. (a) columnar and (b) pyramidal.

The work was further extended to design more complex lattices based on a pyramidal topology, by including more struts into the open pyramidal core structure. This resulted in modified pyramidal truss core lattices, referred to as type-1, -2 and -3. A type-1 (T1) core structures has a central vertical strut through the apex of the pyramidal core. A type-2 (T2) core structure was designed to include another four inclined struts in a pyramidal topology reflecting from the base of the unit cell, and, a type-3 (T3) contained an additional vertical column through the apex of the type-2 core design. These three types of core designs were explored to fully investigate the feasibility of the sacrificial mould method. Figure 3.3 shows the proposed models for lattice core construction. The lattice geometry dimensions and relative densities of cores considered in this study are summarised in Table 3.3.

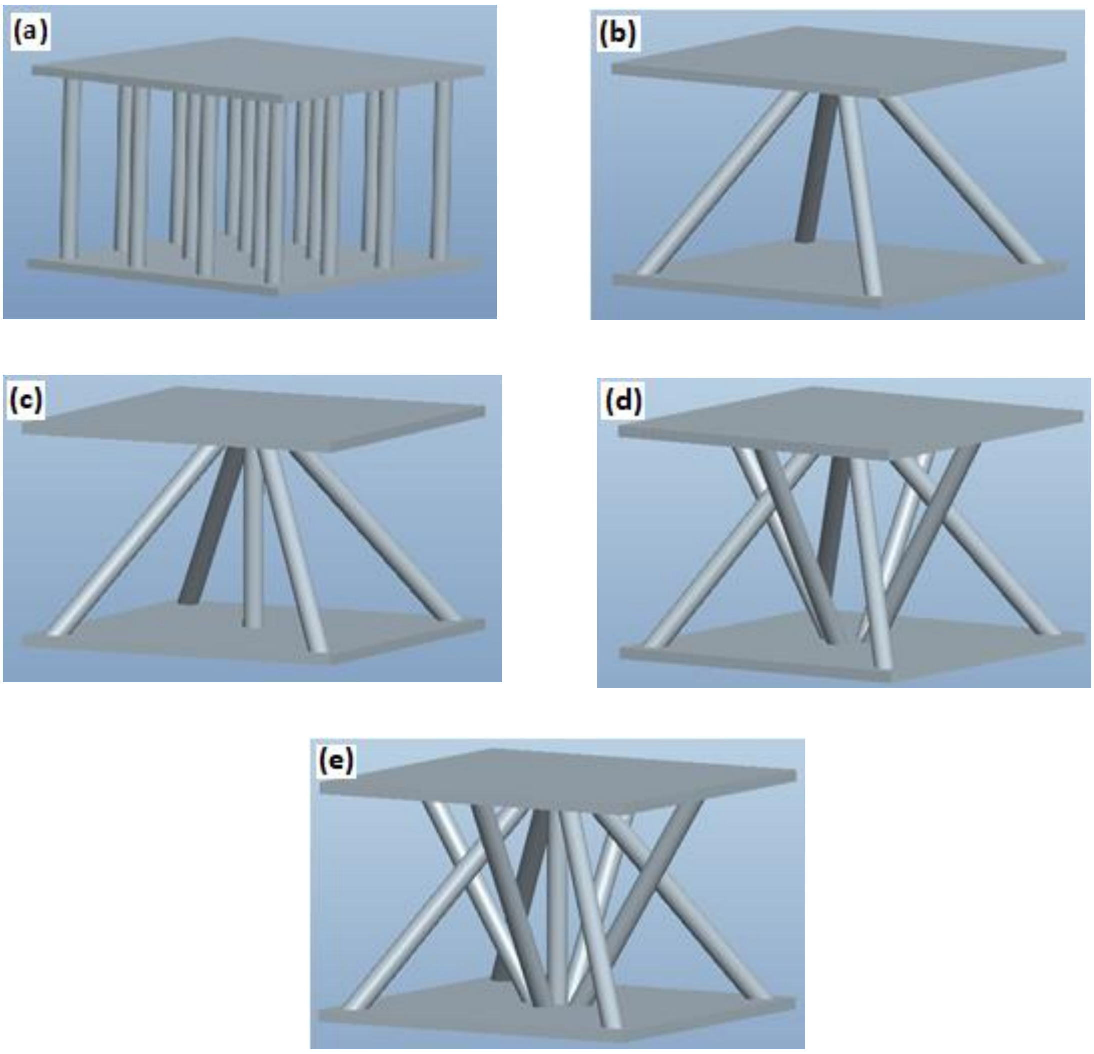

Figure 3.3. 3-D model of a unit cell lattice truss cores. (a) columnar, (b) pyramidal, (c) modified pyramidal (type-1), (d) type-2 and (e) type-3.

Table 3.3. Summary of the dimensions of the lattice cores design.

Design	Dimensions					
Columnar	d (mm)	b (mm)	w (mm)	h (mm)	$\tilde{\rho}$ (%)	ω (°)
C1	2	47	47		2.28	
C2	3	48	48	39	4.91	
C3	4	49	49		8.37	
Pyramidal	d (mm)	l (mm)	t (mm)	h (mm)	$\tilde{\rho}$ (%)	
P1	2				0.48	45
P2	3	52.3	10	37	1.06	
P3	4				1.84	
Modified-Pyramidal	d (mm)	l_1 (mm)	l_2 (mm)	h(mm)	$\tilde{\rho}$ (%)	
T1	2, 3, 4		-		0.57, 1.24, 2.16	
T2	3	52.3	44.5	37	1.95	
T3	3		44.5		2.14	

3.3.2 Sandwich structure fabrication

The sandwich structures were fabricated in a single manufacturing process, without secondary bonding. This manufacturing process eliminates the weak interface between the core and facesheets, a common problem with sandwich structures. This technique is based on stitching continuous fibres into a salt block that acts as a sacrificial mould and through the dry fabric (facesheets) placed on the top and bottom of the salt block. By repeated regular stitching of the fibre from one side to the other through the thickness of the salt block, a truss-like cellular core was produced. The salt block which was machined to the desired core height containing the features of the truss core construction by means of drilling holes into it. In this work, the salt block, as per received condition, was machined to dimensions of 300 x 200 x 37 mm in the length, width and thickness directions, respectively.

The machining operation of the rock salt was performed on a numerical control (NC) milling machine in a very careful manner. A rectangular wood pad which acts as a cushion for the rock salt was used in this machining operation to protect the salt block from breaking when it was clamped on the machine bed. By careful selection of machining parameters, the rock salt, which was received in uneven shape on all sides was machined to the required rectangular dimensions. This process could be accelerated by using computer a numerical control machine (CNC) using the same conditions. During this operation, the salt block was drilled according to the truss core configuration designed. For the vertical truss core (columnar), a drill bit with diameters of 2, 3 and 4 mm were chosen to perform the drilling operation to produce composite column truss cores which were also integrated with facesheets through stitching. Here, a series of holes were drilled into the salt block in four by four arrays to form a unit cell columnar lattice, as illustrated in Figure 3.4.

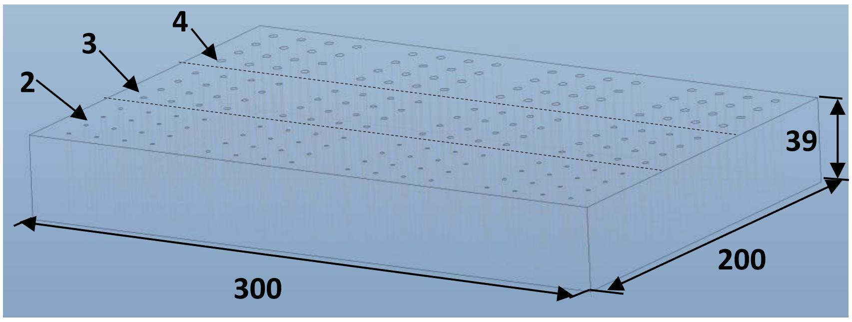

Figure 3.4. Holes with different diameters were drilled into salt block (units in mm).

Schematic diagrams of the location of the holes of 2, 3 and 4 mm diameter in the test samples, yielding cores with relative densities of 2.28, 4.91, and 8.37% respectively, are shown in Figure 3.5. The drilling operation was carried out using a CNC machine or a vertical drill by controlling the orientation of the mould to obtain the desired core configurations.

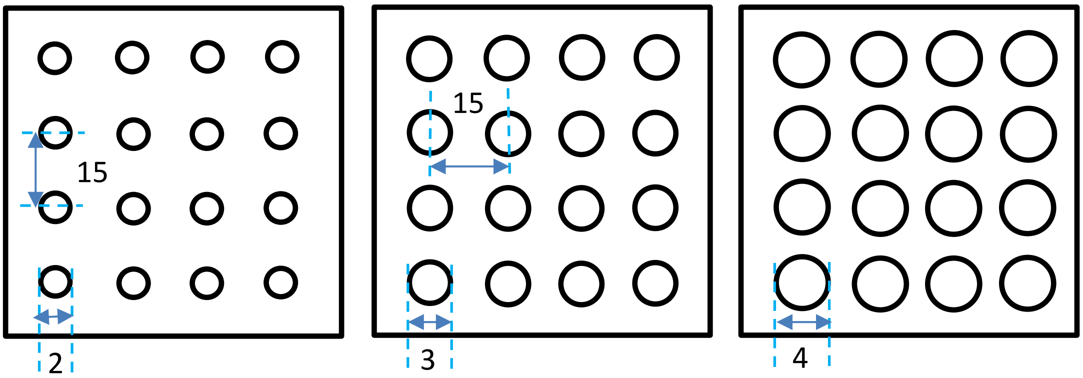

Figure 3.5. Schematic diagrams of the holes in the test samples (units in mm).

The pyramidal core configuration was achieved in the salt block by first designing a jig to guide the drilling operation in an inclined direction. This jig was placed on the salt block following the positioning for manual drill the holes at 45° to form a pyramidal configuration. Firstly, the salt block was placed on a rectangular wooden board slightly larger than the salt block. This wooden board served as a cushion to minimise the vibrating impact during the drilling operation on the salt block, since it is prone to breaking. Then, the aluminium jig part was positioned on the salt block according to the desired pyramidal orientation, and as shown schematically in Figure 3.6. Following this, the entire part was fixed in a G-clamp used for metal and woodworking applications. This set-up was then secured on a bench vise to hold them firmly for drilling, as illustrated in Figure 3.7. The drill bit with sizes of 2, 3 and 4 mm were used to create pyramidal samples with different diameters.

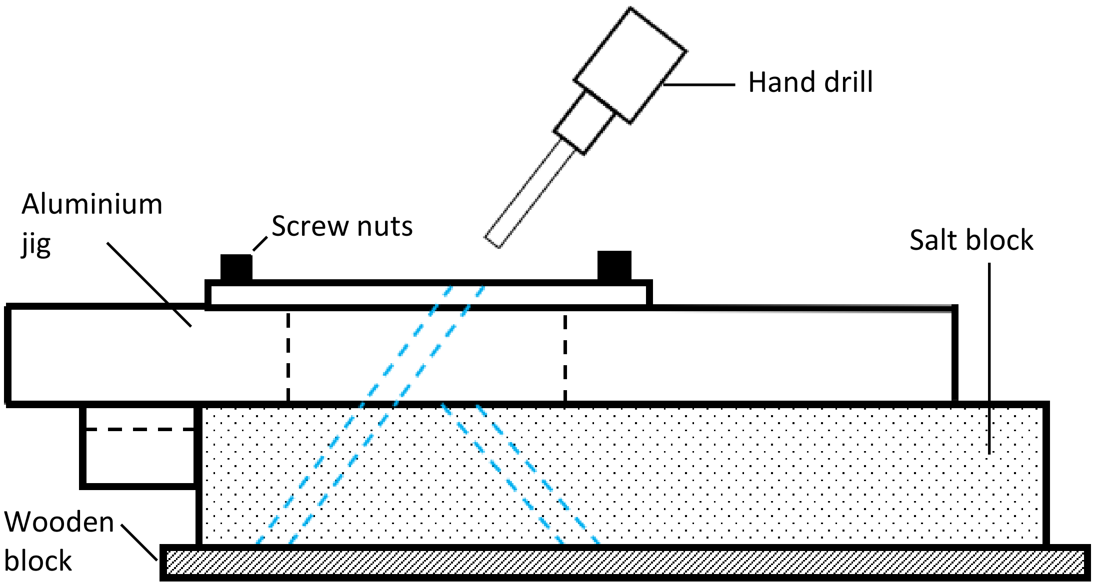

Figure 3.6. Schematic drawing of the assembly of the parts and salt block.

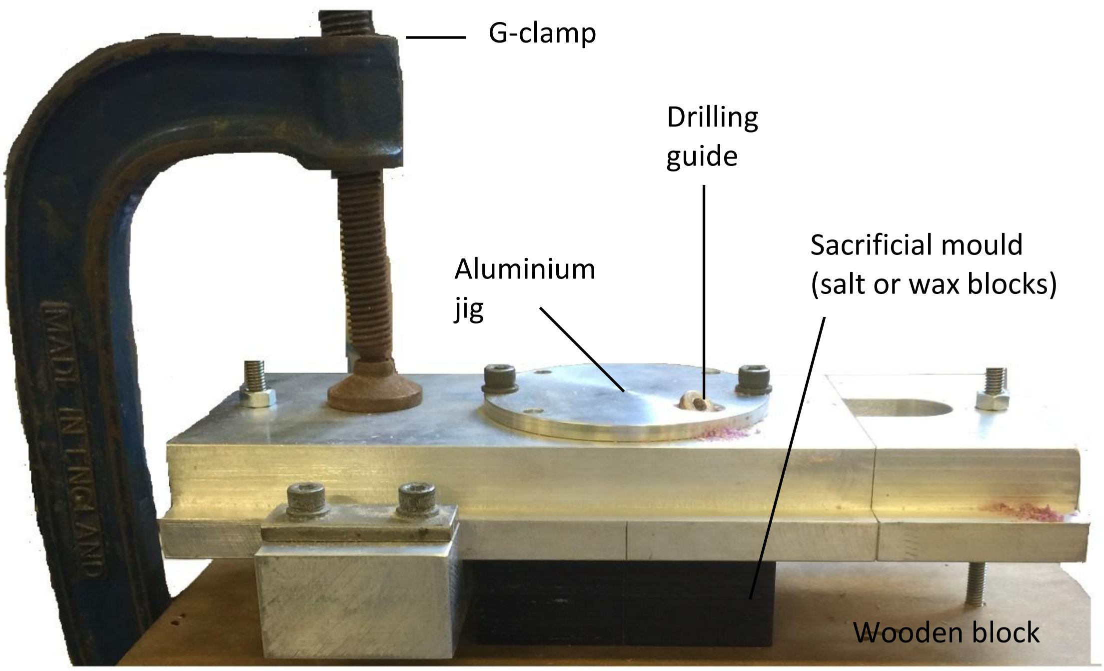

Figure 3.7. The set-up for drilling of an inclined angle.

The modified type-1 core configuration was prepared from a salt block by simply adding a vertical hole through the apex of the pyramidal geometry using a vertical drill machine. The modified type-2 core configuration was created in the salt block following the same drilling operation method as for the pyramidal configuration. Upon completion of the pyramidal core configuration holes, the salt block was turned on another side and the same procedure is repeated to complete the core design drilling. Finally, the modified type-3 core design was achieved in the salt block by adding a vertical hole centrically to pyramidal design of the type-2 core configuration. The drilling operation was carried out manually using a hand drill in this work, however, this procedure can be accelerated by using CNC machine.

Following the above procedure, the holes were drilled in the salt block according to the desired lattice truss core configuration. Then, four layers of woven fabric were cut to a size larger than the salt block and overlaid on the top and bottom surfaces of the salt block, respectively. The dry fabrics were held together on the salt block and kept in place using masking tape. Prior to fibre stitching, the filaments in the carbon fibre tow were held in place by dipping one end of the dry fibre tow in distilled water, and then pulling through a small hole in a rubber membrane to squeeze out the excess water [6]. By doing this, fibre damage during sewing as the tow contacts the surface of the holes was minimized. Following this, the end of the wetted fibre was tied to a thread and fixed to the end of a needle for stitching. A continuous carbon fibre tow was manually stitched from one side to another side of the salt block in the through thickness direction. The process was repeated until the truss configuration was complete. Interestingly, the same fibre tow was used to stitch all of the holes in a unit cell lattice truss, thereby ensuring that there were no fibre discontinuities in the entire structure. The weaving pattern depicted in this study is illustrated schematically in Figure 3.8.

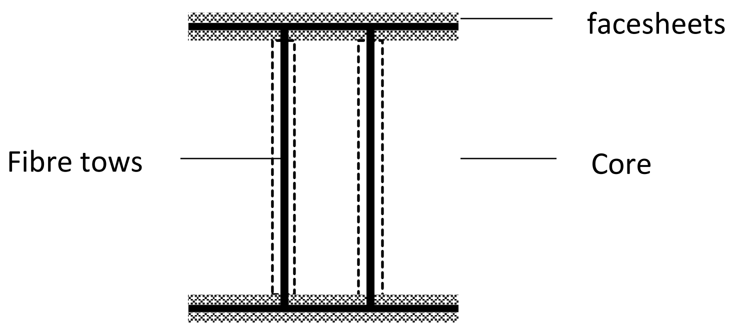

Figure 3.8. Schematic illustration of the sewing pattern used to stitch the samples.

After stitching, the assembly was heated up to 60°C for 1 hour in an oven to remove any moisture. Then, the stitched dry assembly was covered with an additional four woven fabric layers. Finally, the sample was resin infused through the vacuum assisted resin transfer method (VARTM). This process would be described in the next section. Following this, the sample was then cured at room temperature under vacuum pressure for 24 hours before demoulding.

It is worth noting that a constant fibre volume fraction was ensured by altering the number of fibre tows during stitching to produce three distinct sizes of composite strut. The carbon fibre tow had a designation of 12K, consisting of 12,000 filaments. The volume fraction of fibres was estimated from the cross-sectional area of the filaments in the tow and the cross-sectional area of the struts as follows:

$$V_f = \frac{12000\, n\, {d_f}^2}{{d_c}^2} \tag{3.3}$$

where n , d_f and d_c denote the number of fibre tows, filament diameter and the diameter of the struts. Alternatively, the fibre volume fraction can also be estimated using the fibre mass per unit length, following the ratio of the volume of fibre to that of the volume of the struts.

$$V_f = \frac{Volume\ of\ fibre}{Volume\ of\ composite} = \frac{{mass\ of\ fibre}/{fibre\ density}}{\pi r^2 l} \tag{3.4}$$

The number of fibre tows stitched through a hole controls the fibre volume fraction within the struts. The fibre tows measured one meter in length, weighing 0.8 g, according to the manufacturer’s data. This was also confirmed via laboratory measurements. The mass of fibres in each strut is estimated as follows:

$$Mass\ of\ fibre = No.of\ fibre\ tows\ \times Fibre\ mass\ per\ unit\ length\ \times l \tag{3.5}$$

Finally, the fibre volume fraction reduces to,

$$V_f = \frac{n \times Fibre\ mass\ per\ unit\ length}{\pi r^2 p_f} \tag{3.6}$$

where p_f is the density of the carbon fibre, l and r are the strut length and radius respectively. In this work, two different fibre volume fractions were studied for the columnar lattice core samples to examine the influence fibre volume fraction on the compression properties of the vertical truss structures. The fibre volume fraction studied was in the range of 13 – 39 % for vertical truss core (columnar lattice). Meanwhile, the fibre volume fraction studied for the pyramidal and the modified samples ranged 42 – 46 %. The fibre volume fraction estimation was also determined by conducting fibre volume determination tests in the laboratory, which would be elaborated in the test methods section.

3.4 Resin infusion process

The vacuum resin infusion method is a sophisticated technique for manufacturing high performance, void free composites, even on large or complicated moulds. The dry assembly of the perforated salt block with the skin stitched sandwich panel was prepared for the resin infusion process. All the equipment and supplies necessary to undertake vacuum resin infusion are shown in Figure 3.9.

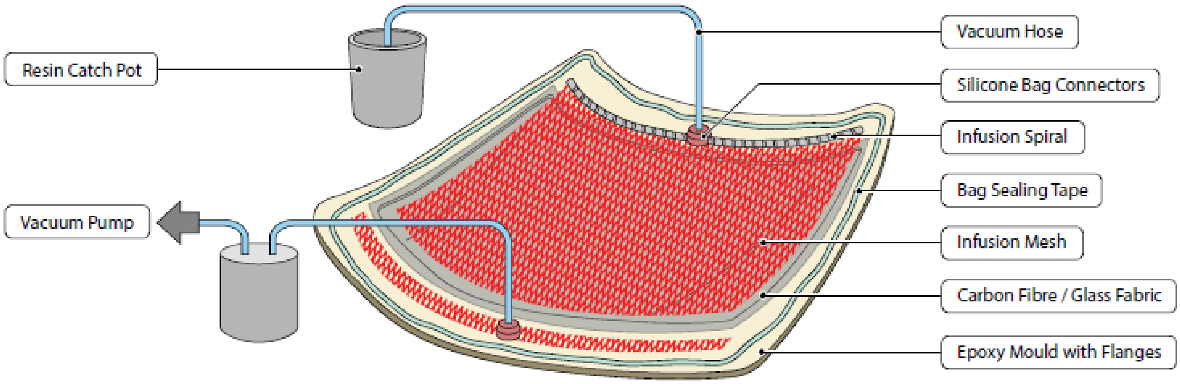

Figure 3.9. Common configurations used for resin infusion.

An IN-2 epoxy resin with hardener was used for the polymer matrix. This is a high performance low viscosity epoxy resin formulated specifically for use in resin infusion composite production. As an infusion resin, it is ultra-low viscosity, ensuring that it can quickly infuse through a range of reinforcements. Its excellent mechanical strength makes it ideally suited for use with high performance reinforcements, such as carbon fibre and aramids like Kevlar.

Vacuum assisted resin infusion process (VARTM) was used to infuse the dry assembly of stitched carbon fibre structures. The set-up prior to infusion is illustrated schematically in Figure 3.10. The infusion and cure cycle were performed at ambient temperature throughout the process. A flat steel platen was first prepared by coating it with a mould release agent prior to the stacking process. This allowed for the release of the cured component from the mould surface. The dry sample assembly stitched sample was placed on the mould and then enclosed in a specially-configured stack of bagging materials (such as a peel ply, infusion mesh and bagging film) before being subjected to vacuum pressure using a composite vacuum pump. Inlet and an outlet tubes were also inserted in the vacuum bagging. The outlet tube was connected to a resin catch pot and the inlet tube was connected to the resin container.

The panel was infused using an epoxy resin to hardener ratio of 100:30. Once all the air had been removed from the bag and the sample was fully compressed under this pressure, and epoxy resin was introduced to the sample panel. The epoxy resin was led by opening the inlet line and the resin allowed to flow through the part to the exit through the outlet tube under the vacuum pressure. Once the resin had been fully infused through the reinforcement, the supply of resin was cut off using a tube clamp and the resin was left to cure and the pump turned off. The infused part was then allowed to cure at room temperature for 24 hours. A complete set-up for the VARTM process is shown in Figure 3.11.

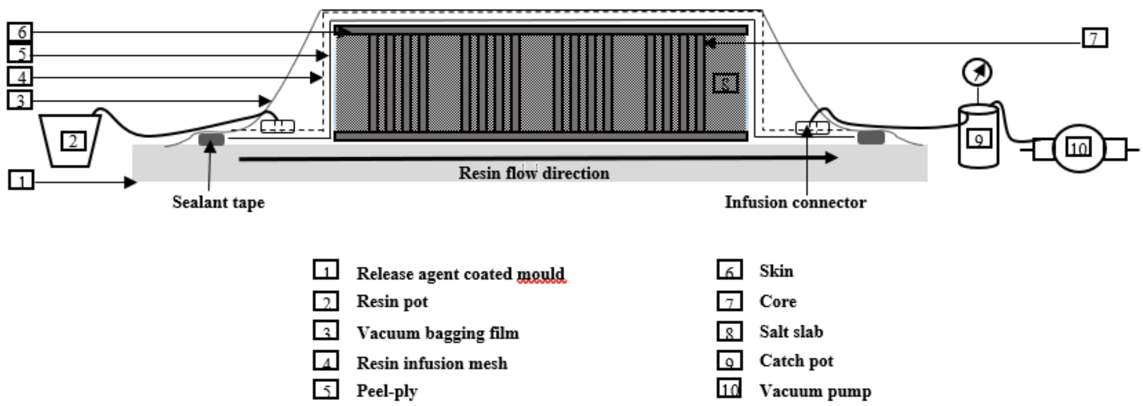

Figure 3.10. Schematic diagram used for the VARTM process.

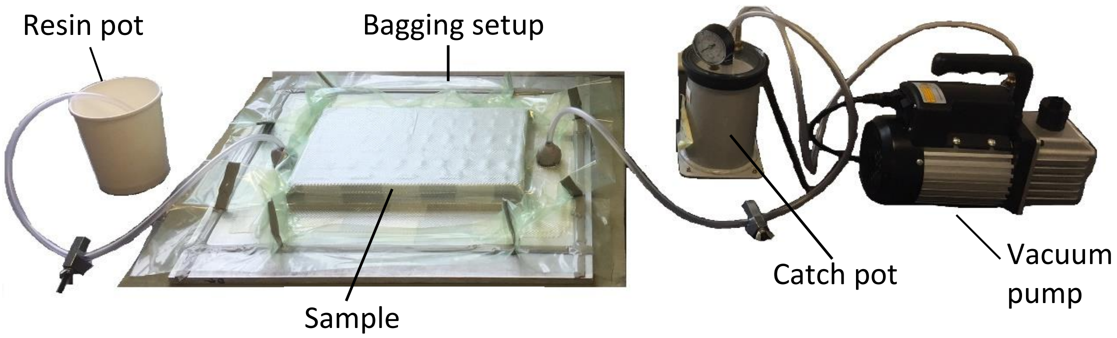

Figure 3.11. A complete setup for resin infusion process.

After cure, the panel was removed from the infusion bagging materials and the panel with the infused salt block subjected to the rock salt removal process. The panel block was kept in warm water for a few hours. Thereafter, the salt was seen completely dissolved leaving sandwich panel structure only. The panel was then machined to the appropriate dimensions for testing. The entire process was repeated to make more complex lattice core sandwich panels, such as pyramidal and modified pyramidal lattices based on 300 x 200 x37 mm salt blocks. Figure 3.12 shows photographs of the sandwich panel taken after the post-infusion process and subsequent work to cut the sample for testing.

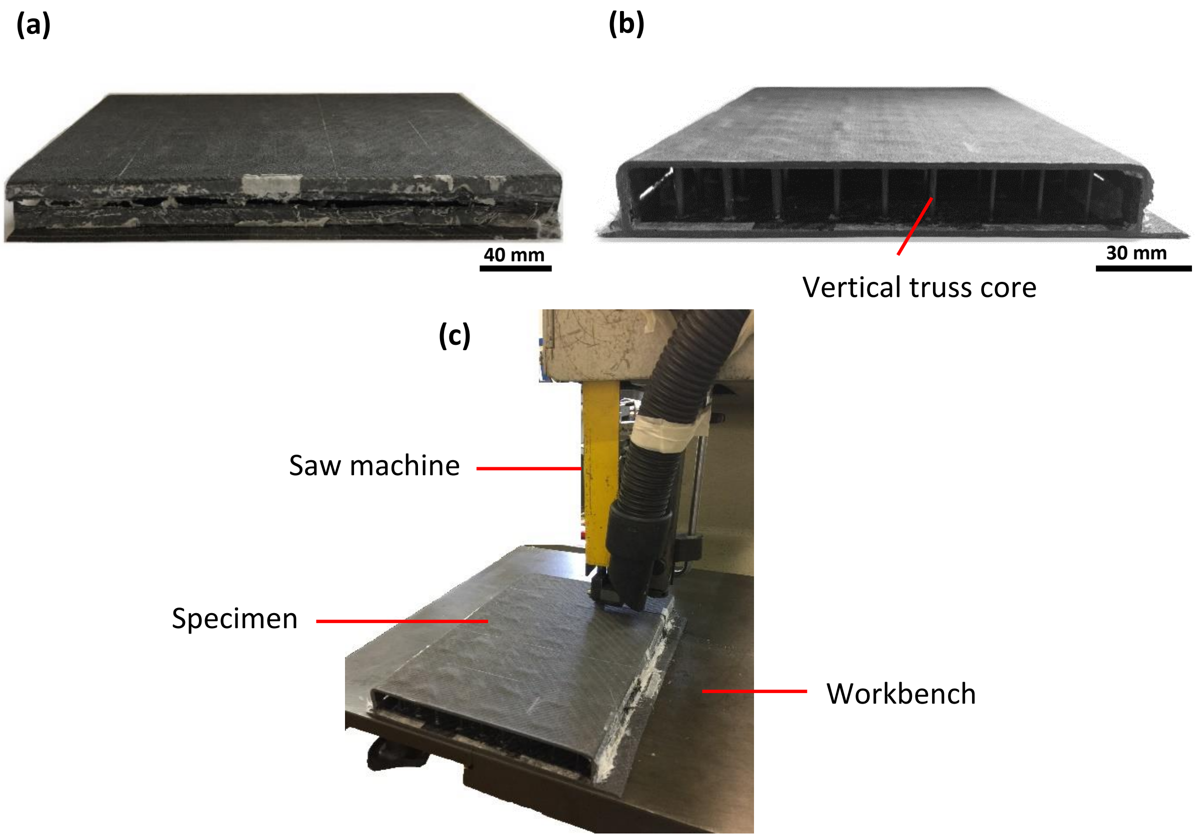

Figure 3.12. The photographs of the panel removed from infusion tooling. (a) sandwich panel (b) panel edge was trimmed and (c) panel was cut for testing.

Following a closer examination on the composite truss manufactured using this method it was evident that the resin had completely enriched the struts as illustrated in Figure 3.13. The range of composite lattice truss structures manufactured using the sacrificial mould technique are shown in Figure 3.14. The vertical lattice truss, pyramidal lattice and modified pyramidal (type-1) were manufactured in three different diameters (2, 3 and 4 mm). For the type-2 and type-3 samples, only 3 mm struts panels were manufactured.

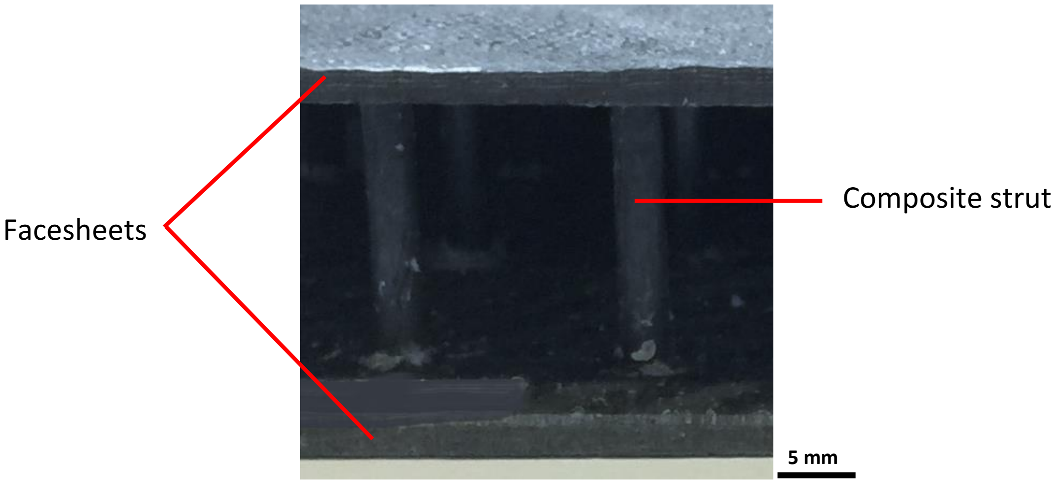

Figure 3.13. The infusion resin filled the hole completely achieving a good finish of composite strut within the panel.

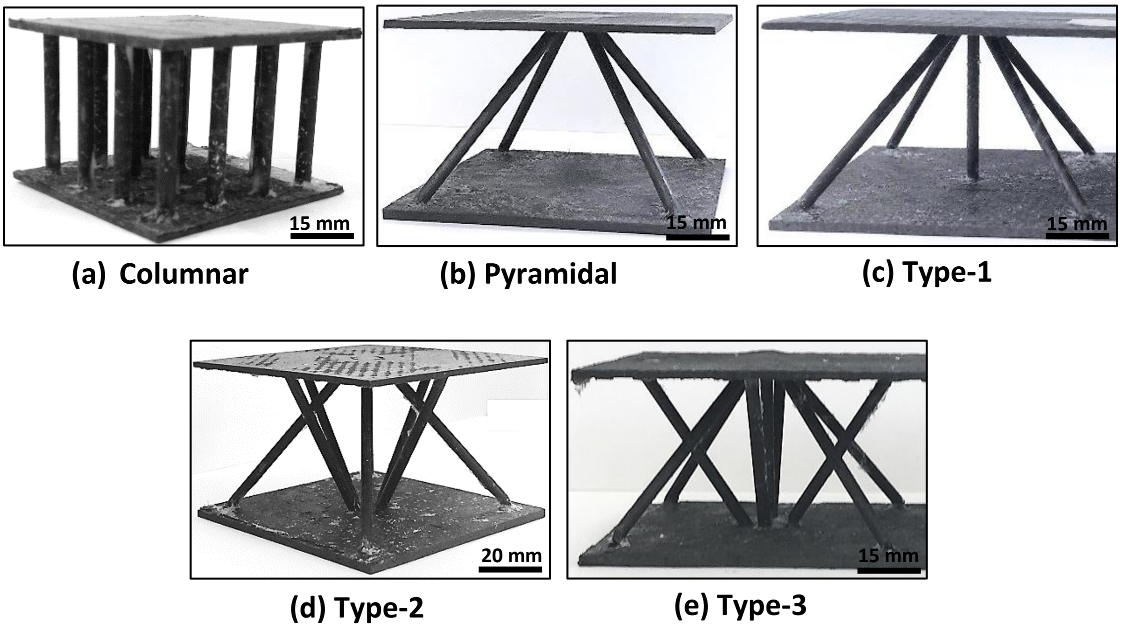

Figure 3.14. Photographs of the range of lattices core sandwich structure produced using sacrificial mould method.

3.5 Test method

The primary aim of this research was to investigate the crushing response of composite lattice structures manufactured by a sacrificial mould method. It is understood that the mechanical properties of the composite lattice core sandwich structures depend on the mechanical properties of the parent material and the geometry of the lattice core. Therefore, initial focus was to determine the fibre volume content of the composite struts which was estimated using well adopted techniques. Following this, the properties of the constituent materials were obtained by column compression tests. Thereafter, the through-thickness compressive response of composite lattice truss core sandwich structures was studied under quasi-static and dynamic loading. Quasi-static compression tests were undertaken at a constant crosshead speed to facilitate understanding the failure mechanisms and modes. In contrast, dynamic tests were carried out to imitate the actual crush impact where the velocity decreases from the initial high impact velocity to rest as the structure absorbs energy. A drop-tower is commonly used to simulate the actual impact conditions and investigate the behaviour of composite materials under dynamic condition. In this section, the test methods used to conduct the experiments are primarily described.

3.5.1 Fibre volume determination test

In the fibre reinforced material, the fibres are distributed throughout the matrix in a pattern either repeating or periodic. The cross-sectional area of the fibre relative to the total cross-sectional area of the unit cell is a measure of the volume of fibre relative to the total volume of the composite. This fraction is an important parameter in composite materials and is called the fibre volume fraction and it has a value between 0 and 1. Since the fibre and resin content affect the material's mechanical response and properties, they should be measured for each material tested and accounted for in predicting mechanical response. Here, fibre burn-off test and optical microscopy-based method were used to measure the fibre volume fraction in the composite struts.

3.5.1.1 Burn-off tests

'Burn-out' tests were carried on the composite strut specimens manufactured from sacrificial mould method to measure the fibre and resin volume fractions. This test method was conducted following ASTM D2584 "Standard Test Method for Ignition Loss of Cured Reinforced Resins" [7]. Three identical samples were tested for each carbon composite strut diameters for repeatability to obtain the average results. Before testing, the samples were measured to record the length and average diameter of the struts using calliper. Following this, the mass of an empty crucible was recorded.

A 37 mm height of carbon fibre reinforced composite struts were placed in the crucible and the total mass was determined. The crucible containing the sample was placed in a furnace which was then heated to a temperature up to 560°C and maintained at that temperature for forty-five (45) minutes.

Following this step, only the reinforcement material was left in the crucible with no visible resin remaining. The crucible was taken out of the furnace and left to cool to room temperature in a desiccator. The mass of the sample together with crucible was recorded to the nearest 0.01 g. Using this data, the mass of the sample after the burn-off test was calculated by subtracting the mass of the crucible. Terminologies and formulas used for the burn-off test are provided in Appendix.

3.5.1.2 Optical microscopy method

Composite volume fraction determinations based on an image analysis technique have been conducted with the intention of supplanting method employing matrix removal by combustion. The optical analysis of a unidirectional carbon composite strut was conducted in the following manner. The samples were sectioned along a plane perpendicular to the fibre orientation and three specimens from each were mounted in a resin as illustrated in Figure 3.15. The mounted specimen in resin was then cured for 24 hours. After cure, the mounted specimen was taken out from its container. The surfaces were then polished using standard composite microstructure preparation techniques using firm polishing laps, light pressure, and sharp abrasives to minimize the surface relief between the harder fibre-rich and softer matrix-rich regions, followed by thorough ultrasonic cleaning to remove particulate residue. Care was also taken to ensure that the polished surfaces were flat and parallel with the bottoms of the specimen mounts in order to minimize focusing errors.

Prior to image analysis, the specimens were observed in an optical microscope to obtain cross-sectional photographs at different magnifications. Epiphot 300 (Nikon Corp., Japan) microscope was used for this purpose. The equipment can be classified as an inverted microscope which can cover a range of magnification between 25x to 1000x. These are a combination between 10x of eyepiece lens and 2.5x, 5x, 10x, 20x, 40x, 60x and 100x of objective lens. This microscope was employed with an Infinity 2 microscopy monochrome CCD camera (Lumenera Corporation Inc., Canada) in order to capture digital images of microstructures. The camera comes with a resolution of 1616 x 1216 (2 megapixel). The USB 2.0 interface was used to connect this camera with software packages, Infinity Analyze and Infinity Capture (Lumenera Corporation Inc., Canada), for advanced camera control, image processing, measuring and annotation.

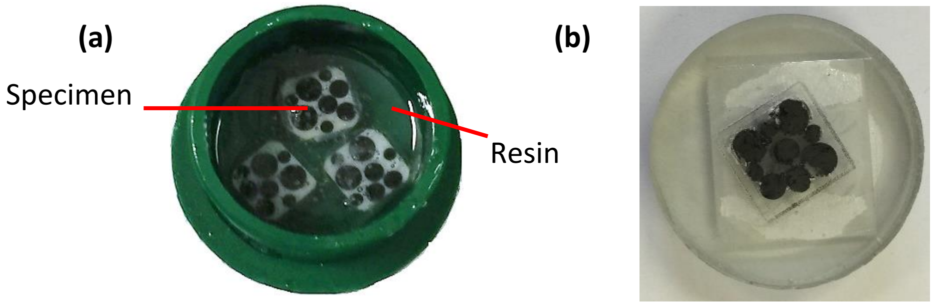

Figure 3.15. Carbon composite strut was sectioned into three section along its length and mounted in resin. (a) Specimen mounted in a resin (b) the specimen after curing.

3.5.2 Parent material compression test

As is well known, compressive responses of lattice core sandwich panels are relied on the mechanical properties of the composite struts. Consequently, such the properties can be used to predict not only the structural strength and stiffness of the structure but also the failure modes. Thus, the compressive properties of a circular cross section of carbon fibre reinforced composite was first determined before assessing the crushing response of the lattice core sandwich structures. Prior to testing, a similar fabrication method was used to produce a range of single straight rods with varying diameter and fibre volume fraction to match their corresponding lattice core sandwich structures in order to satisfy the boundary conditions of the rods. Yin et al. [9] used an approach to produce single straight composite tube from the same fabrication technique as used in their corresponding pyramidal lattice sandwich structures. The samples were cut in a square (20 x 20 mm) containing the single rod integrated with facesheets. The compressive tests on the columns were performed according to ASTM D695-15 [10] on a universal testing machine at a constant displacement rate of 1 mm/min. Five samples were tested for each test condition to take account of the variability in the test measurements. The manufactured rods and a schematic diagram of test specimen are shown in Figure 3.16. The stress-strain responses for the various rod diameters (2mm, 3mm and 4mm) and varying fibre volume fractions (0.14, 0.28, 0.37, 0.42 and 0.57) were measured. Images of the specimen deformation were also taken using a digital camera during the tests to reveal the failure modes.

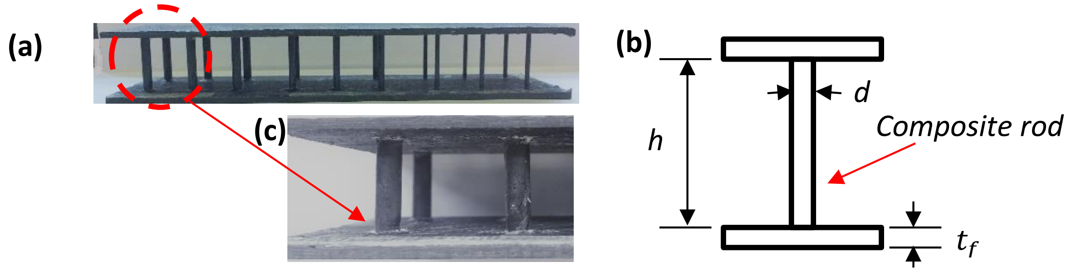

Figure 3.16. (a) Photograph of individual columns or rods (b) the dimension of the specimen, the length, h = 25 mm and facesheet thickness t_f = 2 mm (c) Connection between the skin and core via fibre stitching.

3.5.3 Quasi-static tests

To quantify the performance of the lattices, through-thickness compression tests on the composite lattice cores sandwich structures were performed at a displacement rate of 0.5 mm/min at room temperature between two steel platens. The columnar cores were constructed in arrays of four by four to form a unit cell and the square specimen was cut into dimensions of 60 x 60 mm with a core height of 39 mm. The pyramidal and modified-pyramidal (T-1) truss core sandwich structures were cut into 1x1 and 2x1 unit cells that were produced using 2, 3 and 4 mm diameter rods. The dimension of the specimens was 75 mm × 75 mm in the width and length directions, with 37 mm core thickness. Finally, the unit cells of the more complex lattice core structures referred to as of type T-2 and T-3 were manufactured using 3mm rod diameters.

A universal testing machine (INSTRON 4505) with a 100 kN load cell was used for the compression tests, and tests were performed according to the ASTM C365 Standard [11] to determine the out-of-plane compressive properties and to investigate the failure mechanisms under this loading condition. The static test set-up is as shown in Figure 3.17. At least three tests were conducted for each sample type to confirm the repeatability of the measurement and average readings were taken. The samples were compressed until the structures had been crushed up to 60 % from their original height. The applied load was measured via the load cell on the test machine, and the stress applied to the structure was obtained by calculation. The compressive stress over the specimen was calculated by dividing the measured load by the surface area of the unit cell of lattice core sandwich. The compressive strain was calculated by dividing the measured displacement by the core height assuming that the facesheets exhibit small out-of-plane displacement compared to the core [12]. Using these compression stress - strain traces, the compressive strength and compression modulus were determined. The compression modulus was obtained from the two points of the straight section of the stress-strain traces.

Furthermore, the load-displacement data were used to determine the energy absorption and specific energy absorption of the structures. The energy absorbed by the lattice core sandwich structures was calculated from the area under the load-displacement traces using the trapezoidal rule. The specific energy absorption of the structure was calculated by dividing the energy absorbed by the mass of the lattice cores. Moreover, the resultant values for the energy absorbed can be used as a parameter for undertaking the low velocity impact test, since this result is equivalent to the energy needed to completely fracture the sample.

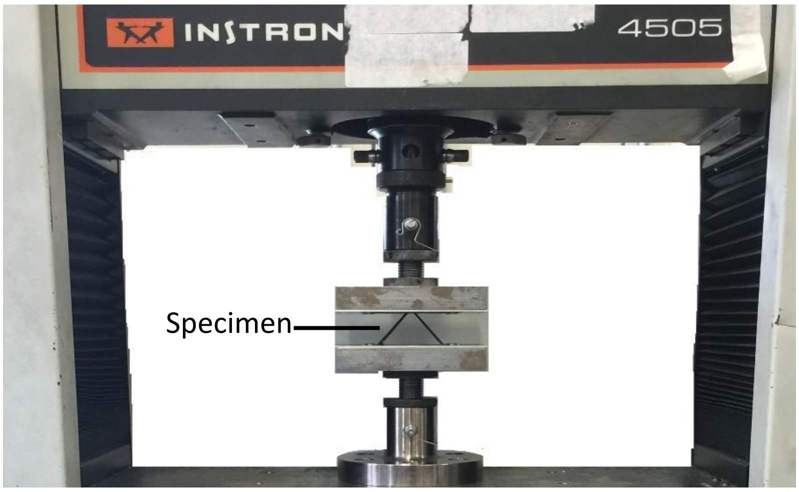

Figure 3.17. A specimen under compression loading using the Universal Testing Machine Instron 4504.

Generally, it is convenient to start the investigation by conducting quasi-static tests due to two reasons [13]. Firstly, the experimental setup for quasi-static loading is simpler than that for impact tests. Second, a quasi-static test enables us to observe, with relative ease, the detailed deformation history. However, this type of testing cannot be considered to be a true simulation of the actual event. In an actual event of a crash, a structure dissipates energy through several mechanisms during the crush process. Therefore, it is insufficient to interpret data based solely on quasi-static testing when selecting crashworthy structure. Nevertheless, information from quasi-static testing can be used in preliminary design and selection before the sample is crushed dynamically. Since an impact test requires expensive equipment, such as a high-speed video camera, high frequency data loggers and load cells, data from quasi-static tests can be used in predicting the failure modes and the energy absorption characteristics of a sample to prevent potential damage of equipment.

3.5.4 Low velocity impact tests

It is well known that sandwich panels are susceptible to impact damage caused by runway debris, hailstones, dropped tools and others. Therefore, the low velocity response of composite lattice cores sandwich structures is investigated using flat head impact mass. The low velocity impact tests were conducted using a drop-weight tower. The impact machine was built 'in house' and had a height of 2 m with the impact mass being guided on the steel rails as depicted in Figure 3.18. The impact test relies on the free falling of a known mass from a given height that carrying a certain amount energy to deform the specimen, which is loaded axially. Relatively, the mass and the height of the impactor can adjust to obtain the desired impact energy, E based on test requirements. This energy can be obtained using the following formula:

$$E = mgh \tag{3.7}$$

Here, the m is the impactor mass in kilograms (kg), g is the gravitational constant (9.81 m/s^2) and h is the impactor height in metre (m).

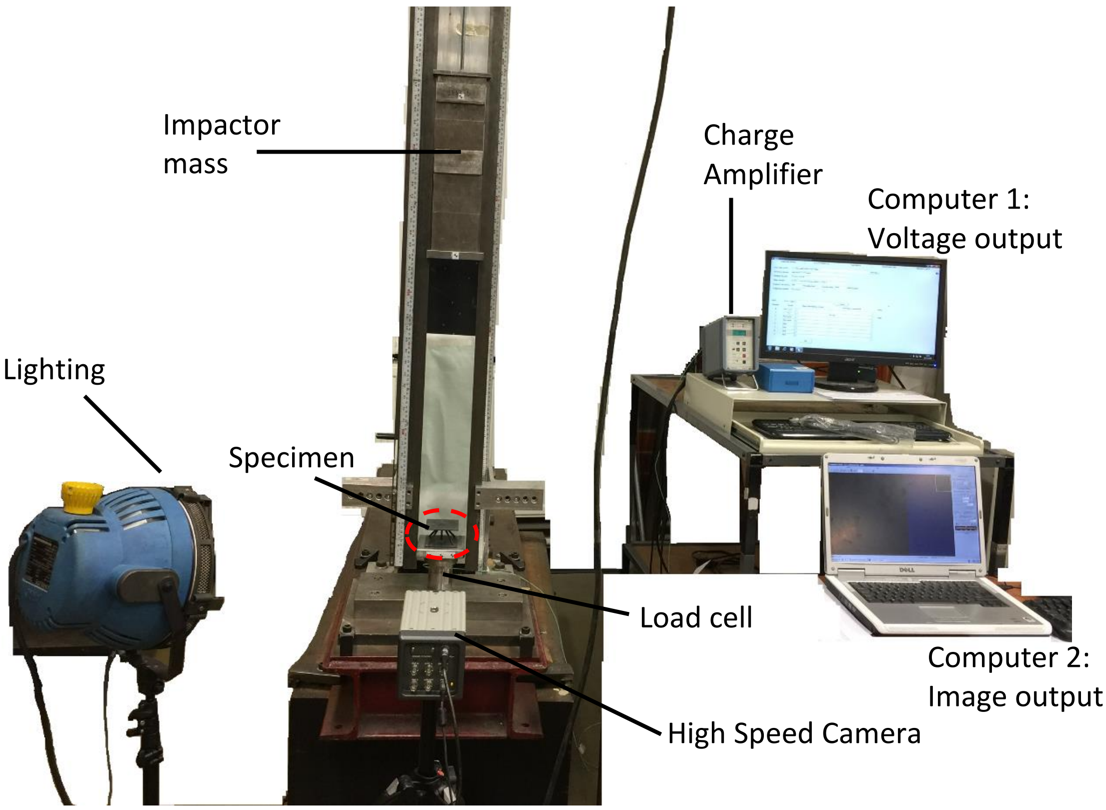

Figure 3.18. The drop-weight impact test facility at the University of Liverpool.

Prior to testing, the test specimens were placed on the impact plate and positioned parallel to the direction of the impactor, as shown in Figure 3.19. Initially, a flat rectangular impactor, with dimensions of 120 mm x 80 mm was raised to a predefined level depending upon the velocity and impact energy. The movement of the impactor was guided by two greased steel rails with a ±0.5 mm clearance. Therefore, the contact between the impactor and rails was assumed to be frictionless. The impactor was released once the entire test configuration was ready. The dynamic compression tests were stopped when the specimens had been completely crushed and bottomed-out [14]. Load data were collected from a piezoelectric load cell, while the displacement during crushing was recorded by the high-speed video camera. A load-cell mounted underneath the impact plate measured the voltage-time histories during the impact event. The Kistler type 9363A load cell, with measuring range of 120 kN, was connected to a charge amplifier using an insulated co-axial cable. Details of the load cell and the charge amplifier are given in Table 3.4 and Table 3.5, respectively [15,16].

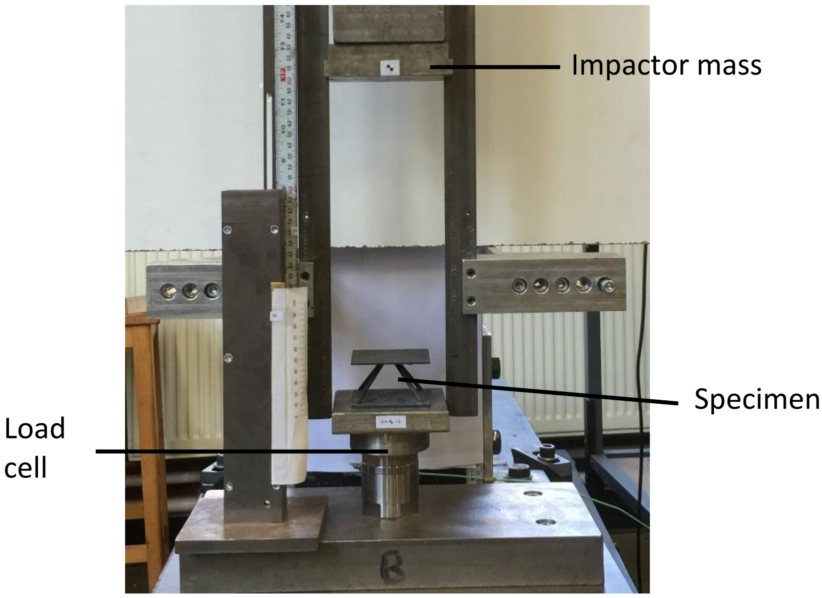

Figure 3.19. Position of the specimen on the load cell and impactor.

Table 3.4. Details of the piezoelectric load cell (Kistler type 9363A) [14].

	Unit	Value
Measuring range	kN	0 – 120
Sensitivity	pC/N	– 3.8
Natural frequency	kHz	>35
Weight (without cable)	g	800

Table 3.5. Details of the Kistler amplifier type 5011B [15].

	Unit	Value
Measuring range for 10 V FS	pC	± 10 – ± 999 000
Sensor sensitivity (M.U. = mechanical units)	pC/M.U.	± 0.01 – ± 9 999
Frequency range (-3db, Filter "OFF"	kHz	≈ 0 – 200
Weight	kg	≈ 2

During an impact event, the mechanical force was recorded by a pressure sensor in the load cell and converted to an electrical signal. Since the electrical signal is in order of millivolts, amplification of the signal was undertaken by a charge amplifier. A digitiser device was used to convert the analogue signals into digital signals, and these were recorded using a computer. Finally, the force (in Newton) readings were obtained by converting the voltage using a scaling factor of 12,000 N/V which was found by conducting a static calibration on the Instron Machine.

The motion of the impactor was captured using a high-speed video MotionPro X4, model no. X4CU-U-4 with a standard F/0.95-50 mm lens positioned in front of the impact rig, as shown in previous Figure 3.18. For all impact tests, the frequency of the high-speed video was set to 5,000 frames per second. Before conducting the test, a target with a 15 mm scale was placed on the surface of impactor to enable the high-speed video to track the motion. The video file was captured and processed using MotionPro software, Version 2.30.0. This video file was then analysed and calibrated using the 15 mm scale and the motion analysis software, ProAnalyst, to produce the displacement data. A further analysis using Mathlab 2014a software was required to calibrate the force data to the displacement data.

3.5.4.1 ProAnalyst motion analysis

ProAnalyst is a leading software package for automatically measuring moving objects recorded in video. ProAnalyst enables to import any video and quickly extract and quantify motion within that video [17]. ProAnalyst is the ideal companion software to any prosumer, scientific and industrial video camera which is used extensively by engineers and researchers. Any digital video camera becomes a measurement instrument with ProAnalyst. Given the capabilities of ProAnalyst software, all impact tests conducted in this research project were captured using high-speed camera and stored as video files. The video file was then processed using ProAnalyst extract motion features from video sequences and to track those features throughout the crushing sequence of the specimens.

For example, Figure 3.20 shows the video image acquired from the impact test on pyramidal lattice core sandwich specimen. Initially, the video file imported to ProAnalyst software was set 5000 frames per second to match with frequency set in high-speed camera. Following this, the video image was calibrated to set the scale length using the target scale marking on the platen as shown in Figure 3.20. Once the impactor touch the specimen, the tracking feature calibration tool was then used to track the motion of the platen as it crushes the specimen fully. Following the tracing of the motion using feature tracking tool in a ProAnalyst, resulting data, for example, displacement, velocity and time were extracted from this analysis.

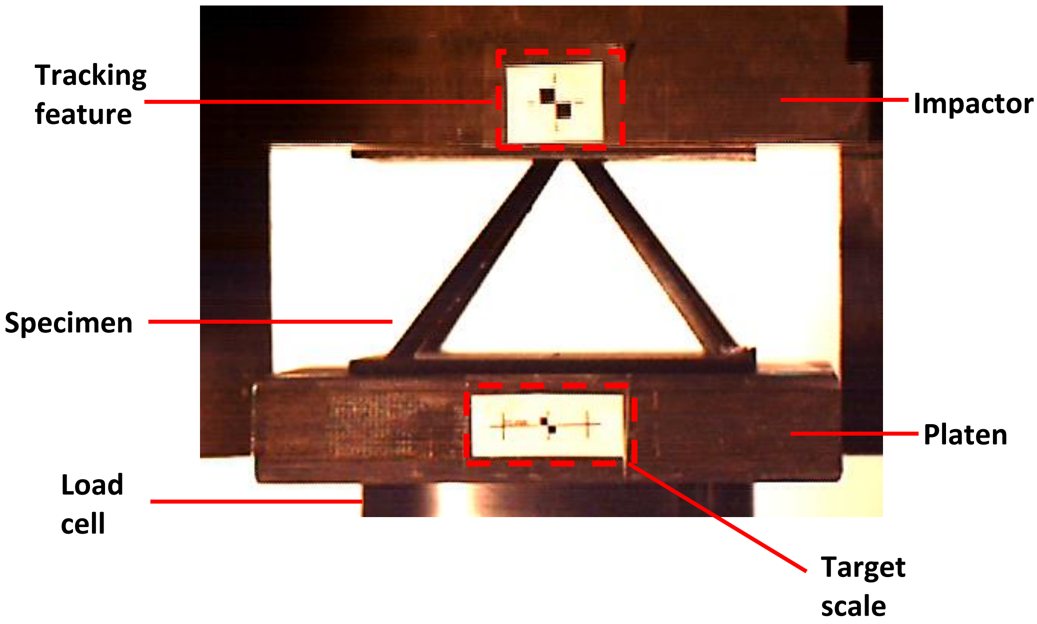

Figure 3.20. The motion captured in high-speed camera which is imported to ProAnalyst for an analysis.

3.6 Summary

This chapter has presented the manufacturing method of fabricating carbon fibre reinforced composite lattice cores sandwich structures using sacrificial mould method. Firstly, it covers the preparation of materials and the procedures to configure the features of lattice cores on the sacrificial mould. This is followed by the detailed manufacturing method to fabricate the lattice core sandwich panel samples. Finally, the experimental set-up for various tests on fibre volume determination, quasi-static compression and low-velocity impact are described.

References

[1] Y. Sun and L. Gao, Mechanical behavior of all-composite pyramidal truss cores sandwich panels, Mechanics of Materials, 65, 2013, pp56–65.

[2] Pyrofil TR Series Fibre DataSheet, Mitsubishi Rayon Co., Ltd., 2013. Available: https://www.mrc.co.jp.

[3] GRAFIL 34-700 12k Fibre Datasheet, Mitsubishi Chemical Carbon Fiber and Composites, Inc., 2013. Available: http://mccfc.com.

[4] https://westlabsalts.co.uk/collections/shower-washes.

[5] https://www.cousinsuk.com/product/wax-blocks.

[6] H. Kim, B. H. Cho, H.-K. Hur, and K.-J. Kang, A composite sandwich panel integrally woven with truss core, Materials and Design, 65, 2014, pp231–242.

[7] ASTM D2584 − 11. Standard test method for ignition loss of cured reinforced resins, ASTM, PA, USA; 2011.

[8] I.M Daniel and O. Ishai, Engineering mechanics of composite materials, 2nd Edition, Oxford University Press, 2006.

[9] S. Yin, L. Wu, L. Ma, and S. Nutt, Pyramidal lattice sandwich structures with hollow composite trusses, Composite Structures, 93, 2011, pp3104–3111.

[10] ASTM D695 – 15. Standard test method for compressive properties of rigid plastics, ASTM, PA, USA; 2015.

[11] ASTM C365 – 15. Standard test method for flatwise compressive strength of sandwich cores, ASTM, PA, USA; 2015.

[12] C. Schneider, M.N. Velea, S. Kazemahvazi, and D. Zenkert, Compression properties of novel thermoplastic carbon fibre and poly-ethylene terephthalate fibre composite lattice structures, Materials and Design, 65, 2015, pp1110–1120.

[13] G. Lu and T. Yu, Energy absorption of structures and materials, Woodhead Publishing Limited, Cambridge, England, 2003.

[14] N. Jones, Structural impact, 2nd Edition, Cambridge University Press, 2011.

[15] www.kistler.com

[16] www.intertechnology.com/Kistler/pdfs/ACC_5011B_Charge_Amplifier.pdf.

[17] www.xcitex.com/Literature/ProAnalystBrochure.pdf

4 Results and Discussion

This chapter presents the results obtained from the experiments and discusses the outcomes. Initial attention is focused on fabricating simpler lattice core sandwich panels made of vertical struts based on a carbon fibre reinforced epoxy composite. The mechanical response of this panel was obtained following quasi-static compression tests. The influence of the fibre volume fraction and strut diameter were also investigated and presented. Prior to this, the column compression test results on individual reinforcing members with varying fibre volume fraction and strut diameter are discussed. This is followed by the results on carbon fibre reinforced epoxy pyramidal based lattice core sandwich structures under quasi-static and dynamic loading. Finally, the failure mechanisms on the structures that were observed during and after the tests are presented and characterised.

4.1 Fibre volume fraction

The fibre volume fraction within each individual member was varied by increasing the number of fibre tows during stitching process. The study aims to maintain the fibre volume fraction in different member sizes to near agreement as possible as to permit a fair comparison between them. Initially, the fibre volume fraction considered for reinforcing the strut was calculated using Equation 3.3 or 3.6 in Chapter 3. For example, by considering the 2 mm circular cross-section of the composite strut, the fibre volume fraction of the carbon fibre containing single tow is computed by:

$$V_f = \frac{12000\, n\, {d_f}^2}{{d_c}^2} = \frac{12000\,(1)(7\times10^{-3})^2}{(2)^2} = 0.147 \tag{4.1}$$

or

$$V_f = \frac{n \times Fibre\ mass\ per\ unit\ length}{\pi r^2 p_f} = \frac{1\times 0.0008}{\pi \times 1^2 \times 0.0018} = 0.141 \tag{4.2}$$

where , d_f, ρ_f, and d_c or r denote the number of fibre tows, filament diameter, fibre density and the diameter or radius of the struts. Table 4.1 gives details of the carbon fibre tows used to produce different groups of fibre volume fractions for various sizes of composite strut obtained from the above relationships. The carbon fibre tow has a designation of 12K, consisting of 12,000 filaments.

Table 4.1. Summary of the carbon fibre tow in composite strut.

Fibre volume fraction range	Strut diameter (mm)		
	2	3	4
	Carbon fibre tow counts		
0.126 – 0.147	1	2	4
0.353 – 0.392	2.5	6	10
0.424 – 0.457	3	7	12

Here, 2.5 carbon fibre tow count refers to two strands of carbon fibre containing 12K filaments and 1 strand of carbon fibre containing 6K filaments of the same fibre type. The estimated carbon fibre volume fraction is further verified by conducting resin burn-off tests.

A burn-off test is a common approach to measure the volume fraction of the constituent of a composite material. The samples for this test were the individual carbon fibre composite struts that were detached from vertical truss core sandwich panels. Three different struts sizes with diameters of 2, 3 and 4mm, were investigated. Figure 4.1 shows the vertical truss core sandwich panels that were manufactured using the sacrificial method with a different content of carbon fibre volume fractions consisting various strut sizes. The struts were based on a unidirectional carbon fibre reinforced epoxy resin that produced using vacuum assisted resin infusion process.

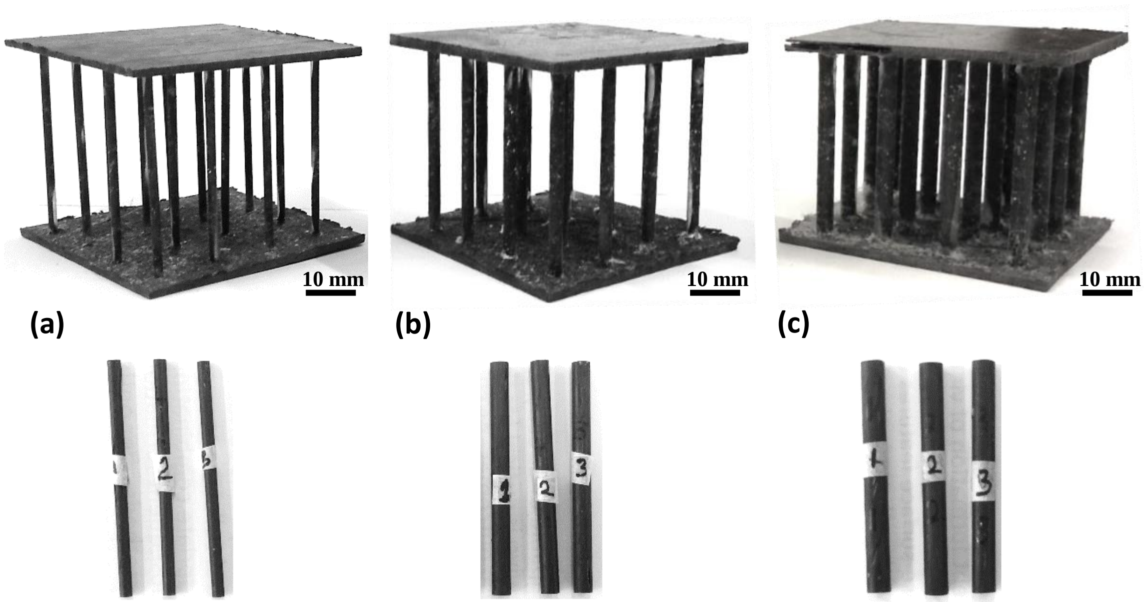

Figure 4.1. Vertical truss core sandwich panels with various sizes and the individual members that cut from the panels for burn-out test (a) 2mm (b) 3mm and (c) 4mm.

Three identical struts were selected from each size to weigh the mass of the sample due to lightness of the strut. Following this, three samples were taken for considering each strut size according to different group carbon fibre tow counts for repeatability. The volume fraction of the fibres in the composite struts was obtained by burning off the resin in a furnace at a temperature of 560 °C [1,2]. This temperature was found to be sufficient to remove the resin completely leaving the fibres remaining. Table 4.2 gives a summary of the carbon fibre reinforced epoxy resin struts following the burn-off tests. By weighing the fibre residue from the burn-out test, parameters such as the volume fraction, V, volume of the sample, v_s, weight fraction, W and density, ρ_s, were determined. For example, by considering the G3-4 sample, the weight fraction of the carbon fibre and epoxy resin matrix were determined by [3]:

$$1 = W_f + W_m \tag{4.3}$$

$$W_f = \frac{m_f}{m_s} = \frac{1.455}{2.719} = 0.535$$

$$W_m = \frac{m_m}{m_s} = \frac{1.264}{2.719} = 0.465$$

The volume of a sample is related to the density of the constituents of the composite material in which the density of the carbon fibre it was given as 1.8 g/cm^3 and 1.1 g/cm^3 for epoxy resin according to manufacturer catalogue. Thus, the volume of the G3-4 sample can be calculated by:

$$v_s = v_f + v_m \tag{4.4}$$

$$v_f = \frac{m_f}{\rho_f} = \frac{1.455}{1.8} = 0.808$$

$$v_m = \frac{m_m}{\rho_f} = \frac{1.264}{1.1} = 1.149$$

$$\therefore \; v_s = 1.957$$

Volume fraction which refers to the fibre content is given by:

$$1 = V_f + V_m \tag{4.5}$$

$$V_f = \frac{v_f}{v_s} = \frac{0.808}{1.957} = 0.413$$

$$V_m = \frac{v_m}{v_s} = \frac{1.149}{1.957} = 0.587$$

The density of the sample is obtained from the relationship that known as rule of mixtures:

$$\rho_s = \rho_f V_f + \rho_m V_m \tag{4.6}$$

$$\rho_s = (1.8)(0.413) + (1.1)(0.587)$$

$$\rho_s = 1.39\ g/cm^3$$

By referring to the results obtained from the burn-off tests for fibre volume content it was found that there are slight discrepancies between the values obtained between the measurements and predictions. However, these values are closer to the estimated values using the method of fibre mass per unit length following the ratio of volume of fibre to that of volume of the struts compared to that of cross-sectional area ratio method. Figure 4.2 illustrates the fibre volume content in the composite struts for different diameters using the theoretical formula (volume ratio) and by burn-off tests. Here, the terms G1, G2 and G3 refer to the different groups of estimated fibre volume range.

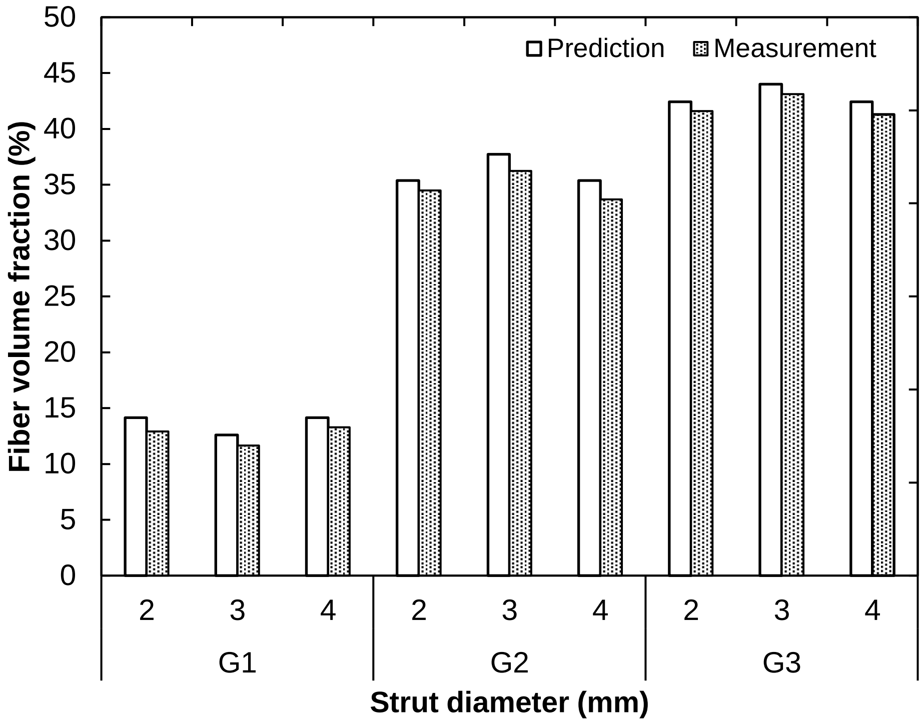

Figure 4.2. Fibre volume fraction in composite strut manufactured using various number of continuous carbon fibre tow by resin infusion process

Table 4.2. Summary of the carbon fibre tow in composite strut with various diameters following burn-off tests.

Specimen	Sample ID	Mass sample, m_s [g]	Mass fibre, m_f [g]	Mass matrix, m_m [g]	Fibre volume fraction, V_f	Matrix volume fraction, V_m	Fibre weight fraction, W_f	Matrix weight fraction, W_m
G1	G1-2	0.427	0.083	0.343	0.129	0.871	0.194	0.803
	G1-3	0.977	0.173	0.803	0.117	0.884	0.177	0.822
	G1-4	1.713	0.343	1.370	0.133	0.867	0.200	0.800
G2	G2-2	0.447	0.207	0.240	0.345	0.655	0.463	0.537
	G2-3	1.017	0.490	0.527	0.362	0.638	0.482	0.518
	G2-4	1.843	0.837	1.007	0.337	0.663	0.454	0.546
G3	G3-2	0.707	0.380	0.326	0.416	0.584	0.538	0.461
	G3-3	1.565	0.866	0.699	0.431	0.569	0.553	0.447
	G3-4	2.719	1.455	1.264	0.413	0.587	0.535	0.465

Overall, based on the results obtained from burn-off tests for G1, G2 and G3 ranges, it was found that the values differ from the estimated value on average less than 5%. Furthermore, it was noticed that the percentage of differences is much lesser when the number fibre tows were increases in the making of composite struts from G1 to G3 range. In this case, the differences were related to uncertainties in the measurements and imperfections caused during the manufacturing process such as voids and impurities. Nevertheless, the predictions from the volume ratio method are considered reliable and in good agreement with the measurement values. This was further verified using image analysis with optical microscopy.

Optical microscopy was used to qualitatively image the fibre packing arrangement and resin rich region in the composites. Samples from carbon fibre composite struts having different diameters were subsequently sectioned and polished to characterise the arrangement of fibres in the cross-section. Here, three cross-sections from each composite strut were taken. The samples were sectioned by cutting them across their diameters using a diamond-tipped saw to obtain the cross-section. Each sample was then mounted in a resin pot and post-cured in preparation for the grinding and polishing process. A Buehler grinding and polishing machine was used, according to the recommended four step procedures for preparing polymer-matrix composite samples. An image analysis of each cross-section was undertaken, and the fibre volume fraction was calculated using Image J software.

The micrographic images captured using the microscope over a range of magnifications between 25x to 1000x were imported to Image J to be analysed. The images are then prepared for particle analysis by converting the image to an 8-bit image. Following this, the particles were detected by adjusting the threshold parameters until the phase for which to determine the volume fraction is all red. The grey background of original image would just be disappeared under the red. By applying this condition, the image was turned to black and white. Finally, particle analysis was performed by running the analysis to determine what fraction of the area of this image is black. Through a repeated process, the fibre volume measurements can be obtained. Figure 4.3 depicts some portion of the image of particles representing the individual filament of a carbon fibre tow that distributed across the cross section of the strut. This individual filament has been numbered according to particle counts across the cross-section that obtained through particle analysis in Image J. The particle in the area fraction measurement was also included in Figure 4.3.

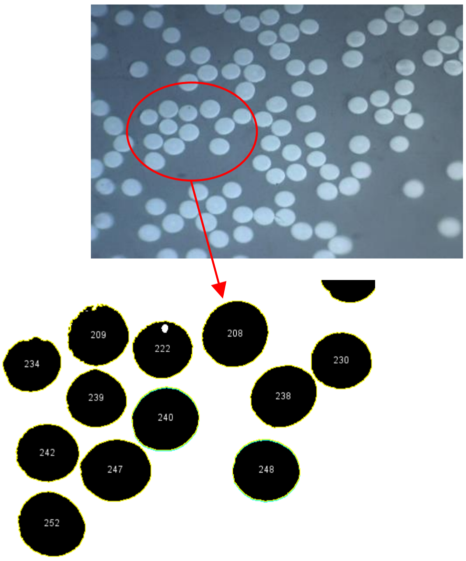

Particle	Area (μm^2)
208	34.733
209	31.193
222	30.465
230	31.339
234	30.320
238	34.116
239	31.105
240	33.092
242	31.230
247	34.693
248	32.785
252	34.849

Figure 4.3. An example of the image after running a successful particle analysis using Image J and their corresponding area measurement.

It was evident that from the particle analysis the cross-section of individual fibre filament is not in a uniform diameter. The fibre volume fraction which was estimated using the cross-sectional area of the filaments is found to be overestimated the values as it uses filament diameter of 7 µm as provided by the manufacturer. The average filament diameter that found from the particle analysis was 6.4 µm. This further suggested that the fibre volume fraction obtained using fibre mass per unit length following the ratio of volume of fibre to that of volume of the struts was reasonable. In this study, the highest fibre volume fraction achieved for measurement purposes was ranging from 42 to 44%, whilst the lowest content was about 13% to 14%. Figure 4.4 shows the typical cross-section images of the composite struts under optical microscopy for different fibre content.

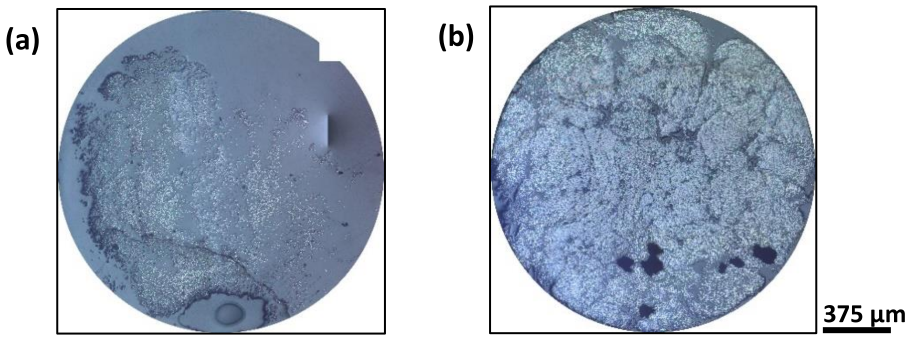

*Note: Difference in colour due to the effect of lighting in microscope while capturing the images.

Figure 4.4. Optical micrograph of the composite struts (a) 3 mm diameter, $V_f = 0.14$ (b) 3 mm diameter, $V_f = 0.42$.

Figure 4.5 shows some of the images captured for different diameter struts following manufacture. An examination of the cross-section indicates that the fibres are distributed across the sample as the fibre content increases, although there is a small region of resin enrichment in one region close to the surface of the cylinder. It is also clear that the fibres appear to be fully impregnated by the resin, with no evidence of any voiding in a lower fibre content and slightly little voids being there for higher fibre volume that can be visually observed from the microscopic images. It was reported by Shah et al. [4] in his work that this is possibly due to the changing resin flow dynamics with fibre content although there was no clear correlation between composite fibre volume fraction and porosity. In essence, fibre content may not have an obvious effect on void content, but it does influence the type of voids formed. Nevertheless, an examination of the cross-section images of the composite struts revealed having good fibre-matrix bonding across the region.

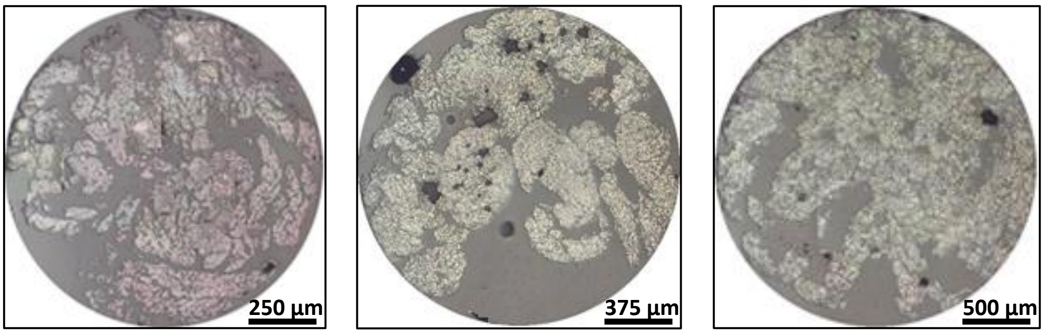

(a) **(b)** **(c)**

*Note: Difference in colour due to the effect of lighting in microscope while capturing the images.

Figure 4.5. Optical micrograph of the composite struts (a) 2 mm diameter, $V_f = 0.35$ (b) 3 mm diameter, $V_f = 0.37$ (c) 4 mm diameter, $V_f = 0.35$.

From the micrograph of the images, it is evident that the fibres are located towards the centre of the cross-section, leaving a distinct resin-rich area close to the circumference of the strut. This is clearer as the fibre fraction volume within the struts increases from 0.14 to 0.42, where more uniform fibre distribution within the cross-section is found, although resin-rich regions are in evidence. It is desirable to have an even distribution of fibre through the cross section of the strut. Resin-rich regions are relatively weaker than the remaining portions of the strut resulted in an undesirable variation in mechanical properties. The fibre spreading within the cross-section of struts during fibre stitching may need to be improved to achieve better fibre distribution.

4.2 Column compression performance

The mechanical properties of composite struts with different aspect ratios (d/l) will vary according to the particular fibre volume fraction. Thus, the carbon fibre individual struts were tested in uniaxial compression along the fibre directions in order to determine the compressive properties of the parent material used to manufacture lattice cores. The circular struts with diameters of 2, 3 and 4 mm have varying fibre volume fractions of 14, 28, 35, 42 and 57 % were tested to measure their compressive properties. Figure 4.6 shows some examples of measured nominal stress-strain curves of individual struts following compression tests for fibre volume fraction of 14 %.

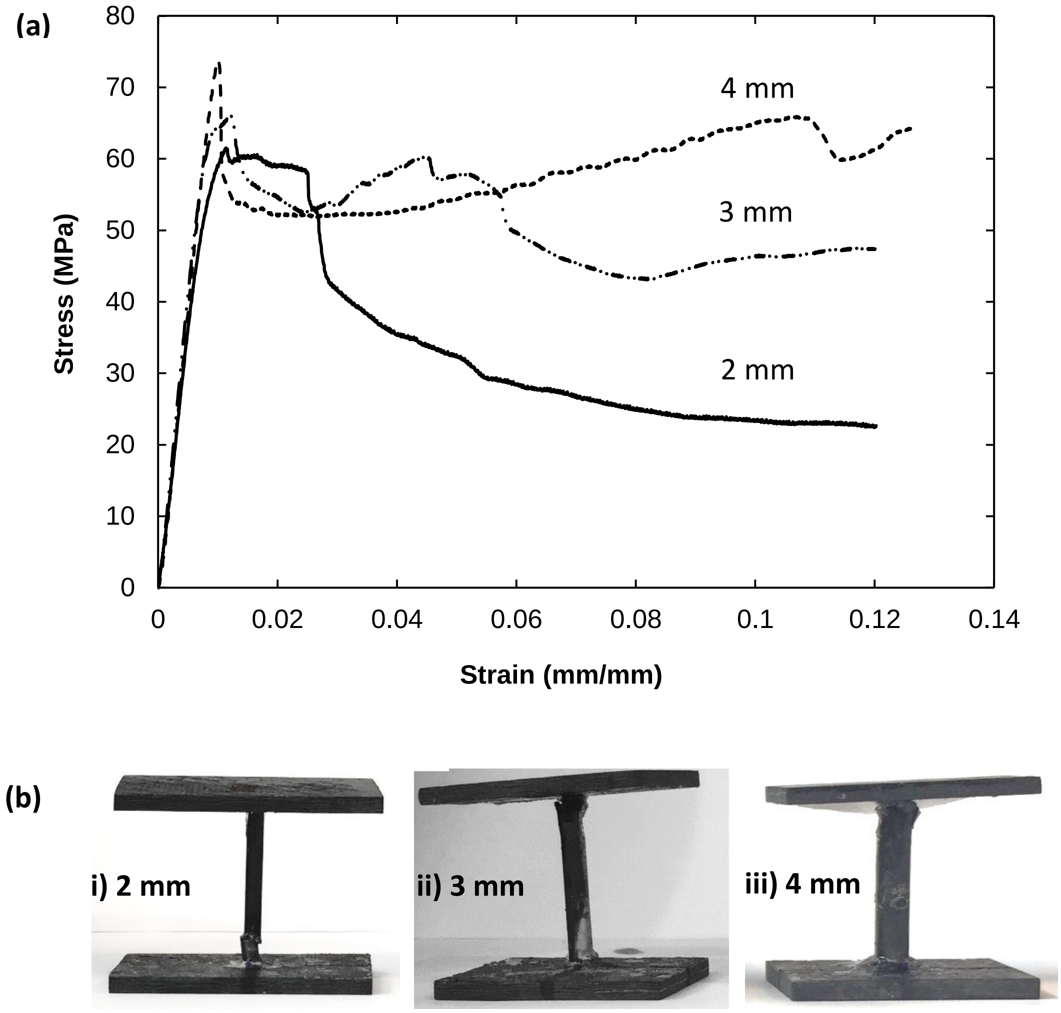

Figure 4.6. (a) The measured compressive stress-strain curves of composite struts (b) The photographs of the failure modes of the struts. $V_f = 0.14$.

The stress-strain curve for 2 mm diameter specimen displays a linear elastic response up to the initial failure at approximately 62 MPa, followed by gradual decrease in stress before an abrupt failure occurs at strain about 2.5 %. It was observed on the specimen during the testing that the initial failure occurred by buckling within the struts. This resulted in microbuckling forming within the strut and a sudden fracture near to one end of the struts slightly distant from the interfacial connection. Photograph (i) in the Figure 4.6b shows the failure process in a typical strut, where it is evident that the strut has failed as mentioned. The curves for the 3 mm diameter specimen also demonstrated that the compression strength increases linearly for strain values up to 0.01 before a failure occurs and the strut begins to be splitting near to the facesheet connection. The stress then decreases slightly with a fluctuation before it begins to drop gradually as the splitting and cracks continue as can be seen in the photograph (ii) in the Figure 4.6b. The stress-strain curve for the 4 mm diameter specimen with a lower fibre volume fraction of 0.14 also exhibit a linear response initially up to a compressive strength at approximately 76 MPa prior to initial failure. An observation of test specimen during the testing indicates that the failure occurred at the one end of strut with localised crushing in the form of splitting noticeable. The photograph (iii) in Figure 4.6c clearly shows that the struts fail via crushing, absorbing significant energy in the process.

Alternatively, Figure 4.7 shows the measured nominal stress-strain curves of individual struts for a higher fibre volume fraction of 57% following compression tests. Here, the stress-strain traces for 2 mm diameter specimen rises in a linear fashion, followed by initial failure at about 180 MPa. At this point, it can be noticed that the stress drops a little and gradually increases to another point where again the stress dropping. This is followed by a gradual increasing prior to an ultimate failure as illustrated in Figure 4.7a. The test specimen during testing shows that initial failure is caused by fibre microbuckling and the subsequent failure initiated by the crushing of the strut at the end of joint. This crushing takes in the form of fibre splitting and cracks at the joint before an abrupt rupture of the strut as shown in photograph (i) in the Figure 4.7b. The stress increases linearly with a strain for 3 mm diameter specimen to the strength value approximately at 215 MPa, then drops slightly and further increases to nearly 285 MPa prior to ultimate failure. Failure of the specimen initiated by fibre microbuckling and followed by splitting and cracking at one end of the strut. During this failure process, greater energy was absorbed by the specimen as characterised by the stress-strain trace in Figure 4.7b and the image of the failed specimen in the Figure 4.7b (ii). A similar incident was observed for 4mm diameter specimen, where the stress increases linearly up to approximately 315 MPa. This is followed by a significant reduction of stress initially and subsequent relatively mild decrease of stress over the strain approaching 24%. The crushing of the strut in the form of splitting and cracking was a dominant failure mode as shown in the photograph (iii) in the Figure 4.7b. It was evident that failure modes were observed to be crushing with no sign of buckling mode when higher fibre volume fraction used.

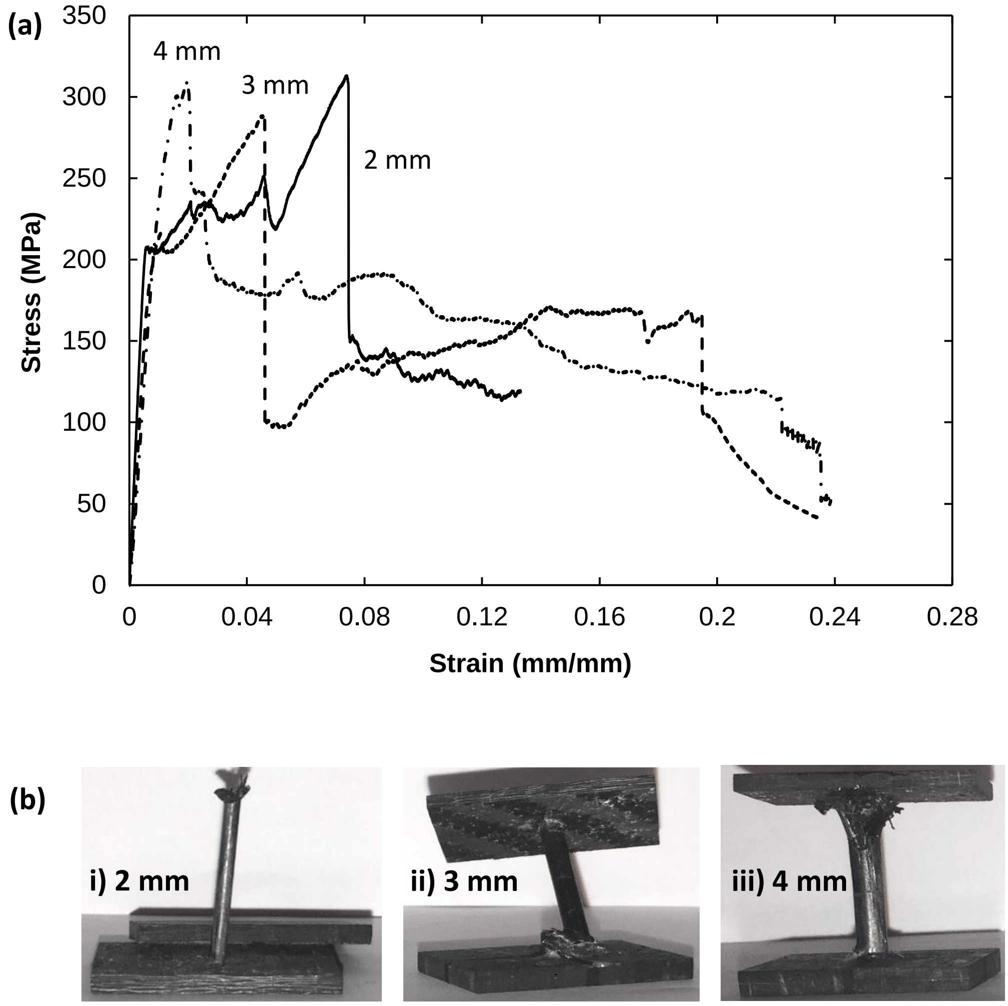

Figure 4.7. (a) The measured compressive stress-strain curves of composite struts (b) The photographs of the failure modes of the struts. $V_f = 0.57$.

It was worth noting that the stress-strain traces of the individual struts following compression tests show a larger strain under compression tests for struts with higher volume fractions (0.35, 0.42 and 0.57) than that of struts with lower fibre volume fraction (0.14 and 0.28). Overall, the failure modes observed for struts compression tests were buckling, fibre micro-buckling, splitting, cracking and crushing of the struts. Figure 4.8 shows the stress-strain curves following compression tests on individual struts with a diameter of 3 mm based on nominal fibre volume fraction of 0.14, 0.28, 0.35, 0,42 and 0.57. The traces for all samples demonstrated a linear region for small strain approximately less than 1 % and subsequent traces reflecting to failures occurred within the struts. It is important to note that the tests for samples with fibre volume fractions of 0.14, 0.28 and 0.35 has been stopped when it approaches strain value of approximately 12 % due to factors that could not be controlled during the testing process. Several factors, such as the struts deviation from the centreline of the fixture and struts slipping, could be observed during struts failure.

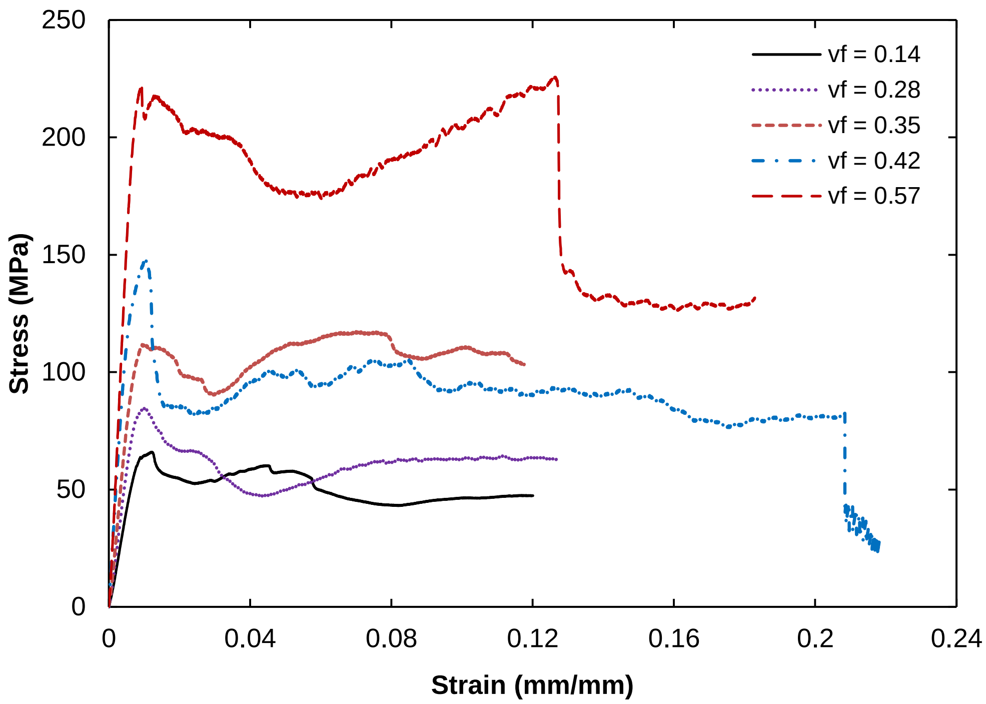

Figure 4.8. Typical measured compressive stress-strain curves of composite struts under various fibre volume fractions, $d = 3\ mm$.

It is worth noticing that increasing the fibre volume fraction of the struts leads to an improvement in strength, as seen in Figure 4.8. Furthermore, increasing the fibre fraction also effectively increases the modulus of the struts, which is evident from the gradient of linear region of the stress-strain traces. Figure 4.9 gives the summary of the compression strength prior to struts initial failure based on various nominal fibre volume fractions for different struts aspect ratio. It is clearly showing that the compression strength is influenced by the fibre content within the composite struts where the measured strength increases with the increasing fibre volume fraction. Subsequently, the compressive strength is also increasing when the strut aspect ratio increased from 0.08 to 0.16. Lower aspect ratio struts failing by plastic microbuckling, exhibited an increase in strength ranging from 44 MPa to 155 MPa when the fibre volume fraction was increased from 14 % to 0.57 %. Meanwhile, the struts failing by crushing at higher aspect ratio indicated that the strength increases from 72 MPa to 213 MPa when fibre fraction increased. This clearly shows an increase of 250% and 196% in strength for the lower and higher aspect ratios, respectively. Alternatively, the compressive strength increased by 64% in samples based on the lowest fibre volume fraction and by 38% for samples at the highest fibre fraction. It is revealed that the failure mode transitioned from microbuckling to crushing of the struts as the fibre volume fracture increased.

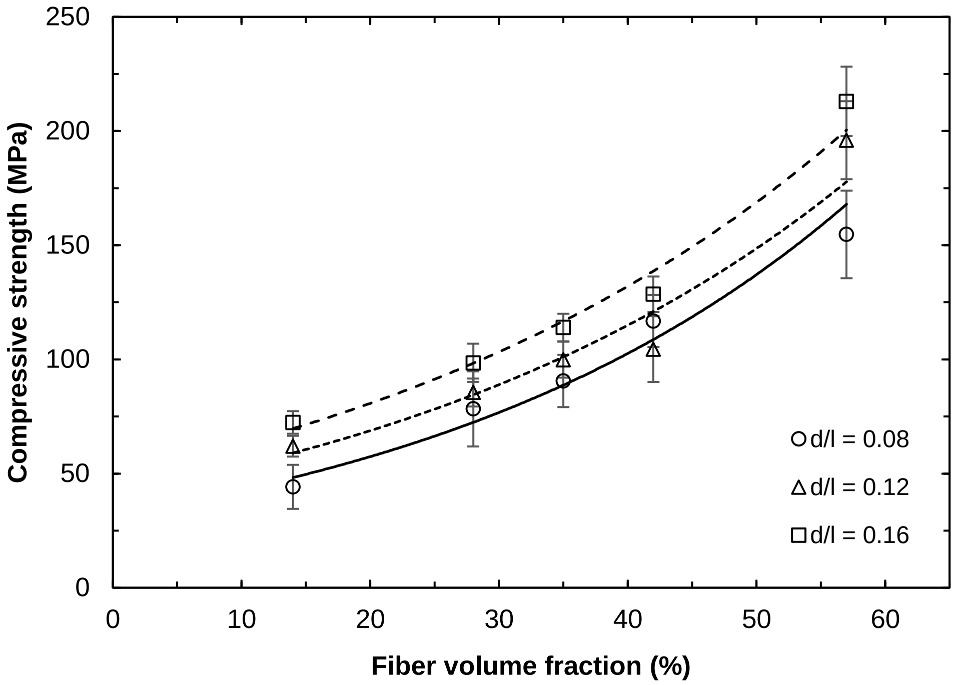

Figure 4.9. Compressive strength as a function of fibre volume fraction for various strut aspect ratios.

The findings of this study on compression tests of composite struts coincides well to the works reported by Che al et. and Xu et al. [5,6] whereby the compressive strength is linearly increased with struts aspect ratio.

4.3 Columnar lattice truss core sandwich structure

Compression tests were performed to determine their compressive stiffness and strength in the out-of-plane direction in accordance with ASTM C 365. The thickness of the facesheets was 2.25 mm, and the total thickness of the specimen is 43.5 mm. The columnar cores were constructed in arrays of four by four to form a unit cell and the square specimen was cut into dimensions of 60 x 60 mm with a core height of 39 mm. The columnar lattice truss was fabricated in three different diameters, i.e. 2, 3 and 4 mm, resulting in relative densities of 2.3, 4.9 and 8.4 %, respectively. Figure 4.10 shows the representative compressive stress-strain responses of these structures based on two different fibre volume fractions. The compressive stress was calculated by taking force divided by the planar area of the columnar truss, while the compressive stiffness was determined from slope of the stress–strain curves within the linear region regime.

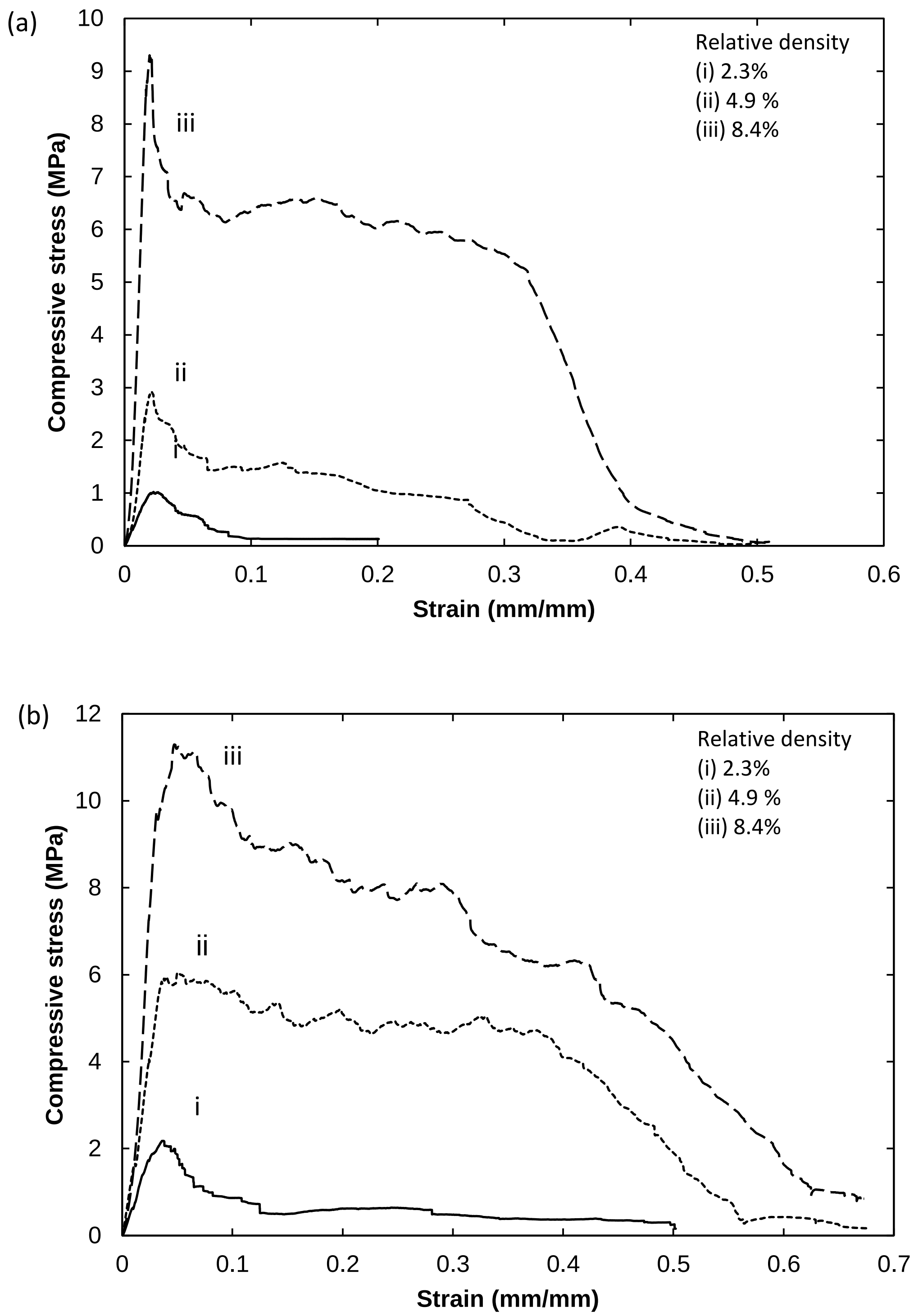

Figure 4.10. Stress versus strain of columnar lattices of varying relative densities at two different fibre volume fractions. (a) $V_f = 0.14$ and (b) $V_f = 0.35$.

Figure 4.10 clearly shows that an initial linear response is observed, followed by a non-linear segment due to the progressive failure of the truss members. After reaching a peak stress, a series of further local failure events in truss members lead to a descent stage with serrations as the crosshead displacement increasing. Columnar lattices based on 2mm diameter members resulting in relative density of 2.3% are observed to be failing by buckling events in the middle of strut members. This is also evident when the fibre volume fraction within 2 mm diameter members was increased from 14% to 35% in Figure 4.10b. The 2 mm column lattice sample having a lower fibre fraction reaches a maximum stress of approximately 0.95 MPa, while the sample with a higher fibre fraction reaches to maximum stress of approximately 2.04 MPa. This shows an increasing compressive strength by 115% for the 2 mm diameter system when fibre volume fraction is increased. In addition, the stiffness of the 2 mm columnar lattice truss cores is 52.5 MPa and 79.2 MPa for the lower and higher fibre volume fraction, respectively.

For columnar lattices having 3 mm truss members, the stress reaches a maximum value of approximately 3.11 MPa prior to initial failure for strut members containing fibre volume fraction of 0.14 (Figure 4.10a). The maximum stress is observed to be 6.23 MPa for 3mm columnar lattices sample having fibre volume fraction of 0.35 which indicates the strength increased by 100% (Figure 4.10b). The failure mode in the strut members with a lower fibre volume fraction is found to be a combined failure of buckling and fibre splitting closer to the joints between the face sheet and the strut. In contrast, the strut members based on higher fibre volume fraction shows a failure mode that predominantly controlled by the crushing of the strut members at the joints from one end to another, although, some members were observed to be failed by a splitting mode as shown in Figure 4.11. Here, the stiffness of the columnar lattice system based on a 3 mm diameter was found to be a slightly increased from 163.9 MPa to 167.8 MPa, a rise of only 2%. Columnar lattices based on 4 mm diameter truss members have shown a drastic increase in maximum compression strength up to approximately 9.13 MPa and 11.06 MPa for lower and higher fibre volume fractions, respectively (Figures. 4.10a and 4.10b). However, it is found that the stiffness of columnar lattice samples based on 4 mm diameter is decreased from 514 MPa to 326.5 MPa although the fibre volume fractions were increased. The failure mode associated with the 4mm diameter rod members was crushing of columnar members at the joints and followed by fracture of the columns.

The failure modes observed during the compression tests on columnar lattices are shown in Figure 4.11. Clearly, the transitions of failure modes can be observed when the aspect ratio of the members is increased. At lower fibre volume fraction of 0.14, the columnar lattices based on 2 mm and 3 mm diameters which fail by buckling of the members only indicates small increasing on the strength. Following this, the failure mode of 4 mm based columnar lattices changed to crushing of their members when it was compressed through the thickness direction. It is evident that the compression strength increased by 3 and 9.6 times in comparison to 3 mm and 2 mm samples, respectively (Figure 4.10). Furthermore, when the compressive stress reaches the maximum strength, there is a large plateau in the stress–strain trace which indicates greater energy absorption as depicted by the area under the stress-strain curve. It is worth noting that the failure modes transitioned from buckling to crushing via splitting and fracture of the members when the diameter of the lattice truss increased from 2 mm to 3mm and 4mm for samples with a fibre volume fraction of 0.35. Figure 4.9b clearly shows a dramatic increase on strength from 2 mm sample to 3 mm and 4 mm samples. Subsequently, a similar stress plateau is distinctly observed for 3mm and 4mm columnar lattices, which undoubtedly indicates that the effects of transition of failure mode while improving the load carrying capacity.

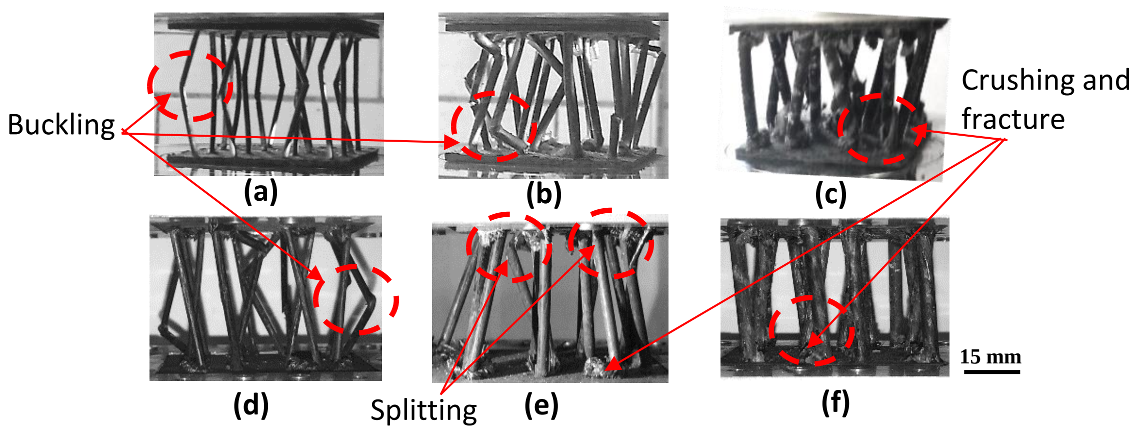

Figure 4.11. Photographs of columnar lattice structures with failure modes. (a) *d* = 2mm and $V_f = 0.14$, (b) *d* = 3mm and $V_f = 0.14$, (c) d = 4mm and $V_f = 0.14$, (d) *d* = 2mm and $V_f = 0.35$, (e) *d* = 3mm and $V_f = 0.35$ (f) *d* = 4mm and $V_f = 0.35$.

Interestingly, the values obtained in the tests on the columnar lattice core sandwich manufactured using novel sacrificial mould method compares favourably well with findings in the literature on carbon epoxy composite column truss sandwich structure manufactured from other techniques. Wang et al. [7] conducted compression tests on vertical truss core sandwich panels fabricated using compression moulding method and recorded strength and modulus values of 8.83 MPa and 424.5 MPa, respectively. The highest values of strength and modulus obtained in current work are 11.06 MPa and 514 MPa, respectively. Similarly, Wang et al. [8] conducted tests on a 3D sandwich structures with foam core reinforced by vertical composite columns and measured strength values from 1.53 MPa to as high as 8.82 MPa. Xiong et al. [9] performed compression tests on vertical metal alloy tubes as core construction with carbon fibre composite facesheets and reported highest strength of 9.38 MPa, respectively. Comparing the strengths, this clearly shows that the panels produced by sacrificial method have superior performance which can be adopted for development of novel light-weight multifunctional structures based on vertical truss core construction.

Figure 4.12 summarizes the specific compression strengths and modulus of the columnar lattice cores sandwich structures based on column member diameter for two different fibre volume fractions. Here, the specific properties are calculated by dividing the strength and modulus of the structures with their relative densities. From the figure, it is again clear that increasing the fibre volume faction within the composite columns and its diameters has a strongly influence on their properties. The specific compression strength values for the lower fibre volume fraction columnar lattices ranges from 42 MPa to 109 MPa and for the higher volume fraction is about 90 MPa to 132 MPa. In the same way, the specific modulus ranges from 2300 MPa to 6100 MPa for the former volume fraction and from 3500 MPa to 3900 MPa for the latter volume fraction. Clearly, the specific modulus is lower in the higher volume fraction lattices based on 4 mm diameter samples.

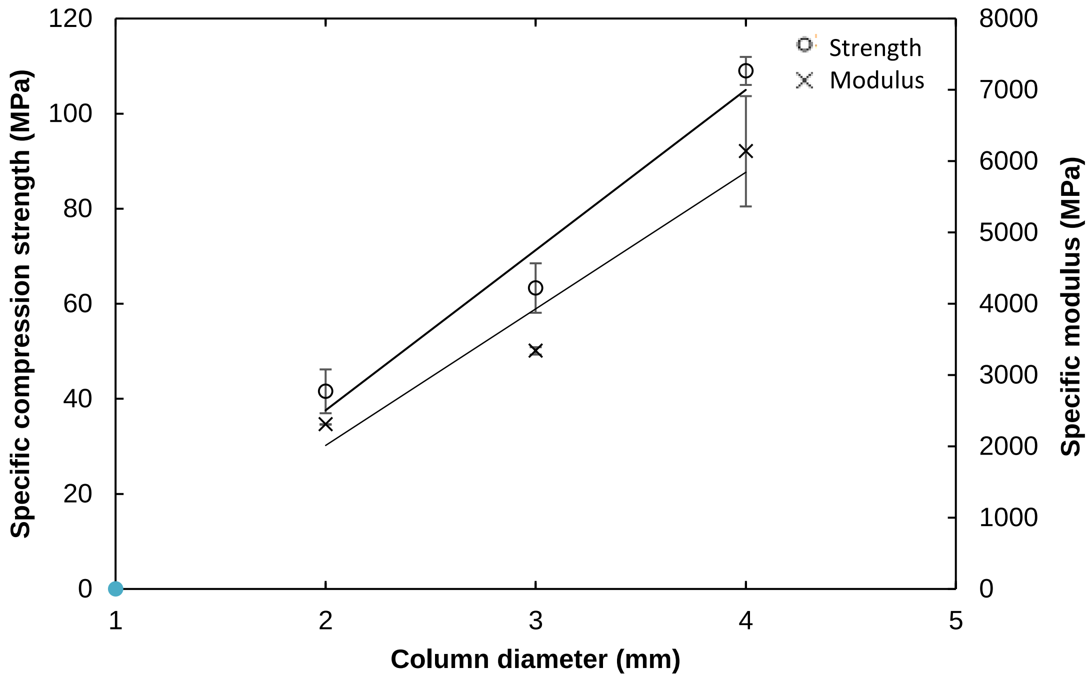

(a)

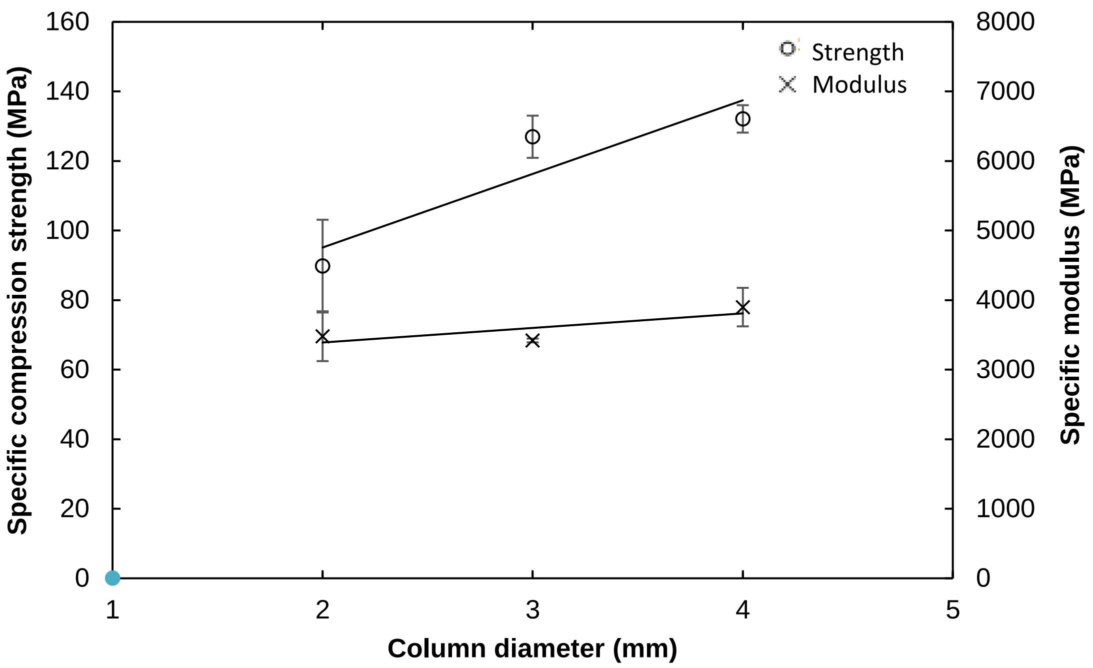

(b)

Figure 4.12. Specific compression properties as a function of column diameter. (a) $V_f = 0.14$ and (b) $V_f = 0.35$.

Figure 4.13 presents the specific energy absorption (SEA) values of the columnar lattice truss core sandwich structures. Here, a distinct difference is observed between the composite column manufactured from two different fibre volume fractions. Such differences are not apparent in the columnar lattices with higher fibre volume fractions when it is passing from the 3 to 4 mm diameter column, which may be due to the fact that columns of the 3 and 4mm diameter failed in a similar mode via crushing of column members during testing. The SEA of the lower fibre volume fraction lattice configuration increases by 200% following the incorporative of 4 mm diameter composite column, the corresponding percentage increase for the higher volume fraction is approximately 100%. The maximum value of SEA in the figure is approximately 39 kJ/kg. The values of SEA evident in Figure 4.13 compare favourably with values measured on foam cores reinforced with carbon composite rods (29 kJ/kg) [10], multidirectional carbon fiber tubes (45 kJ/kg) [11] and carbon epoxy composite tubes (as high as 81.7 kJ/kg) [12]. It is likely that value of 39 kJ/kg could be increased significantly by increasing both the relative density and the fibre volume fraction within the individual trusses (the current value is approximately, V_f =35%).

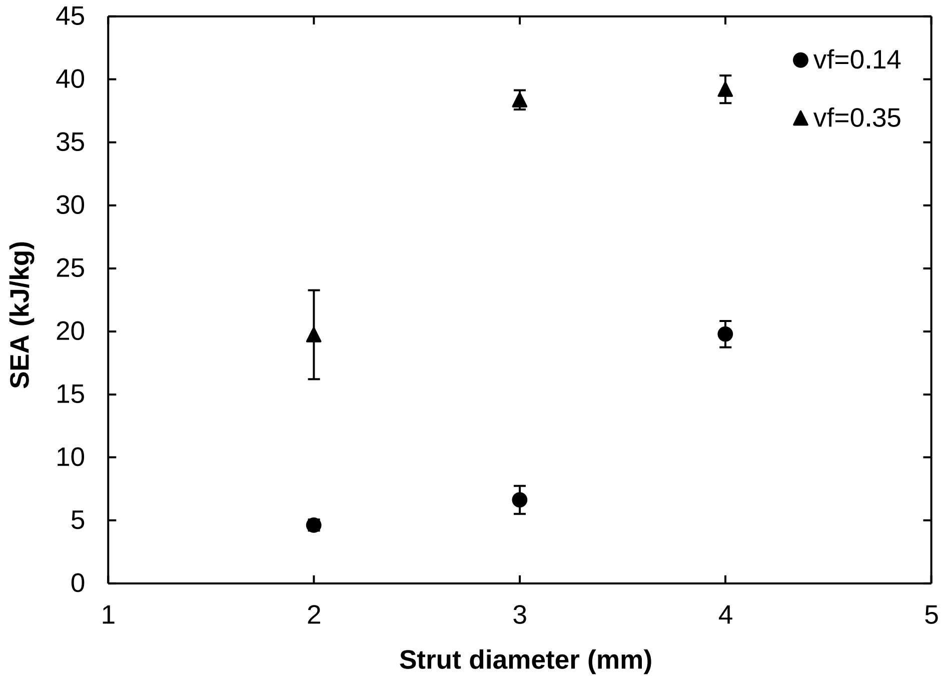

Figure 4.13. The influence of the diameter of the core truss and fibre volume fraction on SEA.

4.4 Pyramidal lattice truss core sandwich structure

Following the study on the columnar lattice core sandwich, the study was further focused on the carbon fibre composite pyramidal lattice core sandwich structures using this new technique, i.e. the sacrificial mould method, and assessing their mechanical behaviour under quasi-static and dynamic loadings. Here, the pyramidal lattice cores were manufactured based on three different sizes of strut, ranging from 2 mm to 4 mm yielding cores with relative densities of 0.48, 1.06, and 1.84 % respectively. The fibre volume fraction within an individual strut was approximately 42 %. The pyramidal truss core sandwich structures were cut into 1x1 and 2x1 unit cells with 37 mm core thickness for testing. Firstly, the compressive properties of the pyramidal lattice structures were evaluated under quasi-static compression tests and then the dynamic response of these structures was obtained following drop weight impact tests.

4.4.1 Quasi-static compression tests

Figure 4.14 shows the compression stress-strain curves of the pyramidal truss core specimens for three strut sizes based on diameters of 2, 3 and 4 mm. The compressive responses in all cases was initially elastic. After the stress reached a maximum at a relatively low strain of 0.02, the load dropped gradually and subsequent failure in truss members leads to stress dropped rapidly as the crosshead displacement continues. There were no obvious plateau regions in the stress-train curves following the initial stress drop, indicating that most struts failed simultaneously in a brittle manner. For pyramidal cores made up from 2 mm struts 0.48 % of relative density, initial failure occurred at the peak approximately of 0.26 MPa as a result of local Euler buckling of the thin struts. This is followed by a sudden break in the middle of one strut forming the pyramidal core, manifest as a sharp drop in supported load as shown in the Figure 4.14 for 2 mm curve. Finally, the subsequent buckling of the other struts in the pyramidal core resulted in the complete damage on this structure.

Interestingly, it is worth noting that pyramidal cores with 3 and 4 mm diameters strut which yielding with relative densities of 1.06% and 1.84%, respectively, are not susceptible to the buckling failure. Instead, the crushing of struts at the node via fracture or rupture leads to a reduction of stress after an initial linear response. The maximum strength achieved by pyramidal cores consisting 3 and 4 mm diameter struts are 0.68 MPa and 1.03 MPa, respectively. Following this, the damage is gradually induced by the subsequent crushing of the core-struts at the end of struts (node) via splitting or rupture and sometimes a break occurred at the ends of the struts. Clearly, the strength is increasing when core-struts diameter (relative density) is increased from 2 mm to 4 mm. The strength is increased by 162% when the relative density increases from 0.48% to 1.06% and by 296% when it increased from 0.48% to 1.84%. This increase is attributed to the failure mode associated with the pyramidal core transitioned from local buckling to crushing of the struts when the diameter of the strut is increased. Figure 4.15 shows the sequence of failure in the pyramidal cores based on 2, 3 and 4 mm strut cores.

The measured average compressive modulus of the composite pyramidal lattice cores sandwich structures is 37.9, 84.5 and 114.4 MPa for 2, 3 and 4 mm core-struts, respectively. This shows an increase of 123% and 200% when the diameter of the strut within the pyramidal core is increased from 2 mm to 3mm and then based on to 4 mm, respectively. Figure 4.16 presents the specific compressive strength and modulus of the composite pyramidal core sandwich structures against their relative densities. Here, the specific compression strength increases as the relative density of the core increasing. However, such increment is not much when it is passing from 3 to 4 mm diameter strut cores, as shown in the Figure 4.16 (a). On the other hand, the specific compression modulus of the pyramidal lattice core sandwich is slightly increased with increasing relative density from 0.48% to 1.06% corresponding to strut diameter increased from 2 to 3 mm. However, the specific modulus is dropped when higher relative density core is tested. The reason is that the mechanical properties of the parent material are sensitive to fabrication defects that might be introduced during the manufacturing process when higher fibre volume ($\approx V_f = 42\%$) within the struts is used.

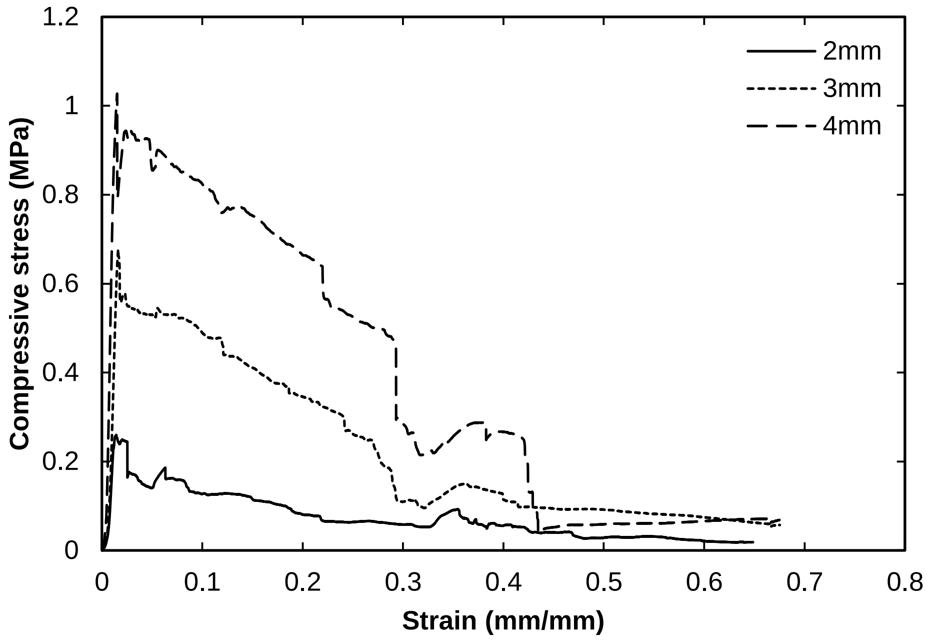

Figure 4.14. Stress versus strain plots of pyramidal lattices with three different diameters strut.

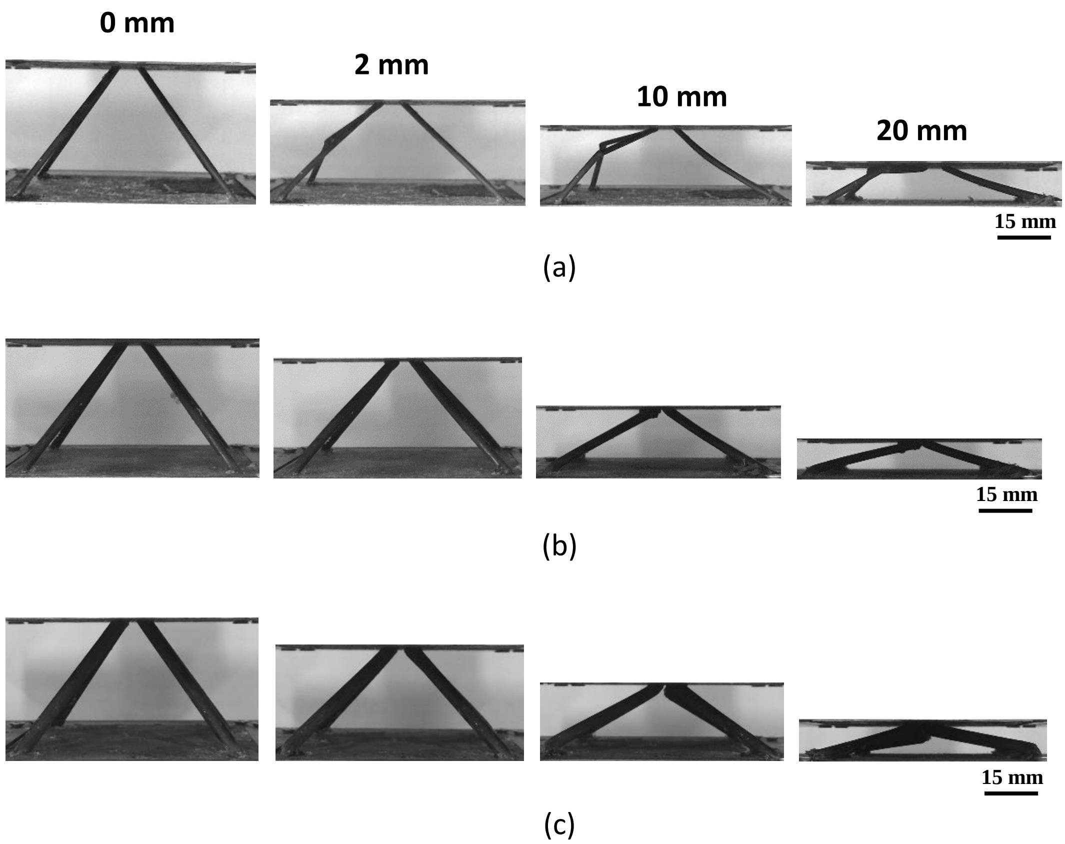

Figure 4.15. Sequence of failure during testing (a) 2 mm (b) 3 mm and (d) 4 mm.

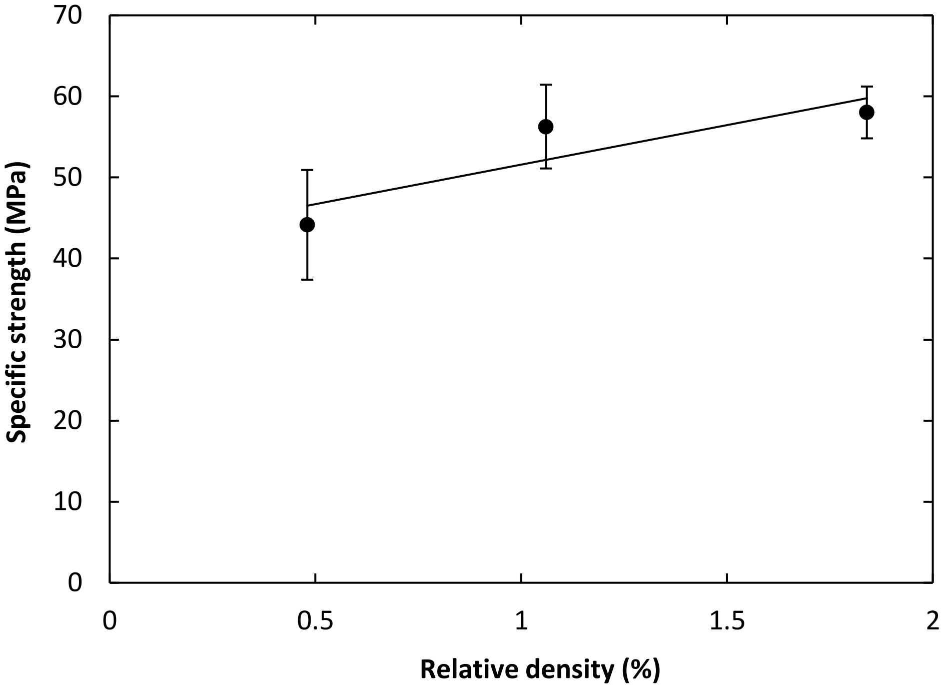

(a)

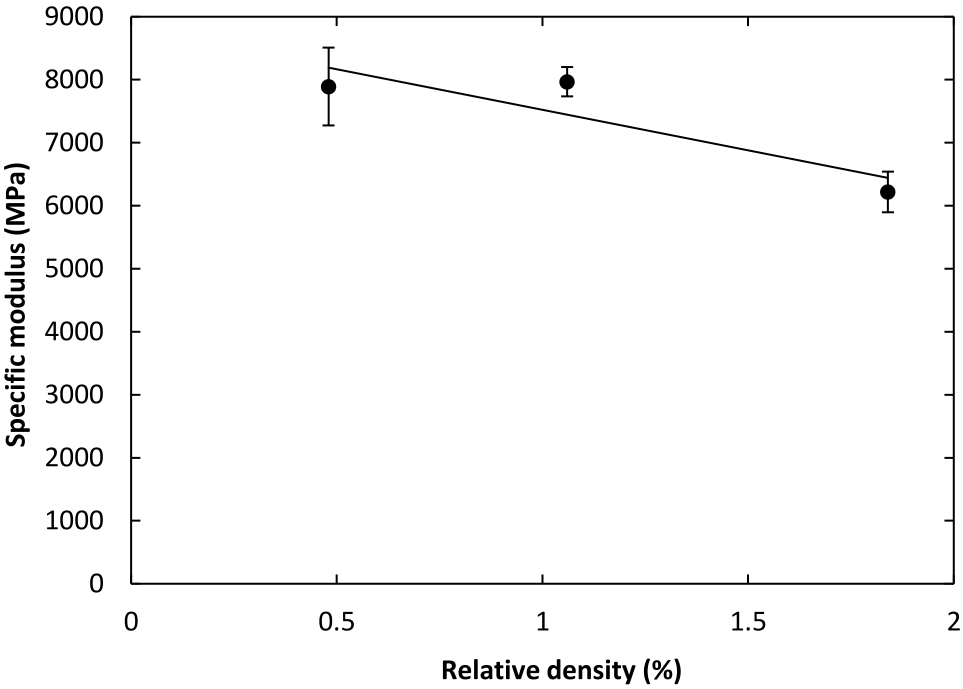

(b)

Figure 4.16. Specific compression properties as a function relative density for pyramidal lattice core sandwich structure (a) Strength and (b) Modulus.

The variation of the SEA values of the composite pyramidal lattice core sandwich structure manufactured the using sacrificial method is shown in the Figure 4.17. The energy absorbed by the pyramidal core structures was measured from the area under the load-displacement curves that obtained from compression tests. The value then was normalized by the mass of the struts occupying the open core, as indicated in Figure 4.17. It is evident that that the SEA of the composite pyramidal core sandwich structures increases with increasing relative density of the cores. The pattern shows a linear fashion resulting in increasing the relative density of the cores influencing the SEA of the structures linearly. The SEA of the pyramidal lattice core is increased by 42% following the incorporation of 4 mm diameter core-struts than that of 2 mm diameter core-struts. An examination of the figure indicates that the maximum SEA value is approximately 11.4 kJ/kg. It is interesting to note that the pyramidal core failed by progressive crushing via node rupture absorb more energy than that of failing by buckling mode.

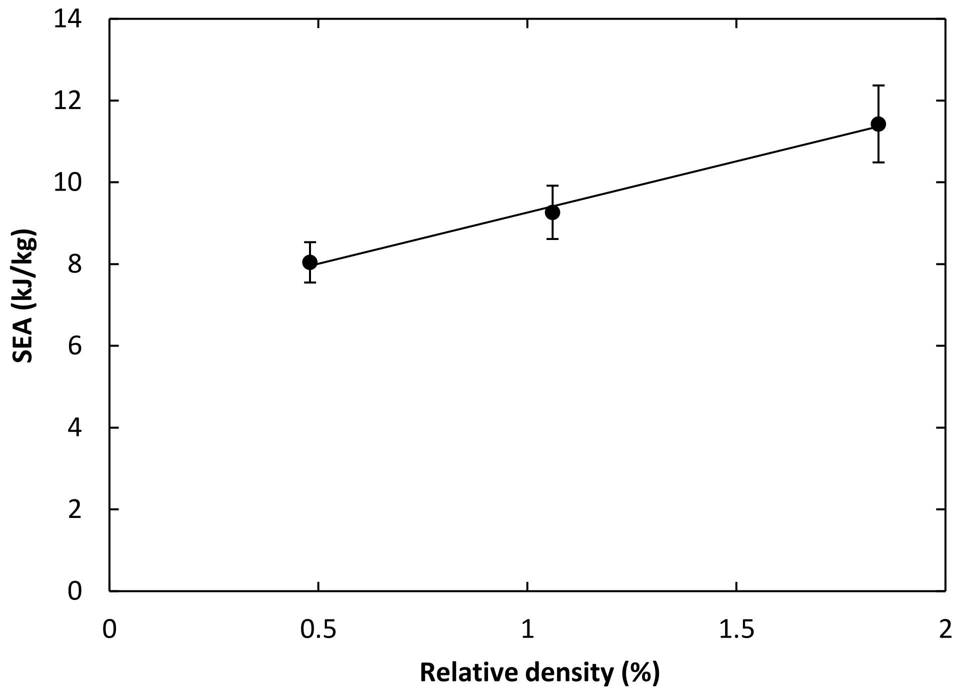

Figure 4.17. The variation of the SEA value of pyramidal lattice cores sandwich structures based on three different relative densities.

The influence of the number of cells on the performance of the pyramidal lattice cores samples was also investigated in quasi-static compression loading. The following section describes the test results for 2x1 unit cell number specimen to explore the size effect on the structural out-of-plane compressive load-bearing capacity.

4.4.1.1 The effect of varying the unit cell numbers

Figure 4.18 shows the representative compressive stress-strain responses of pyramidal lattice core sandwich structures based on (2x1) unit cell number. The stress-strain traces demonstrate that all pyramidal cores with varying relative densities exhibit the similar characteristics, as observed for (1x1) unit cell specimens. However, the peak strength obtained by (2x1) unit cell specimens is slightly lower than that of (1x1) unit cell specimens (Figure 4.14 and Figure 4.18). During the compression of a (1x1) unit cell for 2 mm core-struts, the collapse process was initiated by buckling of struts and followed by breaking in the middle of the struts. This is attributed to the fact that the pyramidal core with 2 mm diameter core-struts has lowest aspect ratio (d/l) tends to be failing by global buckling and the failure mode will be transitioned from buckling to fracture as the aspect ratio increases. This agrees well with the work presented by Che al et. and Xu et al. [5,6]. Buckling of struts were also observed during compression response of the (2x1) unit cell specimens as shown in the Figure 4.19 (a).

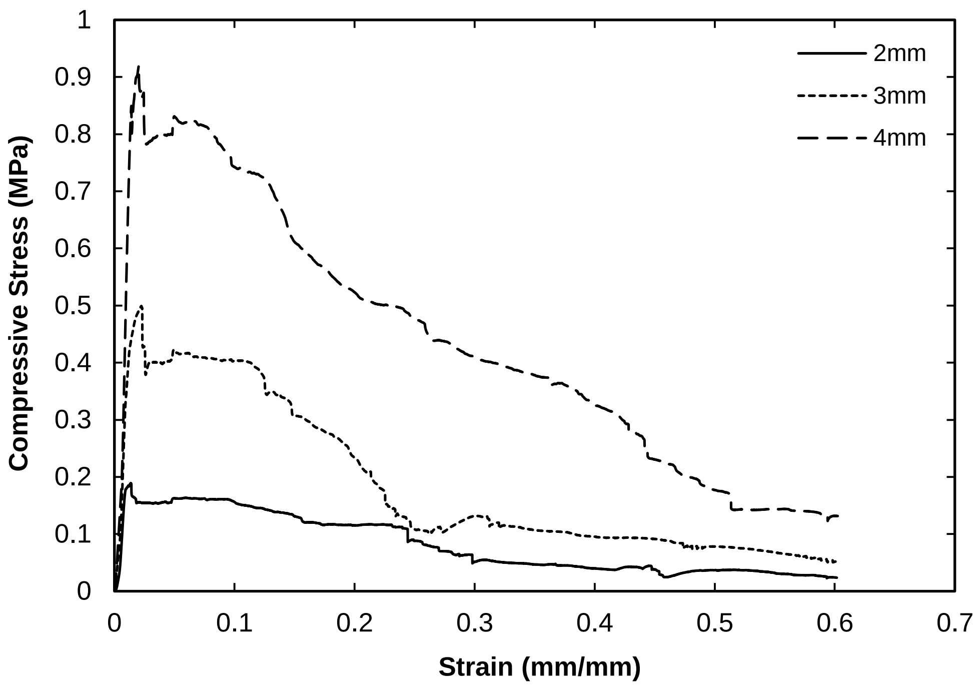

Figure 4.18. Stress versus strain of pyramidal lattices with (2x1) unit cells consisting 2, 3 and 4mm core-struts.

For 3 and 4 mm diameters core-struts, the (2x1) unit cell specimens displayed the similar failure modes after reaching a peak value whereby crushing of struts via fracture or node rupture and splitting were seen predominantly controlling the failure process during compression as monitored for (1x1) unit cell specimen. Figures 4.19 (b) and (c) show images of the crushing process in the struts of pyramidal cores based on 3 and

4 mm core-struts. An examination of these photographs highlights the transition of failure modes from buckling to crushing of the struts as the core-strut diameter increasing. Close inspection of the 3 and 4 mm pyramidal core-struts indicates the crushing of struts initiated from one end of the strut to other end, specifically at the nodes.

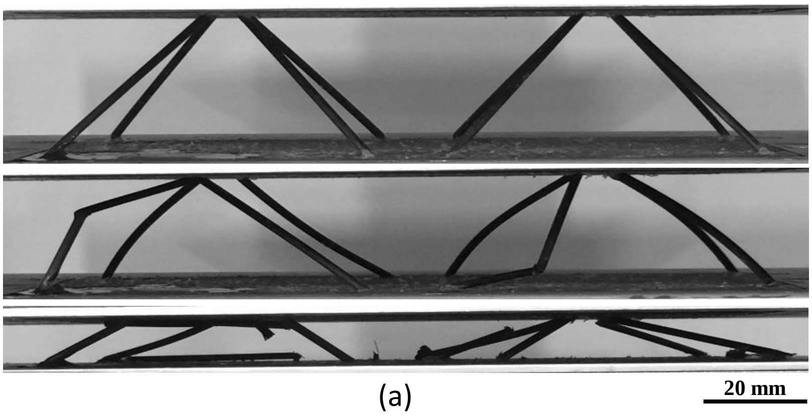

(a)

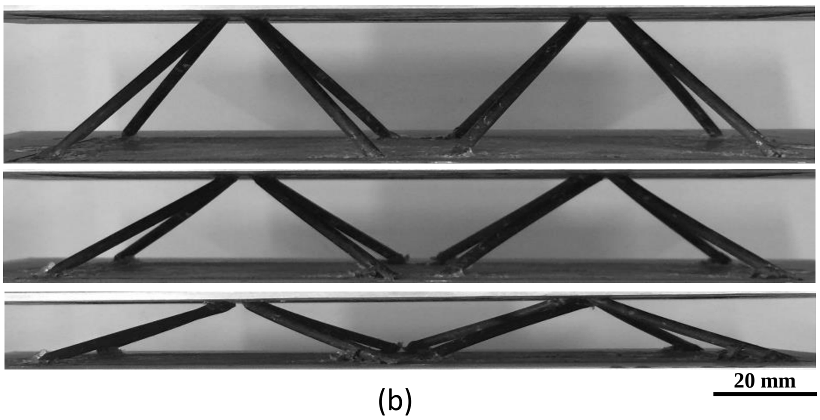

(b)

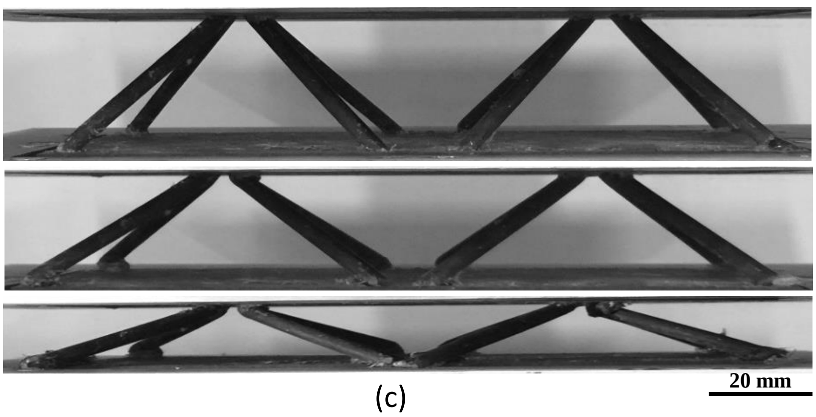

(c)

Figure 4.19. Photograph of failure mode in pyramidal cores with (2x1) unit cell based on varying core-strut diameters.

The effect of varying the number of cells on the specific compression strength and modulus of the pyramidal lattice cores of various relative densities is shown in the Figure 4.20 (a) and Figure 4.20 (b), respectively. An examination of the figure clearly indicates that the specific strength and modulus decrease with an increase in the unit cell number to a certain extent. Therefore, the size effect actually exists in the range of specimen size, and the effect is likely weakened with the increase of the specimen size due to increasing imperfections. These results also highlight the influence of the connected neighbourhood cells in which they are separated in a certain distance. The specific properties of (2x1) unit cell core specimens could be improved if the adjacent cells are closer to each other. The resulting values of SEA are compared with unit cell number in Figure 4.21. Increasing the unit cell number to (2x1) cells of (1x1) unit cell resulted in an increase of SEA measurement compared to (1x1) unit cell. Here, it is clear that the energy absorption of 4 mm diameter strut core (2x1 unit cells) indicates an increase by 20% in comparison to (1x1) unit cell.

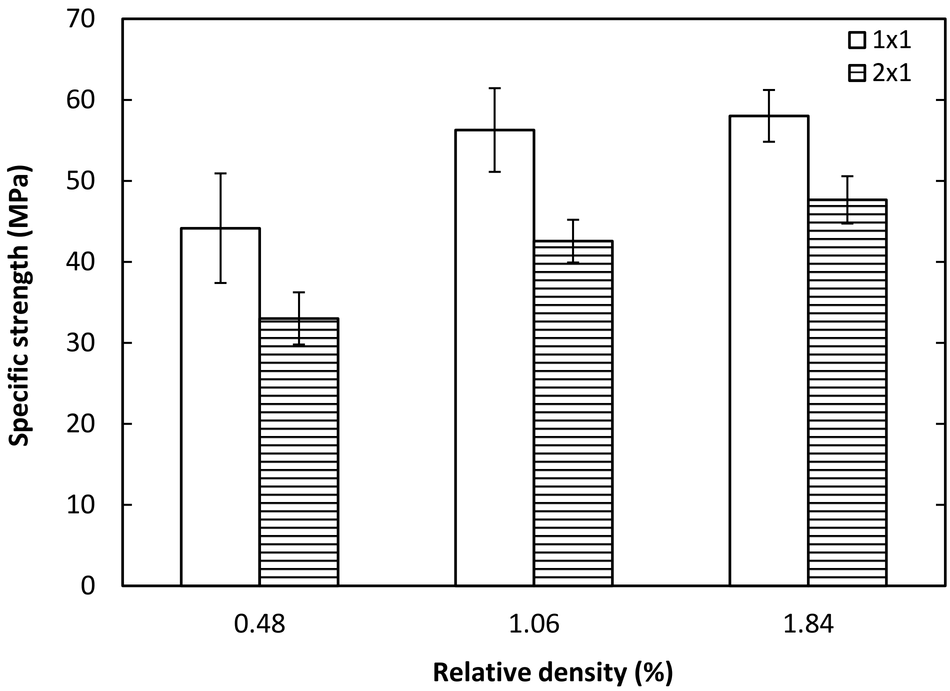

(a)

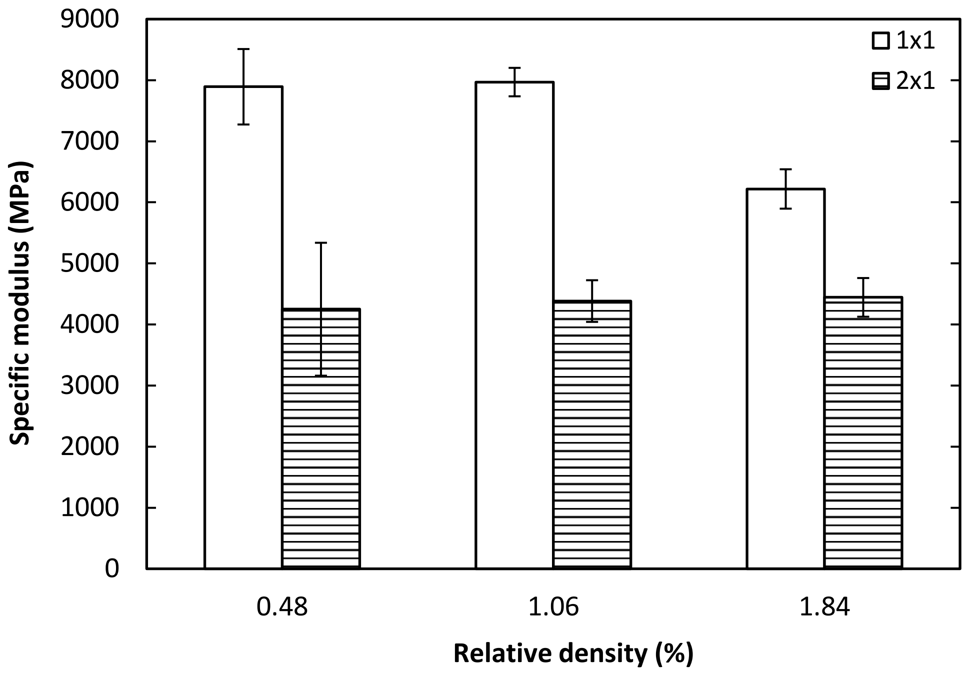

(b)

Figure 4.20. Specific compression properties as a function relative density for pyramidal lattice core sandwich structure with varying unit cell (a) Strength and (b) Modulus.

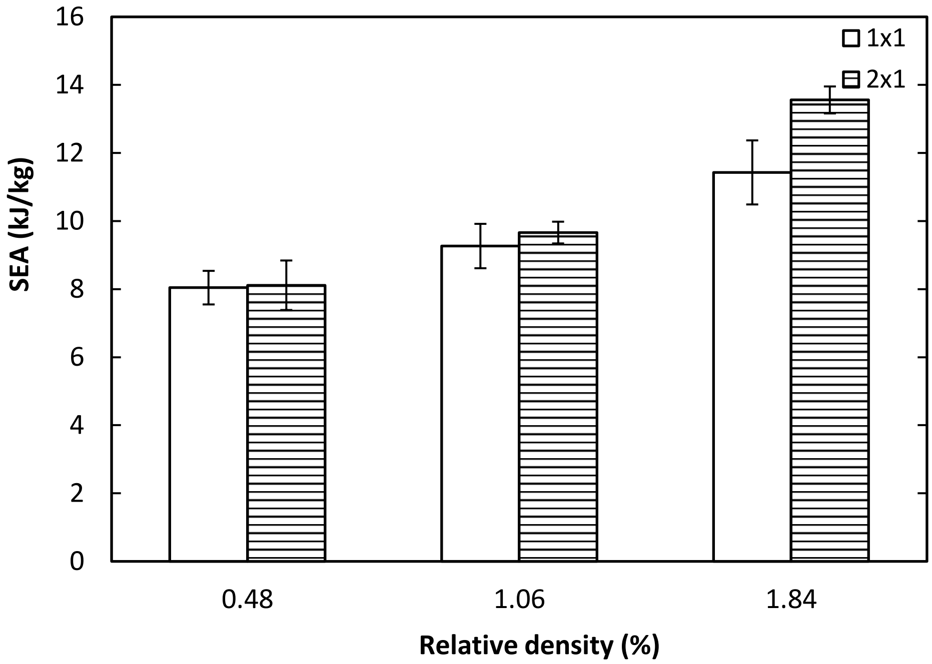

Figure 4.21. The comparison of the SEA value of pyramidal lattice cores with varying number of unit cell.

4.4.2 Dynamic tests

Dynamic tests were performed by conducting low velocity impact tests using a drop-weight tower. Here, a mass (m) of 25.6 kg was dropped from a predefined height to crush the samples. In this study, the height from which the mass was dropped is pre-determined based on the energy absorption data measured from the quasi-static compression tests. Table 4.3 summarises the test parameters used to evaluate the impact response of the composite pyramidal lattice core sandwich structures. A flat rectangular impactor that capable of carrying a mass was used to strike the specimens. The impactor was guided by two parallel columns to ensure that the impactor struck the specimen centrically. The specimen was progressively crushed from the top to the bottom once the impactor made contact with the top surface. All tests were limited to (1x1) unit cell specimens only.

Table 4.3. Test values used during the low velocity impact tests on the different core-struts diameters.

Structure	Relative density (%)	Drop height (m)
Pyramidal core	0.46	0.06
	1.06	0.16
	1.84	0.32

Figure 4.22 shows typical load-displacement traces following dynamic crushing tests on the carbon fibre composite lattice core sandwich structures based on three core-strut diameters. A comparison of the quasi-static load-displacement traces of pyramidal core and their equivalent relative densities were also included in the figure with red lines.

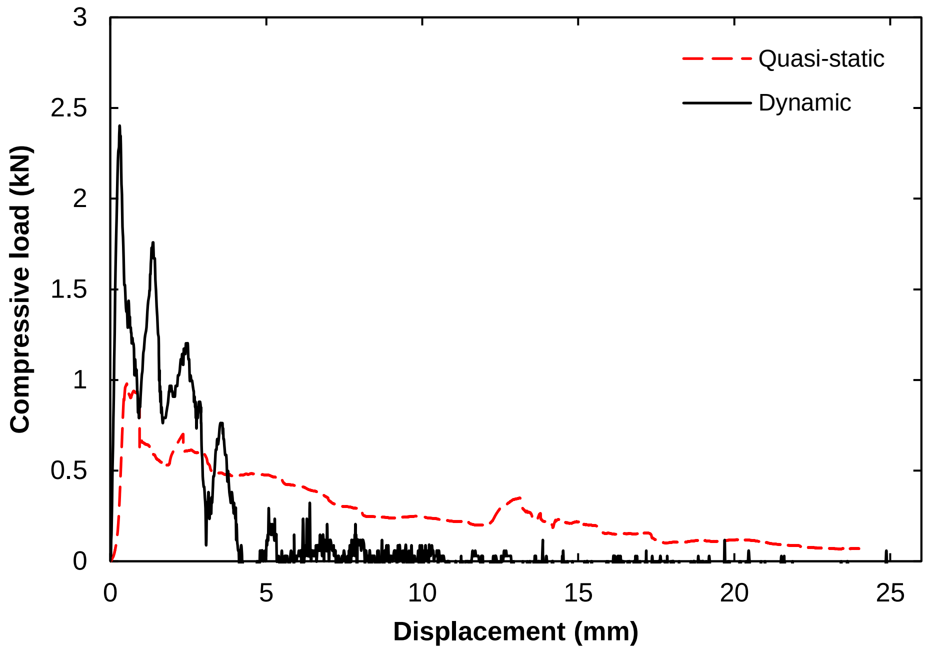
Quasi-static
Dynamic
Compressive load (kN)
Displacement (mm)
0
0.5
1
1.5
2
2.5
3
0
5
10
15
20
25

(a) 2 mm

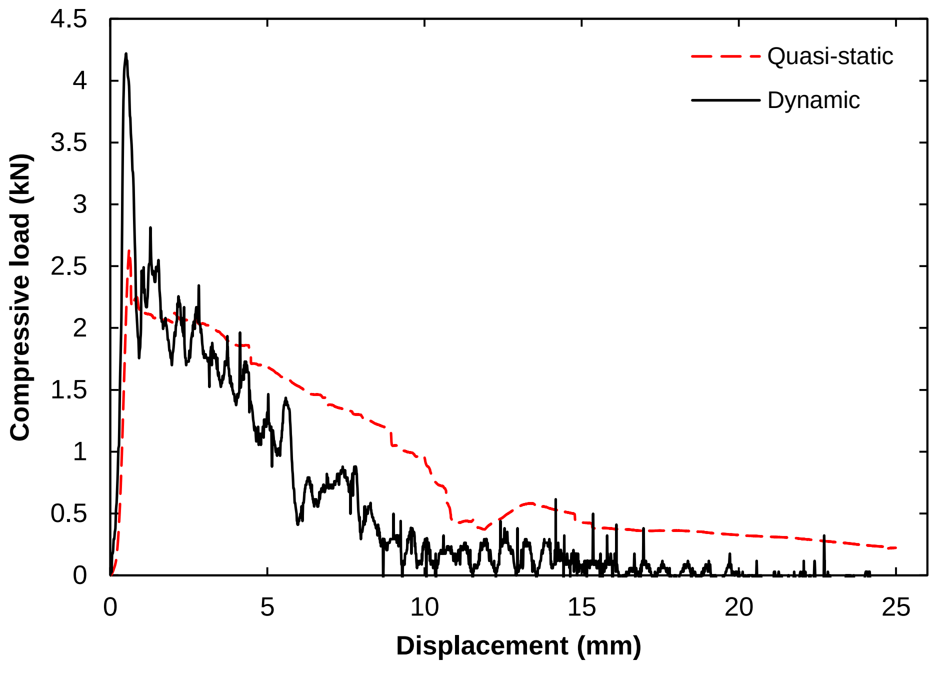
Quasi-static
Dynamic
Compressive load (kN)
Displacement (mm)
0
0.5
1
1.5
2
2.5
3
3.5
4
4.5
0
5
10
15
20
25

(b) 3 mm

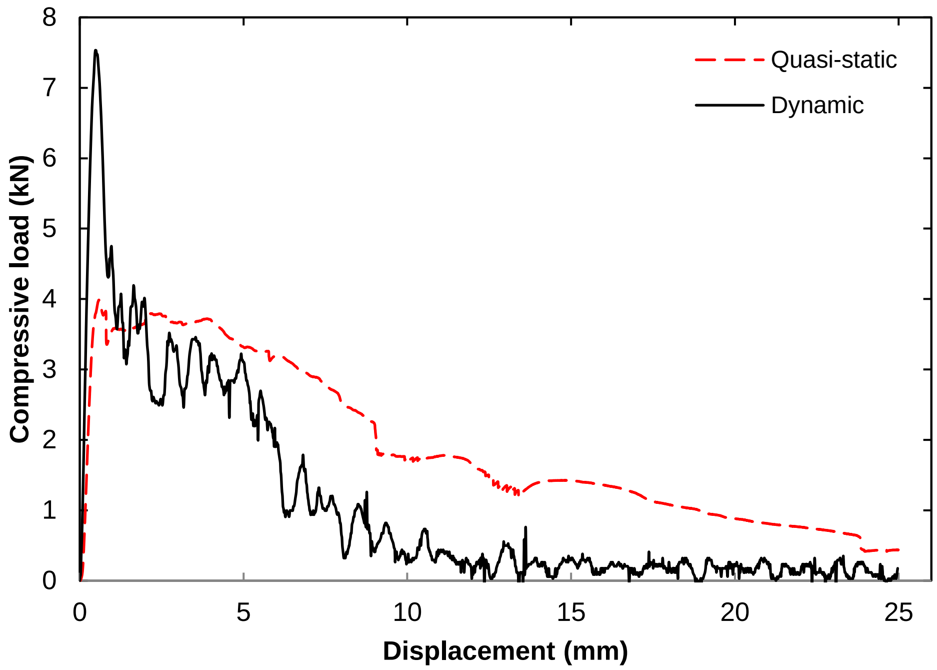

(c) 4 mm

Figure 4.22. Load-displacement traces following drop impact test on pyramidal lattice cores sandwich structures (a) 2 mm (b) 3 mm and (c) 4 mm.

Close inspection of the traces following impact testing indicates that the force initially increases in a linear fashion, before reaching a peak value. The force then drops rapidly as the core-struts begin to fail followed by fracture at the nodes. All four struts occupying the pyramidal core fail by fracture at the strut ends within a crosshead movement reaching 5 to 10 mm, with core-struts diameter increasing from 2 to 4 mm. After onset failure there is clearly force oscillation upon completion of the impact events. Such behaviour is likely due to dynamic effects in the load cell and drop weight carriage as well as instabilities during the failure process of the core-struts. Interestingly, it is found that the peak force during impact testing is higher than that of the quasi-static counterpart. An examination of the dynamic traces in the Figure 4.22 suggests that the impact-loaded samples absorb less energy than their quasi-static counterparts.

Figure 4.23 shows the stress-strain traces following drop-weight impact tests on pyramidal lattice cores with varying core-strut diameter. The response curves are presented in terms of the nominal stress (equal to the applied load divided by edge planar area of the specimen) and nominal strain (equal to the displacement divided by the original specimen core height). The energy absorption of the specimen was determined from the area under the load-displacement trace up to 60% crushing from specimen height. In general, the stress-strain traces exhibit a linear trend up to the peak stress, followed by drop in stresses reflecting to failure process as explained for the corresponding force-displacement traces in Figure 4.22. The average peak stress for the 2 mm pyramidal core-struts is 0.59 MPa, it is 1.09MPa for the 3 mm diameter core-struts and finally the peak stress for the 4 mm diameter core-struts is approximately 1.92 MPa. This clearly shows that the peak stress is increased by 85% when the core-struts diameter is increasing from 2 mm to 3 mm, whereas it is increasing by 225% when the core-strut dimeter passing from 2 mm to 4 mm.

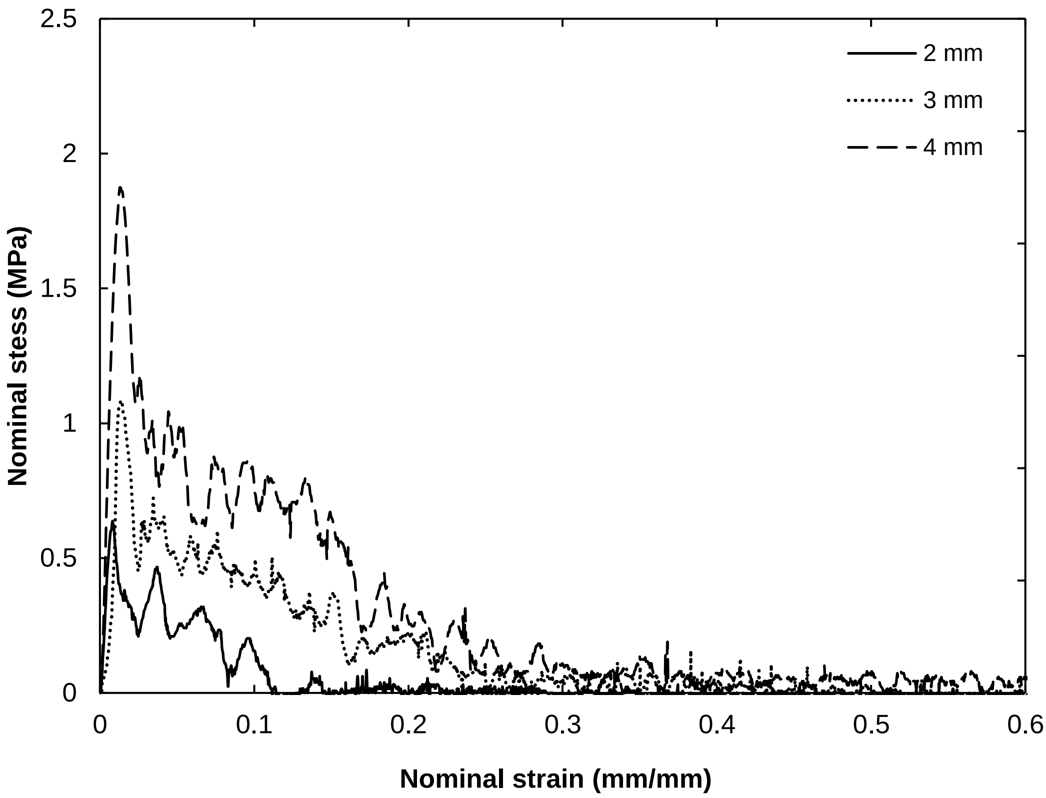

Figure 4.23. The stress-strain relationship following drop impact test on pyramidal lattice cores sandwich structures based on different core-struts diameter.

As evidenced in the Figures 4.22 and 4.23, the average compressive forces or stresses are higher at dynamic rates of loading within an elastic regime, which in turn gives slightly higher energy absorption up to the peak forces or stresses than their quasi-static counterparts. However, the overall energy absorption capabilities in dynamic loadings are lower compared to that of quasi-statically loaded specimens. Figures 2.24 (a) – (c) present the energy absorbed by the specimens over the crosshead movement based on quasi-static and dynamic loadings for three repeated tests of three different core-strut diameters.

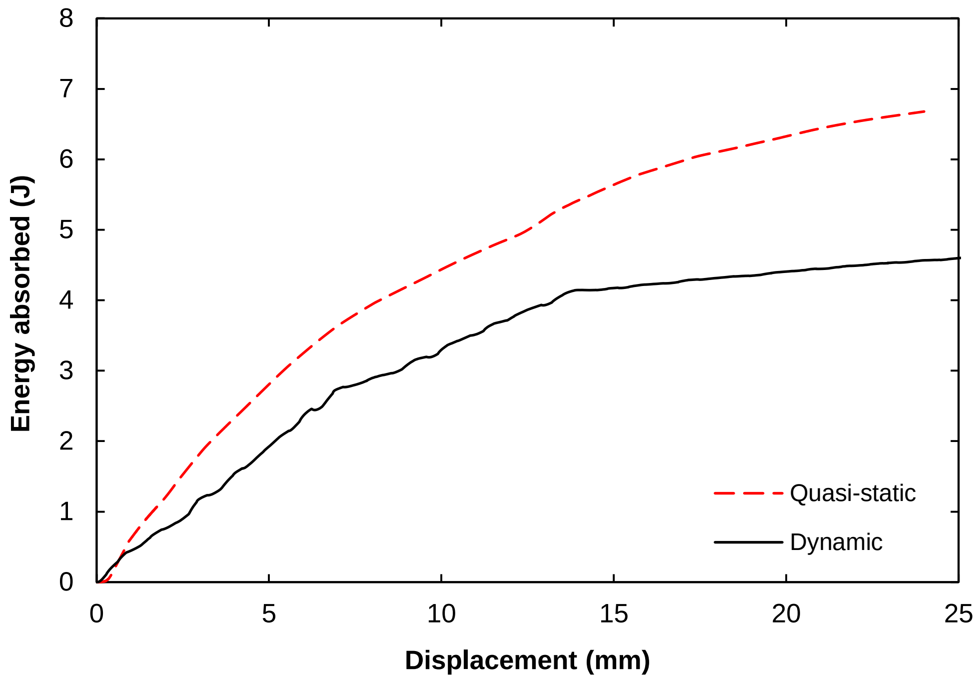
Energy absorbed (J)
0
1
2
3
4
5
6
7
8
0
5
10
15
20
25
Displacement (mm)
Quasi-static
Dynamic

(a) 2 mm

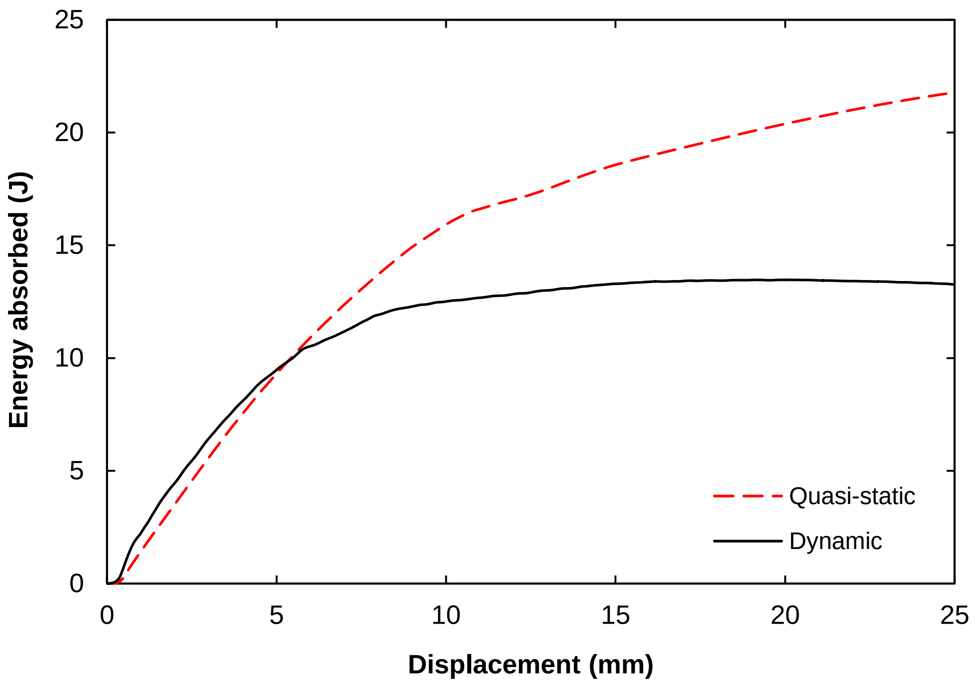
Energy absorbed (J)
0
5
10
15
20
25
0
5
10
15
20
25
Displacement (mm)
Quasi-static
Dynamic

(b) 3 mm

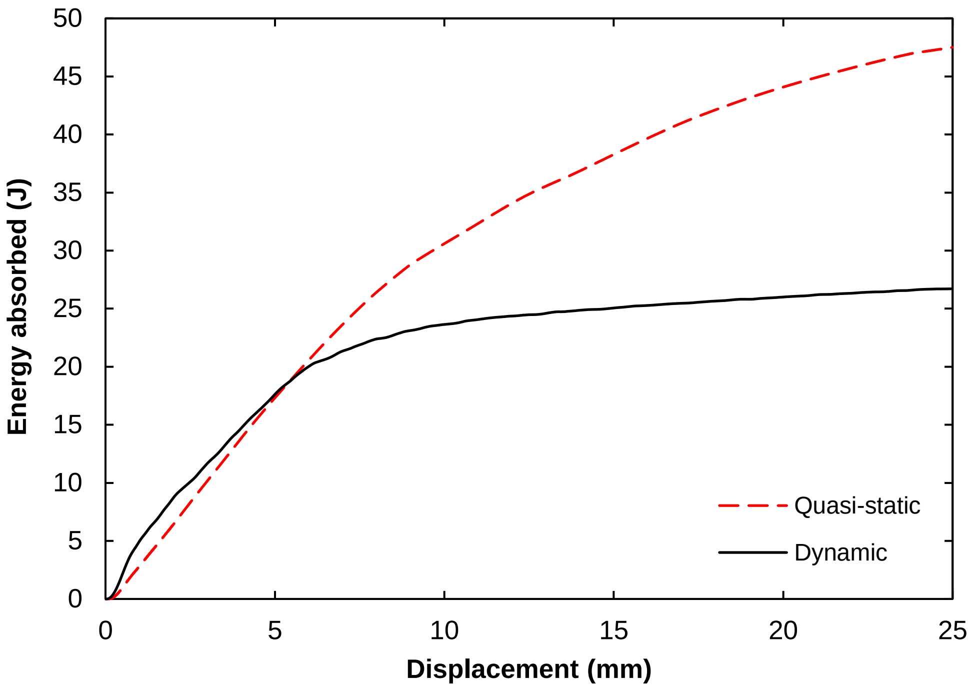

(c) 4 mm

Figure 4.24. The energy absorbed by the pyramidal core specimens under quasi-static and dynamic tests.

From the figure, it is clear that the energy absorbed by the specimens is higher in initial stage under dynamic loadings which indicates the structures were failing abruptly compared to the specimens under quasi-static loadings. Subsequently, the energy absorption is increasing for quasi-static loading surpassing their dynamic counterpart values, which indicates still more energy is needed to crush the samples under quasi-static mode. Following this, the specific energy absorption (SEA) characteristics of the pyramidal core sandwich panel were calculated by dividing the energy absorbed by the mass of the core. The variation of the SEA values of the pyramidal core sandwich structure tested under the dynamic loading are compared with their quasi-static counterparts, as shown in Figure 4.25. It is indeed clear that the dynamic values of SEA are lower than those of quasi-static ones.

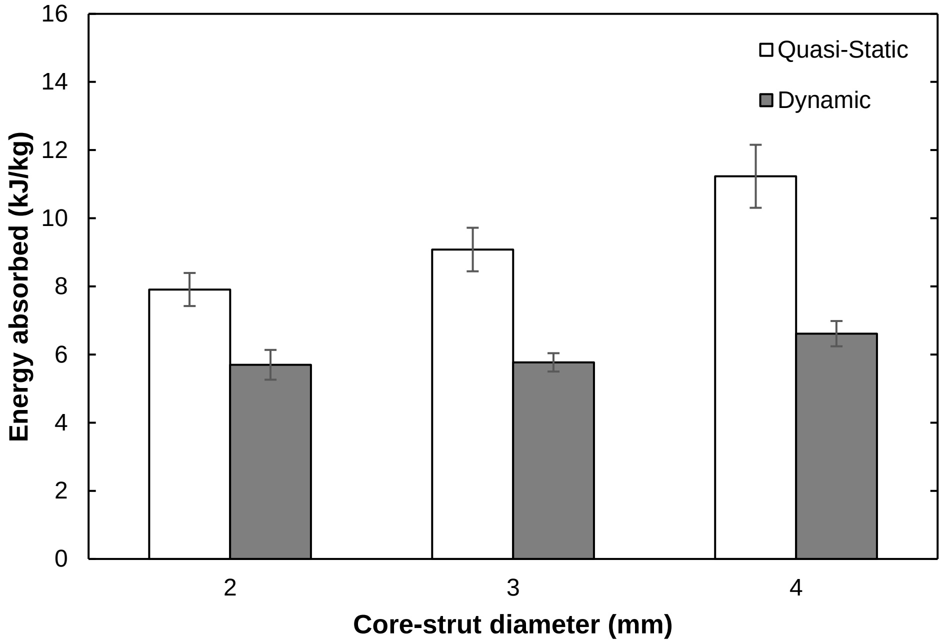

Figure 4.25. The variation of the SEA of the composite pyramidal lattice core sandwich structure at quasi-static and dynamic rates with different core-struts diameter.

4.5 Modified-Pyramidal lattice truss core sandwich structure

Here, the all-carbon composite modified-pyramidal lattice core sandwich structures were manufactured by introducing an additional central column through its apex based on simple pyramidal lattice structures using the sacrificial mould method. The resulting samples were then tested in quasi-static and dynamic loading to examine their mechanical performance. The modified-pyramidal lattice core structures were produced based on three different diameters of 2, 3 and 4 mm, yielding cores with relative densities of 0.57, 1.24, and 2.16% respectively. The core has a thickness of 37 mm and the fibre volume fraction within an individual strut was approximately 42%.

4.5.1 Quasi-static compression tests

Figure 4.26 shows typical stress-strain traces following compression tests on the modified pyramidal core with a unit cell structure. From the figure it is evident that there are two distinct regions within the trace, one being linear before reaching the peak stress, followed by non-linear region corresponding to failure process in the struts comprising the lattice structure. The resulting average peak stresses before initial failure were 0.42 MPa, 0.91 MPa and 1.71 MPa based on 2, 3 and 4 mm core-strut diameters, respectively. After achieving the peak values at relatively a low strain ranging from 0.01 – 0.03, the following crosshead movement caused a series of failure events in the lattice truss members as indicated by sharp or gradual drop in load until total damage occurred. An observation of the specimen during failure reveals that 2 mm diameter modified-pyramidal core-struts failing by buckling of the truss members and followed by breaking in the middle of struts. Similar observation are witnessed for simple-pyramidal lattice core structures with 2 mm diameter members as well. Concurrently, the column through the apex of the modified sample fails by crushing near the connecting ends and followed by sudden break in the within the column. A sharp drop in the stress-strain trace for 2 mm diameter core-struts indicates the breaking experienced by the struts during failure process. The subsequent loading caused fracture to the ends of the struts connecting with bottom facesheet until complete failure occurred.

Failure in modified-pyramidal core structures based on 3 and 4 mm diameter core struts was initiated by crushing the vertical column through the apex initially, followed by concurrent crushing via fibre splitting and fracture to other truss members in the structure which eventually caused node rupture upon completion of the series of the failure events. The insertion of the vertical column in the modified-pyramidal leads to increasing peak stress values as compared to their simple-pyramidal counterparts. Furthermore, the peak stress is increased with the increasing diameter of the core-struts. With increasing diameter of the core struts from 2 mm to 3 mm, the compressive stress rises significantly by 115% and by 307% when it increases from 2 mm to 4 mm diameter core-struts. Figure 4.27 shows the progressive failure in the modified-pyramidal cores during compression testing.

Furthermore, the resulting average modulus values calculated from the slope of the linear region (as indicated in the Figure 4.26) of repeated three tests were 50.3, 108.9 and 136.4 MPa for 2, 3 and 4 mm core-strut diameters, respectively. This shows that the modulus of the modified-pyramidal core structure is increased as the size of the core-struts increase, also with evidence for the maximum strength. Figure 4.28 presents the specific compressive strength and modulus of the all-carbon composite modified-pyramidal core sandwich structures with respect to their relative densities. An examination of the figure revealed a similar trend with the pyramidal core lattices whereby the specific compression strength increasing when the relative density of the core increased. Despite showing an increasing trend, the increase is not significant as evidence in the Figure 4.28 (a). Here, it is clear that the specific modulus of the modified-pyramidal lattices is decreased significantly as the strut size is increased from 2 mm to 4 mm diameter of the core-struts, however it is less significant when it increases from 2 mm to 3 mm.

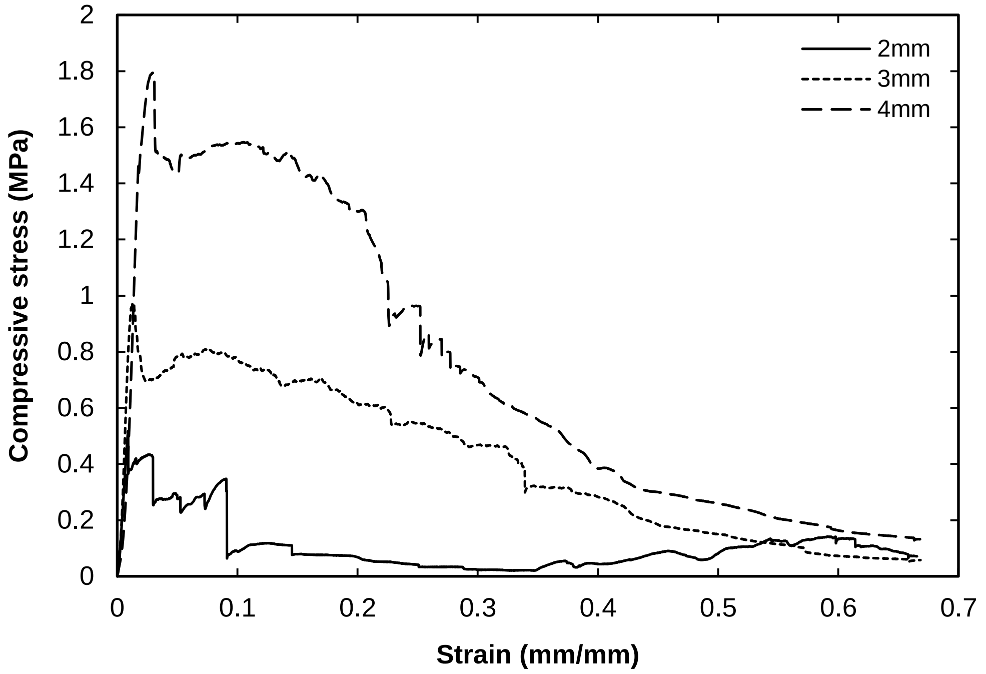

Figure 4.26. Typical stress-strain curves of modified-pyramidal lattice core structures based on various diameters.

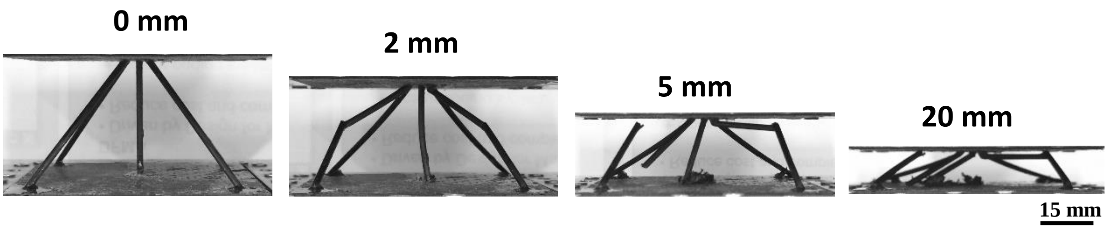

(a) 2mm

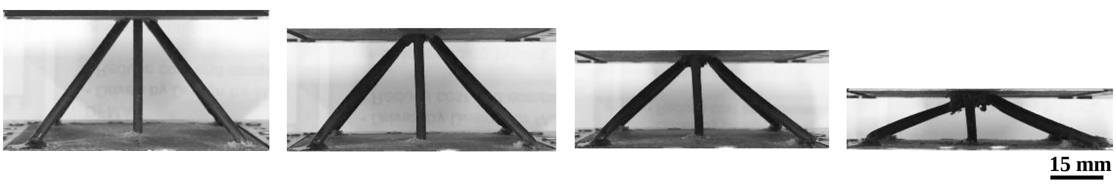

(b) 3mm

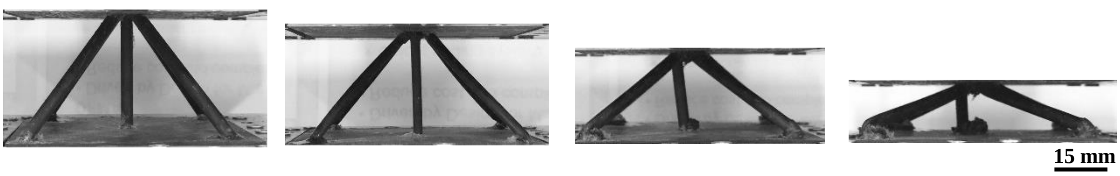

(c) 4mm

Figure 4.27. Photograph of progressive failure in modified-pyramidal lattices.

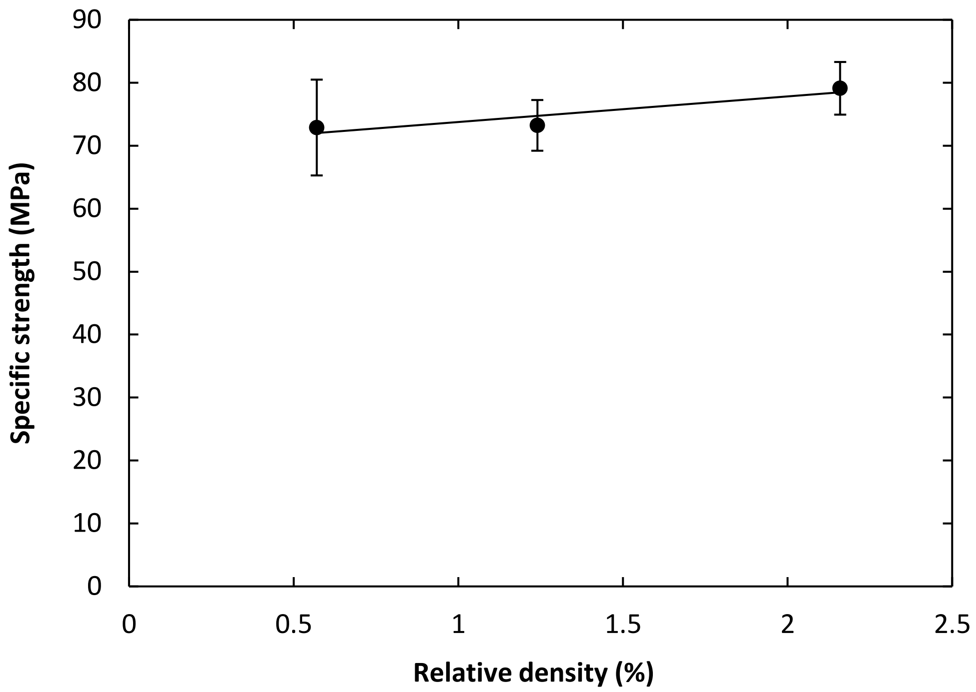

(a)

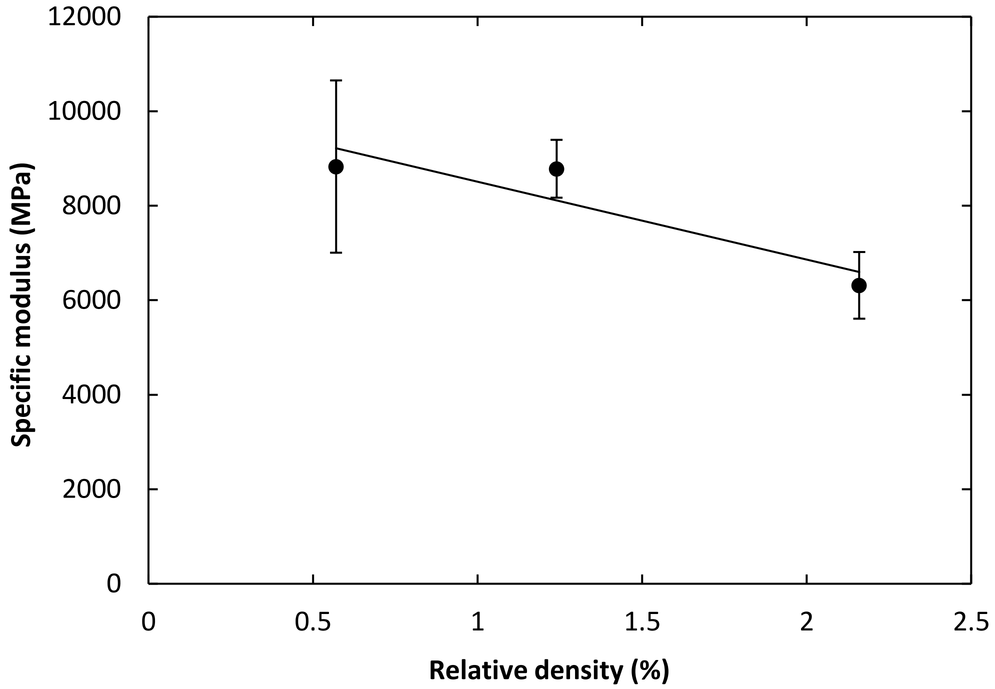

(b)

Figure 4.28. Comparison of the specific properties of the modified-pyramidal lattice core structures based on different relative densities. (a) Strength (b) Modulus.

An attempt to further investigate the mechanical response of the modified-pyramidal core was carried out using different numbers of unit cell. Specimens with (2x1) unit cells were tested for assessing their performance as compared to that of (1x1) unit cell. Figure 4. 29 shows the typical compressive stress-strain response for the modified-pyramidal lattices with (2x1) unit cells under three different truss member diameter. Based on this observation, it is again clear that there are two distinct regions within the trace, i.e. linear and non-linear stage as evidenced for (1x1) unit cell compression testing. An examination of the figure indicates the stress increases linearly before the onset of the initial failure, followed by subsequent progressive failure events. The average peak strengths of these lattices are 0.28, 0.70 and 1.27 MPa, whereas their modulus is 27.5, 50.9 and 81.7 MPa for 2, 3 and 4 mm diameter core-struts, respectively. An identical failure mode was observed with their (1x1) unit cell counterparts. Figure 4.30 shows the progressive failure in the (2x1) unit cells modified pyramidal lattices system. Close examination of the failure mechanisms reveals transitions in the failure mode from buckling to progressive local crushing via fibre splitting and fracture at both ends of the struts. Clearly, the vertical column in the modified lattices failed by crushing of column and sometimes fractured.

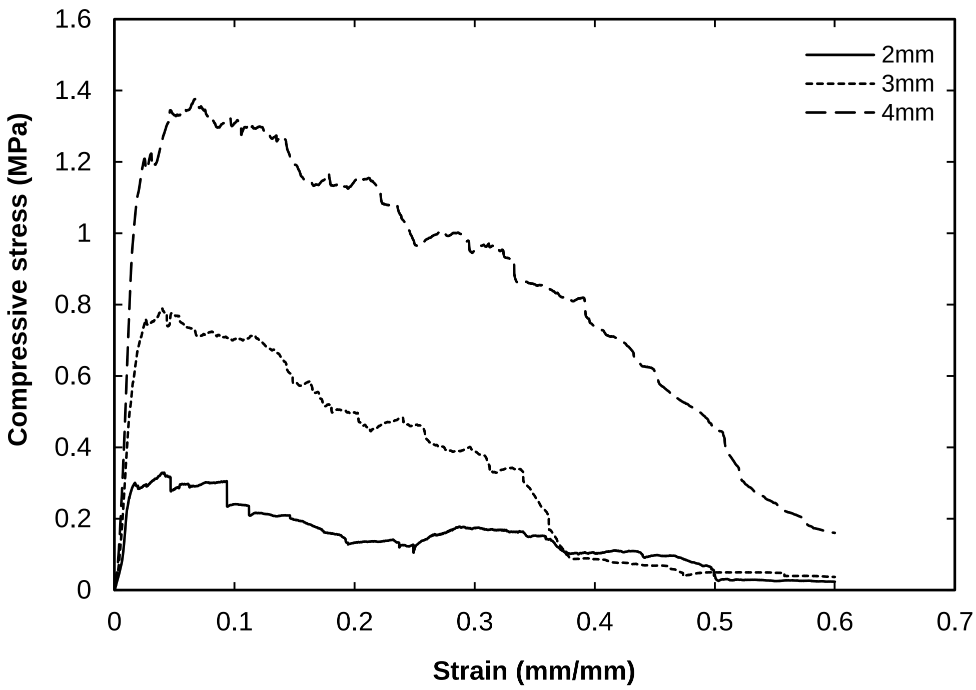

Figure 4.29. Typical stress-strain curves of (2x1) unit cells modified-pyramidal lattices based on various diameters.

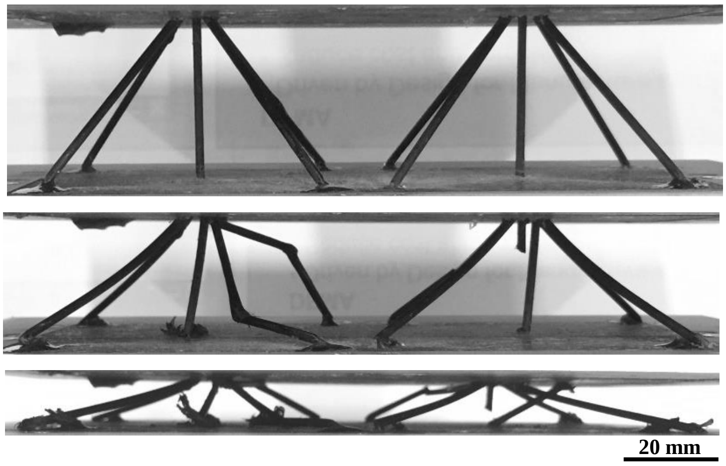

(a) 2 mm

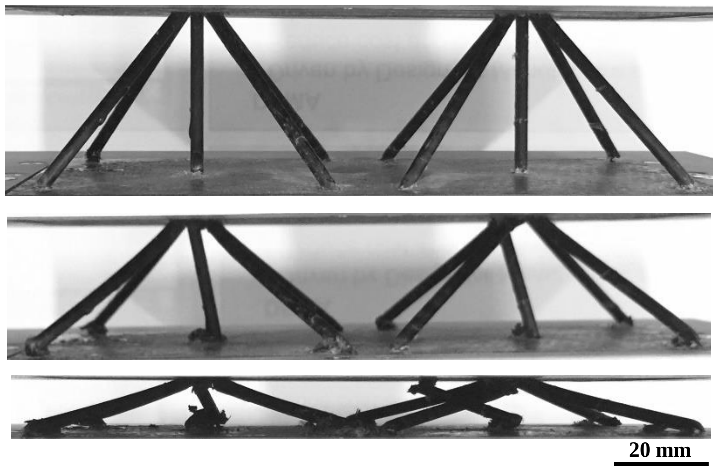

(b) 3 mm

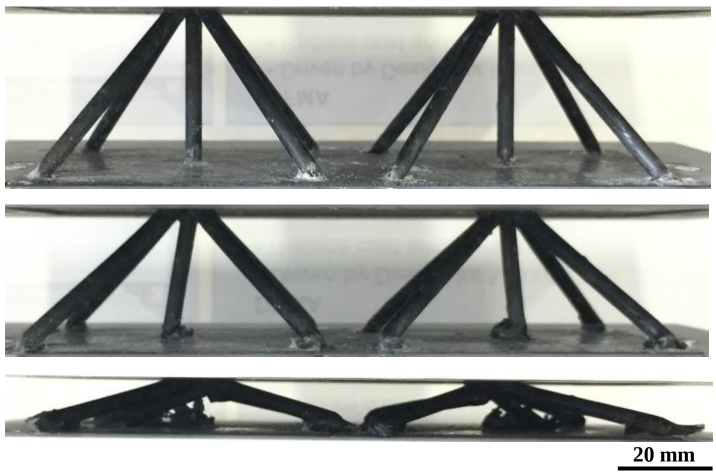

(c) 4 mm

Figure 4.30. Photographs of the modified-pyramidal lattices based on (2x1) unit cells during crushing under quasi-static loading.

The specific compression properties of the modified pyramidal lattice core based on (2x1) unit cells are presented in the Figure 4.31. As evidenced for (1x1) unit cell, an examination of the figure indicates the similar trend for (2x1) cells with increasing specific strength as the relative densities increase. However, the specific modulus of the panel is decreased with their relative densities. Moreover, following a close observation of Figure 4.31 as compared with Figure 4.28, it is found that the specific properties of the (2x1) unit cells are lower than that of (1x1) unit cell counterparts. The effect of varying the number of unit cells on the SEA values of the modified pyramidal lattice is compared in Figure 4.32. It is found that the SEA values of the (2x1) unit cells are slightly lower or equivalent to the (1x1) unit cell. This finding is different from that of the simple-pyramidal lattices, however the SEA values are higher compared to that of the pyramidal counterparts.

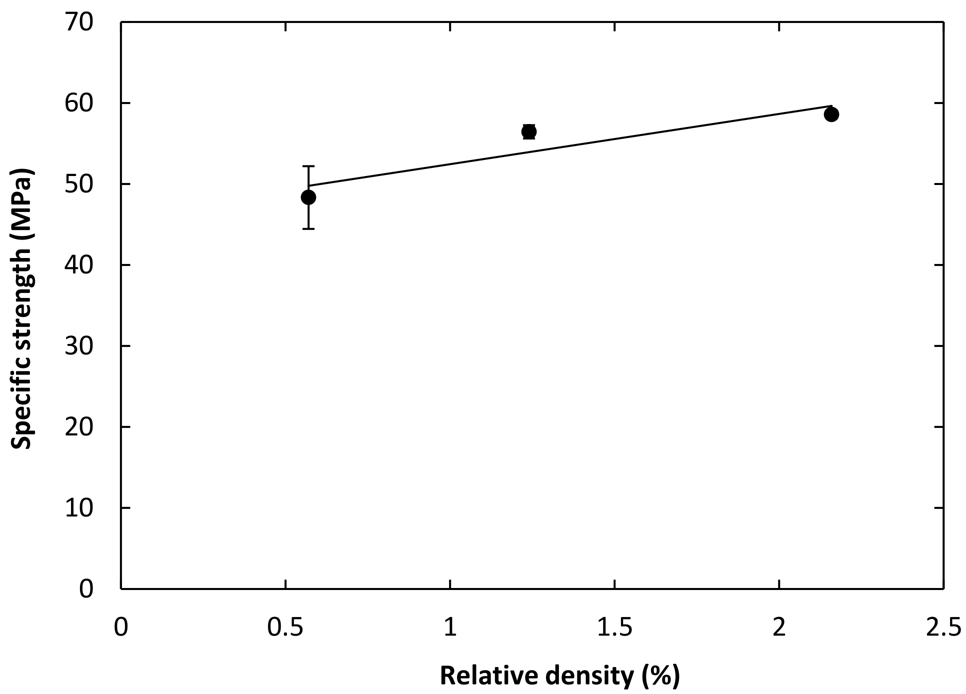

(a)

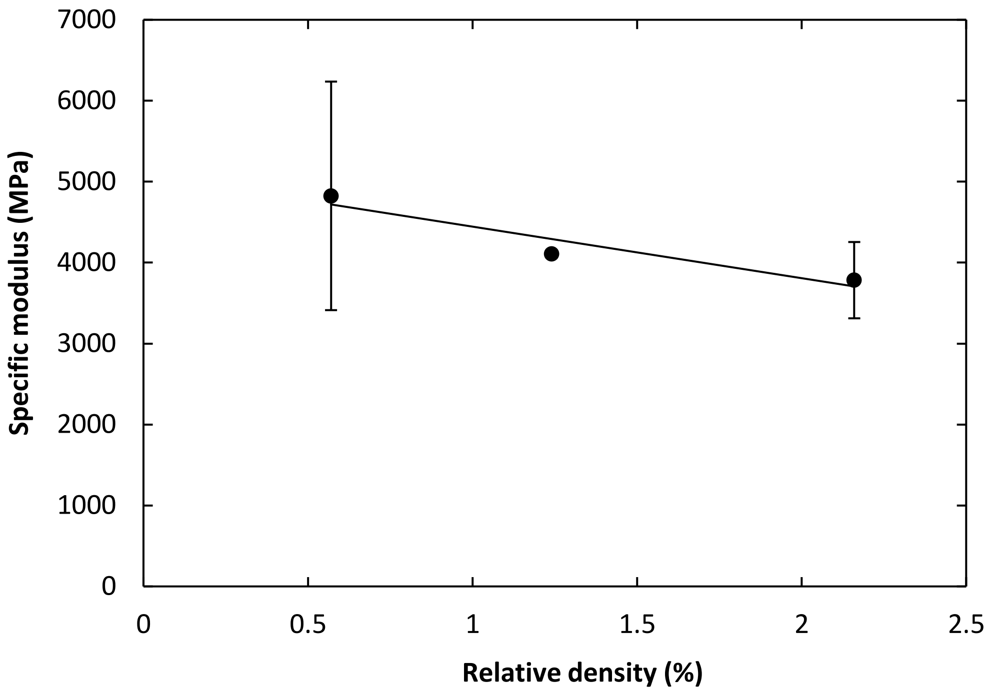

(b)

Figure 4.31. Comparison of specific properties of the modified-pyramidal lattice core structures based on (2x1) unit cells. (a) Strength (b) Modulus.

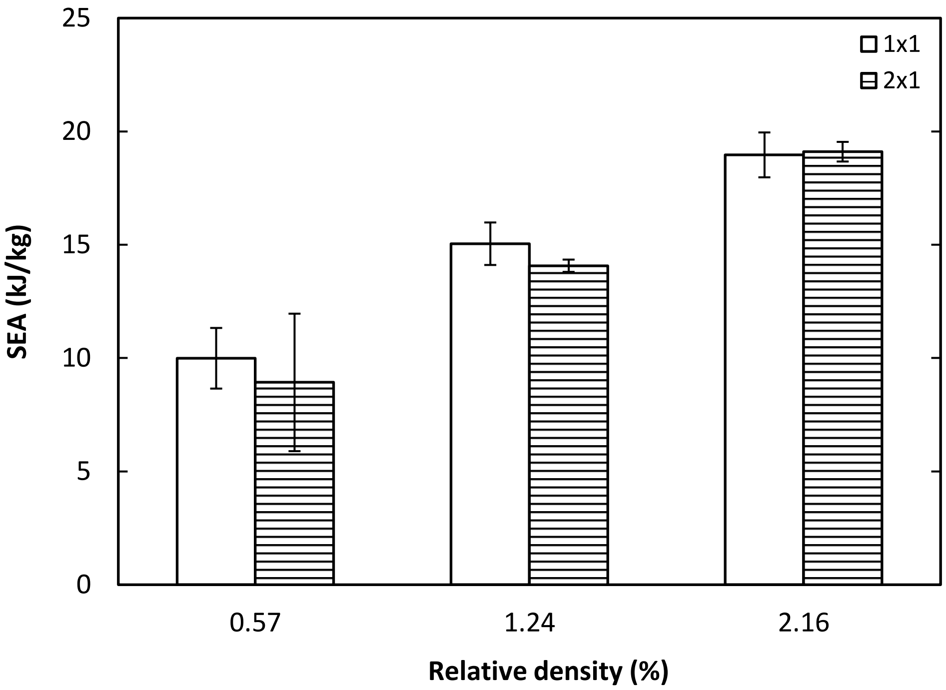

Figure 4.32. Comparison of the SEA values of the modified-pyramidal lattices with different numbers of unit cells.

4.5.2 Dynamic tests

The dynamic loading response of the modified-pyramidal lattice core structures has been evaluated and their tests are limited to (1x1) unit cell specimens only. Similarly, a mass (m) of 25.6 kg was used to crush the samples from a predefined height. Here, this mass was dropped from heights of 0.1, 0.28 and 0.64 m to strike the samples with 2, 3 and 4 mm diameter core-struts, respectively. Figure 4.33 shows the load-displacement traces following impact tests on the modified pyramidal lattices system. For comparison, load-displacement traces of the quasi-static test counterparts are included in Figures 4.33 (a) – (c). From the figure, it is clear that the force increases linearly up to the maximum value before a drastic drop of the force due to the progressive failure, followed by oscillation in which the load gradually decreases until the specimen experiencing a total damage and leads the force close to zero. An examination of the load-displacement trace indicates that the initial stiffness and the average peak load in the dynamic tests are higher than their quasi-static counterparts. Such a situation is possibly due to strain-rate effects in the composite, i.e. the material is strain-rate-dependant. It is also worth mentioning that buckling failure mode is not visible for 2 mm modified pyramidal lattice core structures under dynamic tests as evidenced for pyramidal lattice core counterparts. The presence of the vertical column in the centre of four-membered trusses results in the structures to fail by crushing the column initially and simultaneously crushing via node rupture for the other member at the joints.

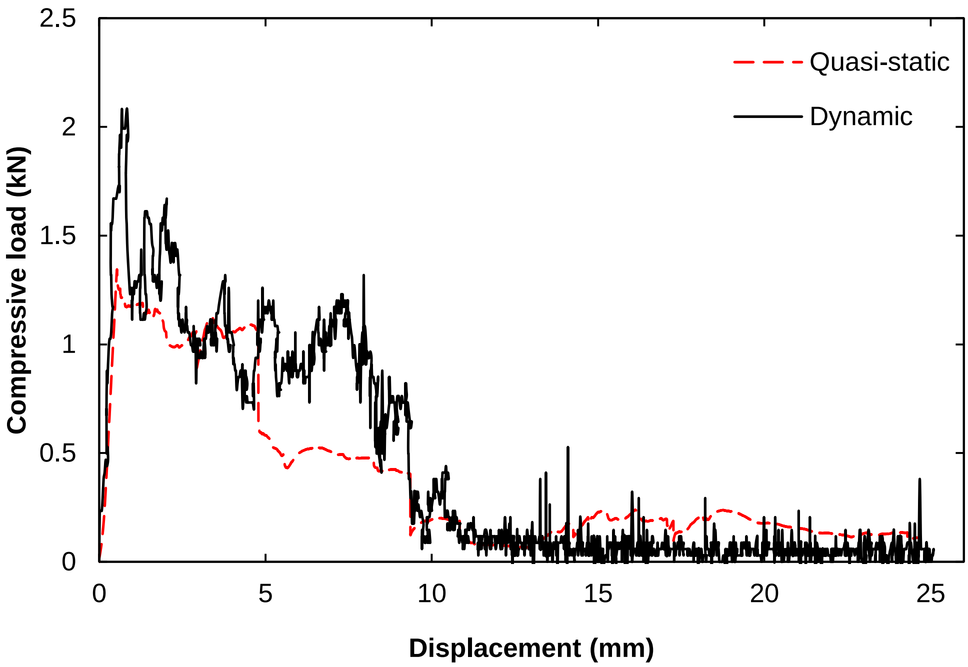

(a) 2 mm

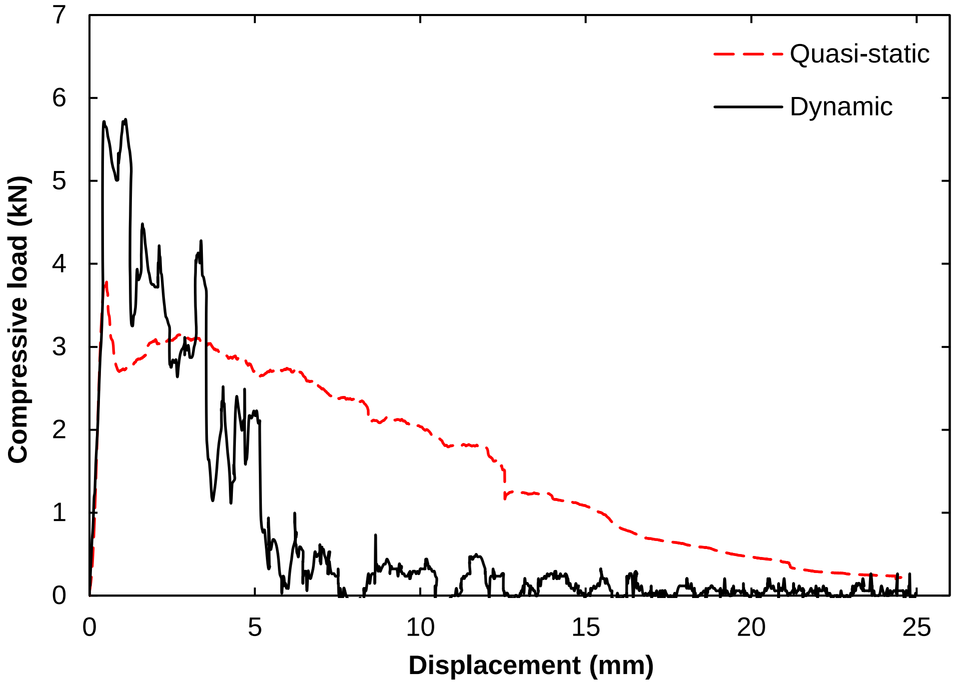

(b) 3 mm

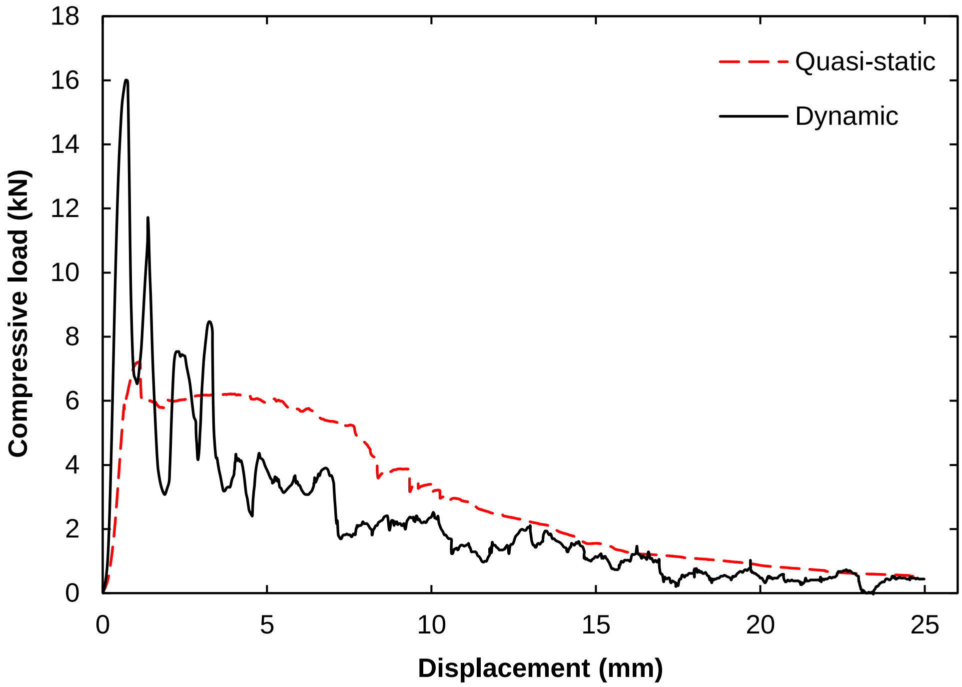

(c) 4 mm

Figure 4.33. Load-displacement traces following drop impact test on modified-pyramidal lattice cores sandwich structures.

Following this, typical stress-strain traces of modified-pyramidal specimens tested in dynamic loadings are presented in Figure 4.34. The peak stress increases when the diameter of the core-struts is increased. A comparison of the quasi-static compression and impact strength of the modified-pyramidal lattices is shown in Figure 4.35. In the figure, it is evident that the strength offered under dynamic conditions is much higher than that of their quasi-static counterparts. The trend shows an increasing pattern on both loadings with increasing core-struts diameter. For the 4 mm diameter, the modified-pyramidal lattice offers significant rise in the strength under impact loading compared to that quasi-static.

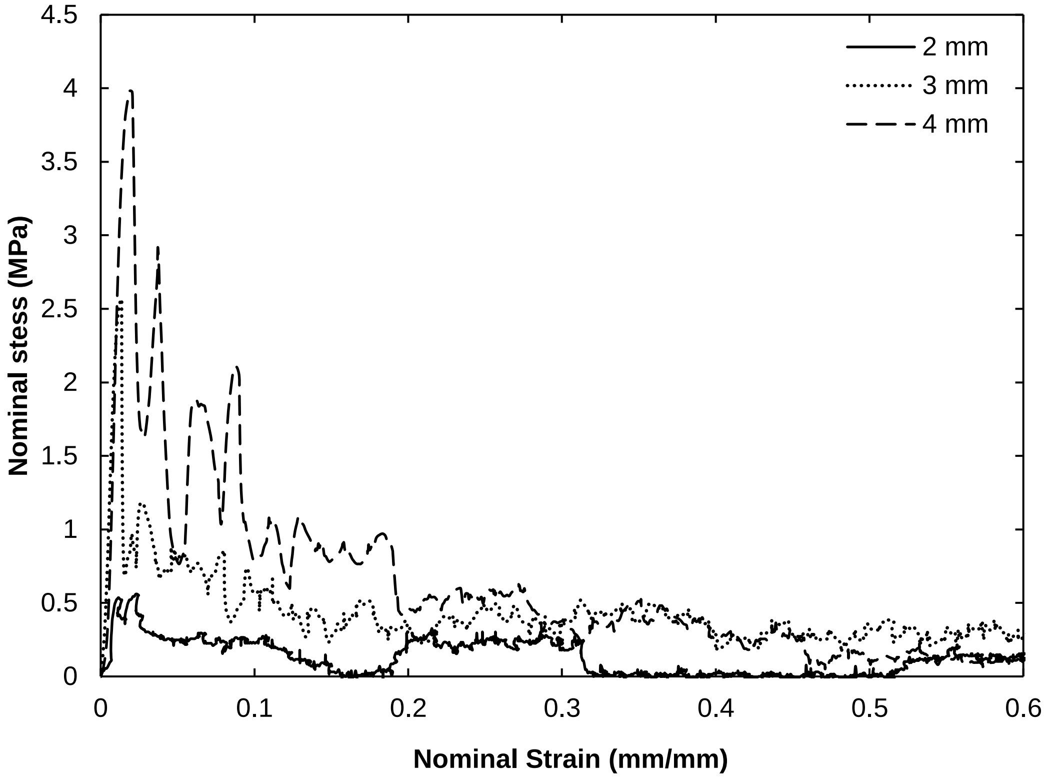

Figure 4.34. Typical stress-strain response under dynamic loading conditions for three different diameters of modified-pyramidal lattice core-strut.

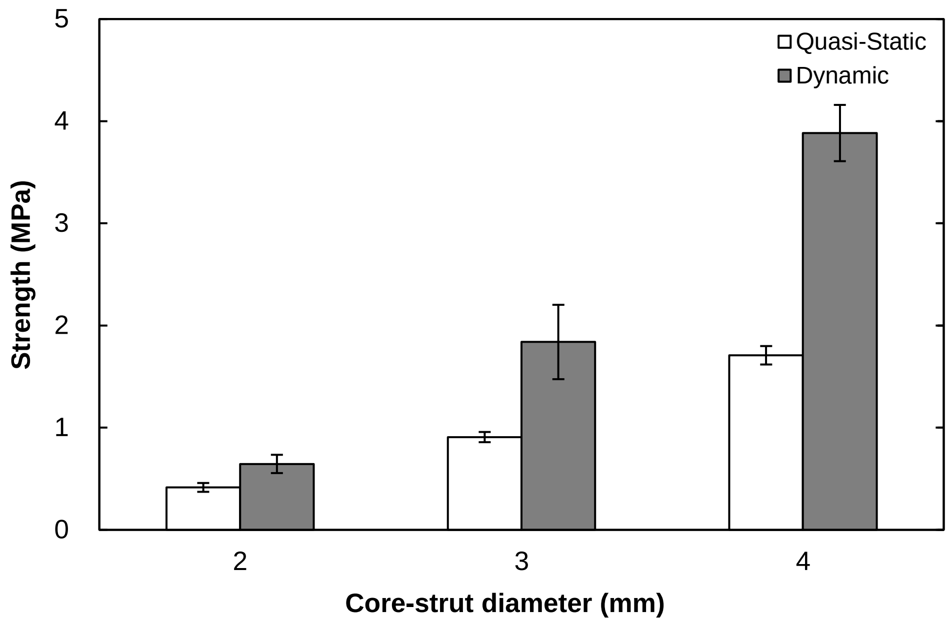

Figure 4.35. The variation of the strength of the specimens under quasi-static and dynamic conditions based on three diameters.

Furthermore, it is necessary to examine the energy absorption capabilities of the structures under quasi-static and dynamic conditions. Close examination of area under the curve force-displacement traces in former Figure 4.33 indicates that the impact-loaded samples absorb more energy in the initial stage of crushing compared with the quasi-static counterparts. Interestingly, the resulting energy absorption capacity are greater in dynamic loading than that in quasi-static loading for 2 mm core struts, however the lattices of other two diameter core-struts (3 mm and 4 mm) give lower energy absorption than their quasi-static loading counterparts, which is shown in Figure 4.37. Figures 4.36 (a) – (c) present the energy absorbed by the specimens over the crosshead movement based on quasi-static and dynamic loadings for three repeated tests of lattices with three different core-strut diameters. Figure 4.37 includes the SEA values resulting from the dynamic tests on modified-pyramidal lattice core structures as compared to their quasi-static counterparts.

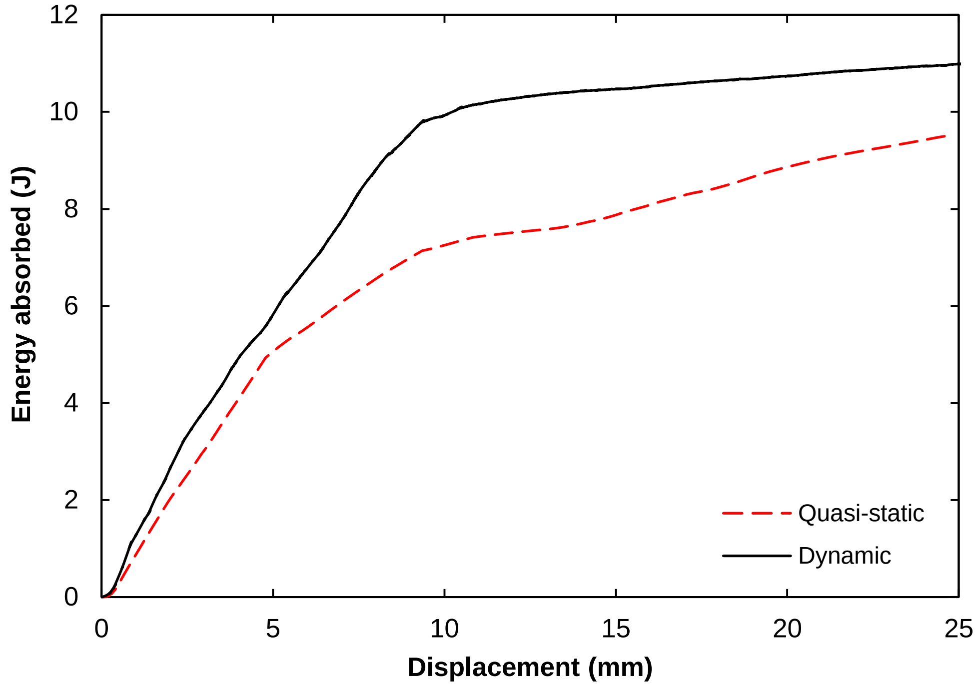
12
10
8
6
4
2
0
Energy absorbed (J)
0
5
10
15
20
25
Displacement (mm)
Quasi-static
Dynamic

(a) 2 mm

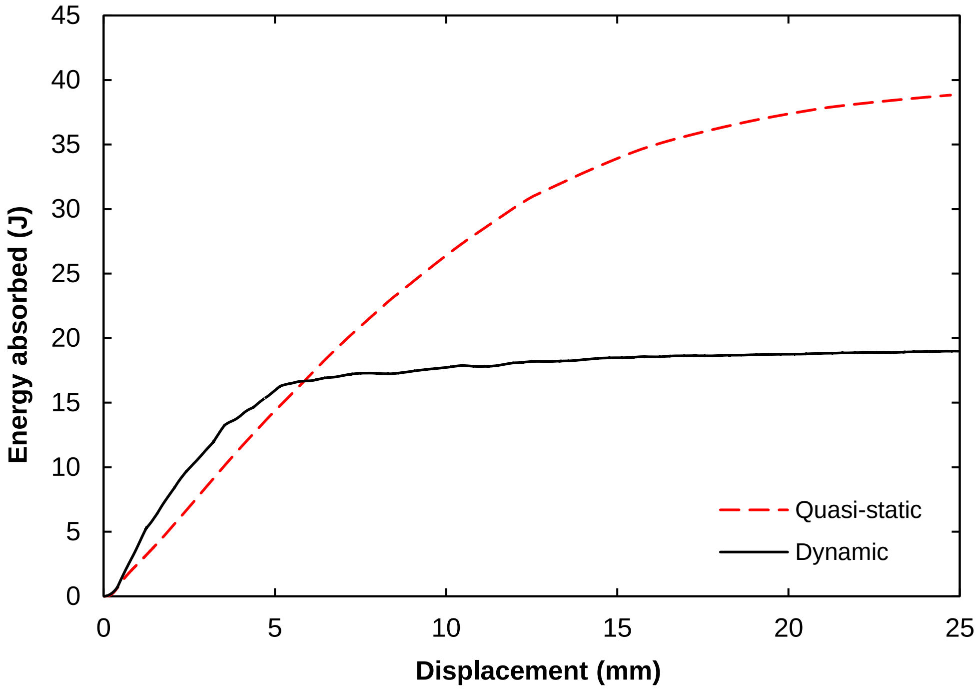
45
40
35
30
25
20
15
10
5
0
Energy absorbed (J)
0
5
10
15
20
25
Displacement (mm)
Quasi-static
Dynamic

(b) 3 mm

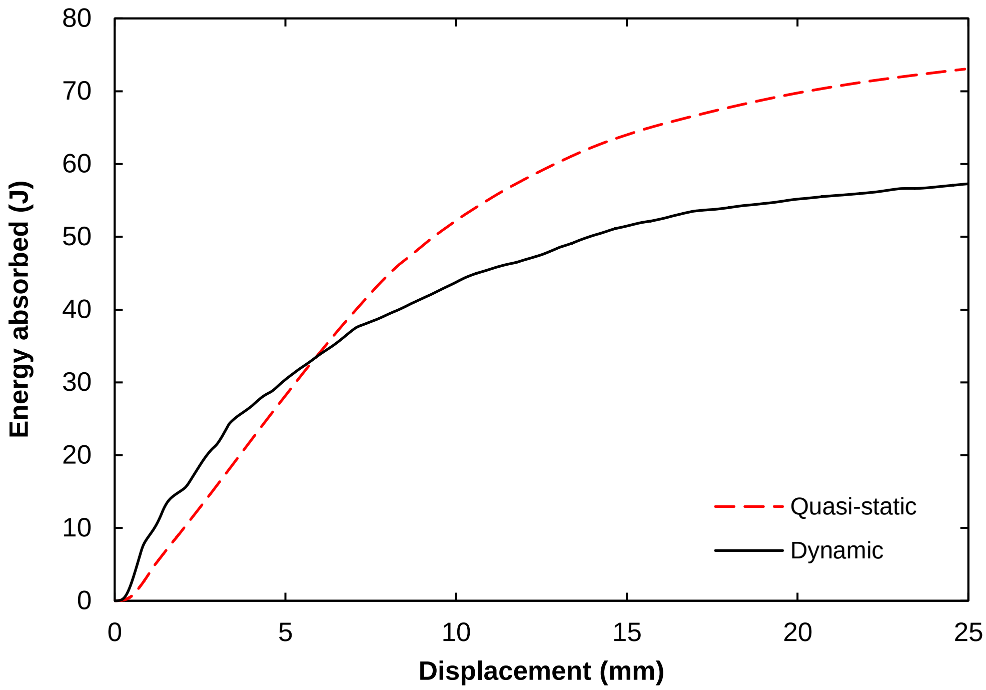

(c) 4 mm

Figure 4.36. The energy absorption traces for the modified-pyramidal core specimens under quasi-static and dynamic tests.

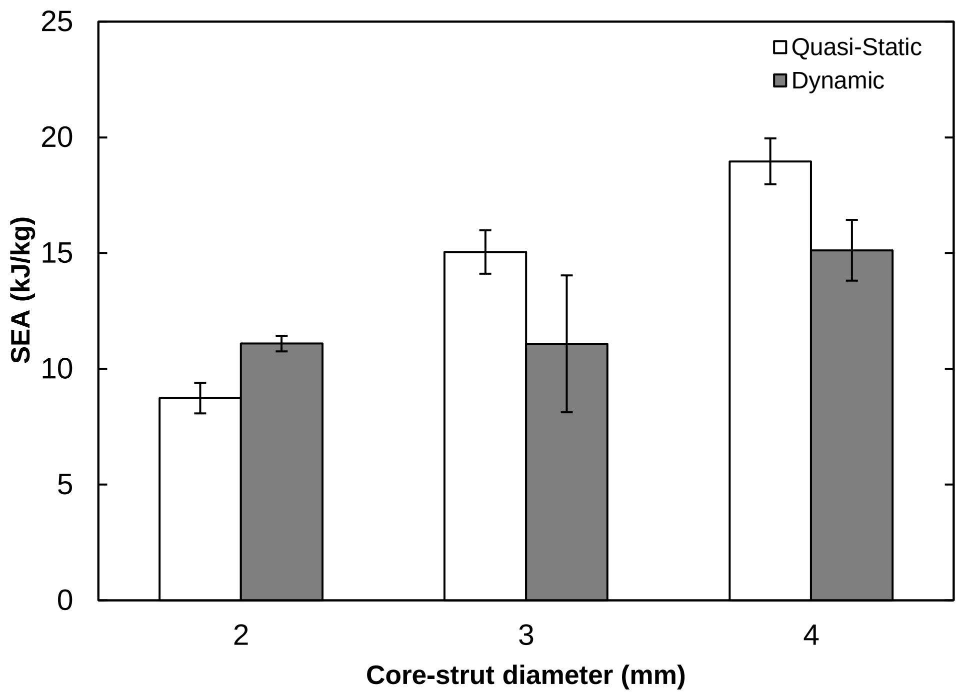

Figure 4.37. The variation of the specific energy absorption of the modified-pyramidal lattice cores under quasi-static and dynamic rates.

4.6 Complexity lattices based on pyramidal design

The next stage of this investigation focused on exploring the potential offered by sacrificial mould manufacturing method to fabricate the complex lattice structures based on the pyramidal topology by including more struts into the plain pyramidal core structure. The resulting lattice structures are then tested in both quasi-static and dynamic compression loadings to examine their mechanical behaviour and assessing energy-absorbing capabilities. Here, two different lattice structures were manufactured with 3 mm diameter core-struts identified as type-2 (T2) and type-3 (T3) modified designs yielding cores with relative densities of 1.95% and 2.14%, respectively. Again, the fibre volume fraction within an individual strut is kept as 42%.

4.6.1 Quasi-static compression tests

Figures 4.38(a) and (b) show stress-strain traces for the T2 and T3 structures under quasi-static loading. These two traces display the similar characteristics with two distinct regions. The first region is an elastic region with the stress linearly approaching the first peak value before an initial failure encountered. This is followed by the second region, being the non-linear segment associated with a series of failure events in the core truss members. In this region, the stress decreases with increasing strain, associated with serrations in the stress-strain traces until it is completely damaged at a strain of 0.6 mm/mm. The average maximum stresses measured for T2 and T3 lattice cores structures are 1.15 MPa and 1.66 MPa, respectively. The presence of vertical column in T3 lattice core has improved the load carrying capacity by 44% compared with T2 lattice core. An examination of the failure modes during the compression loading, shown in Figure 4.39, indicates both structures failed as a result of crushing via fibre splitting or facture at ends of truss members. This can be clearly seen at joints connecting the truss members to facesheets of the test samples, as shown in Figure 4.39. The vertical column in the T3 lattice core collapses by crushing of the column in a progressive manner as observed for the modified-pyramidal lattice core.

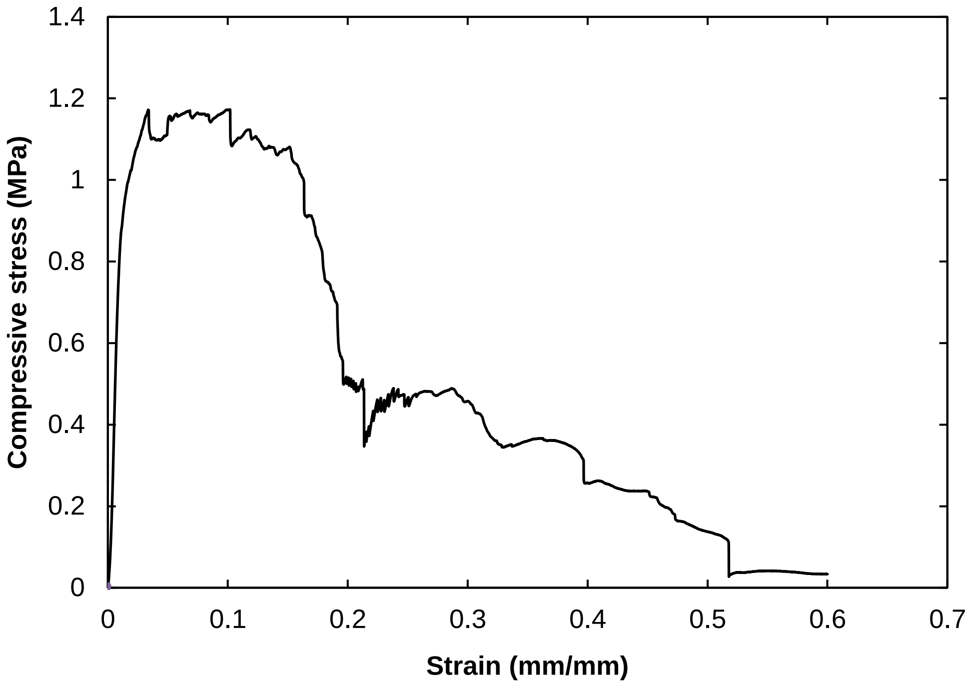

(a) T2 – 3mm

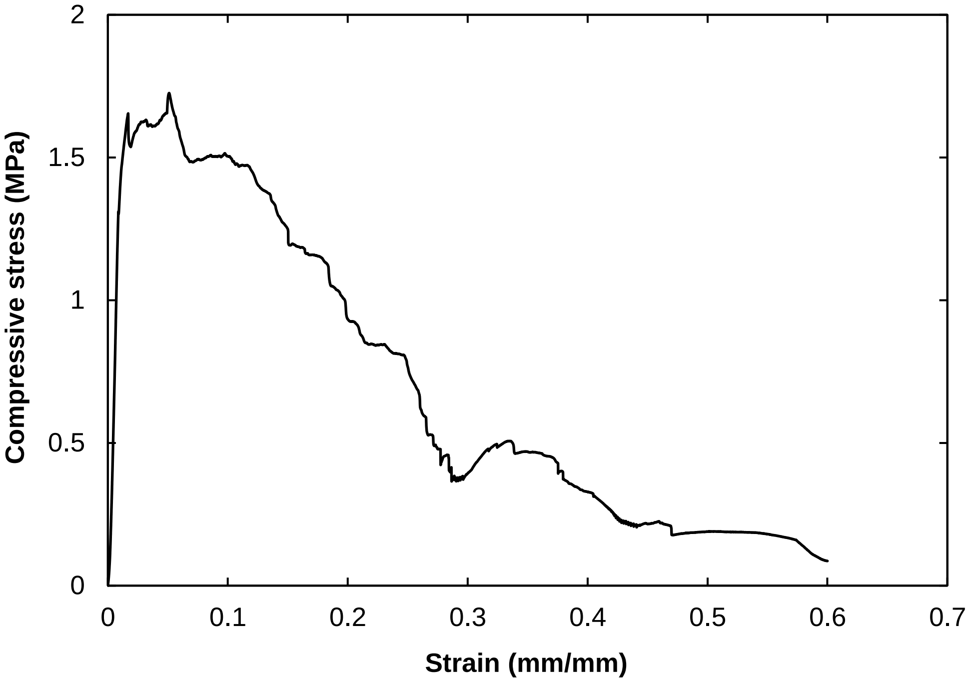

(b) T3 – 3mm

Figure 4.38. Typical stress-strain traces following quasi-static tests on complex lattice cores based on 3 mm diameter core-struts (a) T2 and (b) T3.

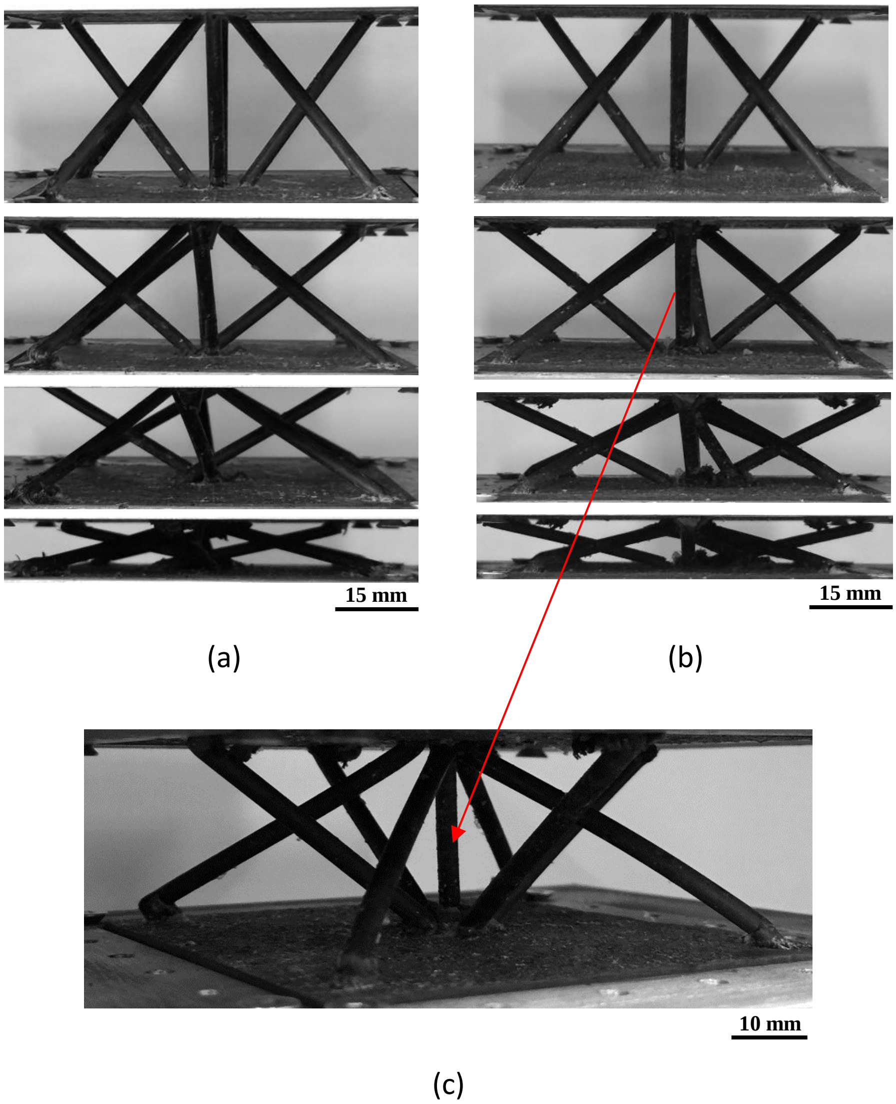

Figure 4.39. Sequences showing the failure modes in the complex lattice cores (a) T2 (b) T3 and (c) Closer photograph of vertical strut in T3 lattice.

The normalised compression strength and modulus of these lattice cores-based sandwich structures (type-2 and type-3) are presented in Figure 4.40. Normalised values are calculated by taking the measured values divided by the core density which gives an appropriate comparison between different lattices due to reason that their relative densities of the lattices are different. A comparison of the pyramidal and the modified-pyramidal (type-1) is also included in the figure to examine the performance of the manufactured composite lattice core sandwich structures. From the figure, it is clear that the T3 structure out-performs its T2 counterparts, for a given core density. For example, the normalised compression strength of the T3 lattice core structure with a density of 29.4 kg/m^3 is over twenty percent higher than that of T2 lattice core with a density of 25.3 kg/m^3. Similar trends are apparent in the normalised compression modulus data for these structures, shown in Figure 4.40(b). Here, the normalised modulus of the T3 structure is significantly higher than that of T2 structure, by showing an increase by 67%. However, close inspection of the figure indicates that the normalised strength and modulus by T2 and T3 structures are not showing much improvement when it compared to the values obtained by the plain pyramidal and the modified-pyramidal (T1) structures. For example, the value of the normalised strength only passes from approximately 41.26 kNm/kg for pyramidal lattice core with a density of 14.5 kg/m^3 to 45.25 kNm/kg for the T2 lattice core with density of 25.3. In addition, the normalised modulus of the T2 lattice core is significantly lower than the plain pyramidal lattice core structures and the other two designs as indicated in Figure 4.40(b). The highest values obtained for normalised strength and modulus are 56.35 kNm/kg and 6489.5 kNm/kg achieved by T3 lattice core structure. This is followed by the modified-pyramidal (T1) lattice core structure with specific strength of 55.03 kNm/kg and specific modulus of 6600 kNm/kg. From lightweight-perspective, it can be concluded that the modified-pyramidal (T1) lattice core sandwich structure offers superior properties to the other structures by just adding one vertical column to their open plain pyramidal core counterparts. Although T3 lattice core structure shows slightly better performance than the modified pyramidal, it needs more struts to achieve this, which directly increases the mass of the core. Despite of this, the sacrificial mould method offers a potential to manufacture a variety of core topology to produce lattice core panels with optimised specific properties.

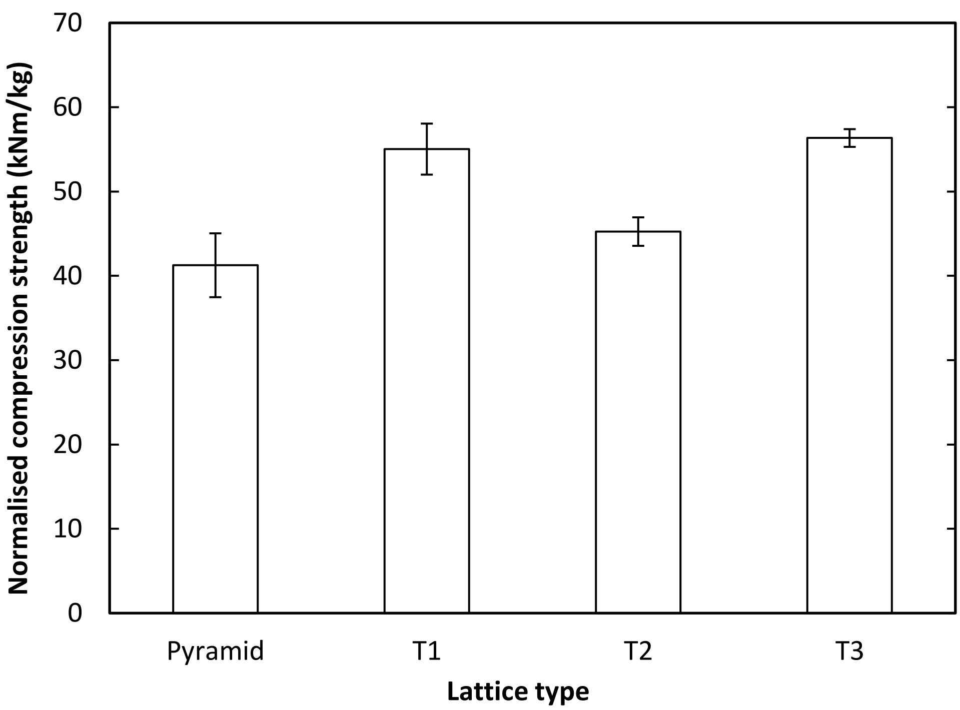

(a)

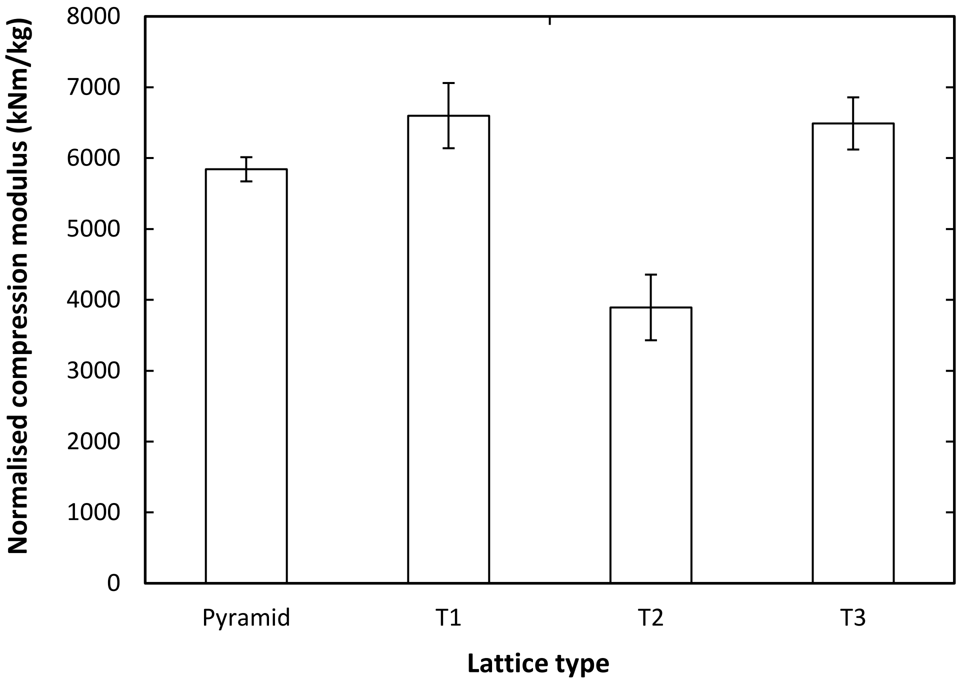

(b)

Figure 4.40. Comparison of specific properties of the composite lattice core structures (a) Strength (b) Modulus.

The energy required to crush the composite lattice core structures were again determined from the area under the load–displacement trace. Figure 4.41 shows the variation in the values of SEA for the T2 and T3 lattice core structures as a function of relative density. The values of SEA of the pyramidal and the modified-pyramidal (T1) counterparts are also included in the figure for comparison. The SEA values obtained following quasi-static testing are ranging approximately from 9 kJ/kg to 16 kJ/kg. It is again evident from the figure that the modified pyramidal lattices (T1, T2 and T3) outperform their plain pyramidal lattice core structure counterparts. This means the inclusion of the struts into plain pyramidal core requires higher force to initiate failure within the struts which in turns increases the energy absorption capabilities. However, it is clear that by only adding one vertical column in the plain pyramidal cores it is able to achieve SEA value equivalent to T3 structure which requires more struts within pyramidal topology.

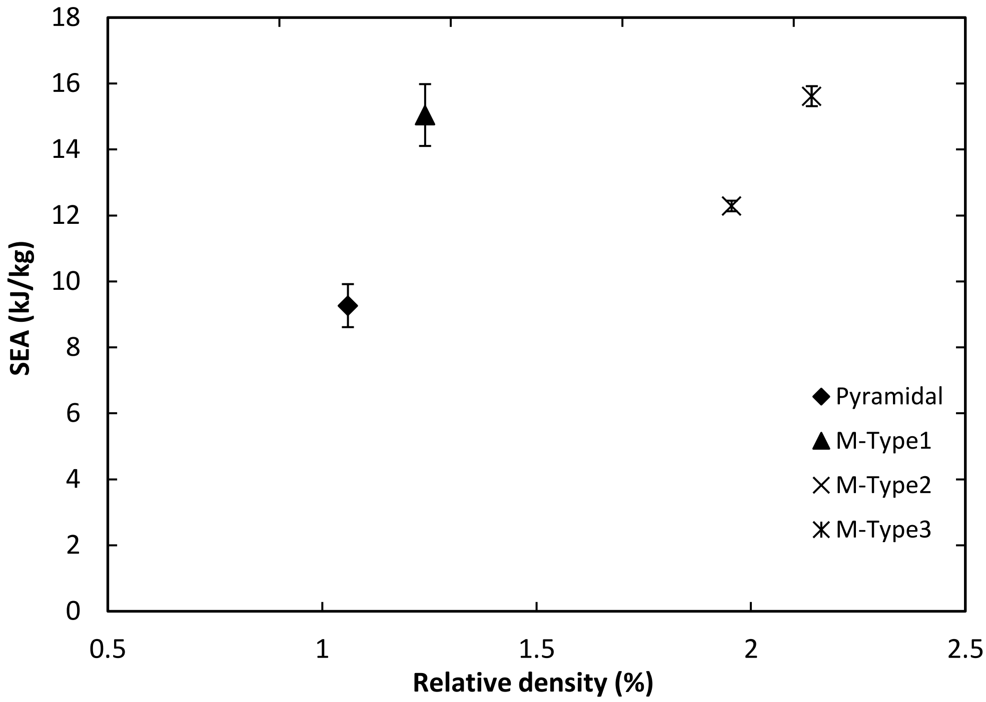

Figure 4.41. Variation of the SEA values of the manufactured the all-carbon composite lattice core sandwich structures.

4.6.2 Dynamic tests

Low-velocity impact tests were undertaken on the T2 and T3 lattice cores structures based on 3 mm diameter core-struts. Here, a mass (m) of 25.6 kg was used to crush the samples from height of 0.36 m and 0.52 m for T2 and T3 lattices, respectively. Figure 4.42 presents the dynamic load response of the complex lattice core structures. In the figure, both curves display a linear response prior to the load reaching a maximum value, followed by a significant drop before the load approaches to zero with increasing displacement manifesting a total damage in the structure. The peak loads in the dynamic tests are significantly greater than quasi-static counterparts, a phenomenon observed in other lattices tested formerly in dynamic loadings, which is once again showing strain-rate sensitivity of the structure. The failure mechanisms under dynamic loading are similar to those under quasi-static loading. This includes the struts failed by crushing via rupture and fibre splitting in the nodal connectivity in a brittle manner.

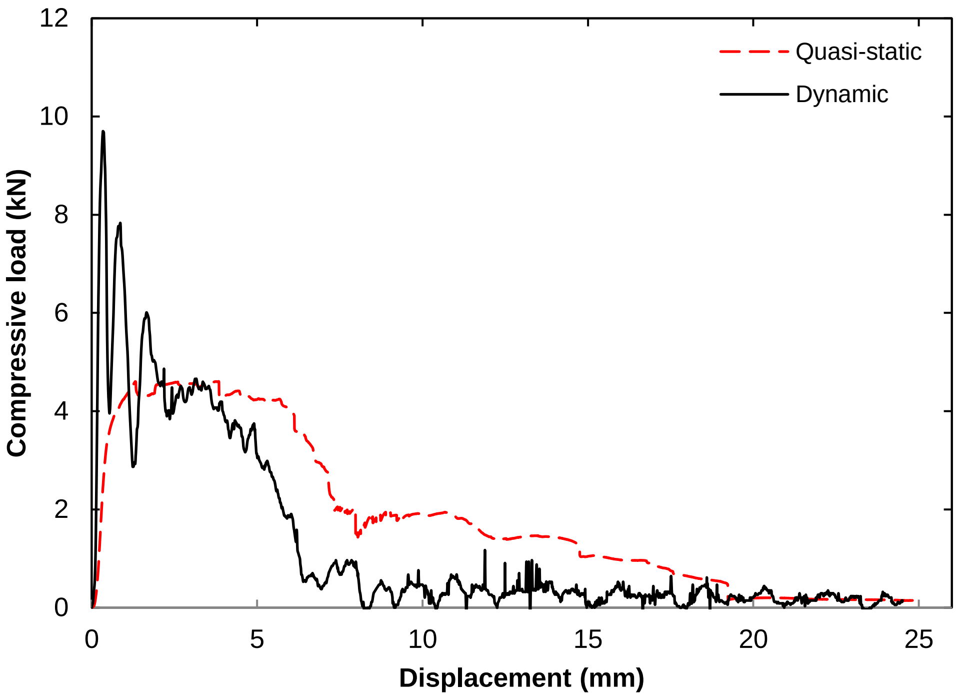

(a) T2 – 3mm

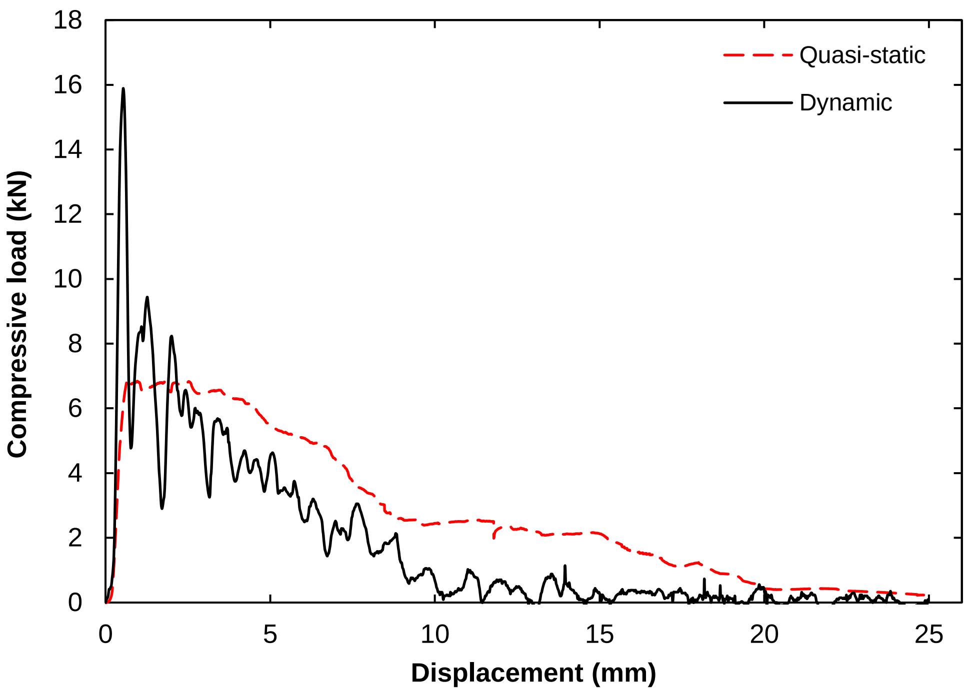

(b) T3 – 3mm

Figure 4.42. Compressive load-displacement traces of the lattice cores structures under dynamic and quasi-static loading (a) type-2 (T2) and (b) type-3 (T3).

Figure 4.43 shows typical stress-strain traces following impact tests on T2 and T3 lattice cores structures. Here, the nominal stress is obtained from the average applied load in Figure 4.42 divided by the planar area of connecting struts and the nominal strain is taken to be the crush length divided by the uncrushed lattice core height. It should be noted that the strength of type-3 structures are higher than those of type-2 lattice core, which is attributed to the higher relative density of the core. It is evident that from the Figure 4.43, the strength of the lattice structures increases with the number of struts included within the space of the core. Also, the dynamic strength is always higher than its quasi-static counterparts in all cases, as shown in Figure 4.44.

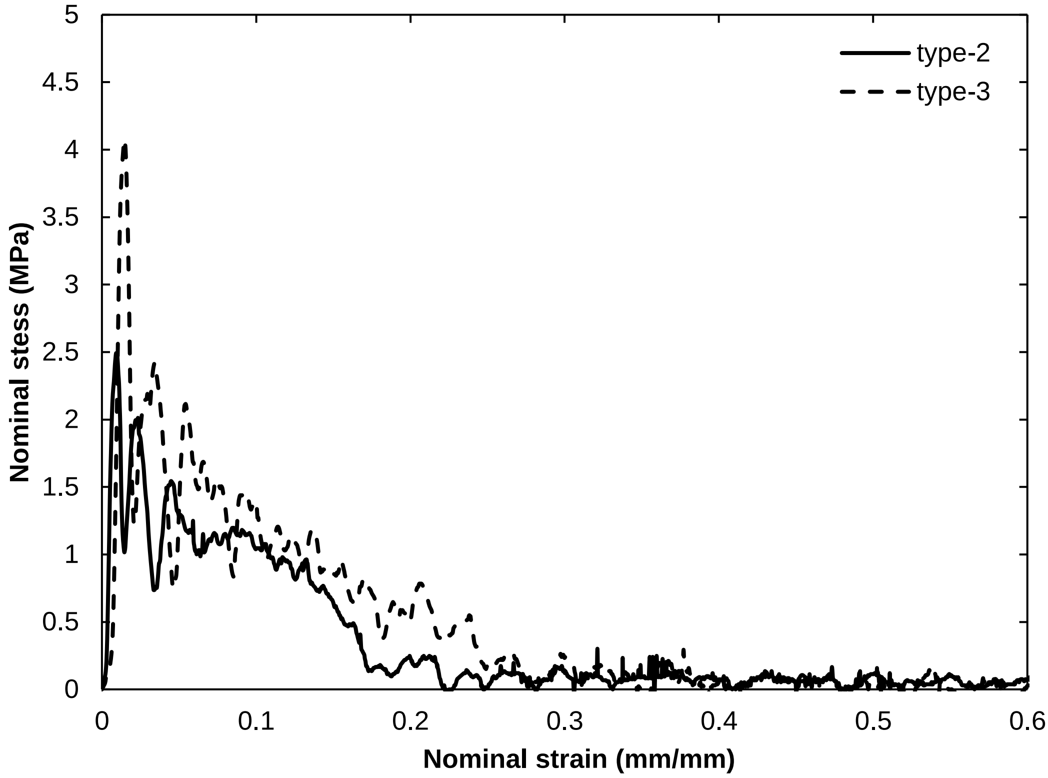

Figure 4.43. Typical stress-strain traces of the lattice cores structures under dynamic loading.

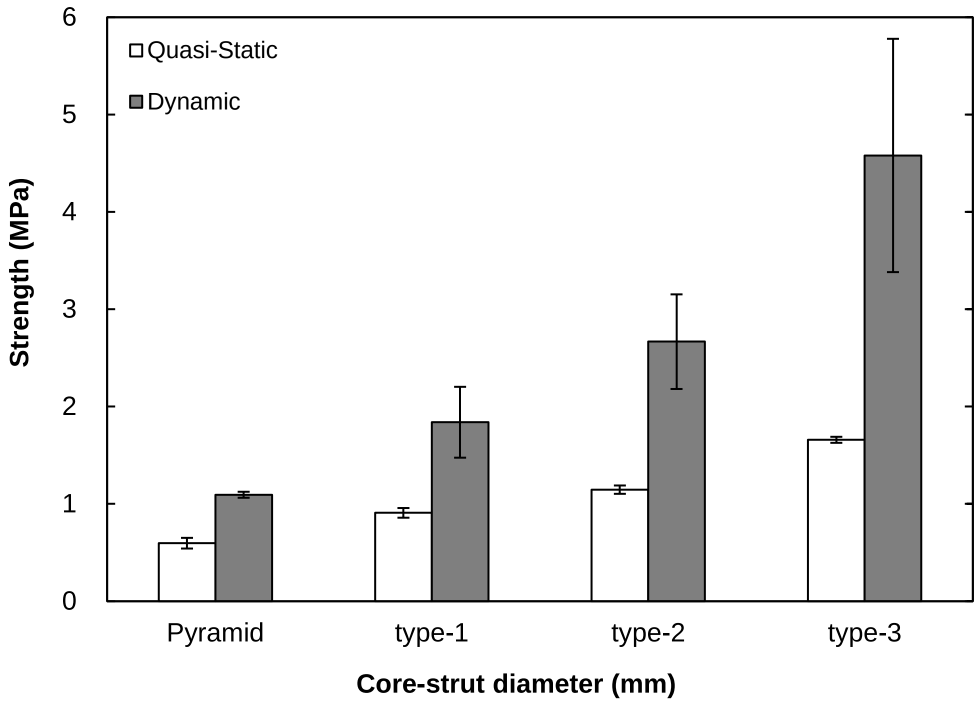

Figure 4.44. The compressive strength of various lattices based on 3 mm diameter core-struts under quasi-static and dynamic conditions.

Figure 4.45 includes the traces of the energy absorption of the T2 and T3 structures, crushing under impact loading. It again highlights the incident of absorbing more energy during initial crushing of the specimens under dynamic loading compared with their quasi-static counterparts. Subsequently, the energy absorption of the specimens under quasi-static loading surpasses their dynamic counterpart, which indicates more energy needed to crush the samples under the quasi-static mode. Figure 4.46 compares the SEA values of T2 and T3 lattices based on the plain pyramidal and the modified pyramidal (T1) lattices systems under quasi-static and dynamic loading. Interestingly, close examination of the figure indicates the SEA value of the modified-pyramidal is significantly greater than those of other lattices in dynamic condition, while the value is slightly lower or equivalent to T3 lattice core in quasi-static loading. In general, the modified-pyramidal of type-1 (T1) simply offers the superior SEA values in both quasi-static and dynamic events, which is potentially the best candidate for energy absorbing structures among others investigated.

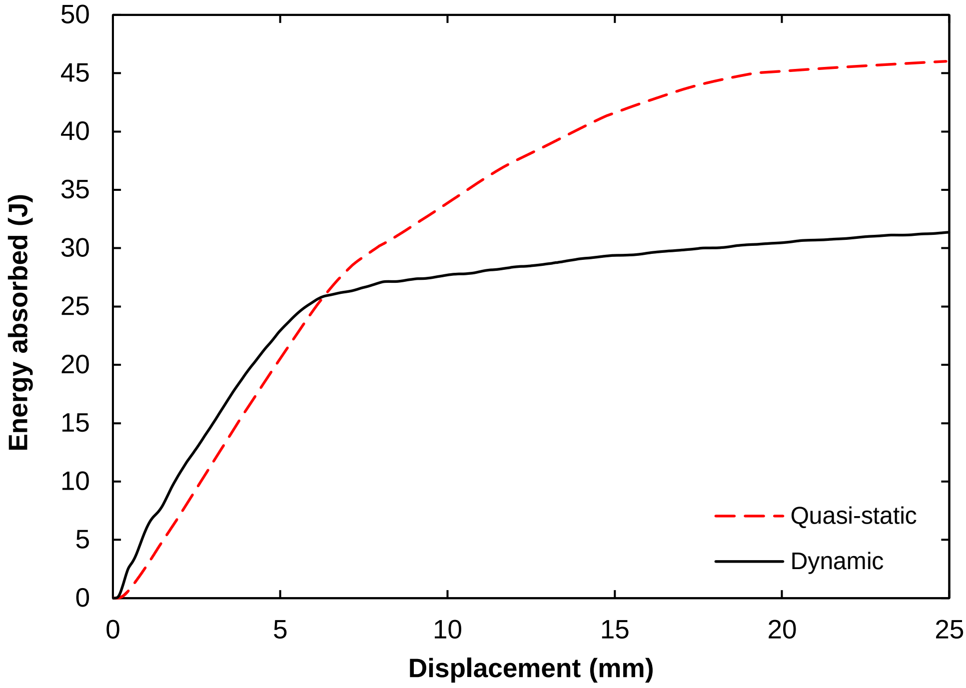

(a) T2 – 3mm

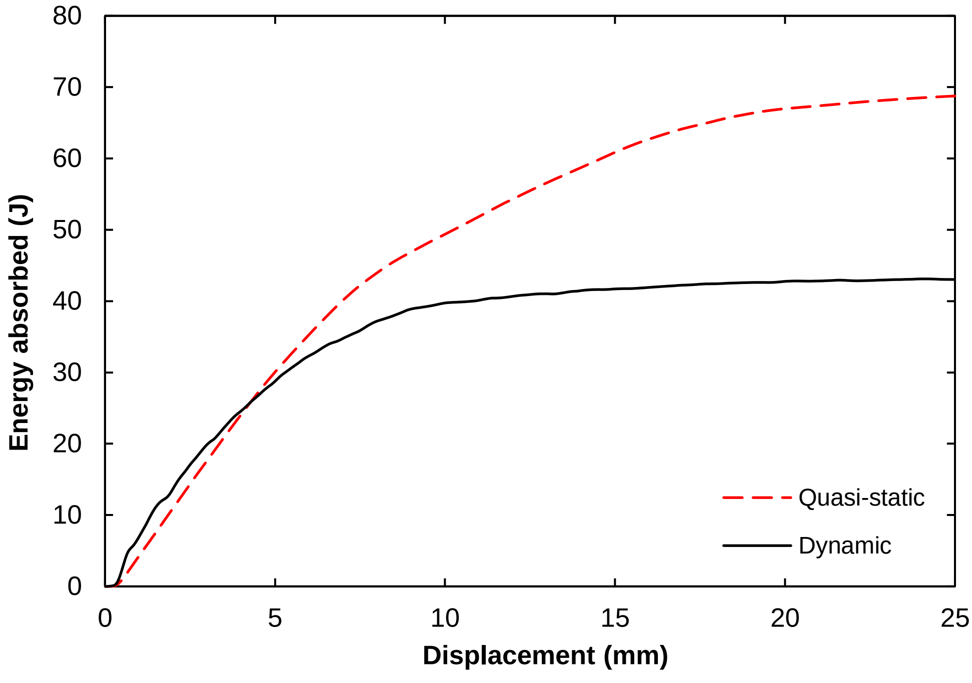

(b) T3- 3mm

Figure 4.45. The energy absorption traces following quasi-static and dynamic tests of the T2 and T3 lattice cores.

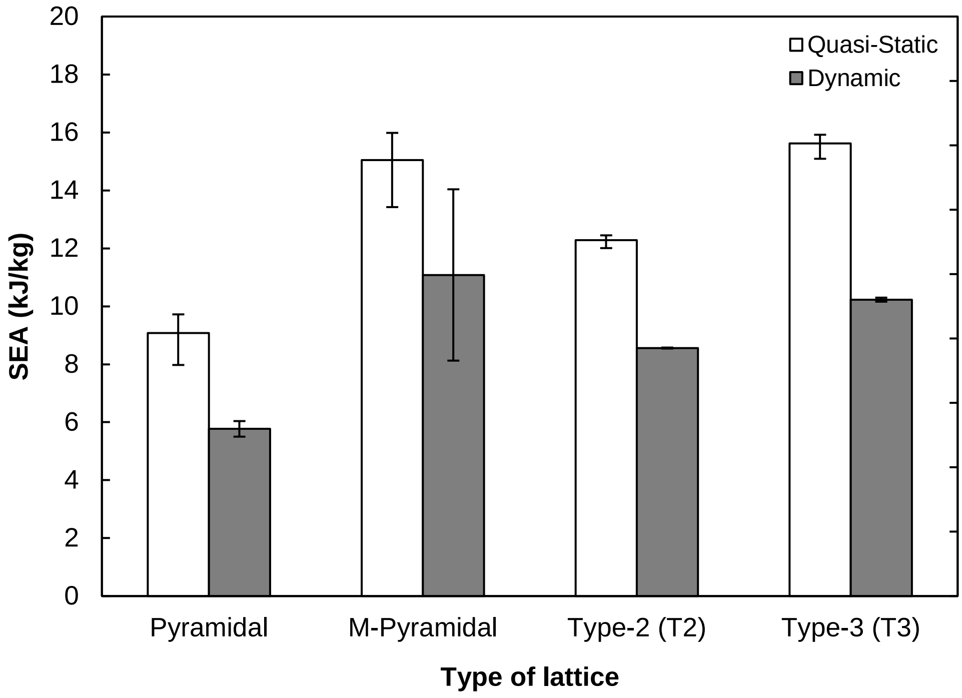

Figure 4.46. Comparison of quasi-static and dynamic SEA values of the manufactured composite lattices.

4.7 Comparison with competing structures

Stretching-dominated lattice truss structures made from range of materials for example, metal, polymer and composites are the focus in the research field of lightweight materials. Owing to lightweight characteristic, one of the main applications of lattice truss materials is as the core material in sandwich structures. Typically, the aim is to maximize the stiffness and/or strength-to-weight ratio of the lattice materials so as to enhance the performance of the sandwich structure in which they are employed. Based on the manufacturing method explored in this research, a range of all carbon composites lattices sandwich were produced. The compressive strength and stiffness of the carbon fibre reinforced composite pyramidal lattices investigated here are compared with other pyramidal lattice materials in an Ashby style plot in Figure 4.47 (a) and (b) respectively. In these figures, the strength and moduli are plotted as function of the lattice truss core density. Although not all previous studies report stiffness properties, the out-of-plane stiffness as function of density is plotted for a selected number of sandwich pyramidal core materials in Figure 4.47 (b). It is evident from the figures that the range of lattices manufactured using the sacrificial mould method has comparable properties (strength and modulus) to the other pyramidal lattice truss material. With density varying from 6 kg/m^3 to 30 kg/m^3 the composite lattice is much lighter. Within the scope of low density, the carbon fibre composite lattices have better strength and modulus, as shown in Figure 4.47.

(a)

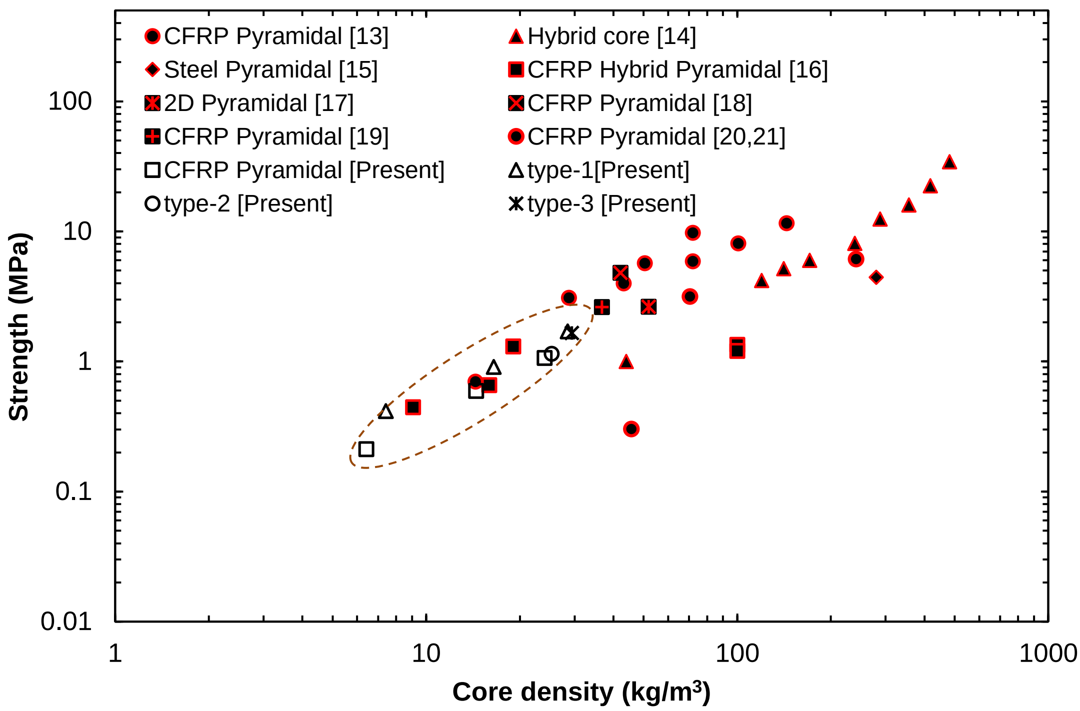

(b)

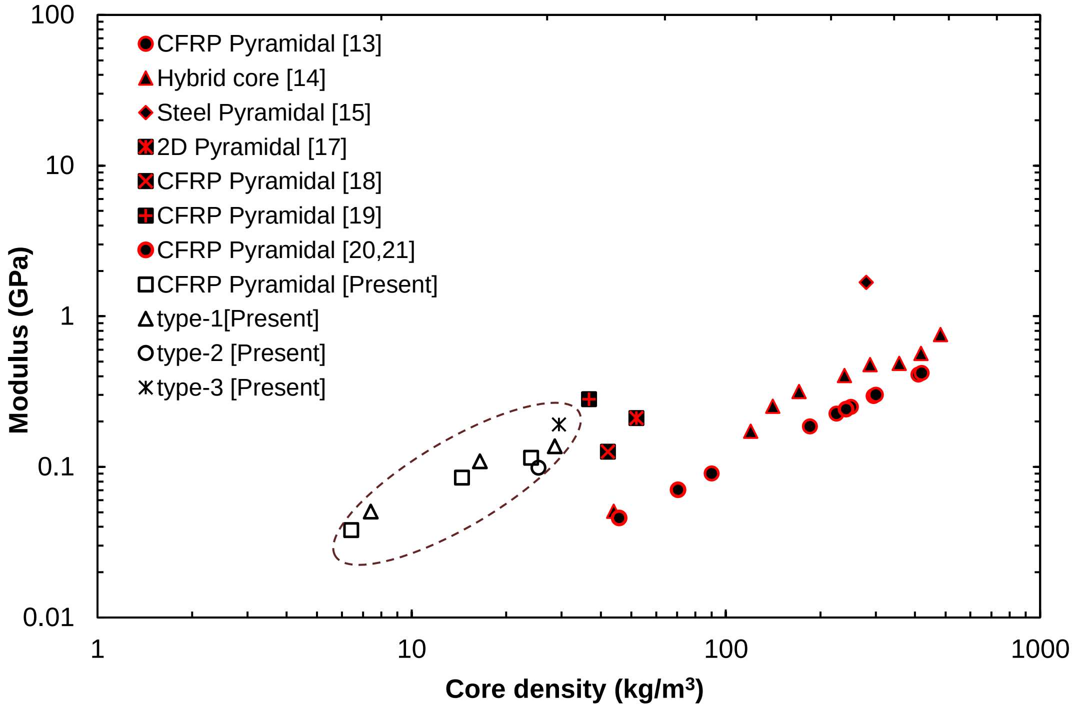

Figure 4.47. Out-of-plane compressive strengths and modulus for various pyramidal lattice structures as function of the density.

It is worth mentioning that the pyramidal lattices here were manufactured with a fibre volume fraction of approximately 42% only. This is much lower compared to those lattices presented for comparison in figures which some of them were manufactured from fibre volume fraction ranging from 50% to 60%. If the fibre volume fraction within an individual strut is much higher than 42%, it is likely much larger increases in strength and modulus can be achieved for the lattice cores presented in this research within the scale of much lower core density. Interestingly, the strength and modulus of the pyramidal and modified pyramidal lattice core system studied in this research are also compared with those other lattice topologies as illustrated in Figure 4.48 (a) and (b) respectively. For the range of metal and composite lattice topologies compared in the figures, for example, kagome, tetrahedral, octahedral, octet and many others, the lattices produced in this work have comparable and superior strength and modulus for the low-density regime at only 42% fibre volume fraction. At these low core densities has no competing metallic cores exist.

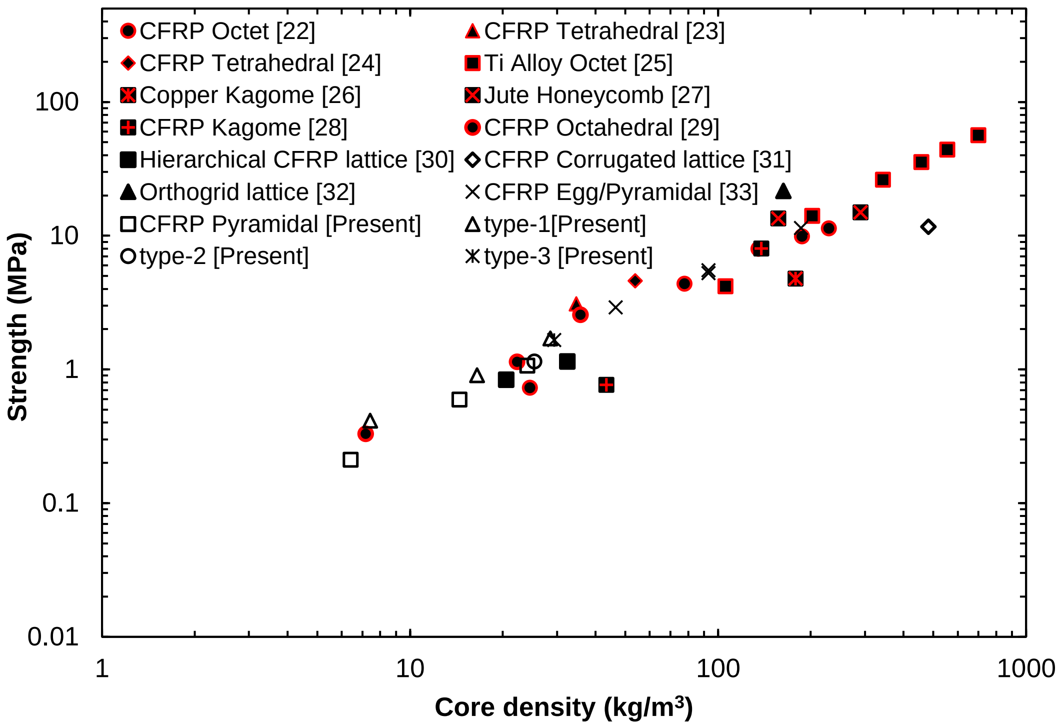

(a) Strength

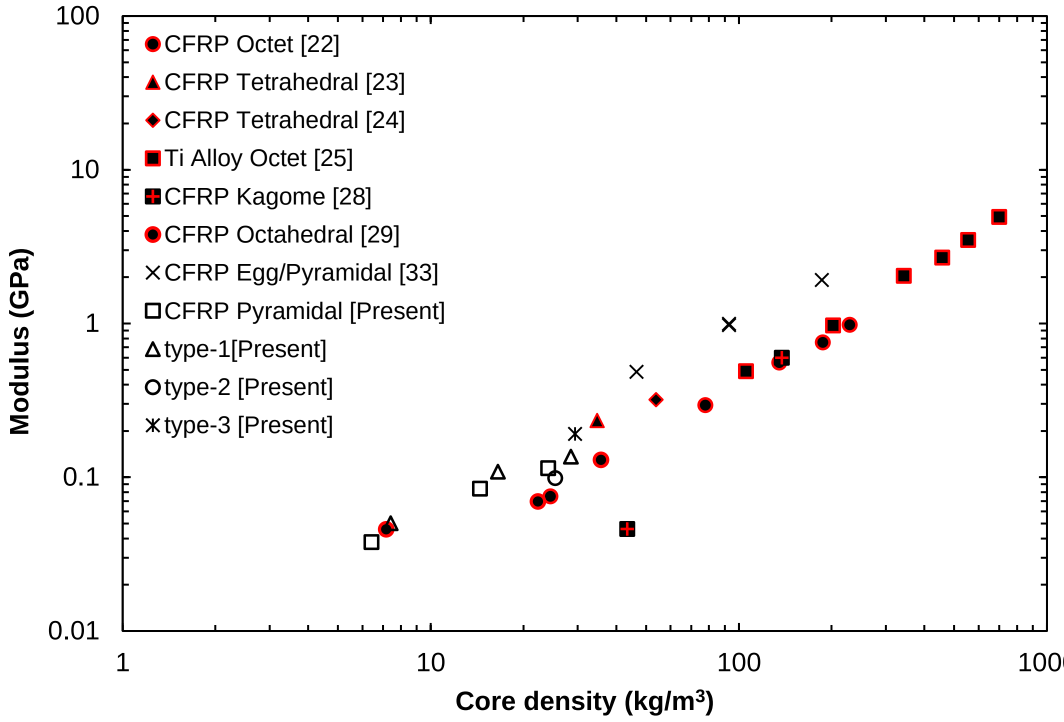

(b) Modulus

Figure 4.48. Core strength and modulus as function of core density for a range of different sandwich lattice core topologies materials.

In addition, they also possess good energy absorption characteristics, as shown in Figure 4.49. The energy absorption capability per unit mass is compared and it is suggested in the figure that the specific energy absorption of the lattices manufactured via sacrificial mould method is outstanding within the scope of low density. This indicates the columnar, pyramidal and modified lattice cores sandwich structures may potentially be good energy absorbing materials for lightweight applications.

Finally, the measured compressive strengths and moduli of the carbon fibre composite truss lattices investigated here were included in the material property charts. Material property charts are a useful way to compare the mechanical properties of varying density materials and allows us to position different materials on the figure. A chart of strength/modulus versus density is presented in Figure 4.50, where fully-dense materials such as metals, ceramics, composites and polymers are compared to foams and lattices.

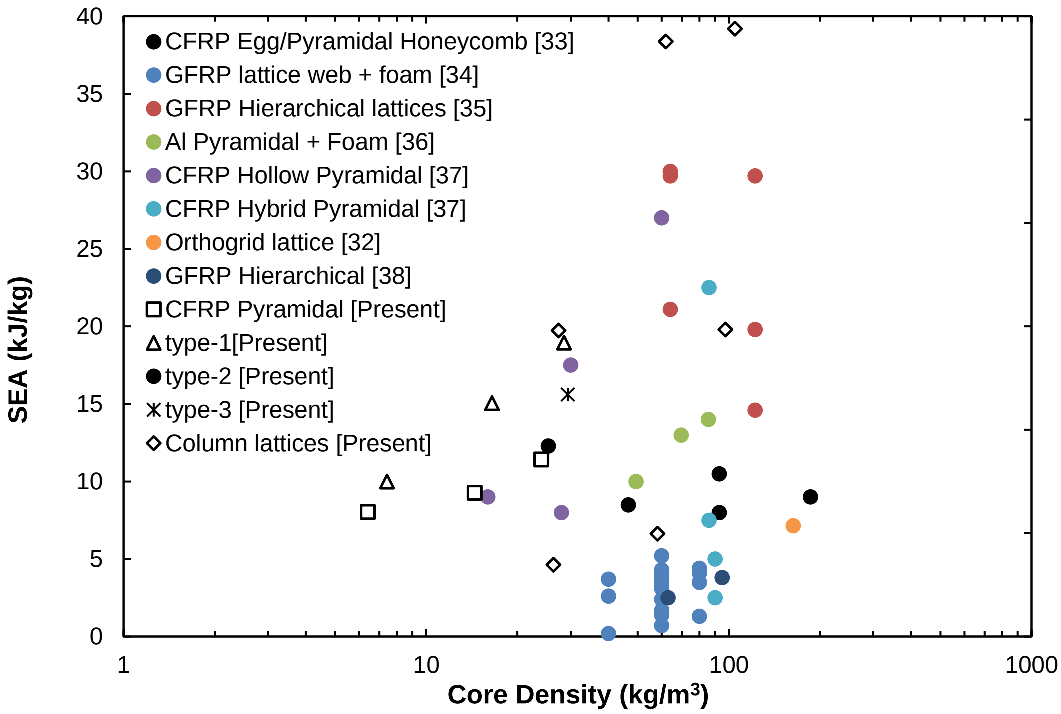

Figure 4.49. SEA values of lightweight truss core materials.

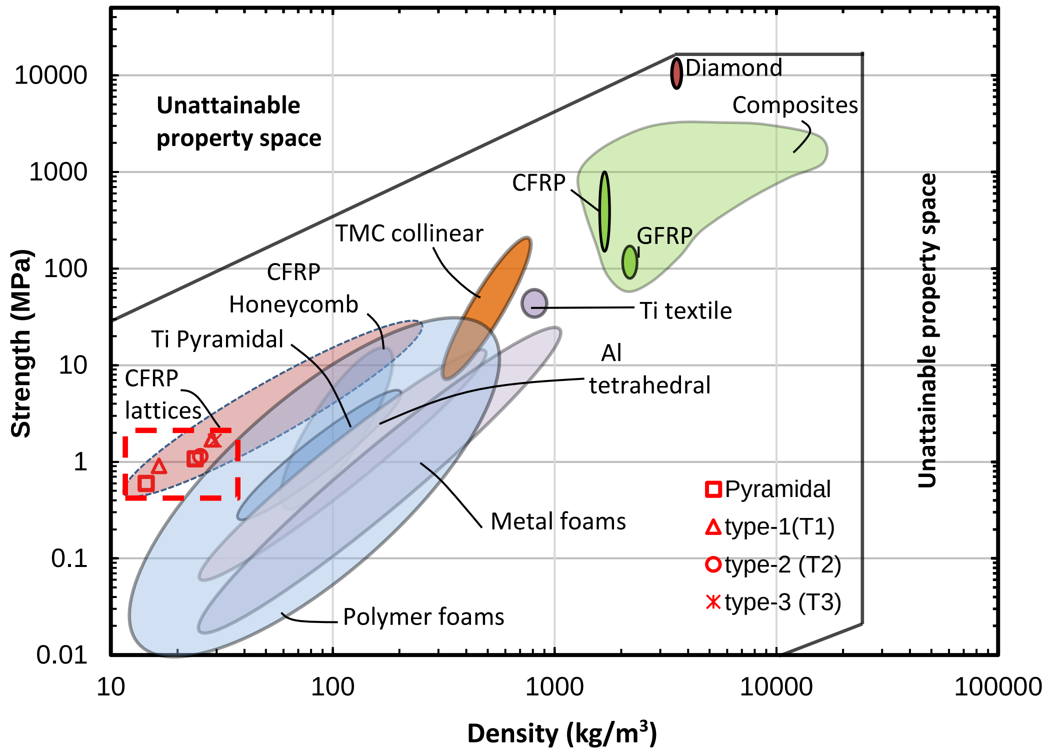

(a) Strength

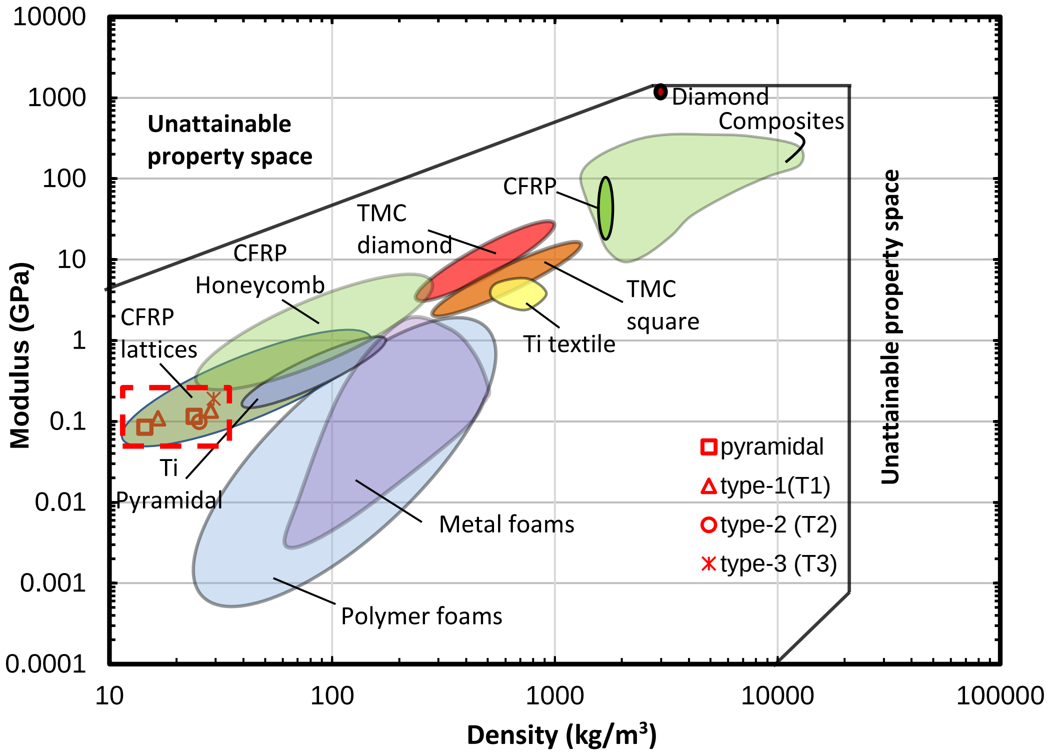

(b) Modulus

Figure 4.50. Material property chart comparing material properties against density (a) Strength (b) Modulus.

4.8 Summary

Chapter 4 has presented the manufacturing method to produce a range of lattice truss core sandwich structures based on carbon fibre composite using sacrificial mould method. This process included the manufacturing of the columnar, pyramidal and modified-pyramidal based lattice truss configuration. Initially, the fibre volume fraction within an individual composite column was characterised by conducting burn-off tests. The study aimed to maintain the fibre volume fraction in different member sizes to near agreement as possible as to permit a fair comparison between them.

This section has investigated the quasi-static and dynamic response of a range of all-carbon composite lattice cores sandwich structures manufactured using sacrificial mould method based on different fibre volume fractions and core-strut diameters. The data for the lattice cores sandwich specimens under quasi-static and dynamic compression tests were presented, and the failure mechanisms were discussed in detail. The study has shown that the failure modes of the lattices were predominantly controlled by Euler buckling and fracture of the struts.

It has been shown that by adding a vertical strut to the plain pyramidal unit cell, the mechanical properties of the lattice are improved significantly. It is likely that optimisation of the unit cell geometry could further enhance these properties and increase the potential for use in load-bearing applications. The possibility of manufacturing the such lattices configuration using sacrificial mould method proved to be an advantage over other techniques, which extremely challenging to manufacture using composite material.

Dynamic testing has shown an increase in the peak load of the range of lattices structures studied. However, the overall energy absorption capacity of lattice structures in dynamic loading showed a decrease of approximately 30% compared to structures tested in most of quasi-static cases due to more significant drop of load carrying capacity after the damage initiation.

Improvements in the sacrificial mould method, producing composite struts with fewer imperfections, could also lead to an enhancement of the structures properties.

References

[1] I.M. Daniel and O. Ishai, Engineering Mechanics of Composite Materials, 2nd Edition, Oxford University Press, 2006.

[2] ASTM D2584 – 11 Standard test method for ignition loss of cured reinforced resins, ASTM, PA, USA; 2011.

[3] ASTM D3171 – 15 Standard test methods for constituent content of composite materials, ASTM, PA, USA; 2015.

[4] D.U. Shah, P.J. Schubel, P. Licence and M.J. Clifford, Determining the minimum, critical and maximum fibre content for twisted yarn reinforced plant fibre composites, Composites Science and Technology, 72, 2012, pp1909–1917.

[5] L. Che, G. Xu, T. Zeng, S. Cheng, X. Zhou, and S. Yang, Compressive and shear characteristics of an octahedral stitched sandwich composite, Composite Structures, 112, 2014, pp179–187.

[6] G. Xu, J. Zhai, T. Zeng, Z. Wang, S. Cheng, and D. Fang, Response of composite sandwich beams with graded lattice core, Composite Structures, 119, 2015, pp666–676.

[7] B. Wang, L. Wu, L. Ma, Q. Wang, and S. Du, Fabrication and testing of carbon fiber reinforced truss core sandwich panels, Journal of Materials Science and Technology, 25, 2009, pp547–550.

[8] B. Wang, L. Wu, X. Jin, S. Du, Y. Sun, and L. Ma, Experimental investigation of 3D sandwich structure with core reinforced by composite columns, Materials and design, 31, 2010, pp158–165.

[9] J. Xiong, L. Ma, L. Wu, M. Li, and A. Vaziri, Mechanical behavior of sandwich panels with hollow Al–Si tubes core construction, Materials and design, 32, 2011, pp592–597.

[10] J. Zhou, Z. W. Guan, W. J. Cantwell, and Y. Liao, The energy-absorbing behaviour of foam cores reinforced with composite rods, Composite strctures, 116, 2014, pp346–356.

[11] G.L. Farley, Energy absorption of composite materials, Journal of Composite Materials, 17, 1983, pp267–279.

[12] J.S Kim, H.J Yoon and K.B Shin, A study on crushing behaviors of composite circular tubes with different reinforcing fibers, International Journal of Impact Engineering, 38, 2011, pp198 – 207.

[13] K. Finnegan, G. Kooistra, H.N.G. Wadley, and V.S. Deshpande, The compressive response of the carbon fiber composite pyramidal truss sandwich cores, International Journal of Materials Research, 98, 2007, pp1–9.

[14] T. George, V.S. Deshpande, K. Sharp, and H.N.G. Wadley, Hybrid core carbon fiber composite sandwich panels: Fabrication and mechanical response, Composite Structures, 108, 2014, pp696–710.

[15] R. Biagi and H. Bart-Smith, Imperfection sensitivity of pyramidal core sandwich structures, International Journal of Solids and Structures, 44, 2007, pp4690–4706.

[16] S. Yin, L. Wu, L. Ma, and S. Nutt, Hybrid truss concepts for carbon fiber composite pyramidal lattice structures, Composites: Part B, 43, 2012, pp1749–1755.

[17] B. Wang, G. Zhang, Q. He, L. Ma, L. Wu, and J. Feng, Mechanical behavior of carbon fiber reinforced polymer composite sandwich panels with 2-D lattice truss cores, Materials and Design, 55, 2014, pp591–596.

[18] Y. Sun and L. Gao, Mechanical behavior of all-composite pyramidal truss cores sandwich panels, Mechanics of Materials, 65, 2013, pp56–65.

[19] M. Li, L. Wu, L. Ma, B. Wang, and Z. Guan, Mechanical Response of All-composite Pyramidal Lattice Truss Core Sandwich Structures, Journal of Materials Science and Technology, 27, 2011, pp570–576.

[20] J. Xiong, L. Ma, L. Wu, B. Wang, and A. Vaziri, Fabrication and crushing behavior of low density carbon fiber composite pyramidal truss structures, Composite Structures, 92, 2010, pp2695–2702.

[21] J. Xiong, L.Ma, A. Vaziri, J. Yang and L.Wu, Mechanical behavior of carbon fiber composite lattice core sandwich panels fabricated by laser cutting, Acta Materialia, 60, 2012, pp5322–5334.

[22] L. Dong and H. Wadley, Mechanical properties of carbon fiber composite octet-truss lattice structures, Composites Science and Technology, 119, 2015 pp26–33.

[23] J. Mei, J. Liu, and J. Liu, A novel fabrication method and mechanical behavior of all-composite tetrahedral truss core sandwich panel, Composites: Part A, 102, 2017, pp28–39.

[24] G. Zhang, L. Ma, B. Wang, and L. Wu, Mechanical behaviour of CFRP sandwich structures with tetrahedral lattice truss cores, Composites: Part B, 43, 2012, pp471–476.

[25] L. Dong, V. Deshpande, and H. Wadley, Mechanical response of Ti-6Al-4V octet-truss lattice structures, International Journal of Solids and Structures, 60–61, 2015, pp107–124.

[26] J. Wang, A.G. Evans, K. Dharmasena, and H.N.G. Wadley, On the performance of truss panels with Kagomé cores, International Journal of Solids and Structures, 40, 2003, pp6981–6988.

[27] A. Stocchi, L. Colabella, A. Cisilino and V. Álvarez, Manufacturing and testing of a sandwich panel honeycomb core reinforced with natural-fiber fabrics, Materials and Design, 55, 2014, pp394–403.

[28] H. L. Fan, F. H. Meng, and W. Yang, Sandwich panels with Kagome lattice cores reinforced by carbon fibers, Composite Structures, 81, 2007, pp533–539.

[29] L. Che, G. Xu, T. Zeng, S. Cheng, X. Zhou, and S. Yang, Compressive and shear characteristics of an octahedral stitched sandwich composite, Composite Structures, 112, 2014, pp179–187.

[30] Y. Liu, C. Zhou, B. Cen, Z. Zeng, X. Lu, and X. Zhu, Compression property of a novel lattice sandwich structure, Composites Part B, 117, 2017, pp130–137.

[31] S. Yin, L. Wu, and S. Nutt, Stretch–bend-hybrid hierarchical composite pyramidal lattice cores, Composite Structures, 98, 2013, pp153–159.

[32] Y. Hu, W. Li, X. An, and H. Fan, Fabrication and mechanical behaviors of corrugated lattice truss composite sandwich panels, Composites Science and Technology, 125, 2016, pp114–122.

[33] S. Jiang, F. Sun, X. Zhang and H. Fan, Interlocking orthogrid: An efficient way to construct lightweight lattice- core sandwich composite structure, Composite Structures, 176, 2017, pp55–71.

[33] J. Xiong, A. Vaziri, R. Ghosh, H. Hu, L. Ma and L.Wu, Compression behavior and energy absorption of carbon fiber reinforced composite sandwich panels made of three-dimensional honeycomb grid cores, Extreme Mechanics Letters, 7, 2016, pp114-120.

[34] Q. Zheng, H. Fan, J. Liu, Y. Ma and L. Yang, Hierarchical lattice composites for electromagnetic and mechanical energy absorptions, Composites: Part B, 53, 2013, pp152–158.

[35] G. Zhang, B. Wang, L. Ma, L. Wu, S. Pan, and J. Yang, Energy absorption and low velocity impact response of polyurethane foam filled pyramidal lattice core sandwich panels, Composite Structures, 108, 2014, pp304–310.

[36] S. Yin, L. Wu, L. Ma, and S. Nutt, Pyramidal lattice sandwich structures with hollow composite trusses, Composite Structures, 93, 2011, pp3104–3111.

[37] J. Xiong, A. Vaziri, L. Ma, J. Papadopoulos, and L. Wu, Compression and impact testing of two-layer composite pyramidal-core sandwich panels, Composite Structures, 94, 2012, pp793–801.

[38] H. Fan, L. Yang, F. Sun, and D. Fang, Compression and bending performances of carbon fiber reinforced lattice-core sandwich composites, Composites: Part A, 52, 2013, pp118–125.

5 Micromechanical Modelling

This chapter provides the derivation of analytical expressions for the “effective” compressive stiffness and strength of the composite lattice cores, sandwiched between two facesheets. The lattice core struts are made from unidirectional carbon fibre tows infused with epoxy resin via resin transfer moulding, such that one set of fibres were aligned with the axial direction of the struts of the lattice truss. The quasi-static compression response of a range of all-carbon composite lattices that manufactured using a sacrificial mould method in Chapter 4 were used to compare with the analytical calculations derived in this chapter in an effort to further understand the behaviour of carbon composite lattice structures with various core configurations.

5.1 Analytical predictions of a columnar lattice truss core

In this section, the elastic properties and the collapse strength of the vertical columnar lattice core sandwich structures are obtained as a function of the apparent composite material properties and its relative density.

5.1.1 Relative density

The relative density of the lattice core depends on the geometrical properties of the struts and the unit cell of the structures. The relative density ($\bar{\rho}$) is defined as the density of the lattice core (ρ_c) divided by that of the solid material (ρ_s) from which it is made. As such, this simply means that the ratio of the material volume in a unit cell to that of the unit cell gives the relative density of the cores. The representative unit cell of the vertical columnar lattice core is shown in Figure 5.1. The geometrical parameters of the vertical columnar lattice core include the vertical truss height, h, with a circular cross-section of diameter, d, arranged within a square core base consisting of length, b, and width, w. The columns were equally spaced within the core planar base for all geometric variations of the columnar core construction. Based on the Figure 5.1 and its description, the effective relative density of the vertical columnar core is given by:

$$\bar{\rho}_{COLUMNAR} = \frac{n\pi d^2}{4A} \tag{5.1}$$

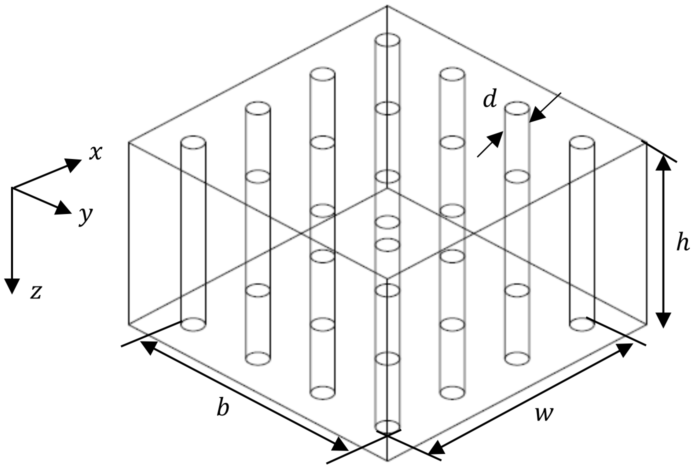

Figure 5.1. Schematic of the unit cell of a columnar lattice truss core.

where n is the number of columns within the core and A is the planar area of the unit cell.

5.1.2 Compressive modulus

To interpret the quasi-static compression data obtained in experiments, analytical expressions are derived for the compressive modulus and strength of the composite vertical columnar lattice core sandwich structures. Here, a local coordinate system is utilized, with the axes x, y, and z in the width, length, and height directions of the unit cell as illustrated in Figure 5.1. An analytical analysis of the effective compressive modulus of the composite vertical columnar lattice truss core is undertaken by analysing the deformation of a single vertical column initially and the analysis extended to evaluate the effective properties of the entire core.

Consider an out of plane compressive force that is applied to the top of rigidly supported vertical columnar lattice core unit cell in the z-direction of global coordinate system, as shown in Figure 5.2(a), with the effect that their top end of the individual struts can only move along the z-direction. For an imposed displacement δ in the z-direction of global coordinate system as illustrated in Figure 5.2(b), the applied axial force F_A in a strut are given by the elementary beam theory as [1]:

$$F_A = \frac{E_s \pi d^2 \delta}{4h} \tag{5.2}$$

where E_s denotes the apparent elastic modulus of individual composite struts.

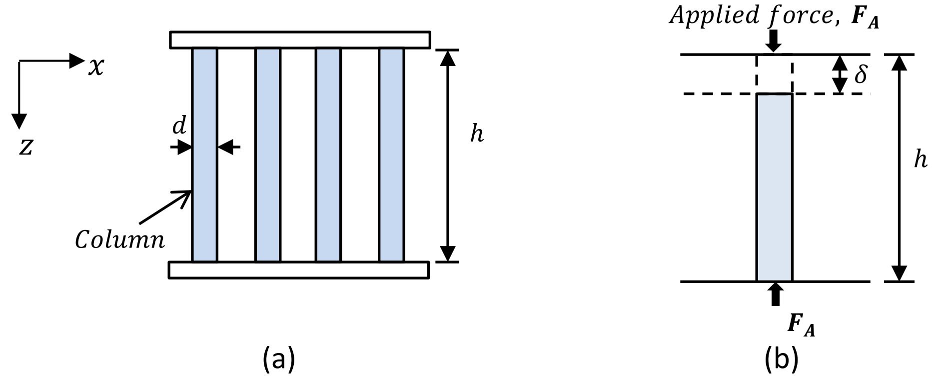

Figure 5.2. a) Side view of the columnar core (b) Schematic of a single strut deformation under compression.

Given each column within the core supports an applied force F_A, the total force F_{TOTAL} in the z-direction is obtained as a function of number of columns, n presents in a predetermined unit cell.

$$F_{TOTAL} = nF_A = \frac{nE_s \pi d^2 \delta}{4h} \tag{5.3}$$

Now consider the unit cell of the columnar core sketched in Figure 5.1. The stress and strain applied to columnar core are related to the force F_{TOTAL} and displacement δ. Therefore, the nominal compressive stress, $\sigma_{COLUMNAR}$ in the vertical columnar lattice truss structure for a unit cell is given by:

$$\sigma_{COLUMNAR} = \frac{F_{TOTAL}}{A} \tag{5.4}$$

and the corresponding nominal axial strain in the z-direction of the unit cell is given by:

$$\varepsilon_{COLUMNAR} = \frac{\delta}{h} \tag{5.5}$$

Thus, by assuming linear elasticity is applied, the effective compressive modulus $E = \sigma/\epsilon$ of the vertical columnar lattice truss structures from equations (5.3) – (5.5) is given by:

$$E_{COLUMNAR} = \frac{n\pi d^2 E_s}{4A} \tag{5.6}$$

The effective compressive modulus of the columnar core is related to the relative density of the columnar core via:

$$E_{COLUMNAR} = \bar{\rho}_{COLUMNAR} E_s \tag{5.7}$$

5.1.3 Compressive strength

The peak compressive strength of a unidirectional carbon fibre reinforced composite columnar lattice truss core sandwich structure is dependent on the initial failure mode of the manufactured composite struts. For the vertical columnar lattice core, the compressive strength is governed by strut failure due to elastic buckling or member crushing via plastic micro-buckling as evidenced in the experiments.

5.1.3.1 Fracture of struts

For the fracture failure mode, the failure stress, σ_c, of the columnar core is determined from the parent material, i.e. individual column compression tests using direct measurement rather than by the predictions of micromechanical models. Knowing the maximum failure stress ($\sigma_c = \sigma_{max}$) of the parent material, the peak compressive strength $\sigma_{columnar}$ of a vertical columnar lattice core can be deduced as:

$$\sigma_{COLUMNAR} = \frac{n\pi d^2}{4A} \sigma_{max} \tag{5.8}$$

Thus, the relation between compression strength and the unit cell relative density of the columnar core can be expressed via:

$$\sigma_{COLUMNAR} = \bar{\rho}_{COLUMNAR} \sigma_{max} \tag{5.9}$$

5.1.3.2 Euler buckling

For columnar lattice structures composed of columns with medium to high slenderness ratios (low aspect ratios), the failure stress σ_c will be replaced by the critical buckling stress σ_{cb}. This is a geometric instability failure mode observed in slender structural members. Euler buckling theory is used to calculate the buckling stress as given by:

$$\sigma_{cb} = \frac{\pi^2 E_x}{(SR)^2} \tag{5.10}$$

where E_x is the axial stiffness in the direction of the compressive loading and SR is the slenderness ratio calculated as:

$$SR = \frac{L_e}{R_g} \tag{5.11}$$

Here, $L_e = KL$ is an effective length with K being an effective length factor (depending on the condition of column ends), L is unsupported specimen length and $R_g = \sqrt{I/A_c}$ is a radius of gyration with I and A_c are the moment of inertia and cross-sectional area of the column member, respectively. This Euler buckling formula is generally developed for isotropic materials. Thus, to account for the influence of material orthotropy, this formula is then modified as follows [2]:

$$\sigma_{cb} = \frac{\pi^2 E_x}{(SR)^2 + 1.2\pi^2 \left(\frac{E_x}{G_{xz}}\right)} \tag{5.12}$$

where G_{xz} is the shear stiffness in the through-thickness direction ($G_{xz} = G_{xy}$ for transversely-isotropic material). In such instances, the second term in the denominator of the modified Euler buckling in Equation (5.12) is representing the influence of material orthotropy.

In this work, a unidirectional fibre reinforced composite column is considered transversely-isotropic material through the cross-section with a plane containing fibre direction is a plane of symmetry with an assumption that the fibres are randomly distributed in the cross-section [2]. By taking consideration of Equation (5.12), the critical Euler buckling strength for a pin-ended composite column (K=1), σ_{cb} , is given by:

$$\sigma_c = \sigma_{cb} = \frac{\pi^2 E_x}{\left(\frac{4h}{d}\right)^2 + 1.2\pi^2 \left(\frac{E_x}{G_{xz}}\right)} \tag{5.13}$$

The peak compressive strength due to critical buckling strength of the vertical columnar lattice core can be found by substituting σ_{cb} for σ_{max} in Equation (5.9).

$$\sigma_{COLUMNAR} = \bar{\rho}_{COLUMNAR}\sigma_{cb} \tag{5.14}$$

5.2 Analytical predictions of the compressive response of a pyramidal truss core

In this section, analytical models for predicting the compressive response of the carbon fibre reinforced composite pyramidal lattice truss core sandwich structures is presented. Few studies have been carried out on this type of structure to estimate their stiffness and strength that will be used as a basic in developing analytical relation in this work [3-8].

5.2.1 Relative density

The unit cell of pyramidal truss core is sketched in Figure 5.3. There is a small span between the truss apexes, and such a span is denoted by symbol t. The other parameters describing the geometry include the truss length, l, the diameter, d, and the inclination angle between the truss members and the base of the unit cell, ω. The pyramidal truss structure shown in Figure 5.3 has $l = 52.3\ mm$, $t = 10\ mm$, $\omega = 45°$. Here, three different diameters of the truss members were considered, i.e. 2, 3 and 4 mm. The dimensionless relative density is determined by calculating the volume of the truss members within a unit cell and dividing it by the volume of the unit cell. The relative density of the pyramidal core is given by:

$$\bar{\rho}_{pyr} = \frac{\pi d^2}{2 \sin\omega\,(\,l\cos\omega +\ t)^2} \tag{5.15}$$

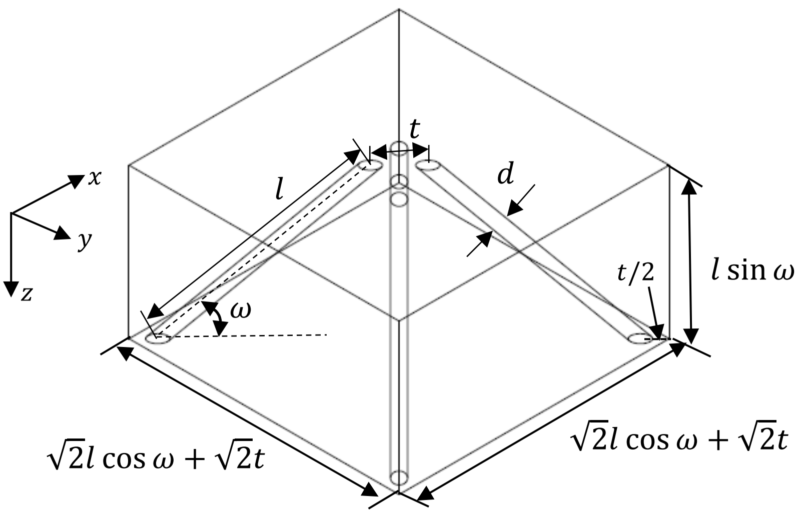

Figure 5.3. Schematic illustration of the pyramidal unit cell.

5.2.2 Compressive modulus

Analytical expressions for the compressive modulus E_{pyr} of the composite pyramidal lattice truss cores are given by first analysing through the elastic deformations of a single strut of the pyramidal lattice truss cores and then extending the results to evaluating the effective properties of the whole core. The analytical model of truss structure deformation attached to two rigid (assumed) flat plates is shown in Figure 5.4. Considering a strut of a length l and circle cross-section of diameter d as shown in Figure 5.4 (b), symmetry conditions indicate that the top end of the strut is only free to move along the z-direction. For an imposed displacement δ in the z-direction, the axial F_A and shear F_S forces in the strut are given by the elementary beam theory as:

$$F_A = \frac{AE_s\delta_A}{l} \tag{5.16}$$

and

$$F_S = \frac{12E_sI\delta_S}{l^3} \tag{5.17}$$

where $\delta_A = \delta \sin\omega$ and $\delta_S = \delta \cos\omega$ are two perpendicular displacement components in the x-direction and z-direction whereas $A = \frac{1}{4}\pi d^2$ and $I = \frac{1}{64}\pi d^4$ are the cross-sectional area and second moment of area of the strut. Thus, the axial and shear forces, F_A and F_S, in the composite strut are expressed as:

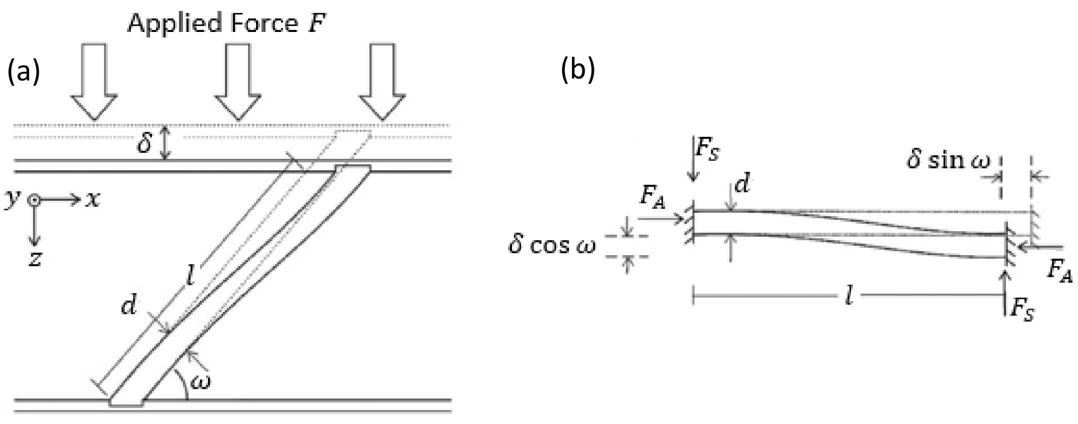

Figure 5.4. (a) Schematic diagram of the deformation of a single strut of the pyramidal core under uniaxial compression and (b) the free-body diagram of a strut loaded in a combination of compression and shear.

$$F_A = \frac{\pi d^2 E_s \delta \sin\omega}{4l} \tag{5.18}$$

and

$$F_S = \frac{3\pi d^4 E_s \delta \cos\omega}{16 l^3} \tag{5.19}$$

The total force acting on truss structure, , can be obtained using the energy method. Assuming $\Delta\omega \approx 0$, gives:

$$F = F_A \frac{\delta_A}{\delta} + F_S \frac{\delta_S}{\delta} = F_A \sin\omega + F_S \cos\omega$$

$$= \frac{\pi d^2 E_s \delta}{4l}\left(\sin^2\omega + \frac{3d^2\cos^2\omega}{4l^2}\right) \tag{5.20}$$

Considering four struts to form a unit cell of pyramidal lattice truss core as shown in Figure 5.3, the through-height stress σ_{pyr} and strain ε_{pyr} applied to the pyramidal cores are related to the force F and displacement δ via:

$$\sigma_{pyr} = \frac{4F}{A} = \frac{\pi d^2 E_s \delta}{2l(l\cos\omega + t)^2}\left(\sin^2\omega + \frac{3d^2\cos^2\omega}{4l^2}\right) \tag{5.21}$$

and

$$\varepsilon_{pyr} = \frac{\delta}{l\sin\omega} \tag{5.22}$$

respectively. Following this, combining Equations (5.20) – (5.22) then gives the effective nominal compressive modulus $E_{pyr} = \sigma_{pyr}/\varepsilon_{pyr}$ of the pyramidal cores as:

$$E_{pyr} = \frac{\pi d^2 E_s \sin\omega}{2(l\cos\omega + t)^2}\left(\sin^2\omega + \frac{3d^2\cos^2\omega}{4l^2}\right) \tag{5.23}$$

Thus, considering Equations (5.15) and (5.23), the compression modulus can be expressed in terms of the relative density by:

$$E_{pyr} = E_s\bar{\rho}_{pyr}\sin^4\omega + \frac{3}{4}E_s\bar{\rho}_{pyr}\left(\frac{d}{l}\right)^2\cos^2\omega\sin^2\omega \tag{5.24}$$

The first and second terms in Equation (5.24) represent the stiffness of the pyramidal lattice core associated with stretching and bending of the struts, respectively. Compared with the first term, the second term is a small quantity and can be neglected. Thus, realizing the pin-joint idealization that widely used for truss analysis, Equation (5.24) can be deduced as:

$$E_{pyr} = E_s\bar{\rho}_{pyr}\sin^4\omega \tag{5.25}$$

5.2.3 Compressive strength

There are two competing mechanisms that ultimately determine the peak compression strength of a composite pyramidal lattice truss core, including Euler elastic buckling and fracture of the struts, as evidenced in the compression tests of the pyramidal truss sandwich panels. Among these two modes, the one with the lower value of the failure strength became as the operative failure mode.

5.2.3.1 Fracture of the struts

A force balance along the compression axis can be used to derive an equation relating the peak strength of the pyramidal unit cell to the failure stress of the individual truss. Recalling that the total force, , per strut as follows from Equation (5.20) and relating it to Equation (5.18) for axial force, there is:

$$F = F_A\left(\sin\omega + \frac{3d^2\cos^2\omega}{4l^2\sin\omega}\right) \tag{5.26}$$

Considering the failure load of an individual composite strut is $F_A = \sigma_c(\frac{\pi d^2}{4})$, where σ_c is the strut's failure stress due to fracture. Following this, substituting F_A into the Equation (5.26) gives the applied load to the pyramidal truss core in terms of the composite strut failure stress expressed as:

$$F = \sigma_c(\frac{\pi d^2}{4})\left(\sin\omega + \frac{3d^2\cos^2\omega}{4l^2\sin\omega}\right) \tag{5.27}$$

Then, taking into account that the unit cell of the pyramidal core comprises four struts, the through-thickness nominal compressive strength of the pyramidal core from Equation (5.21) can be given by:

$$\sigma_{Pyr} = \frac{\sigma_c(\pi d^2)\left(\sin\omega + \frac{3d^2\cos^2\omega}{4l^2\sin\omega}\right)}{2(l\cos\omega + t)^2} \tag{5.28}$$

By relating to Equation (5.15), the peak compressive strength due to the fracture failure mode can be related to the relative density as:

$$\sigma_{Pyr} = \bar{\rho}_{pyr}\sigma_c\sin^2\omega + \frac{3}{4}\bar{\rho}_{pyr}\sigma_c\left(\frac{d}{l}\right)^2\cos^2\omega \tag{5.29}$$

Assuming pin-jointed struts, the second term in Equation (5.29) can be neglected leaving only an expression given as:

$$\sigma_{Pyr} = \bar{\rho}_{pyr}\sigma_c\sin^2\omega \tag{5.30}$$

where $\sigma_c = \sigma_{max}$ is the maximum compressive stress of a composite strut obtained from parent material compression tests.

5.2.3.2 Euler buckling

Under through-height compression, the pyramidal core may collapse by the elastic buckling of the constituent strut. Recalling that the Euler buckling load of an end-clamped strut subjected to an axial load is given by:

$$F_E = \frac{4\pi^2 E_s I}{l^2} \tag{5.31}$$

Thus, the nominal compressive collapse strength of a pyramidal core due to the elastic buckling of its constituent struts can be expressed,

$$\sigma_{Pyr} = \bar{\rho}_{pyr}\sigma_c\sin^2\omega + \frac{3}{4}\bar{\rho}_{pyr}\sigma_c\frac{d^2}{l^2}\cos^2\omega \tag{5.32}$$

where $\sigma_c = \sigma_{cb}$ is the strut's Euler buckling stress. This can be estimated as follows:

$$\sigma_{cb} = \frac{\pi^2 E_x}{\left(\frac{2l}{d}\right)^2 + 1.2\pi^2\left(\frac{E_s}{G_s}\right)} \tag{5.33}$$

However, for the assumption of a pin-jointed strut, Euler buckling load of a pin-jointed strut subjected to an axial load is given by:

$$F_E = \frac{\pi^2 E_s I}{l^2} \tag{5.34}$$

Realizing the compressive failure stress of pin-jointed composite strut due to elastic buckling is given by:

$$\sigma_c = \sigma_{cb} = \frac{\pi^2 E_x}{\left(\frac{4l}{d}\right)^2 + 1.2\pi^2\left(\frac{E_x}{G_{xz}}\right)} \tag{5.35}$$

Following this, the peak compressive stress of the pyramidal core for the Euler buckling failure mode in the case of pin-jointed strut can be obtained by substituting Equation (5.35) into Equation (5.30) resulting is as:

$$\sigma_{Pyr} = \bar{\rho}_{pyr}\sigma_{cb}\sin^2\omega \tag{5.36}$$

5.3 Analytical predictions of the compressive response of a modified pyramidal truss core

In this section, analytical models for predicting the compressive response of the carbon fibre reinforced composite modified pyramidal lattice truss core (type-1) sandwich structures is presented.

5.3.1 Relative density

A representative unit cell of the modified-pyramidal lattice truss core is shown in Figure 5.5 which is similar to a pyramidal unit cell. This modified pyramidal lattice core considered as a type-1 (T-1) core structure includes a central vertical strut through the apex of the pyramidal core as illustrated in Figure 5.5 (b).

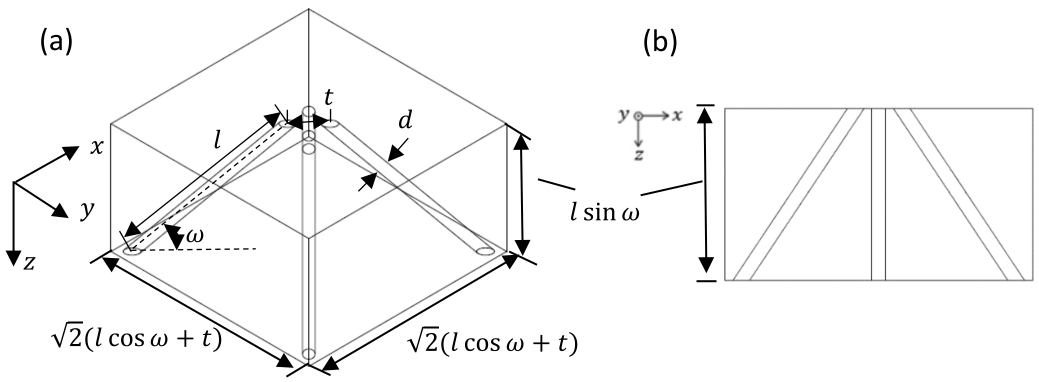

Figure 5.5. (a) Schematic illustration of the modified-pyramidal unit cell (b) Side view of the core structure.

The critical parameters describing the geometry of the modified-pyramidal core unit cell include the inclined truss length, l, the diameter of the truss member, d, and the inclination angle between the inclined truss members and the base of the unit cell, ω. There is a small span between the inclined truss apexes denoted as t and the vertical truss through the centre of the core is perpendicular to the base of the unit cell. The inclination angle of the truss, ω, with respect to the base is $45°$ and the modified pyramidal core were manufactured with struts having a cross sectional diameters of 2,3 and 4 mm resulting in core with different relative densities. The truss core has $l = 52.3\ mm$ and $t = 10\ mm$. Following this, the relative density of the modified pyramidal core, which includes an additional strut through the center of pyramidal core, can be calculated by dividing the volume of struts comprising the core to that volume of a unit cell given as:

$$\tilde{\rho}_{MP} = \frac{\pi d^2 \left[1 + \left(\frac{1}{4}\right) \sin\omega\right]}{2 \sin\omega\,(l \cos\omega + t)^2} \tag{5.37}$$

5.3.2 Compressive modulus

A theoretical analysis of the effective compressive modulus of the truss composite modified pyramidal core lattice structure is undertaken by analysing the deformation of a single inclined strut and the vertical strut of the core and then applying the results to evaluate the effective properties of the entire core. Consider the schematic of the unit cell shown in Figure 5.6 (a) with an applied force F being imposed on the core in the through-height direction. Considering the strut is a beam. The applied force F that generates a displacement δ in the z-direction creating an axial F_A and shear F_s forces in each of the inclined struts, while an axial force, F_{AC}, is created on the vertical column truss, as shown in Figure 5.6 (b) and Figure 5.6 (c) respectively. Thus, the axial force, F_A, and shear force, F_s, in an inclined strut are given by the elementary beam theory as:

$$F_A = \frac{\pi d^2 E_s \delta \sin\omega}{4l} \tag{5.38}$$

and

$$F_S = \frac{12 E_s I \delta \cos\omega}{l^3} \tag{5.39}$$

respectively. Given that the vertical column in the centre within the core also supports an applied force F, the reactive force component in the z-direction, F_{AC}, is given as:

$$F_{AC} = \frac{A E_s \delta}{l \sin\omega} = \frac{\pi d^2 E_s \delta}{4l \sin\omega} \tag{5.40}$$

Given that a unit cell of modified-pyramidal core contains four inclined struts and one vertical column truss, the total resisting force of the core structure against through-height compression can be obtained using the energy method. The total force F_{TOTAL} is given by:

$$F_{TOTAL} = 4(F_A \sin\omega + F_S \cos\omega) + F_{AC} \tag{5.41}$$

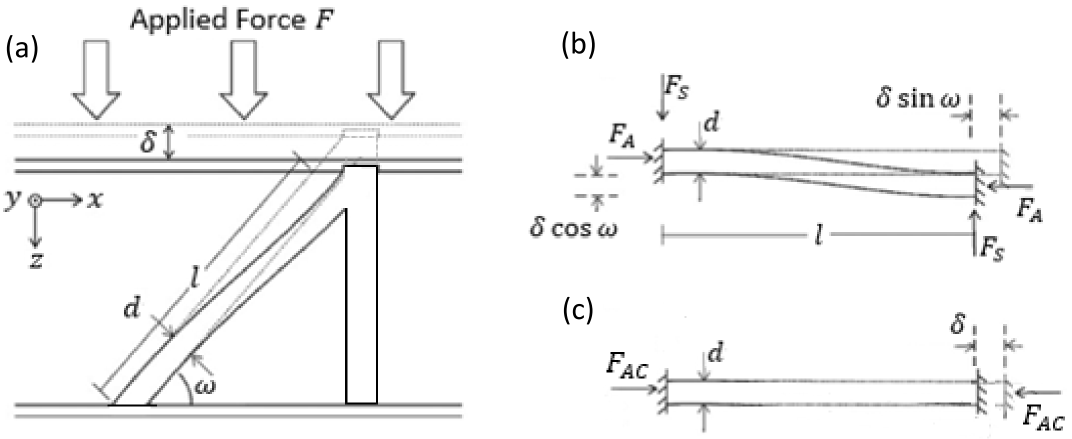

Figure 5.6. (a) Schematic diagram of the deformation of a single strut of the modified-pyramidal core under uniaxial compression and (b) the free-body diagram of an inclined strut loaded in a combination of compression and shear (c) the free-body diagram of a vertical strut in compression.

Knowing the total applied force on the modified pyramidal core, the nominal stress acting on the structure is estimated by:

$$\sigma_{MP} = \frac{F_{TOTAL}}{A} = \frac{F_{TOTAL}}{2(l\cos\omega + t)^2} \tag{5.42}$$

Similarly, the nominal strain acting on the modified pyramidal core is given by:

$$\varepsilon_{MP} = \frac{\delta}{l\sin\omega} \tag{5.43}$$

It is known that within the elastic region, the stress-strain relationship follows Hooke's law resulting in $\sigma_{MP} = E_{MP}\varepsilon_{MP}$. Thus, the effective elastic modulus of the modified-pyramidal core is as follows:

$$E_{MP} = \frac{\pi d^2 \left[1 + \left(\frac{1}{4}\right)\sin\omega\right] E_s \sin^2\omega}{2\sin\omega\,[4 + \sin\omega](l\cos\omega + t)^2}\left(4\sin^2\omega + \frac{3d^2\cos^2\omega}{l^2} + \frac{1}{\sin\omega}\right) \tag{5.44}$$

By relating this expression to Equation (5.37), the effective compressive modulus can be written in the form of relative density as:

$$E_{MP} = \frac{4\bar{\rho}_{MP}E_s\sin^4\omega}{4 + \sin\omega} + \frac{3\bar{\rho}_{MP}E_s d^2\cos^2\omega\sin^2\omega}{l^2[4 + \sin\omega]} + \frac{\bar{\rho}_{MP}E_s\sin\omega}{4 + \sin\omega} \tag{5.45}$$

It is worth noting that the first and third terms represent the contribution to stiffness of the core due to stretching of all the struts, while the second term represents the contribution from the bending of the inclined struts. Following this, consider the pin-jointed struts, a first order approximation for the compressive modulus of the core can be obtained. In the absence of the bending effects on the pin-jointed struts, the effective compression modulus can be expressed as follows:

$$E_{MP} = \frac{4\bar{\rho}_{MP} E_s \sin^4 \omega}{4 + \sin \omega} + \frac{\bar{\rho}_{MP} E_s \sin \omega}{4 + \sin \omega} = \bar{\rho}_{MP} E_s \left(\frac{4 \sin^4 \omega + \sin \omega}{4 + \sin \omega} \right) \tag{5.46}$$

5.3.3 Compressive strength

5.3.3.1 Fracture of the struts

A force balance along the compression axis is employed to derive an equation relating the peak strength of the modified-pyramidal unit cell to the failure stress of the individual truss via inclined struts or vertical strut. The total applied force acting on the unit cell of the modified-pyramidal core is given as:

$$F_{TOTAL} = \frac{\pi d^2 E_s \delta \sin^2 \omega}{l} + \frac{3\pi d^4 E_s \delta \cos^2 \omega}{4 l^3} + \frac{\pi d^2 E_s \delta}{4 l \sin \omega} \tag{5.47}$$

Equation (5.47) can be expressed in terms of the axial load, F_A, for an inclined strut and F_{AC} for the vertical truss member. This gives the total applied force expressed as:

$$F_{TOTAL} = F_A \left(4 \sin \omega + \frac{3 d^2 \cos^2 \omega}{l^2 \sin \omega} \right) + F_{AC} \tag{5.48}$$

Realizing the failure load of an inclined strut is $F_A = \sigma_c (\frac{\pi d^2}{4})$ and the failure load of a vertical truss is $F_{AC} = \sigma_{cc} (\frac{\pi d^2}{4})$, where σ_c and σ_{cc} are the critical axial stresses to initiate failure in the inclined strut and vertical strut respectively. Substituting Equation (5.48) into Equation (5.42), the nominal compressive strength of the modified-pyramidal core can be expressed via:

$$\sigma_{MP} = \frac{\pi d^2 \sigma_c \sin \omega}{2(l \cos \omega + t)^2} \left(1 + \frac{3 d^2 \cot^2 \omega}{4 l^2} \right) + \frac{\pi d^2 \sigma_{cc}}{8(l \cos \omega + t)^2} \tag{5.49}$$

The peak compressive strength can also be related to relative density of the modified-pyramidal core structure as follows:

$$\sigma_{MP} = \frac{4\bar{\rho}_{MP}\sigma_c \sin^2\omega}{4+\sin\omega} + \frac{3\bar{\rho}_{MP} d^2 \sigma_c \cos^2\omega}{l^2[4+\sin\omega]} + \frac{\bar{\rho}_{MP}\sigma_{cc}\sin\omega}{4+\sin\omega} \tag{5.50}$$

Within the elastic region ($\sigma = E\varepsilon$), the critical axial stresses, σ_c and σ_{cc} of the inclined and vertical struts respectively can also be given by:

$$\sigma_c = \frac{E_s \delta \sin\omega}{l} \tag{5.51}$$

and

$$\sigma_{cc} = \frac{E_s \delta}{l \sin\omega} \tag{5.52}$$

Combining Equations (5.51) and (5.52), σ_c and σ_{cc} can be related by an expression written as follows:

$$\sigma_c = \sigma_{cc}\sin^2\omega \tag{5.53}$$

By assuming that the modified pyramidal core fails when the inclined trusses reach their strength limit σ_c, and knowing that $\sigma_{cc} = \sigma_c/\sin^2\omega$ from Equation (5.53), the peak compressive strength of the core can be given as:

$$\sigma_{MP}^{UPPER} = \bar{\rho}_{MP}\sigma_c\left(\frac{4\sin^2\omega}{4+\sin\omega} + \frac{3d^2\cos^2\omega}{l^2[4+\sin\omega]} + \frac{1}{\sin\omega\,[4+\sin\omega]}\right) \tag{5.54}$$

This resulting in an upper bound approximation of the compression strength of the modified-pyramidal core. similarly, a lower bound approximation is derived by assuming that the core fails when the vertical strut reaches its strength limit σ_{cc} as given in Equation (5.53), the compression strength is given by:

$$\sigma_{MP}^{LOWER} = \bar{\rho}_{MP}\sigma_{cc}\left(\frac{4\sin^4\omega}{4+\sin\omega} + \frac{3d^2\cos^2\omega\sin^2\omega}{l^2[4+\sin\omega]} + \frac{\sin\omega}{4+\sin\omega}\right) \tag{5.55}$$

where $\sigma_{cc} = \sigma_{max}$ when shear loading is not considered on the vertical strut. Finally, by assuming that the inclined and the vertical struts fail simultaneously, an approximate value of the compression strength of the core is obtained from Equation (5.50).

Assuming the presence of pin-jointed struts, the second term in Equations (5.50), (5.54) and (5.55) contributed due to bending effects can be vanished, leaving only expressions given by:

$$\sigma_{MP} = \frac{\tilde{\rho}_{MP}}{4+\sin\omega}\left(4\sigma_C \sin^2\omega + \sigma_{CC}\sin\omega\right) \tag{5.56}$$

$$\sigma_{MP}^{UPPER} = \frac{\tilde{\rho}_{MP}\sigma_C}{4+\sin\omega}\left(4\sin^2\omega + \frac{1}{\sin\omega}\right) \tag{5.57}$$

$$\sigma_{MP}^{LOWER} = \frac{\tilde{\rho}_{MP}\sigma_{CC}}{4+\sin\omega}\left(4\sin^4\omega + \sin\omega\right) \tag{5.58}$$

respectively. In the absence of the shear loading on the pin-jointed inclined struts, $\sigma_c = \sigma_{cc} = \sigma_{max}$.

5.3.3.2 Euler buckling

The elastic buckling strength of the core is obtained by first calculating the buckling strength of the axially-loaded struts, i.e. inclined and vertical struts. For an end-clamped strut that subjected to an axial load, the Euler buckling strength is given by:

$$\sigma_c = \frac{\pi^2 E_s}{\left(\frac{2l}{d}\right)^2 + 1.2\pi^2\left(\frac{E_s}{G_s}\right)} \ and\ \sigma_{cc} = \frac{\pi^2 E_s}{\left(\frac{2h}{d}\right)^2 + 1.2\pi^2\left(\frac{E_s}{G_s}\right)} \tag{5.59}$$

Nevertheless, by assuming a pin-jointed strut that subjected to an axial load, the Euler buckling strength can be estimated by:

$$\sigma_c = \frac{\pi^2 E_s}{\left(\frac{4l}{d}\right)^2 + 1.2\pi^2\left(\frac{E_s}{G_s}\right)} \ and\ \sigma_{cc} = \frac{\pi^2 E_s}{\left(\frac{4h}{d}\right)^2 + 1.2\pi^2\left(\frac{E_s}{G_s}\right)} \tag{5.60}$$

where σ_c and σ_{cc} are the Euler buckling strength of the inclined and vertical strut, respectively. The results are then substituted into Equations (5.56) – (5.58).

5.4 Analytical predictions of the compressive response of a modified pyramidal truss core (type-2)

Here, analytical models for predicting the compressive response of the carbon fibre reinforced composite modified-pyramidal lattice truss core (type-2) sandwich structures is presented. This truss core is manufactured to explore the potential offered by the manufacturing method via sacrificial mould method by simply adding more struts into the space of a unit cell of the core based on pyramidal configuration.

5.4.1 Relative density

A unit cell of the lattice structure based on the pyramidal structure referred as type-2 (T2) lattice truss core is shown in Figure 5.7. The cell structure has four more struts included in pyramid pattern to the regular pyramidal core topology. The lattice material is constructed from circular cylindrical struts. The important geometrical parameters describing the configuration of a T2 unit cell include the truss lengths, l_1 and l_2, diameter, d and inclination angles with respect to the base of a unit cell, ω and α.

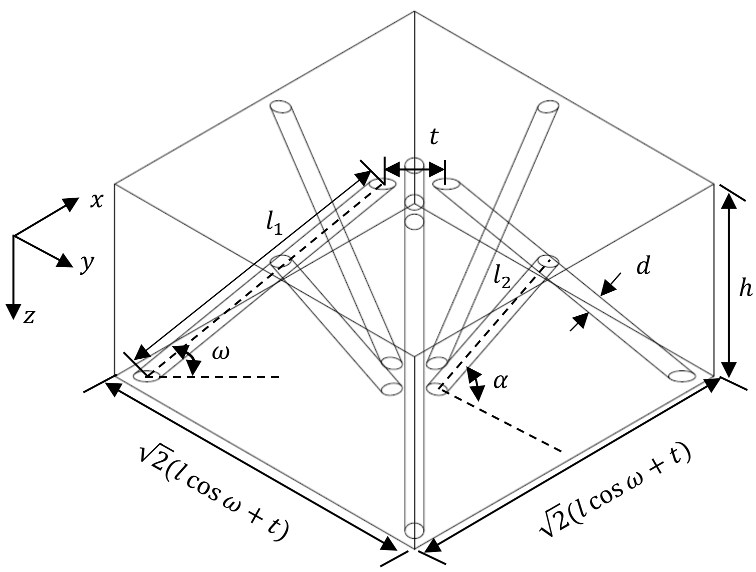

Figure 5.7. Schematic illustration of the modified-pyramidal unit cell.

Here, the inclined strut with a length of $l_1 = 52.3\ mm$ has an angle of $\omega = 45°$, while another angled strut with a length of $l_2 = 44.5\ mm$ has an inclination angle of $\alpha = 56°$. The diameter of the all struts is $d = 3\ mm$. The relative density of the core material can be calculated from the ratio of the truss volume to the volume of the unit cell which is given by:

$$\bar{\rho}_{T2} = \frac{\pi d^2 (l_1 + l_2)}{2(l_1 \cos\omega + t)^2 h} \tag{5.61}$$

It is known that $h = l_1 \sin\omega = l_2 \sin\alpha$, giving l_2 can be expressed as a function of l_1 using a relation, $l_2 = l_1 \emptyset$, where $\emptyset = \sin\omega / \sin\alpha$ is a dimensionless quantity describing the ratio of given angles. Thus, the effective relative density of the core is given by:

$$\bar{\rho}_{T2} = \frac{\pi d^2 (1 + \emptyset)}{2 \sin\omega\, (l_1 \cos\omega + t)^2} \tag{5.62}$$

5.4.2 Compressive modulus

Using the same approach described in Section 5.2.2 for the pyramidal lattice core, the analytical expression for the compressive modulus of the T2 unit cell is obtained as a function of the core geometry and the elastic properties of the parent material. Here, the deformation of a single strut is analysed first and then extending the results to evaluating the effective properties of the whole core. Consider inclined trusses at two different angles (α and ω) separately with an applied force in the z-direction resulting in a displacement δ, as shown in Figure 5.8. The free body diagram showing the force components in strut-1 with an angle of ω and strut-2 with an angle of α is shown in Figure 5.8 (b) and Figure 5.8 (c) respectively.

For a displacement δ imposed in the through-height direction, considering all bending and shear deformations besides stretching, the axial and shear force components in both struts are given following the beam theory:

For strut-1:

$$F_{A1} = \frac{\pi d^2 E_s \delta \sin\omega}{4 l_1} \; and \; F_{S1} = \frac{3\pi d^4 E_s \delta \cos\omega}{16 {l_1}^3} \tag{5.63}$$

and strut-2:

$$F_{A2} = \frac{\pi d^2 E_s \delta \sin\alpha}{4 l_1} \, and \; F_{S2} = \frac{3\pi d^4 E_s \delta \cos\alpha}{16 {l_1}^3} \tag{5.64}$$

respectively.

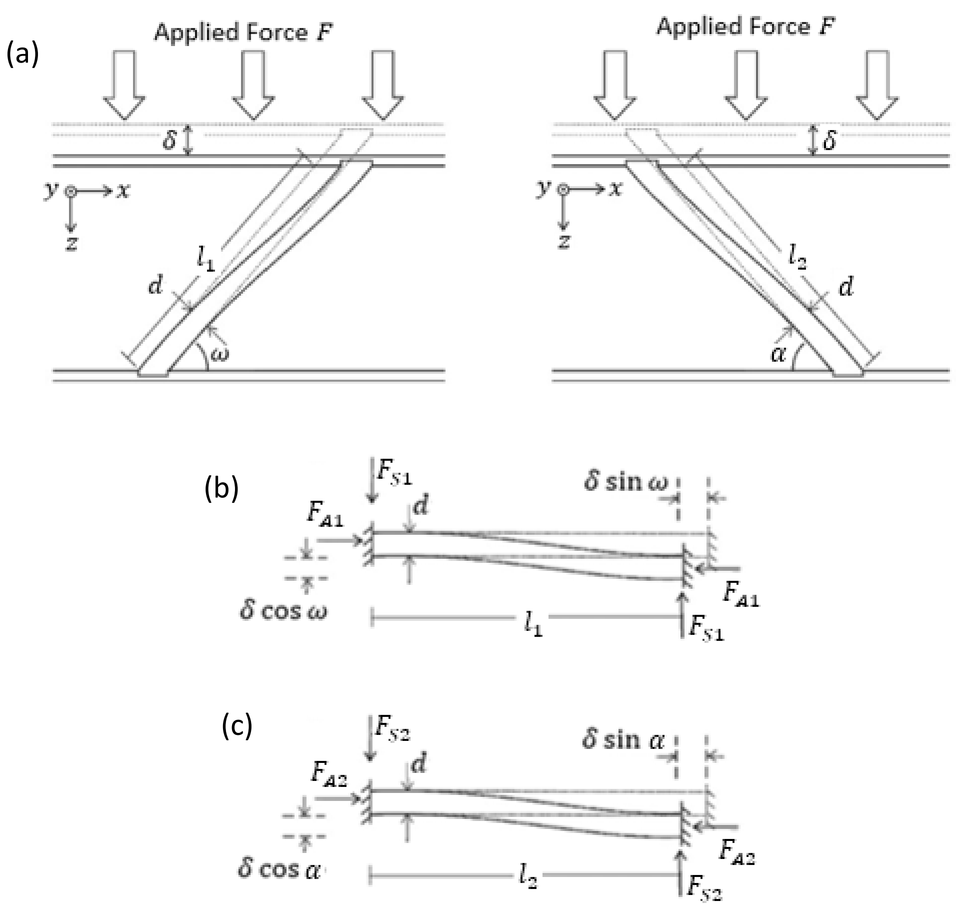

Figure 5.8. (a) Schematic diagram of the deformation of a single strut of the T2 core under uniaxial compression and (b) the free-body diagram of an inclined strut-1 loaded in a combination of compression and shear (c) the free-body diagram of an inclined strut-2 loaded in a combination of compression and shear.

As the unit cell has eight trusses in total, i.e. four strut-1 members and four strut-2 members, the net applied force F_{TOTAL} within the unit cell of T2 lattice structure is given by:

$$F_{TOTAL} = \frac{\pi d^2 E_s \delta}{l_1}\left(\sin^2 \omega + \frac{3d^2 \cos^2 \omega}{4{l_1}^2}\right) + \frac{\pi d^2 E_s \delta}{l_2}\left(\sin^2 \alpha + \frac{3d^2 \cos^2 \alpha}{4{l_2}^2}\right) \tag{5.65}$$

Then, the through-height stress σ_{T2} and strain ε_{T2} applied to the type-2 lattice cores are related to the net force F_{TOTAL} and displacement δ via:

$$\sigma_{T2} = \frac{F_{TOTAL}}{2(l_1 \cos \omega + t)^2} \tag{5.66}$$

and

$$\varepsilon_{T2} = \frac{\delta}{h} \tag{5.67}$$

respectively. Combining Equations (5.65) – (5.67) then gives the effective compressive modulus of the T2 cores:

$$E_{T2} = \frac{\pi d^2 E_s h}{2l_1(l_1\cos\omega + t)^2}\left(\sin^2\omega + \frac{3d^2\cos^2\omega}{4{l_1}^2}\right) + \frac{\pi d^2 E_s h}{2l_2(l_1\cos\omega + t)^2}\left(\sin^2\alpha + \frac{3d^2\cos^2\alpha}{4{l_2}^2}\right) \tag{5.68}$$

Knowing the relationships of $h = l_1\sin\omega = l_2\sin\alpha$, $l_2 = l_1\emptyset$ and $\emptyset = \sin\omega/\sin\alpha$, the effective nominal compressive modulus can be rearranged as:

$$E_{T2} = \frac{\pi d^2 E_s \sin^2\omega\,(1+\emptyset)}{(1+\emptyset)\sin\omega\left(\sqrt{2}l_1\cos\omega + 2b\cos\omega\right)^2}\left(\sin^2\omega + \frac{3d^2\cos^2\omega}{4{l_1}^2}\right) + \frac{\pi d^2 E_s \sin^2\omega\,(1+\emptyset)}{\emptyset\,(1+\emptyset)\sin\omega\left(\sqrt{2}l_1\cos\omega + 2b\cos\omega\right)^2}\left(\sin^2\alpha + \frac{3d^2\cos^2\alpha}{4{l_1}^2\emptyset^2}\right) \tag{5.69}$$

The compressive modulus in terms of relative density is given by:

$$E_{T2} = \frac{\bar{\rho}_{T2}E_s\sin^4\omega}{(1+\emptyset)} + \frac{3\bar{\rho}_{T2}E_s d^2\cos^2\omega\sin^2\omega}{4{l_1}^2(1+\emptyset)} + \frac{\bar{\rho}_{T2}E_s\sin^4\omega}{\emptyset^3(1+\emptyset)} + \frac{3\bar{\rho}_{T2}E_s d^2\cos^2\alpha\sin^2\omega}{4{l_1}^2\,\emptyset^3(1+\emptyset)} \tag{5.70}$$

The first and third terms are due to stretching of the truss members, while the second and fourth terms represent the contributions to the modulus of the core due to the bending of the struts. In the absence of the shear force in the pin-jointed idealization, this relationship reduces to:

$$E_{T2} = \frac{\bar{\rho}_{T2}E_s\sin^4\omega}{(1+\emptyset)} + \frac{\bar{\rho}_{T2}E_s\sin^4\omega}{\emptyset^3(1+\emptyset)} \tag{5.71}$$

or

$$E_{T2} = \frac{\bar{\rho}_{T2}E_s\sin^4\omega}{\left(1+\frac{l_2}{l_1}\right)}\left(1+\left(\frac{l_1}{l_2}\right)^3\right) \tag{5.72}$$

5.4.3 Compressive strength

5.4.3.1 Fracture of the struts

Prior to failure, it is important to derive expressions relating the failure strength of the T2 core to the compressive failure strength σ_c of a single strut. The net applied force F_{TOTAL} is expressed as a function the axial force F_A as follows:

$$F_{TOTAL} = F_{A1}\left(4\sin\omega + \frac{3d^2\cos^2\omega}{{l_1}^2\sin\omega}\right) + F_{A2}\left(4\sin\alpha + \frac{3d^2\cos^2\alpha}{{l_2}^2\sin\alpha}\right) \quad (5.73)$$

At the onset of failure, consider the failure loads of an inclined composite strut-1 and strut-2 as $F_{A1} = \sigma_{c1}(\frac{\pi d^2}{4})$ and $F_{A2} = \sigma_{c2}(\frac{\pi d^2}{4})$ respectively. Knowing σ_{c1} and σ_{c2} are the axial critical stresses to initiate failure in the composite strut-1 and strut-2, the effective compressive strength σ_{T2} of the T2 cores associated with the onset of strut fracture can be calculated from:

$$\sigma_{T2} = \frac{\pi d^2\sigma_{C1}\sin\omega}{2(l_1\cos\omega + t)^2}\left(1 + \frac{3d^2\cot^2\omega}{4{l_1}^2}\right) + \frac{\pi d^2\sigma_{C2}\sin\alpha}{2(l_1\cos\omega + t)^2}\left(1 + \frac{3d^2\cot^2\alpha}{4{l_2}^2}\right) \quad (5.74)$$

In terms of the unit cell relative density $\bar{\rho}_{T2}$, the above expression becomes:

$$\sigma_{T2} = \frac{\bar{\rho}_{T2}\,\sigma_{C1}\sin^2\omega}{(1+\emptyset)} + \frac{3\bar{\rho}_{T2}\,\sigma_{C1}d^2\cos^2\omega}{4{l_1}^2(1+\emptyset)} + \frac{\bar{\rho}_{T2}\,\sigma_{C2}\emptyset\sin^2\alpha}{(1+\emptyset)} + \frac{3\bar{\rho}_{T2}\,\sigma_{C2}d^2\emptyset\cos^2\alpha}{4{l_1}^2(1+\emptyset)} \quad (5.75)$$

Following this, the axial stresses (σ_{c1} and σ_{c2}) prior to failure are expressed using Hooke's law within the elastic region ($\sigma = E\varepsilon$) for the composite struts as:

$$\sigma_{c1} = \frac{E_s\delta}{l_1\sin\omega} \; and \; \sigma_{c2} = \frac{E_s\delta}{l_2\sin\omega} \quad (5.76)$$

This forms a relationship between σ_{c1} and σ_{c2} which is given by:

$$\sigma_{C2} = \sigma_{C1}\left[\frac{l_1}{l_2}\right]^2 = \sigma_{C1}\left[\frac{1}{\emptyset^2}\right]$$

where $l_2 = l_1 \emptyset$. (5.77)

By assuming that the T2 modified-pyramidal core fails when the inclined trusses reach σ_{C1}, an upper bound approximation of the compression strength of the T2 core can be written as follows:

$$\sigma_{T2}^{UPPER} = \frac{\bar{\rho}_{T2}\,\sigma_{C1}\sin^2\omega}{(1+\emptyset)} + \frac{3\bar{\rho}_{T2}\,\sigma_{C1}d^2\cos^2\omega}{4{l_1}^2(1+\emptyset)} + \frac{\bar{\rho}_{T2}\,\sigma_{C1}\sin^2\alpha}{\emptyset(1+\emptyset)} + \frac{3\bar{\rho}_{T2}\,\sigma_{C1}d^2\cos^2\alpha}{4{l_1}^2\emptyset(1+\emptyset)} \tag{5.78}$$

By assuming that the T2 core fails when the inclined trusses approach their strength limit σ_{C2}, thus it gives:

$$\sigma_{C1} = \sigma_{C2}\emptyset^{\mathbf{2}} \tag{5.79}$$

Therefore, a lower bound approximation σ_{T2}^{LOWER} is obtained by considering the strut-2 fails upon reaching their critical strength results in:

$$\sigma_{T2}^{LOWER} = \frac{\bar{\rho}_{T2}\,\sigma_{C2}\,\emptyset^{\mathbf{2}}\sin^2\omega}{(1+\emptyset)} + \frac{3\bar{\rho}_{T2}\,\sigma_{C2}\emptyset^{\mathbf{2}}d^2\cos^2\omega}{4{l_1}^2(1+\emptyset)} + \frac{\bar{\rho}_{T2}\,\sigma_{C2}\emptyset\sin^2\alpha}{(1+\emptyset)} + \frac{3\bar{\rho}_{T2}\,\sigma_{C2}d^2\emptyset\cos^2\alpha}{4{l_1}^2(1+\emptyset)} \tag{5.80}$$

Finally, by assuming that both inclined struts fails simultaneously, an average value between the upper and lower bounds for the compressive strength of the lattice core is obtained by using Equation (5.75).

For pin-jointed struts, the compressive strength expressions will neglect the bending effects in the calculations. Thus, an upper, lower and average prediction can be expressed as follows:

$$\sigma_{T2}^{UPPER} = \frac{\bar{\rho}_{T2}\,\sigma_{C1}\sin^2\omega}{(1+\emptyset)}\left(1+\frac{1}{\emptyset^3}\right) \tag{5.81}$$

$$\sigma_{T2}^{LOWER} = \frac{\bar{\rho}_{T2}\,\sigma_{C2}\emptyset\sin^2\omega}{(1+\emptyset)}\left(\emptyset+\frac{1}{\emptyset^{\mathbf{2}}}\right) \tag{5.82}$$

$$\sigma_{T2} = \frac{\bar{\rho}_{T2}\,\sigma_{C1}\sin^2\omega}{(1+\emptyset)} + \frac{\bar{\rho}_{T2}\,\sigma_{C2}\emptyset\sin^2\alpha}{(1+\emptyset)}$$

respectively. For pin-jointed struts, it can be noted that $\sigma_{c1} = \sigma_{c2} = \sigma_{max}$ (5.83)
due to the absence of the shear loadings.

5.4.3.2 Euler buckling

For an end-clamped strut that subjected to an axial load, the Euler buckling strength is given by:

$$\sigma_{c1} = \frac{\pi^2 E_s}{\left(\frac{2l_1}{d}\right)^2 + 1.2\pi^2\left(\frac{E_s}{G_s}\right)} \; and \; \sigma_{c2} = \frac{\pi^2 E_s}{\left(\frac{2l_2}{d}\right)^2 + 1.2\pi^2\left(\frac{E_s}{G_s}\right)} \tag{5.84}$$

where σ_{c1} and σ_{c2} are the Euler buckling strength of strut-1 and strut-2 of the angled struts. For a pin-jointed strut that subjected to an axial load, the Euler buckling strength is given by:

$$\sigma_{c} = \frac{\pi^2 E_s}{\left(\frac{4l_1}{d}\right)^2 + 1.2\pi^2\left(\frac{E_s}{G_s}\right)} \; and \; \sigma_{cc} = \frac{\pi^2 E_s}{\left(\frac{4l_2}{d}\right)^2 + 1.2\pi^2\left(\frac{E_s}{G_s}\right)} \tag{5.85}$$

The resulting values are then replaced into Equation (5.83) to obtain the average compressive strength of the core due to elastic buckling of the struts.

5.5 Analytical predictions of the compressive response of a modified pyramidal truss core (type-3)

This section presents analytical solutions of the elastic modulus and strength properties for type-3 pyramidal truss core based on failure modes of the lattices, i.e. fracture of struts and elastic buckling.

5.5.1 Relative density

The geometric configuration of type-3 (T3) lattice core is similar to that shown in Figure 5.7 along with the critical parameters describing the geometry. However, one vertical strut with the same diameter to the inclined strut is introduced in the centre through the apex of the T2 lattice core structures described in Section 5.4.1. The side view of the T3 core is shown in Figure 5.9. The cylindrical struts have a diameter of 3 mm.

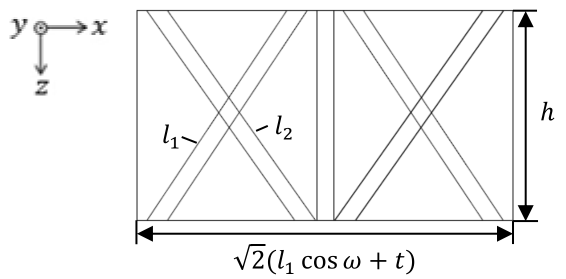

Figure 5.9. Schematic illustration of the side view of the T3-core lattice structure.

Following this, the relative density describing the core configuration is given by:

$$\bar{\rho}_{T3} = \frac{\pi d^2 (1 + \emptyset + \frac{1}{4}\sin\omega)}{2\sin\omega\,(l_1\cos\omega + t)^2} \tag{5.86}$$

where $\emptyset = \sin\omega / \sin\alpha$ is a dimensionless quantity represent the angle ratio of the two inclined struts.

5.5.2 Compressive modulus

The T3 core structure is a combination of a T2 structure and a vertical column through the apex of the core in a unit cell. Using a same approach undertaken for the modified pyramidal and the T2 lattices, the analytical expression for the elastic modulus of the T3 unit cell core lattice is obtained as a function of the core geometry and the elastic properties of the parent material. By referring to the deformation of a single strut as illustrated in Figure 5.6c, Figure 5.8b and Figure 5.8c along with their force components, a force balance analysis is undertaken. The solution is further extended to evaluate the effective properties of the entire T3 unit cell. By considering an analysis performed for the vertical strut in Section 5.3.2 and for the inclined struts (strut-1 and strut-2) in Section 5.4.2, the sum of the axial and shear force components describing the total force F_{TOTAL} applied to the T3 unit cell is given by:

$$F_{TOTAL} = 4F_{A1}\sin\omega + 4F_{S1}\cos\omega + 4F_{A2}\sin\omega + 4F_{S2}\cos\omega + F_{AC} \tag{5.87}$$

and substituting their force components further gives an expression as follows:

$$\begin{aligned} F_{TOTAL} &= \frac{\pi d^2 E_s \delta}{l_1}\left(\sin^2\omega + \frac{3d^2\cos^2\omega}{4{l_1}^2}\right) \\ &+ \frac{\pi d^2 E_s \delta}{l_2}\left(\sin^2\alpha + \frac{3d^2\cos^2\alpha}{4{l_2}^2}\right) + \frac{\pi d^2 E_s \delta}{4h} \end{aligned} \tag{5.88}$$

Based on through-height compressive stress $\sigma_{T3} = F_{TOTAL}/A$ where $A = 2(l_1\cos\omega + t)^2$ and the axial strain $\varepsilon_{T3} = \delta/h$ in a unit cell in the z-direction, the effective nominal modulus of the core is expressed as follows:

$$\begin{aligned} E_{T3} &= \frac{\pi d^2 E_s \sin\omega}{2l_1(l_1\cos\omega + t)^2}\left(\sin^2\omega + \frac{3d^2\cos^2\omega}{4{l_1}^2}\right) \\ &+ \frac{\pi d^2 E_s \sin\alpha}{2l_2(l_1\cos\omega + t)^2}\left(\sin^2\alpha + \frac{3d^2\cos^2\alpha}{4{l_2}^2}\right) \\ &+ \frac{\pi d^2 E_s}{8(l_1\cos\omega + t)^2} \end{aligned} \tag{5.89}$$

The elastic modulus in terms of relative density is written as:

$$\begin{aligned} E_{T3} &= \frac{\bar{\rho}_{T3} E_s \sin^2\omega}{(1 + \emptyset + \frac{1}{4}\sin\omega)}\left(\sin^2\omega + \frac{3d^2\cos^2\omega}{4{l_1}^2}\right) \\ &+ \frac{\bar{\rho}_{T3} E_s \sin\omega\sin\alpha}{(1 + \emptyset + \frac{1}{4}\sin\omega)}\left(\sin^2\alpha + \frac{3d^2\cos^2\alpha}{4{l_2}^2}\right) \\ &+ \frac{\bar{\rho}_{T3} E_s \sin\omega}{4(1 + \emptyset + \frac{1}{4}\sin\omega)} \end{aligned} \tag{5.90}$$

By considering a pin-jointed strut, the compressive modulus E_{T3} for the core is given by:

$$E_{T3} = \frac{\bar{\rho}_{T3} E_s \sin^4 \omega}{1 + (l_2/l_1) + \frac{1}{4}\sin\omega}\left[1 + \left(\frac{l_1}{l_2}\right)^3\right] + \frac{\bar{\rho}_{T3} E_s \sin\omega}{4\left(1 + (l_2/l_1) + \frac{1}{4}\sin\omega\right)} \quad (5.91)$$

where it is known that the relation is $l_2 = l_1 \emptyset$.

5.5.3 Compressive strength

5.5.3.1 Fracture of the struts

Following an approach described in Sections 5.3.3.1 and 5.4.3.1, the net applied force acting in a unit cell along the z-direction for the T3-core is expressed in terms of the axial force of the struts studied in a form below:

$$F_{TOTAL} = F_{A1}\left(4\sin\omega + \frac{3d^2\cot^2\omega\sin\omega}{{l_1}^2}\right) + F_{A2}\left(4\sin\alpha + \frac{3d^2\cot^2\alpha\sin\alpha}{{l_2}^2}\right) + F_{Ac} \quad (5.92)$$

Here, F_{A1}, F_{A2} and F_{AC} is axial forces in the inclined strut-1, inclined strut-2 and vertical strut, respectively. F_{A1} and F_{A2} are given by Equation (5.63) and Equation (5.64), accordingly, while F_{AC} is given by $F_{AC} = \pi d^2 E_s \delta / 4h$ for the central vertical strut.

Considering that the failure load of the composite strut is related to the failure stress within the elastic region, thus the critical force in general is given by:

$$F_A = \sigma_c\left(\frac{\pi d^2}{4}\right) \quad (5.93)$$

Substituting Equation (5.92) into the Equation (5.66) and combining with Equation (5.93), the effective compressive strength σ_{T3} of the T3 core due to strut fracture can be written as:

$$\sigma_{T3} = \frac{\pi d^2 \sigma_{c1}\sin\omega}{2(l_1\cos\omega + t)^2}\left(1 + \frac{3d^2\cot^2\omega}{4{l_1}^2}\right) + \frac{\pi d^2\sigma_{c2}\sin\alpha}{2(l_1\cos\omega + t)^2}\left(1 + \frac{3d^2\cot^2\alpha}{4{l_2}^2}\right) + \frac{\pi d^2\sigma_{cc}}{8(l\cos\omega + t)^2} \quad (5.94)$$

where σ_{c1}, σ_{c2} and σ_{cc} are the critical stress required to initiate failure in the composite struts. Following this, the above expression can be given as a function of unit cell relative density as follows:

$$\sigma_{T3} = \frac{\bar{\rho}_{T3}\sigma_{c1}\sin^2\omega}{(1+\emptyset+\frac{1}{4}\sin\omega)} + \frac{3\bar{\rho}_{T3}\sigma_{c1}\,d^2\sin^2\omega\cot^2\omega}{4{l_1}^2(1+\emptyset+\frac{1}{4}\sin\omega)} + \frac{\bar{\rho}_{T3}\sigma_{c2}\emptyset\sin^2\alpha}{(1+\emptyset+\frac{1}{4}\sin\omega)} + \frac{3\bar{\rho}_{T3}\sigma_{c2}d^2\,\emptyset\sin^2\alpha\cot^2\alpha}{4{l_2}^2(1+\emptyset+\frac{1}{4}\sin\omega)} + \frac{\bar{\rho}_{T3}\sigma_{cc}\sin\omega}{4(1+\emptyset+\frac{1}{4}\sin\omega)} \tag{5.95}$$

For a pin-jointed struts, the compressive strength of the T3 core reduces to

$$\sigma_{T3} = \frac{\bar{\rho}_{T3}\sin^2\omega}{1+(l_2/l_1)+\frac{1}{4}\sin\omega}\left[\sigma_{c1}+\frac{\sigma_{c2}}{(l_2/l_1)}\right] + \frac{\bar{\rho}_{T3}\sigma_{cc}\sin\omega}{4+4(l_2/l_1)+\sin\omega)} \tag{5.96}$$

For pin-jointed struts, $\sigma_{c1} = \sigma_{c2} = \sigma_{cc} = \sigma_{max}$ due to the absence of shear loading in the angled struts, where σ_{max} is maximum strength of the parent material.

5.5.3.2 Euler buckling

The elastic buckling strength of a T3 core unit cell can be calculated using the expressions developed for the modified-pyramidal and the T2 lattice in Sections 5.3.3.2 and 5.4.3.2, respectively.

5.6 Analytical results

In the following sections, the compressive modulus and peak strength values are calculated using the analytical expressions derived in this chapter. It will show the evidence from the calculations that analytical derivation based on the pin-ended assumption results in good agreement with experiments supported by the observed failure modes of the lattices. All the analyses are based on the core strut diameters used in the experiments which results in core with different relative densities.

5.6.1 Parent material properties

Prior to show the analytical results, the elastic properties of the parent material are initially obtained using well established formula in textbooks for predicting engineering properties of the fibre-reinforced material [9,10]. Micromechanics model based on the rule of mixture is used to calculate the engineering properties of the individual strut made up from composite material as basic properties of the constituent materials include the fibre and the matrix. Table 5.1 and Table 5.2 summarise typical basic properties of the carbon fibre and epoxy matrix used for making the composite struts via the sacrificial mould method.

Table 5.1. Typical properties of the carbon fibre material [11,12].

Property	Carbon fibre
Density (ρ)	1800 kg/m^3
Longitudinal modulus (E_{1f})	234 GPa
Transverse modulus (E_{2f})	15 GPa
Longitudinal shear modulus (G_{12f})	27 GPa
Transverse shear modulus (G_{23f})	7 GPa
Longitudinal Poisson's ratio (υ_{12f})	0.2
Transverse Poisson's ratio (υ_{23f})	0.3

Table 5.2. Typical properties of the epoxy material [11,13].

Property	Epoxy
Density (ρ)	1080 – 1120 kg/m^3
Young's modulus (E_m)	3.4 GPa
Shear modulus (G_m)	1.26 GPa
Poisson's ratio (υ_m)	0.36

A unidirectional fibre-reinforced composite material can be considered as an orthotropic material which has three planes of symmetry that coincides with their coordinate planes. One plane of symmetry is perpendicular to the fibre direction, and the other two can be any pair of planes orthogonal to the fibre direction. Only nine constants are required to describe an orthotropic material. However, in this case, cylindrical strut containing unidirectional fibre-reinforced composite can be considered as a transversely isotropic material due to one axis of symmetry, as shown in Figure 5.10. Here, the fibres are aligned in one direction and distributed randomly in the circular cross-section along with the axis-1 of symmetry. Thus, only six constants are required to describe a transversely isotropic material. The six constants are $E_1, E_2, \upsilon_{12}, \upsilon_{23}, G_{12}$ and G_{23} where E_1 and E_2 are elastic modulus in fibre and transverse directions, υ_{12} and υ_{23} are Poisson's ratio and G_{12} and G_{23} are axial and through-thickness shear modulus, respectively. Knowing the fibre and matrix volume fractions and basic properties of the constituent materials as listed in Table 5.1 and Table 5.2, the following expressions show the formula to calculate these constants as follows [9-11]:

$$E_1 = E_{1f}V_f + E_mV_m \tag{5.97}$$

$$E_2 = \frac{E_{2f}E_m}{E_mV_f + E_{2f}V_m} \tag{5.98}$$

$$\upsilon_{12} = \upsilon_{12f}V_f + \upsilon_mV_m \tag{5.99}$$

$$\upsilon_{23} = \frac{\upsilon_{23f}\upsilon_m}{\upsilon_mV_f + V_m\upsilon_{23f}} \tag{5.100}$$

$$G_{12} = \frac{G_{12f}G_m}{G_mV_f + G_{12f}V_m} \tag{5.101}$$

$$G_{23} = \frac{E_2}{2(1 + \upsilon_{23})} \tag{5.102}$$

respectively. Here, V_f and V_m are fibre and matrix volume fractions, accordingly.

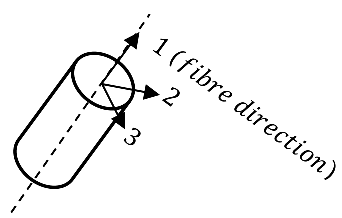

Figure 5.10. Schematic of the fibre-reinforced composite strut.

Using the micromechanics model expressions from Equation (5.97) to Equation (5.102), the elastic properties of the composite struts consisting of different fibre volume fraction are determined. Table 5.3 summarises the values of mechanical properties include elastic and strength parameters.

Table 5.3. Summary of the elastic properties and compression strength of the composite strut.

Engineering properties (Symbol)[Units]	Fibre volume fraction (V_f)		
	0.14	0.35	0.42
Elastic modulus in the fibre direction-1 (E_1) [GPa]	36	84	100
Elastic modulus in the transverse directions-2, -3 (E_2, E_3) [GPa]	3.8	4.8	5.0
Axial Poisson's ratio ($\upsilon_{12}, \upsilon_{13}$)	0.34	0.30	0.29
Through-thickness Poisson's ratio (υ_{23})	0.35	0.34	0.33
Axial shear modulus (G_{12}, G_{13}) [GPa]	1.5	1.9	2.1
Through-thickness shear modulus (G_{23}) [GPa]	1.4	1.7	1.9
Compression strength (σ_{max}) (MPa) [from compression tests]	65	124	141

5.6.2 Columnar lattice

The vertical column lattice cores that were manufactured via the sacrificial mould method produced in three different diameters of the strut based on 2, 3 and 4 mm, yielding a relative density of approximately 2.3, 4.9 and 8.4%, respectively. All columnar lattice systems tested in static compression are then calculated to predict their through-height compression modulus and peak strength using analytical expressions for five different diameters of columns (1, 2, 3, 4 and 5mm). The strut has fibre volume fractions of 0.14 and 0.35. Figure 5.11 shows the predicted compressive modulus for the columnar lattices based on two different fibre volume fractions. The elastic modulus of the vertical column core shows an increasing trend as a function of their relative density in a linear fashion. Column members having the higher fibre volume fraction produces larger modulus values compared to that of the core with lower fibre volume fraction members. The peak strength prediction for the columnar lattices are shown in Figure 5.12. All prediction values are based on the general assumption of the pin-ended joints for truss analysis which produces a good agreement with experimental results as shown in the last part of this chapter.

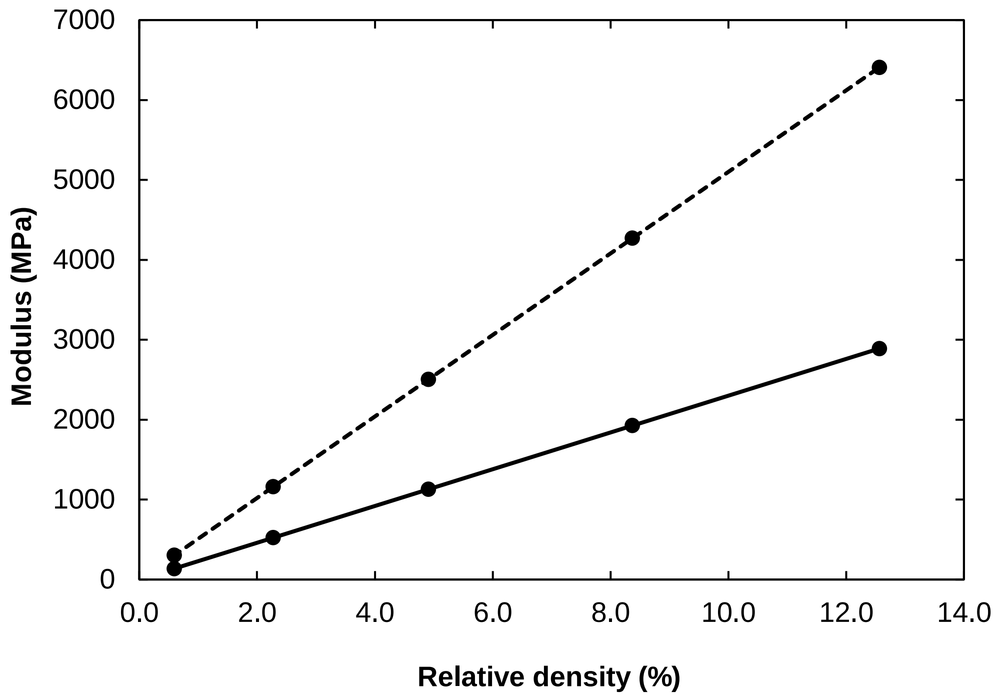

Figure 5.11. Analytical predictions of the compressive elastic modulus of the vertical column lattices. (solid line, $V_f = 0.14$; dashed line, $V_f = 0.35$).

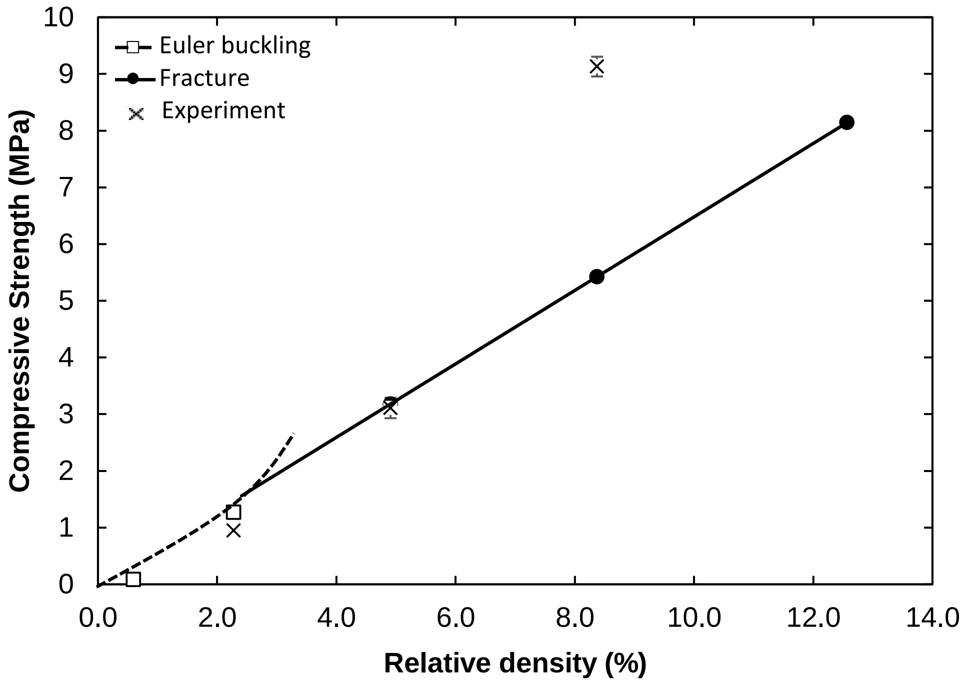

(a) $V_f = 0.14$

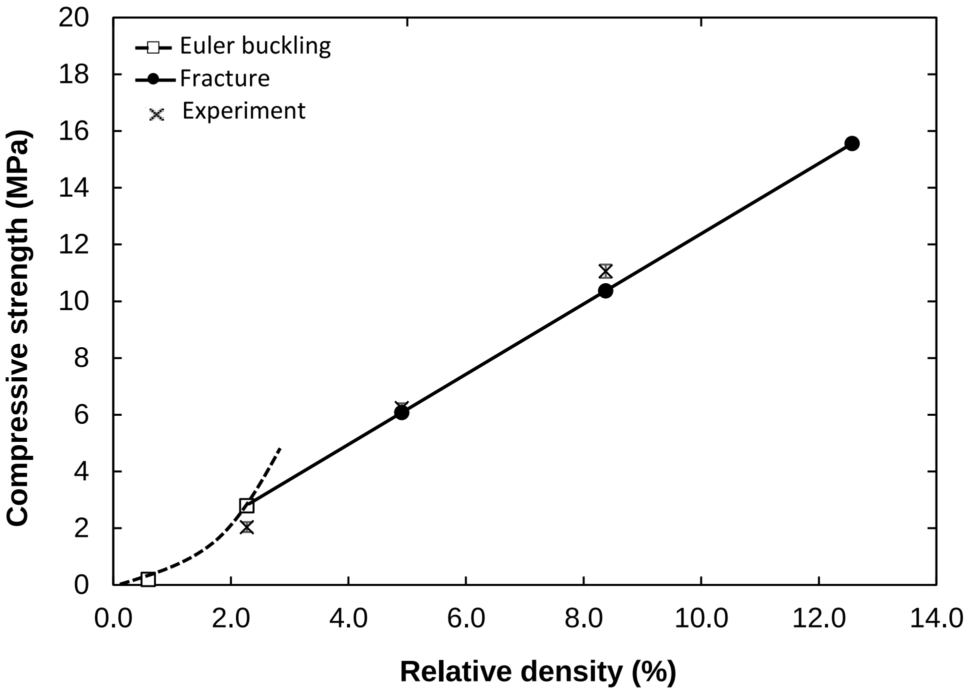

(b) $V_f = 0.35$

Figure 5.12. Peak strength predictions refer to buckling and fracture failure modes of the vertical column lattices.

It is evident from analytical predictions that the dominant failure mode for the columnar lattice with low relative density is Euler buckling of the struts which agreed well with failure mode observed during the experiments (Figure 4.44 in Chapter 4). The failure events matching well with the experiments, however, for column lattices with a fibre volume fraction of 0.14 and a relative density of 4.9%, the dominant failure mode was buckling of the struts which is not agreed with the predictions. This is likely due to the parent material compressive properties obtained from experiments is lower, resulting from manufacturing defects in the making of composite strut. Overall the operating failure modes agree well with analytical expressions and experimental observation.

5.6.3 Pyramidal lattice

The analytical expressions of the pyramidal lattice core sandwich structures were widely reported in the literature and used in this work by adopting the method for the current theoretical analysis. The pyramidal lattice core used in the experiment was for a material having a fibre volume fraction of approximately 42%. Pyramidal lattice cores with three relative densities were examined based on 2, 3 and 4 mm diameter of truss members. The predicted elastic modulus of the pyramidal lattice core is shown in Figure 5.13. The compressive modulus values increase with increasing the relative densities representing a linear function. The figure shows that the core modulus predictions based on pin-ended. This is due to the fact that in an end-clamped strut the contribution to modulus from bending are relatively small compared to that the contribution to stiffness of the core due to stretching of all the struts.

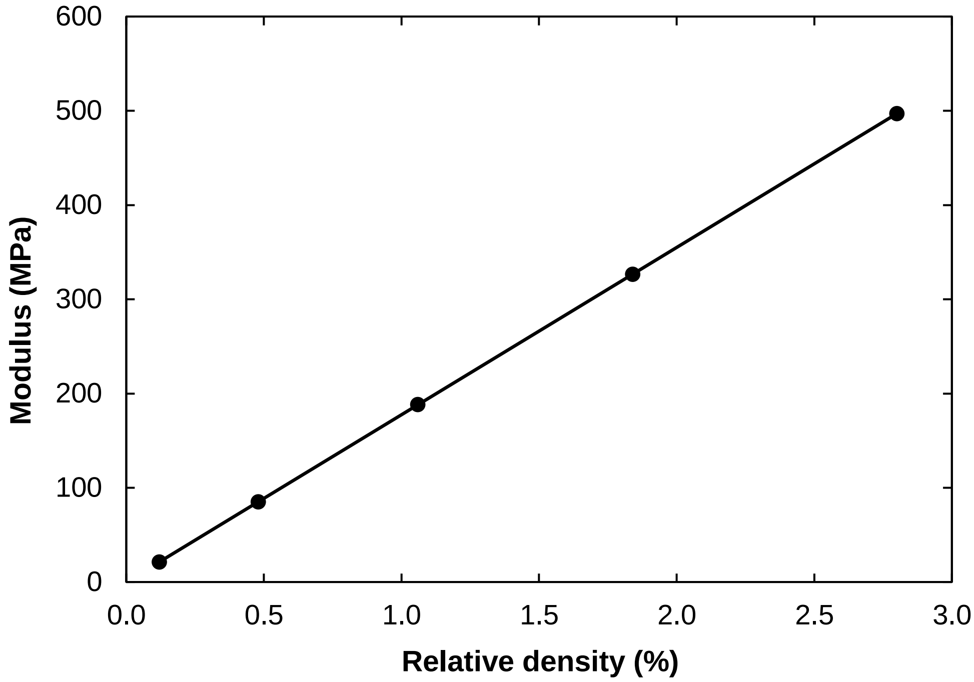

Figure 5.13. Effective elastic modulus of the pyramidal lattice core calculated from the analytical expressions.

The predicted peak strength based on the failure modes is shown in Figure 5.14. The operating failure mode for the lower relative density core is elastic buckling of the struts followed by which the operating failure is transitioned from Euler buckling to fracture of struts. From micromechanical predictions, it is suggested that the transition point is occurring when the relative density of the core is approximately 0.8, which well agreeing with experimental failure modes. The core-strut diameters with 3 mm and 4 mm resulting in relative densities of 1.1 and 1.8 were observed to be failing by fracture of struts via crushing or rupture near the ends of the strut connecting to facesheets.

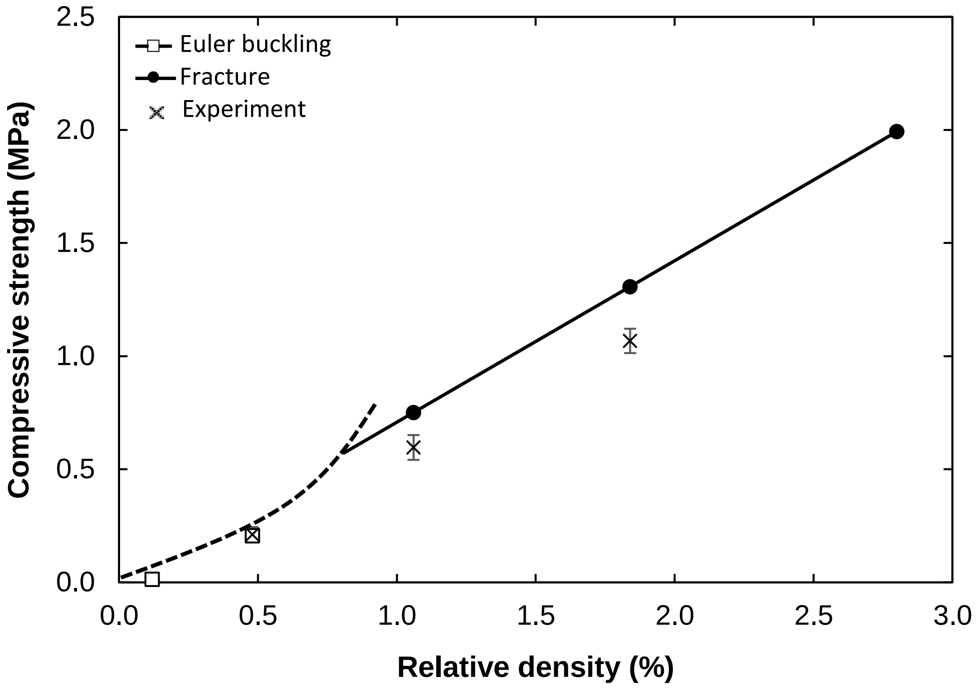

Figure 5.14. Analytical predictions of the pyramidal lattice core compression strength.

5.6.4 Modified-pyramidal lattice (T1)

In this configuration, a central vertical column is added to the plain pyramidal core construction through the apex of the pyramid. Similarly, three core-struts having different diameters were studied with a fibre volume fraction of 42%. Consequently, the relative density was varied by adjusting the strut diameter from 1 mm to 5 mm while keeping all other parameters unchanged. The values of the predicted compressive modulus based on the analytical model are presented in Figure 5.15 based on pin-ended assumptions. Strength predictions based on the pin-joint assumption is illustrated in the Figure 5.16. The strength values presented are calculated using model assuming that both struts (inclined and vertical) are failing simultaneously which gives good agreement with experiments. The model suggested that the modified-pyramidal (T1) core having low relative density collapses by Euler buckling of the struts and the operating collapse modes transitioned at the relative density of approximately 0.7 %. The experimental observations for operating failure modes during compression tests agreeing well with analytical predictions (Figure 4.27, Chapter 4).

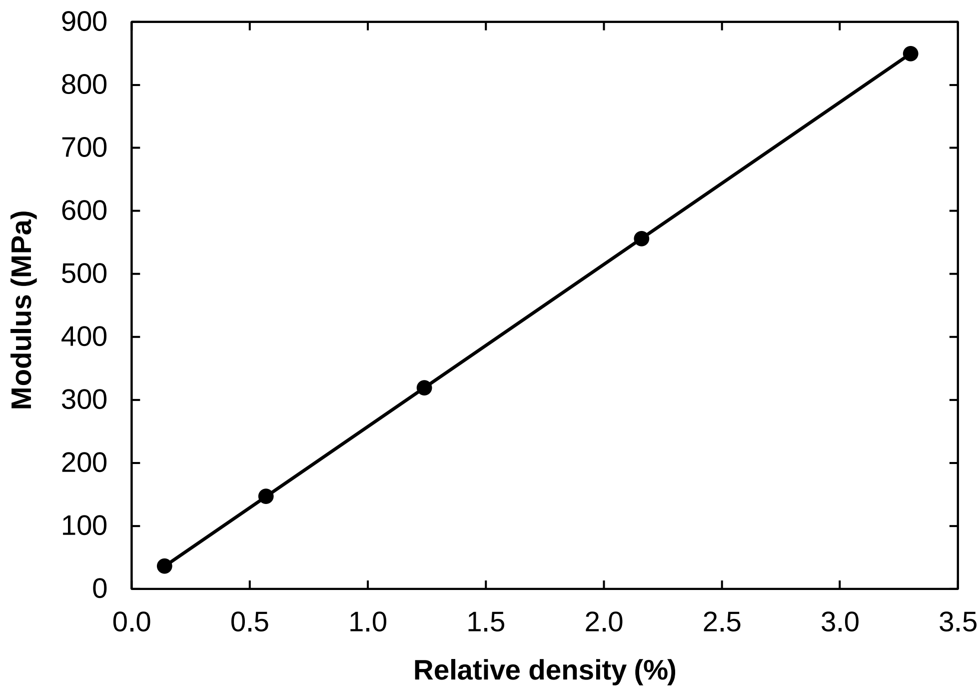

Figure 5.15. Analytical predictions of the modified-pyramidal (T1) lattice core compression stiffness.

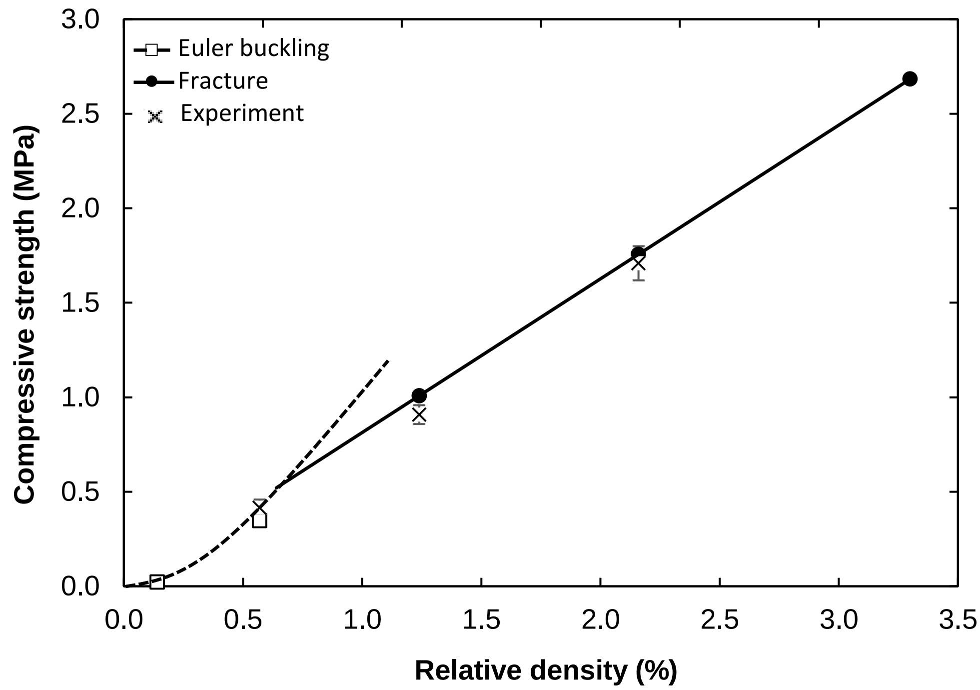

Figure 5.16. Strength values predictions of the modified-pyramidal (T1) lattice core.

5.6.5 Modified-pyramidal lattice (T2)

The type-2 core (T2) based on pyramidal configuration was constructed to examine their compressive behaviour under compression. In this construction, another four struts are added in pyramid configuration to the plain pyramidal core topology. The inclination angle of the strut-1 is $\omega = 45°$ and strut-2 is angled at $\alpha = 56°$, respectively. T2 core lattice was made of struts having fibre volume fraction of 42% with a diameter of 3 mm. However, the prediction results are produced for cores with five different relative densities based on struts having diameters of 1, 2, 3, 4 and 5 mm using the analytical model developed for this core type. The results for the compression stiffness predictions based on pin-ended depicted in Figure 5.17.

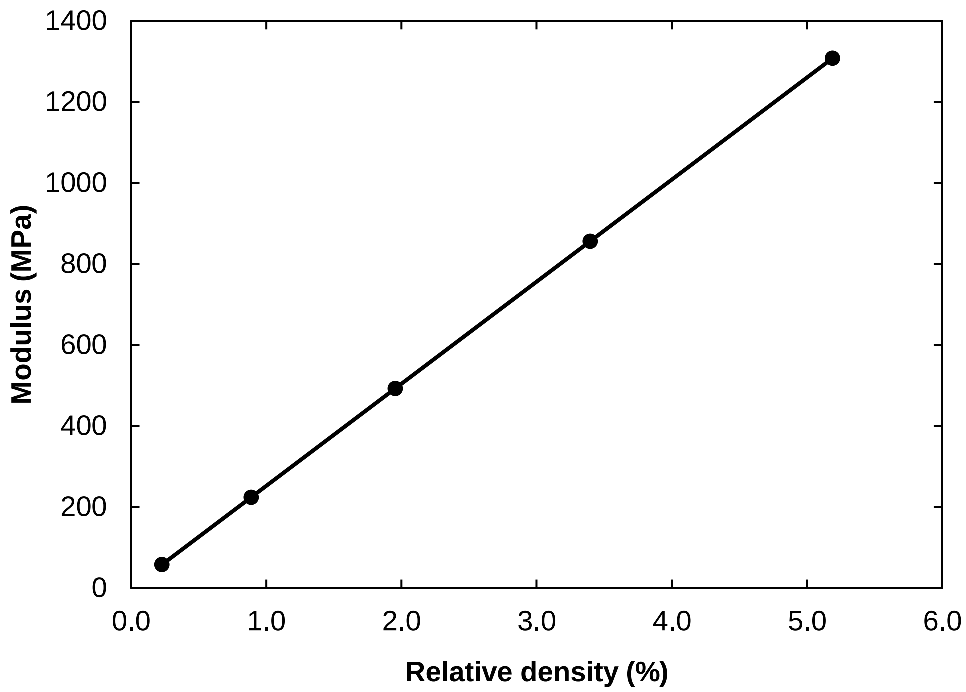

Figure 5.17. Analytical predictions of the modified-pyramidal (T2) lattice core compression stiffness.

The predicted strength results for the T2 lattice core is presented in Figure 5.18. The operating failure mode for 3 mm diameter core-struts is by fracture of struts from analytical model which agrees well with the experiments. The model also suggested that the transition failure mode from Euler buckling to fracture of struts is occurs at the core relative density of approximately 1.2 %.

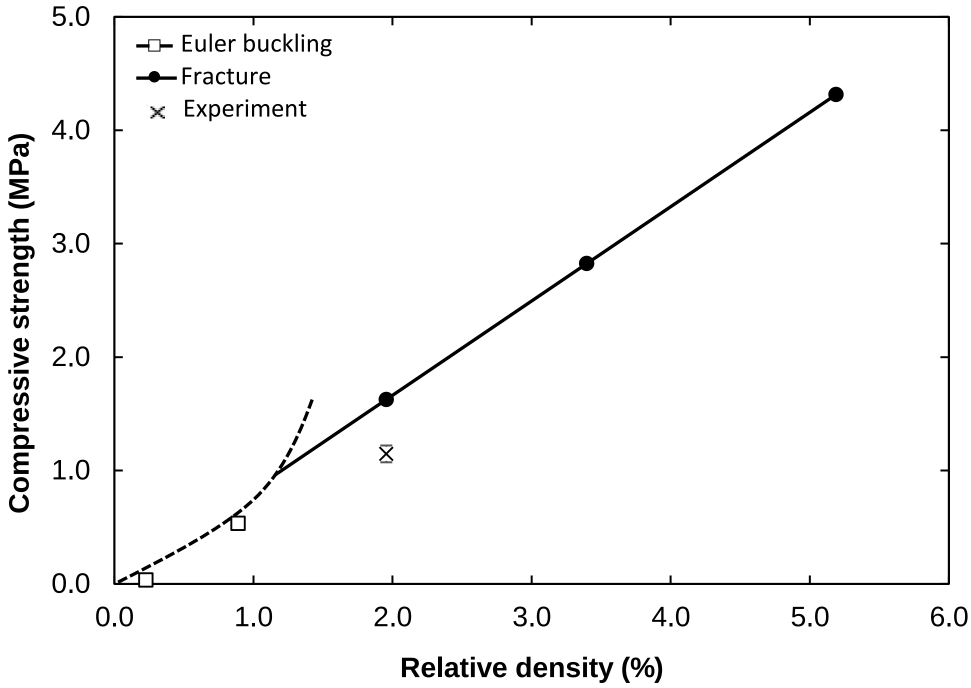

Figure 5.18. Strength values predictions of the modified-pyramidal (T2) lattice core.

5.6.6 Modified-pyramidal lattice (T3)

Type-3 core (T3) construction is based on the T2 lattice structure in which one central vertical column is added to the T2 core construction. The struts in the T3 core having a material of a fibre volume of 42% were manufactured based on 3 mm diameter. Here, the compression modulus and peak stress of the T3 cores are examined using analytical expressions for three different relative densities using Equation (5.91) and Equation (5.92), respectively at five different relative densities based on 1, 2,3, 4 and 5mm. The relative density of the core is controlled by changing the strut diameter, while keeping other geometrical parameters being identical to the T2 core construction including the inclination angles. The stiffness prediction for the pin-jointed struts for a given relative densities is shown in Figure 5.19.

The analytical model for the collapse strength suggests that the core with a low relative density, Euler buckling failure is dominant, as illustrated in Figure 5.20. The predicted failure events for the 3 mm diameter core-struts matching well with failure mode observed during testing in which fracture of struts is operating failure mechanism (Figure 4.39b, Chapter 4).

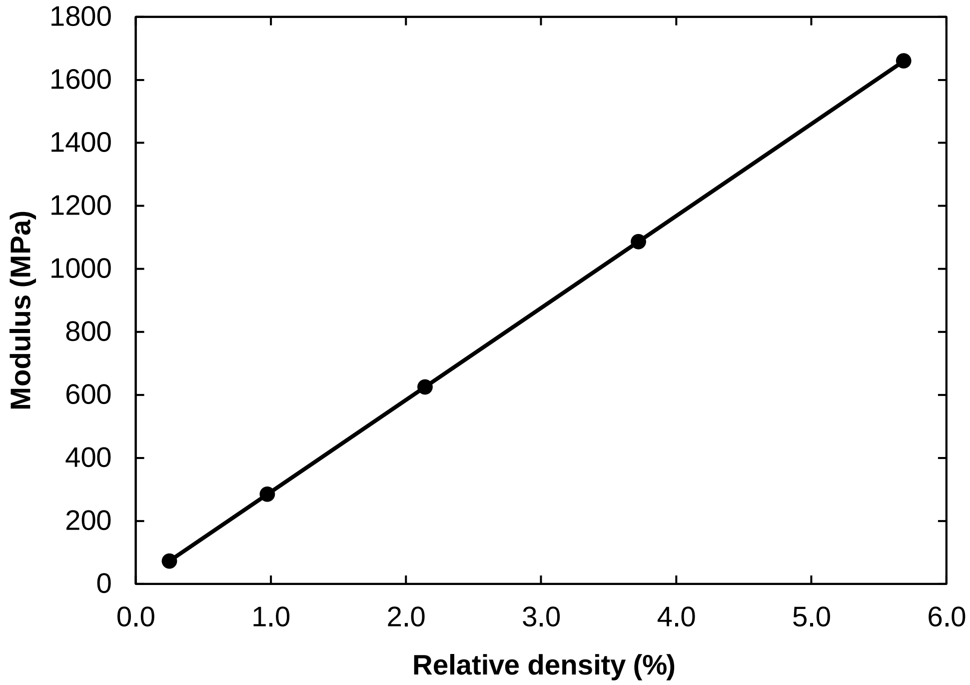

Figure 5.19. Compression modulus of the T3 core using analytical prediction.

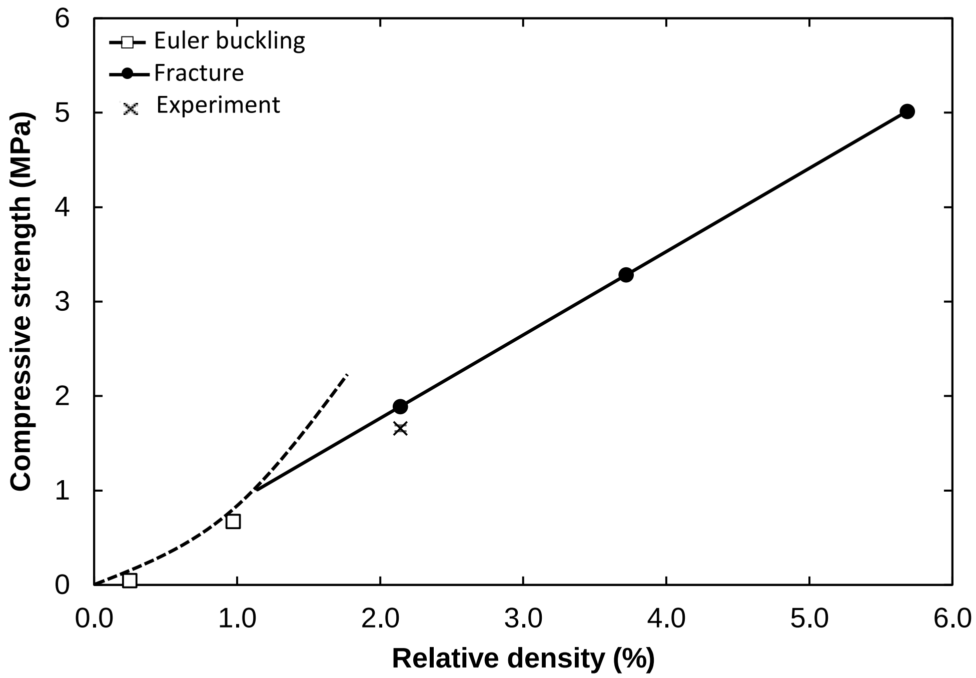

Figure 5.20. Compression strength values prediction of the modified-pyramidal (T3) lattice core.

5.7 Comparisons with experiments for pyramidal-based lattices

Figure 5.21 summarises the compressive stiffness of all four pyramidal based lattice structures based on 3 mm diameter core-struts having a fibre volume fraction of 42% by including the measured values from experiments and the predictions by analytical models. It is evident from figure that the models are over-predicted the modulus in all cases. The analytical models were considered based on ideal condition with general assumptions and simplifications. The effective stiffness prediction is proportional to Young's modulus of the parent material. The elastic modulus of the parent material calculated from rule of mixture based on the ideal situation, where we considered the fibres are evenly distributed across the cross-section. However, images of the cross-section captured from microscope tends to reveal some resin-rich areas with fibre distribution is not perfectly even. This is also attributed to the manufacturing defects in composite struts such as fibre waviness and fibre misalignment. In manufacturing of the lattices, the fibres were handled manually, and stitching process could have led to such fibre waviness and misalignment which can be visually observed for struts having a fibre volume fraction below 14%.

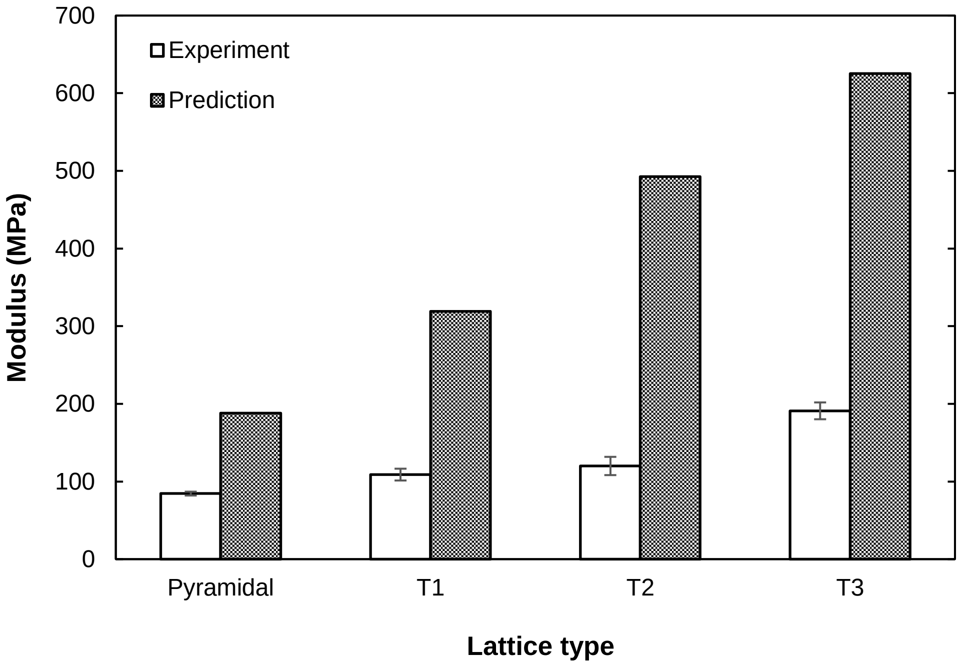

Figure 5.21. Comparison between measured and predicted values of the compression modulus of the pyramidal based-lattice structures.

Apart from parent material properties, the differences between the measured and predicted values are likely due to the error associated with using the crosshead displacement to determine the strain. There are also discrepancies between the assumed and actual boundary conditions at the strut-skin interface. Nevertheless, the models are correctly predicting the general pattern in the experimental data with pyramidal core having least modulus and T3 core showing highest modulus value.

Figure 5.22 compares the compressive strengths measured from the experiments and predicted values from the analytical models. Here, the cores based on 3 mm diameter were observed to be failing by fracture of the struts and these values are presented in Figure 5.22. An examination of the figure indicates that the analytical models overestimated the measured values of the compressive strength. The likely reason for the difference between the measured and estimated values is again due to the defects in the lattices. Although the presence of the defects in the lattices, the models are able to predict the general trend in the compressive strength over the lattice core types.

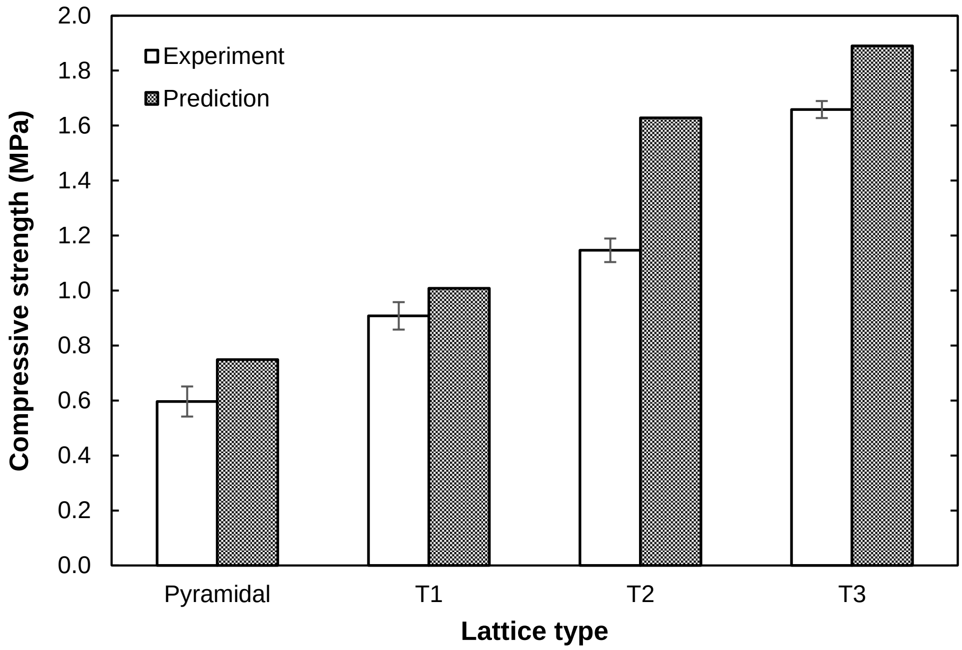

Figure 5.22. Comparison between measured and predicted values of the compression strength of the pyramidal based-lattice structures.

5.8 Summary

Analytical models have been derived to predict the compressive modulus and peak strength of the various types of lattice cores manufactured using the sacrificial mould method. The analytical work is established by employing the beam theory and force balance analysis to conduct the theoretical derivation. The values of the prediction from the analytical models were compared with the experimentally-measured values. The predicted and measured values show good agreement for the compressive strength with some disparities. However, the compressive modulus values from both the predictions and measurements demonstrated large discrepancies due to using the crosshead displacement for strain measurements which significantly under-estimate the modulus. In spite of this, the models were able to predict the general trend in the experimental data for the range of lattices studied.

References

[1] B. Wang, L. Wu, L. Ma, Q. Wang, and S. Du, Fabrication and testing of carbon fiber reinforced truss core sandwich panels, Journal of Materials Science and Technology, 25, 2009, pp547–550.

[2] E.M. Odom and D.F. Adams, Failure modes of unidirectional carbon/epoxy composite compression specimens, Composites, 21, 1990, pp289 – 296.

[3] K. Finnegan, G. Kooistra, H.N.G. Wadley, and V.S. Deshpande, The compressive response of the carbon fiber composite pyramidal truss sandwich cores, International Journal of Materials Research, 98, 2007, pp1–9.

[4] J. Xiong, L. Ma, L. Wu, B. Wang, and A. Vaziri, Fabrication and crushing behavior of low density carbon fiber composite pyramidal truss structures, Composite Structures, 92, 2010, pp2695–2702.

[5] S. Yin, L. Wu, L. Ma, and S. Nutt, Pyramidal lattice sandwich structures with hollow composite trusses, Composite Structures, 93, 2011, pp3104–3111.

[6] S. Yin, L. Wu, and S. R. Nutt, Compressive efficiency of stretch–stretch-hybrid hierarchical composite lattice cores, Materials and Design, 56, 2014, pp731–739.

[7] L. Che, G. Xu, T. Zeng, S. Cheng, X. Zhou, and S. Yang, Compressive and shear characteristics of an octahedral stitched sandwich composite, Composite Structures, 112, 2014, pp179–187.

[8] T. George, V.S. Deshpande, K. Sharp, and H.N.G. Wadley, Hybrid core carbon fiber composite sandwich panels: Fabrication and mechanical response, Composite Structures, 108, 2014, pp696–710.

[9] E.J. Barbero, Introduction to Composite Materials Design, Taylor and Francis, 1999.

[10] M.W Hyer, Stress Analysis of Fibre-Reinforced composite materials, Destech Publications, 2009.

[11] I.M Daniel and O. Ishai, Engineering Mechanics of Composite Materials, 2nd Edition, Oxford University Press, 2006.

[12] GRAFIL 34-700, Mitsubishi Chemical Carbon Fibre and Composites, Inc., Available: http://mccfc.com.

[13] IN2 EPOXY INFUSION RESIN-Technical Datasheet, Easy Composites Ltd., Available: www.easycomposites.co.uk.

6 Conclusions and Recommendations

In this final chapter, the major findings of this research are summarised. Following this, recommendations for future work will also be given.

6.1 General conclusions

The aim of this research was to manufacture composite lattice core sandwich structures in one manufacturing process by integrally stitching truss core with facesheets using a sacrificial mould method. A series of experimental tests have been conducted to investigate the mechanical properties of a range of all-carbon composite lattice cores sandwich structures under quasi-static and dynamic loading conditions. Following this, the collapse and failure mechanisms of the lattice truss cores based on carbon composite material have been characterised under both loading conditions. Analytical models have been proposed to predict stiffness and peak strength of a range of lattice truss configurations under quasi-static compression loading. Considerable work has been carried out to achieve this aim associated with a number of objectives and the following conclusions can be drawn:

- A range of carbon fibre reinforced composite lattice truss cores, based on vertical column, pyramidal, modified pyramidal designs with varying complexity, was successfully manufactured using the sacrificial mould method along with vacuum assisted resin infusion technology.

- The influence of fibre volume fraction on vertical column lattice truss based on strut diameters of 2, 3 and 4mm with resulting relative densities of approximately 2.3, 4.9 and 8.4 % respectively were investigated under quasi-static compression loading. Specific compression strength and modulus values showed an increase when fibre volume fraction within individual struts increased. The maximum value of specific energy absorption value (SEA) is approximately 39 kJ/kg for columnar lattices based on 4 mm diameter struts having a higher fibre volume fraction.

- The collapse processes of the two different columnar structures having varying fibre volume fractions were identified. The failure modes of the columnar lattices were transitioned from Euler buckling to fracture of struts via crushing and splitting for given relative densities.

- Pyramidal lattice cores and modified-pyramidal lattice cores based on varying complexity (type-1, type-2 and type 3) were manufactured and tested under quasi-static compression and low velocity impact tests.

- Key mechanical properties, such as the elastic modulus, peak strength and energy absorption, were recorded for each of lattice core sandwich structures. The structures showed an excellent repeatability in their mechanical response. The mechanical response in compression increases with relative densities.

- The specific properties of all lattice cores were calculated, the structures were shown to compare well with their competitive materials. Based on 3mm core-strut diameter, type-1 and type-3 lattice cores were shown the highest values of specific stress and modulus compared to other two pyramidal-based cores (pyramidal and type-2). This suggested that adding more struts in open plain pyramidal core increased stress and modulus values as expected, however their specific properties were not much improved. Among them, modified pyramidal core (type-1) displayed the optimum characteristics based on their mechanical responses. The resulting SEA values are varied between approximately 9 and 16 kJ/kg.

- The effect of varying unit cell numbers was investigated for the pyramidal and the modified pyramidal (type-1) lattice structures under quasi-static compression loading. It was indicated that the specific strength and modulus decreased with increasing of the unit cell number to a certain extent.

- The primary failure mechanism of the composite pyramidal lattice core based on 2mm truss diameter was controlled by Euler buckling of struts. Meanwhile, the failure mode of the cores based on 3 mm and 4 mm struts was predominantly failed by fracture of the struts at either ends of the struts.

- The impact response of the composite lattice core sandwich structures was investigated. The peak load in dynamic tests are significantly greater than that in the quasi-static counterparts. Similar failure mechanisms were observed in the dynamic tests and the quasi-static tests.

- It was highlighted that the lattice structures absorb more energy during the initial crushing stage under dynamic loading compared with their quasi-static counterparts. However, the overall energy absorption capacity of lattice structures in dynamic loading showed a decrease of approximately 30% compared to structures tested in most of quasi-static cases due to more significant drop of load carrying capacity after the damage initiation.

- Analytical models were presented to predict the response of a range of lattice structures (vertical column, pyramidal, modified-pyramidal type-1, type-2 and type-3) under quasi-static compressive loading. The stiffness and peak failure strength of the lattice cores were predicted by the analytical models.

- The analytical models over-predicted the modulus values in all lattices systems compared to the values measured in experiments, which was likely due to the error associated with using the crosshead displacement to determine the measured strain of the cores and ignoring sample imperfections in the models. However, the models did provide a reasonable prediction of the general pattern in the experimental data with the pyramidal core having least modulus and T3 core showing highest modulus value.

- The maximum strength of the composite lattice core structures was predicted reasonably well by the analytical models. The predictions were slightly higher than from the experimentally measured values for all lattices, due to omitting the presence of the defects such as fibre waviness and uneven fibre distribution within the struts.

- The analytical models also predicted the failure modes observed in experiments for all lattice structures for a given relative density. The dominant failure modes observed in the experiments were primarily buckling and fracture of the struts. This further suggested that the analytical models presented can be effectively used to predict the compressive response of the lattices for the core configurations studied.

- Overall, it has been shown that composite based lattice structures manufactured using the sacrificial mould method offer the potential to demonstrate higher elastic modulus, peak strength and energy absorption by employing higher volume fibre fraction within individual struts.

- Finally, it is believed that this study fills the gap between various aspects of research on cellular core materials, design and manufacture, mechanical properties as well as failure modes in the composite lattice core sandwich structures.

6.2 Recommendations for future work

It has been shown that the performance of current composite lattice core sandwich structures compares well with their competitive cellular cores. The sacrificial mould method has the capability to manufacture different lattice structures with varying degree of complexity and unit cell topologies, which may have superior mechanical properties to the structures presented in this study. Even now, not all of the possibilities have been explored and is an ongoing task. Here, some recommendations for future work are given:

- Additional investigations could be carried out to fully characterise the response of the lattice structures under shear, tensile, bending as well as torsional loading conditions.

- The sacrificial mould technique could be used to manufacture a range unit cell topology lattice structures other than pyramidal configuration. The structures can be optimised to achieve the ideal ratio of weight to mechanical properties. The response of the lattice structures based on different materials, such as, glass fibre or even natural fibre composites can be investigated.

- Work could be carried out to further improve the sacrificial mould method. Studies should be conducted to improve the quality of the struts by evenly distributing the fibre during stitching process as well as to avoid fibre waviness and misorientation during manufacturing process that caused from manual handling. The threading process may be automated to achieve a more even fibre distribution within the strut. This will improve the stiffness and strength properties of the structure.

- Finite element (FE) modelling should be developed and validated against the experimentally measured values. The validated FE models should then be used to assist design the optimum lattice structures and give accurate representation of the cell geometry with damage criteria included in the analysis so that material failure within the cell is captured.

- A systematically designed parametric studies could be carried out by varying the material properties, geometrical parameters and different unit cell topologies to optimised performance of the lattice structures.

Appendix

Terminologies used for the burn-off test are as follows:

m_c	Mass of crucible (g)
m_{c+s}	Mass of crucible + sample (g)
m_s	Mass of sample before burn-out m_{c+s} - m_c (g)
m_{c+f}	Mass of crucible + fiber residue after burn-out (g)
m_f	Mass of fiber m_{c+f} - m_c (g)
m_m	Mass of matrix m_{c+s} - m_{c+f}
ρ_f	Fibre density (kg/m^3)
ρ_m	Matrix density (kg/m^3)
W_m	Weight fraction of matrix
W_f	Weight fraction of fiber
V_m	Volume fraction of matrix
V_f	Volume fraction of fiber

The formulas used to quantify the weight fractions of the fiber and matrix using their corresponding constituent (fiber and matrix) mass are:

$$W_f = \frac{m_f}{m_s} \tag{A-1}$$

The weight fraction is

$$\sum W_i = 1 \tag{A-2}$$

where W_i is the weight fraction of the constituent i. The weight fraction of composite containing the fibers and matrix can be described as:

$$W_f + W_m = 1$$

$$\text{or} \qquad W_m = 1 - W_f \tag{A-3}$$

The volume fraction is represented by:

$$\sum V_i = 1 \tag{A-4}$$

where V_i is the volume fraction of constituent i. The volume fraction of composite containing fiber and matrix can be described as

$$V_f + V_m = 1$$

$$\text{or} \qquad V_m = 1 - V_f \tag{A-5}$$

Generally, the weight fraction and volume fraction values of a composite will not be the same as these values are associated with the constituent densities. Given the densities of the constituents, weight fractions can be converted to volume fractions using the following equation:

$$V_f = \frac{W_f/\rho_f}{\sum W_i/\rho_i} \tag{A-6}$$

and

$$W_f = \frac{V_f \rho_f}{\sum V_i \rho_i} \tag{A-7}$$

In a composite material comprising of only a fibre and a matrix, the fibre volume fraction and weight fraction are given by:

$$V_f = \frac{W_f/\rho_f}{W_f/\rho_f + \left(1 - W_f\right)/\rho_m} \tag{A-8}$$

and

$$W_f = \frac{V_f \rho_f}{V_f \rho_f + \left(1 - V_f\right)\rho_f} \tag{A-9}$$